http://researchspace.auckland.ac.nz

ResearchSpace@Auckland

Copyright Statement

The digital copy of this thesis is protected by the Copyright Act 1994 (New Zealand).

This thesis may be consulted by you, provided you comply with the provisions of the Act and the following conditions of use:

- Any use you make of these documents or images must be for research or private study purposes only, and you may not make them available to any other person.
- Authors control the copyright of their thesis. You will recognise the author's right to be identified as the author of this thesis, and due acknowledgement will be made to the author where appropriate.
- You will obtain the author's permission before publishing any material from their thesis.

To request permissions please use the Feedback form on our webpage. http://researchspace.auckland.ac.nz/feedback

General copyright and disclaimer

In addition to the above conditions, authors give their consent for the digital copy of their work to be used subject to the conditions specified on the Library Thesis Consent Form and Deposit Licence.

Fluoride Emissions from Aluminium Electrolysis Cells

by
Edwin Campbell Patterson

A thesis submitted to the University of Auckland
in fulfilment of the requirements of
Doctor of Philosophy in Chemical Engineering.

Auckland **March 2001**

Abstract.

Modern aluminium electrolysis cells generate between 15 to 40 kg fluoride per tonne of aluminium fluoride produced. This represent a large material recycle load, of which over 99% of this fluoride content is returned to the cell via a dry scrubbing system. Most past research has concentrated on increasing the efficiency of this end scrubbing system, neglecting the actual cause of the fluoride emissions. Lower emissions would reduce this loading, resulting in smaller scrubbing systems, and ultimately lower capital costs. Fluoride emissions also contribute to the changes in heat balance in the cell. The fluoride evolved represents a material loss that requires to be replaced with AlF_3. The addition of this species is a major variable in cell heat balance instability [1]. Overall a better understanding of the contributors to fluoride generation in an aluminium cell would benefit the operation and economics of an aluminium smelter.

Past studies [2-6] have identified most of the important emission contributors to hydrogen fluoride (HF) generation. Two sources were shown to be significant. The most studied source was primary HF generation. This is HF generation from electrolytic reactions between constituents of the fluoride based electrolyte and water from the fed alumina and hydrogen in the anode. Overlooked in some studies were generation reactions outside the electrolyte - defined in this study as secondary HF generation. This source was found to occur mainly from hydrolysis reactions with the generated particulate fluorides. However the results and the relative contributions from these studies are not strictly applicable to the current generation scenario. The present smelting practices and technology, dry scrubbing technology and raw material specifications differ substantially from those used during the period of each past investigation. The present study was designed to identify and quantify emission sources for the current smelter technology and practices. This used controlled laboratory based studies of the individual generation sources complemented by in plant studies analysing the HF emission from production aluminium electrolysis cells.

It was shown that the main contributor to primary HF generation is the addition of water to the electrolyte from the feed alumina. This results in the cyclic short term variations in HF emission, which correlate to the rate of alumina addition to the cell. Laboratory and industrial studies show that only a fraction of the added water reacts. The water reacted is likely the structural water of the alumina. The adsorbed water is thought to be flashed off before addition to the bath. Depending on feeding technology and crust integrity, between 10 to 50% of this water can react. This produces 7 to 14

kgF/tonneAl. This makes it the most significant emission component. The remainder of this structural water is either entrained in the anode gases or forms part of the electrolyte dissolved water content.

Dissolved water generation is the second most significant primary generation contributor, and third most significant emission component. Dissolved water is in equilibrium with the alumina content of the bath. It represents a constant emission source. Depending on feeding technology and cell design, the emission can vary between 3 to 10 kgF/tonneAl.

The final primary HF emission contributor results from electrolytic generation of the hydrogen content of the anode. Laboratory studies found the emission to have a reaction efficiency of approximately 10%. This results in a small emission, of 2 – 5 kg/tonneAl. The remainder of the hydrogen content is expected to be entrained in the anode gases, as the generation of this CO/CO_2 mixture is an order of magnitude greater than the HF generation reaction.

Secondary generation of hydrogen fluoride is also a significant HF emission source. In an industrial cell this results from mainly thermal hydrolysis of the particulate fluoride emissions at the crust–air interface. Laboratory studies have shown that other identified secondary emission sources are unlikely due to the ambient conditions and feeding practices in a modern prebake aluminium electrolysis cell. Hence previously proposed generation from hydrolysis of the particulates in the ducts and desorption of the surface fluoride from the fed secondary alumina, have been found to be insignificant compared to the main HF generation sources.

The thermal hydrolysis emission contributor is the only significant secondary generation emission component. Industrial measurements show that it varies with ambient humidity and crust integrity, two parameters which vary constantly in a modern prebake anode cell. Measurements show that the emission from this source is responsible for 2 to 8 kgF/tonneAl. This makes it the second highest HF emission component. Control of the crust condition and feeder hole states reduces this component significantly.

Hence in a modern prebake aluminium cell, the most significant operational factors affecting emission are related mainly to secondary generation. Industrial measurements show that the long term variations in an emission result from changes in the ambient humidity and the cells crust cover. Control of the crust integrity is thus paramount in

reducing such variations. This relates both to normal operation and batch operations. Reduction of all other sources of emission are a material composition problem. Simply reducing the water content (LOI(300) and LOI(1000)) and reducing the hydrogen content of the anodes will reduce the emission. However material considerations affect other aspects of cell operation and hence these factors are not as simple to adjust.

Acknowledgements.

We all know that three and a bit years brings so many people into ones work and life. Of the countless I have missed in this little note - I thank you whole heartedly.

I can't think a better place to start than with those who have guided me the whole way. Margaret and Barry I'm indebted for you help through all patches, even the rather rough one at the end. Its been fun – and what else is life about. Never fear, I'm glad I've done this and it's finished now ☺.

Those feisty technicians at C&M. Great beer at the end, pity we ran out at the last BBQ. May be a good thing. Still Tom, Keith, Bruce, Alan, Dragan, Bill, Andy and all those past and present – thanks. I love to build stuff, you guys just do it better!!!!

To those at Hydro Aluminium. Victoria thanks for you help, friendship and guidance. Halvor, your advise and help has been invaluable. Bjorn – thanks for the help at the end. To all the rest at ATA in Ardal. Thank you, it was a fun time with a great team. I'll be back some time for a visit.

What is a degree with out friends. All the postgrads past and present – Torsten, Ursula, Derek, Susie, Hoani, Steve (both types), Parin, Dolly, and so many more good friends – thanks. I'll miss those squash nights. And those infamous morning coffees – or morning jolts!

To my Family. Mum, Dad, T and Darrell (and those attention grabbing cats). Thanks for the love and support, where would I be without that sort of foundation.

What else – well I'll end on this – we all need self commentary!!

Its had its ups and downs and side tracks a many
But who could ask for more than this….
Three years of fun, friends, rewards and heartbreak.
But its time to move on now way from all that,
Up and on and flying into the future
With a sprinkling that special nova dust,
Mixed in with sweat and tears.

Contents.

List of Figures.

List of Tables.

List of Symbols.

T	= Temperature	(K)
T_b	= Bath Temperature	(^OC)
P	= Absolute Pressure	(kPa)
p_{H2O}	= Partial pressure of water in the air at a fixed T and P	(kPa)
ΔG	= Gibbs Free Energy	(J)
K	= Equilibrium Constant	(---)
CR	= Cryolite Ratio	(---)
r	= Reaction rate	
k	= Rate constant	
k’	= Pseudo rate constant	
U	= Underfeed HF emission	(kg/h).
O	= Overfeed HF Emission	(kg/h).
A	= OF alumina feed rate	(kg/min).
a	= UF alumina feed rate	(kg/min).
B	= Non alumina emission	(kg/h).
D	= U – O = $D_{feeding}$	(kg/h).
d	= A - α	(kg/min).
α	= Difference between alumina feed normalised overfeeding and underfeeding emission rates	(---).
τ	= Time constant for structural water dissolution	(s).
t	= Time	(s).
A, B, C	= Derived constants for step response analysis.	
a, b, c	= Derived constants for step response analysis.	
F	= Total primary fluoride evolution	(kg/tonne Al)
W	= Bath weight ratio.	
AW	= Alumina water content	(%)
BA	= Bath Alumina content	(%)
CF	= Bath calcium fluoride content	(%)
AE	= Anode effect.	
TR	= Track.	
AF	= Hand fluoride addition.	
HC	= Average hydrogen content of the anodes	(%)
ftc	= Feeding technology coefficient	
OFH	= Open Feeder hole percentage	(%)
P_B	= Ambient Pressure	(kPa)
%CE	= Current Efficiency	(%)
P_{NaF}	= Vapour Pressure of NaF above Bath	(kPa)
R_b	= Weight Ratio NaF/AlF_3 in bath	(---)
HBA	= Hydrolysis by air factor.	

1. Introduction.

Fluoride emissions - both gaseous and particulate - are the major undesirable fume component produced by aluminium smelting. In the last fifty years a great deal of research has been focused on the cleaning of the fumes via post generation scrubbing systems, to reduce the emissions to an accepted level. This somewhat mirrors the current rethink of regional environmental regulations.

The actual process of gaseous hydrogen fluoride (HF) generation has been treated in less detail however. This is peculiar given fluoride emissions are a contributor to the variability that occurs in the operating excess aluminium fluoride concentrations in smelting electrolytes. Directly they represent a material loss, changing the chemical composition of the bath. Indirectly they are the reason AlF_3 is replaced in the electrolyte. Incorrect control of this addition results in cell heat balance instability [1]. Reducing the loss at the generation source would reduce some causes of cell heat balance changes and has the economic advantage of smaller recycle loads within the system. Effectively the post generation scrubbing system could be down sized with lower emission generation, reducing capital costs.

Most of the available information on relative contributions to fluoride emissions is based on modelling, with scant hard data available. While the various generation processes have been investigated in the past, a systematic study of the influence of entrainment of moisture via the alumina and cell room air or even a detailed view of the influence of cell operations on the generation processes is still lacking. Moreover the value of the past studies to modern smelting techniques, technology, materials specifications and the past data's accuracy (due to historical technological limitations on experimental apparatus) makes such studies questionable anyway. Accurate and consistent plant studies on the primary generation of the emissions and the effect of cell dynamics on these mechanisms is still lacking in the published literature. Certainly a clearer understanding of the mechanisms forming the emissions in a modern prebake cell is a fundamental step to reducing the source of the emissions.

Hence it was the overall objective of this thesis to investigate the important process and material variables that influence the rate of evolution of fluorides from smelting electrodes and operating cells. This study attempts to address the actual amounts of these identified sources in the modern smelting environment. Along with the relative

amounts the study always aimed to gain an understanding of the actual generation mechanisms. All contribution factors, moisture content in the air, moisture content of the additives will be investigated.

2. Aluminium Smelting.

2.1. The Aluminium Cell.

Aluminium smelting as an industrial process involves the electrowinning of aluminium from aluminium oxide (alumina) in a high temperature electrolytic cell. The basic layout for a *hooded, point fed, prebaked anode, aluminium cell* is illustrated in figure 2.1. Essentially alumina is added batchwise to the cell via a feeding mechanism and undergoes reaction 2.1 at approximately $960^{O}C$. The most significant side reaction involves the reoxidation of the aluminium product with CO_2 evolved at the anode (reaction 2.2). The overall process, including side reactions requires a voltage of just over 4V.

$$2Al_2O_{3(sol)} + 3C_{(s)} = 4Al_{(l)} + 3CO_{2(g)} \quad (2.1)$$

$$2Al_{(sol)} + 3CO_{2(g)} = Al_2O_{3(sol)} + 3CO_{(g)} \quad (2.2)$$

The carbon for the reaction is provided by a consumable anode with the product aluminium deposited at the bottom of the cell on top of a carbon cathode. Alumina feeding in a prebake cell can either be achieved using large dumps (up to 30 kg), added in a *centre break* channel, or more continuously using several *point feeders*. This design adds smaller amounts of alumina (1-5 kg) more frequently through feeder holes in the frozen electrolyte crust. A point feed cell is illustrated in figure 2.1:

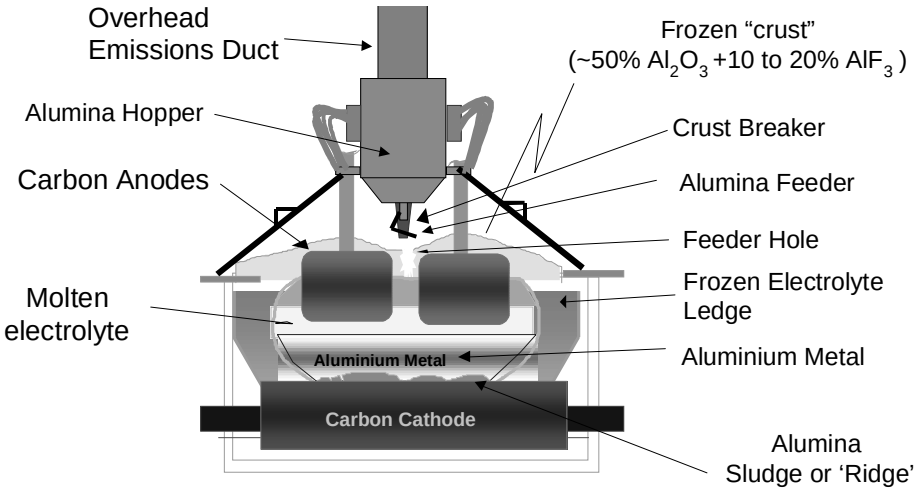

Figure 2.1 – The basic features of an industrial aluminium cell (After [1]).

As illustrated the cell contains approximately 12 tonnes of hot carbon anodes, 3.5 to 4.5 tonnes of molten electrolyte, 8 tonnes of frozen crust, 3.5 to 5 tonnes of frozen cryolite

rich electrolyte ledge on the side walls (at ~900°C) and 7 to 10 tonnes of metal and 0 to 2 tonnes of sludge [1].

Grjotheim and Welch [8] describe concisely the three different fluoride species which form the basis of the electrolyte. These are cryolite (Na_3AlF_6), which is the basic solvent comprising of at least 70 wt% of the total electrolyte mass, aluminium fluoride (AlF_3) which constitutes 2 – 12 wt% (on average around 10%) and calcium fluoride (CaF_2) which is typically in the range of 4 – 8 wt%. Beside these, sodium fluoride (NaF added as Na_2CO_3) is sometimes used in cells. The purpose of the additional additives is to improve the physicochemical properties of the electrolyte, with an emphasis on reducing the liquidus temperature. In this respect AlF_3 is the most suitable additive, though it is consumed at the greatest rate in the process due to its role in the generation of cell emissions.

2.2. Dry Scrubbing.

Essential to all modern day aluminium plants environmental strategy are an emissions cleaning process which meet the present stringent emission regulations. The *dry scrubbing system* (refer to figure 2.2) is the most common process employed at present.

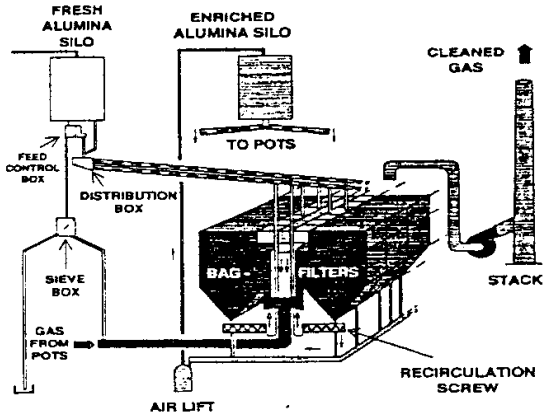

Figure 2.2 - The dry scrubbing process (After [9] figure pg 19-10).

The system consists of a unit which allows hydrogen fluoride to be absorbed onto fresh or unreacted (primary) structural alumina from hot exhaust gas of the cell. This mixture (of reacted alumina and entrained particulate called "secondary alumina") is then collected in a filtration system. This fluoride enriched mixture is then fed into the reduction cell, allowing the recycling the lost fluorides back into the process. Hence the entire process is a closed loop with approximately 98% efficiency. The key unit process in the system is the reaction of hydrogen fluoride on the alumina surface.

3. Alumina.

3.1. Introduction.

Alumina is the elementary raw material the aluminium smelting process is based around. This oxide is reduced to the end product within the electrolysis cell. Due to its regular addition, its properties and impurities have a major effect on both the metal quality, heat balance and cell process dynamics. Along with these process factors the alumina introduces water into the cell via two forms. As chapter 4 will show this results in significant primary HF generation. Overall, all theses factors result in alumina being fundamental to the study of hydrogen fluoride generation from an aluminium cell.

3.2. Alumina Properties.

Alumina is extracted from bauxite, an ore containing hydrated alumina with oxides of iron, silica, and titanium. The aluminus content ranges between 45 to 60% in the form of either trihydrate (gibbsite) or monohydrate (boehmite) and is extracted using the Bayer process [10]. Calcination temperatures of around $1250^{O}C$ are required for complete conversion of this product to conundrum or α-alumina, aluminas stable form. Gamma γ-alumina is the term given to a mixture of intermediate aluminas [10] formed by incomplete calcination.

Alumina with a high alpha alumina content is referred to a *floury alumina*. It has a poor flowability and has many more microcracks through shrinkage accompanying pore closure resulting in a B.E.T. surface area $<5m^2/g$ (refer to the section below). *Sandy alumina* has less severe calcination conditions (calcined at lower temperatures) resulting in lower alpha-alumina content (2-25%) and coarser crystals, with a smoother surface. These have a BET surface area of 30 – 80 m^2/g [8]. This general distinction is useful indicator of the general trends that the tested alumina will give [11].

The properties of interest to an aluminium smelter are listed quite succinctly in Grjotheim and Kvande [11], but for completeness can be summarised as follows:

Chemical purity: This refers to the amount of oxide impurities in the alumina. Smelters specify limits on the major impurity sodium oxide (Na_2O) - present at 0.5 to 0.5 wt% - as it reacts with AlF_3 in the bath, reducing this content. Calcium oxide is

present in lower amounts (less than 0.06%), along with minor amounts of silica, titania, iron oxide, phosphorous and vanadium.

Alpha Alumina: The alpha alumina content is given as a mass percentage of alpha phase in the alumina, and is typically between 10 to 30%. The main importance of this measurement is connected with crust formation, hardness, density and thermal conductivity, though it does affect the BET surface area also.

B.E.T. Surface area: The B.E.T. (Brauner, Emmet and Teller) surface area calculates the surface area of particles using physisorption of nitrogen. This gives an indication of the surface area of the porous network of the crystal (up to the size of the N_2 molecule). It is important in both fluoride adsorption in the dry scrubber and also the rate of dissolution of the alumina in the bath. Smelters generally specify aluminas with a B.E.T. surface area greater than $60 m^2.g^{-1}$.

Density: There are two different types of densities used when describing alumina quality:

Bulk density: Determined by filling the alumina powder in a vertical cylinder and measuring its volume and mass. Typical values range from 0.90 to 1.15 kg/dm^3. This property is important as some point feeders measure alumina feed by volume. Changes in the bulk density change the feed rate, affecting cell operation.

Real or pycnometric density: Determined by filling the void fractions of finely ground alumina (-10μm) with a volume, displacing fluid in a pycnometer. Typical values range from 3.45 to 3.60 kg/dm^3.

L.O.I. – Loss on ignition: This is the mass lost (moisture) of the alumina when heated between two temperatures in an inert atmosphere. Two temperature ranges are commonly analysed:

Humidity	- Heat to 110^OC for 4 hours (from 0^OC).
Moisture in ignition (M.O.I.)	- Heat at 300^OC for 4 hours (from 110^OC).
Loss on Ignition (L.O.I.)	- Heat to 1000^OC for 4 hours (from 300^OC).

These will be further explained in the hydration mechanism section.

Particle size distribution: The normal range of grain sizes is between 20 and 50μm. Smelter specifications tend to restrict the proportion of large particles fines. Large particles have a slow dissolution rate in the bath, while the fines cause mechanical

handling problems and dusting emission. The coarse fraction (+100μm) is usually less than 15%, and the fine fraction (-45μm) is less than 20% (usually less than 8%).

Flow Funnel Time: This is the time required for alumina to flow through a funnel with specific conditions. Typical values range between 4 to 7 minutes, with slow funnel times giving an indication that the alumina will dissolve quickly as it has a lower tendency of clumping on addition.

Angle of Repose: This is defined as the constant angle to the horizon assumed by as cone like pile of alumina powder, and is determined by the resistance of the alumina grains to slide and roll over one another. It typically ranges from 30 to 36^{O}. Only important in side fed cells where a bank of alumina is used and Söderberg cells.

Attrition index: This is a measure of the strength of the agglomerated grains of the alumina to withstand mechanical handling and transport without attrition. Agglomerated particles should withstand the rigours of dry scrubbing and transportation to the cell without producing an excessive proportion of fine (-45μm) powder. The maximum is 10, while 5 is preferred for the attrition index of the –45μm fraction.

3.3. Alumina hydration.

The surface of alumina is polar and has a strong affinity for water. Once adsorbed the water has a large influence on the chemical reactivity of the surface and the physical properties of the bulk alumina, including those properties which are relevant to its application in aluminium smelting [12].

3.3.1. Hydration Mechanisms.

The chemical activity and adsorption sites of the surface results from the defect structure produced during the amorphous to structural transition in the thermal dehydration stage [13]. This makes aluminas properties sensitive to the dehydration process (calcination). Activated aluminas surface (and scrubber grade alumina) is amphoteric, containing both acidic and basic sites of varying strengths and concentrations. The acidic sites result from the presence of coordinately unsaturated Al^{+3} ions and acidic hydroxyls, while the basic sites arise from the presence of O^{-2} anions and basic hydroxyls [13].

Water may be associated with alumina in a variety of forms. It can be held as structural water incorporated into the crystal lattice, or held on the *alumina surface* in a chemisorbed form, physisorbed form or as capillary condensate within the pores.

It is generally accepted that the dehydration process of the *structural water* or trihydrate can proceed in two different ways:

A).Two step:

$$Al_2O_3.3H_2O \xrightarrow{320^OC} Al_2O_3.H_2O + 2H_2O \quad (3.1)$$

$$Al_2O_3.H_2O \xrightarrow{550^OC} Al_2O_3 + H_2O \quad (3.2)$$

B). Single Step:

$$Al_2O_3.3H_2O \xrightarrow{240-300^OC} Al_2O_3 + 3H_2O \quad (2.3)$$

Llavona et al [14] found that industrial gibbsite (trihydrate) follows the first dehydration process.

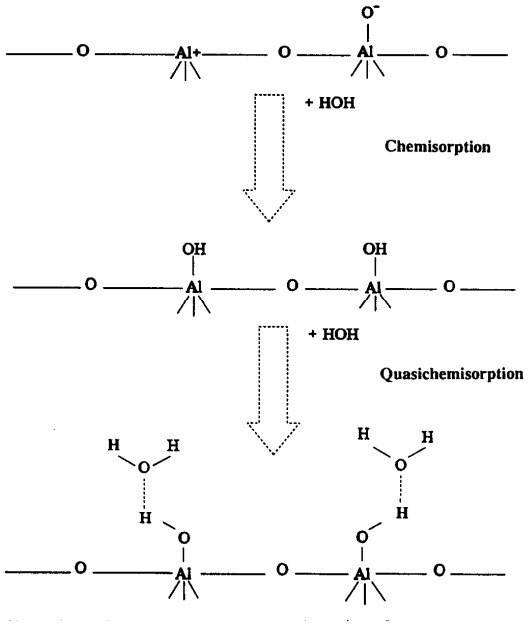

Figure 3.1 - Representation of the chemisorption of water molecules on an activated alumina site. (After [13] figure 7, pg 703).

For the *surface water* Desai et al [13] states that chemisorbed water is really the surface hydroxyl groups. The properties of these groups are determined by their co-ordination number and net electrical charge. Here the initial contact of water vapour with a surface will lead to chemisorption, involving the dissociation of the water molecule into H^+ and OH^- ions which attach to surface sites. The sites for these ions can be oxide ions on the outermost surface layer and an incompletely coordinated aluminium ion in the next layer or an exposed cation located in a hole that is electron deficient and acts as an acid site. The next layer to form is a monolayer of hydrogenly bonded water molecules covering the surface hydroxyls such that the H_2O:OH ratio is 1:2. This hydrogen bonded water is sometimes described as "*quasi-chemisorbed*". Five types of hydroxyl groups are possible [13], though only acidic hydroxyl groups will form strong hydrogen bonds with the water. An additional layer may be adsorbed on top of this hydrogen bonded layer and depending on the pore size and relative pressure, there may also be capillary condensation within the pores

[13]. This understanding is based on severely idealised models. The chemisorbed processes are summarised in figure 3.1.

Using these premises, the aluminium literature generally identifies three processes for characterising the water content of alumina. The loss to 110, 300, and 1000^{O}C is the standard system as it can differentiate moisture, adsorbed water and structural water [14]. As detailed in the properties section these are defined as the Loss On Ignition properties. In some cases L.O.I. is used as a blanket term which covers all the temperature ranges. Humidity (0-100^{O}C) measures some of the physisorbed and some chemisorbed water. MOI (110 - 300^{O}C) removes more chemisorbed and structural water associated with alumina trihydrate, and LOI (300 - 1000^{O}C) removes the strongly chemisorbed water and structural water incorporated into the transition alumina phases. LOI (300 – 1000^{O}C) is the most frequently quoted term, though its use is questionable as it represents a fraction of the water adsorbed (0.3 to 3wt% with an extra 14wt% possible) and it really only reflects the calcination conditions[1]. Moisture pick up under ambient conditions probably best corresponds with LOI (0 - 300^{O}C), although there will be some strong chemisorbed water adsorbed that may not be removed at 300^{O}C [12].

3.3.2. Adsorption studies.

Considering these mechanisms, it is not surprising that water on alumina can be gained or lost rapidly depending on the relative humidity of the surroundings. Hyland et al [12] using adsorption isotherms of hydrated alumina samples, found that pick up and loss of water is rapid, with initial rates of change in adsorbed water in excess of 0.03% per minute. Hyland [12] notes though that it takes between 1 - 3 hours after the water

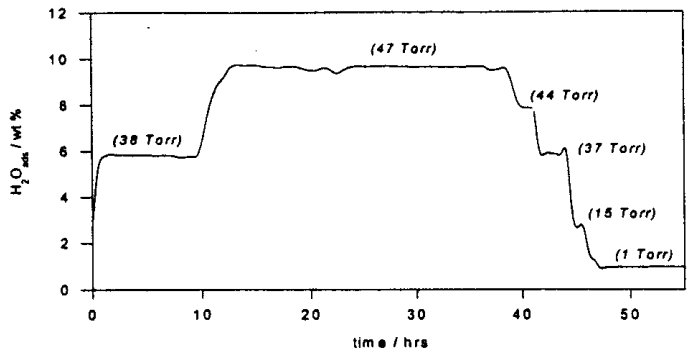

Figure 3.2 - Water adsorption on smelter grade alumina at 40^{O}C. Values in parenthesis are the water vapour pressure at equilibrium. (After [12] figure 3, pg 114).

partial pressure is changed for the new equilibrium moisture content to be reached, even if initial rates are high. Such vast changes in water content can be seen in the following diagram:

Clearly the level of water rises or falls with changes in humidity. More notably at 21^{O}C and 100% relative humidity (RH) up to 14wt% of water is adsorbed. Furthermore, as figure 3.3 illustrates at low temperatures (20^{O}C to 50^{O}C) the most important factor in adsorption is RH rather than temperature.

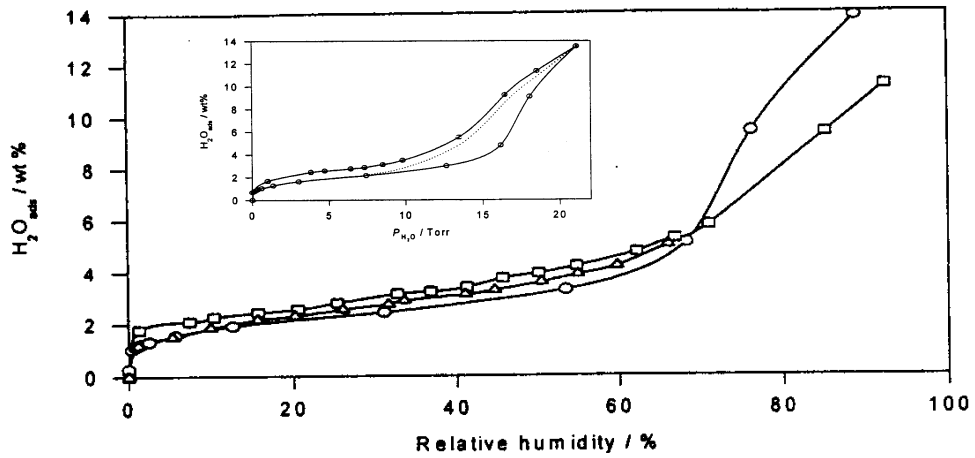

Figure 3.3- Water adsorption isotherms at 21^{O}C (circles), 40^{O}C (squares) and 50^{O}C (triangles). Insert is the 21^{O}C adsorption and desorption curves. (After [12] figure 4&5, pg 115).

Obviously unless extreme care is taken to preserve alumina under local sampling conditions, the alumina will lose or gain moisture depending on the relative humidity of the surroundings. Any insitu measurements made without precautions are unlikely to be accurate.

Both Desai et al [13] and Hyland et al [12] found alumina experiences a *hysteresis effect*. In both studies the adsorption branches sit below the desorption branches over the entire ranges of water pressures indicating that not all the water adsorbed will be desorbed on changing water partial pressures. Both studies attribute the same causes:

- At *high partial pressures* (>7.5 Torr) the large hysteresis is due to capillary condensation - i.e. a slow release of water from small pores [12] [13].

[1] Calcination conditions affects the structural water not the chemisorbed water

- At *low partial pressures* the discrepancy is due to the formation of alumina trihydrates and some strong chemisorption [12] – taken to be the irreversibly chemisorbed monolayer [13] (attributed to the irreversible formation of $Al(OH)_3$ [12]). However Hyland et al [12] found that adsorption and desorption curves, to water pressures in excess of 20 torr, indicate near complete reversibility.

To summarise: Several modes of water/alumina interactions occur for total water adsorption. These are: physisorption, capillary condensation (at high RH), chemisorption (surface hydroxyls) and chemically bound water (crystal lattice water - alumina trihydrate), the latter forms being more strongly bound than the former.

3.4. Alumina Dissolution in an Aluminium Cell.

Grjotheim and Kvande [11] provide an succinct review of the steps of dissolution process of alumina to form a homogeneous solution in the bath. On addition, the cold alumina must be heated up to the bath temperature, be transformed from gamma phase to alpha alumina, dissolve, react chemically with ions in the bath to form complex aluminium oxyfluoride species, and finally be dispersed uniformly throughout the bath. Depending on the path taken, both heat transfer and mass transfer could be rate-determining for this process. Chemical reactions, and also physical properties like dispersion and clump formation can be strongly influencing factors.

Three basic pathways may then be followed once the alumina contacts the bath:

1. It rapidly disperses as discrete grains and dissolves easily.
2. It can agglomerate as a clump and freeze bath around it, which either may float on the surface or sink as a dense crust to the surface of $Al_{(l)}$ or to the cathode surface.
3. It can sink without dispersing (this is the typical behaviour of alpha alumina).

This process can be followed experimentally. Kobbeltvedt *et al.* [15] provide a summary of the steps of alumina dissolution. The dissolution process of alumina when added as one batch on to a restricted bath surface can be divided into several stages.

Figure 3.13 shows the content of alumina in the bath as a function of the time after addition of a batch in a typical dissolution experiment. The first part of the dissolution process is represented by a stage (S1) where the dissolution rate is very high indicating a quick dissolution of dispersed alumina grains. Both measurements and calculations have shown that when the alumina is present in the bath as dispersed grains, it dissolves within approximately 10 seconds. The remainder of the batch dissolves at a remarkably slower rate because alumina agglomerates have been formed. Formation of such agglomerates substantially reduces the contact area between alumina and bath, strongly affecting the dissolution kinetics. This stage is subdivided into two stages (S2 and S3). It can be seen from figure 3.13 that the rate of dissolution changes by a factor of 8 moving from S2 to S3. This can not be explained by mass transport limitation only because the melt is so far from alumina saturation that the decrease in the driving force for mass transport is negligible. This change is more likely a reflection of a great diminution of the contact area, A. Kobbeltvedt *et al.* [15]found it reasonable to interpret this change in the contact area A as a deceleration of the agglomerate disintegration towards the end of dissolution.

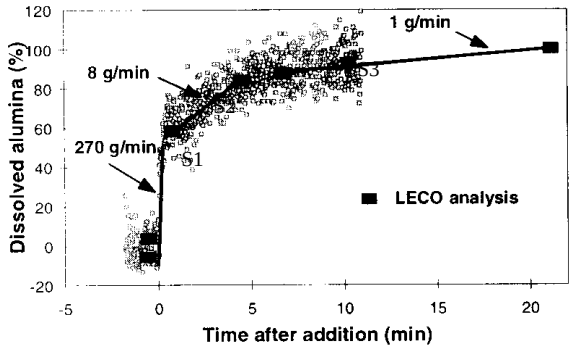

Figure 3.4 - Typical dissolution curve for batchwise feeding of alumina to a cryolite melt. (After Kobbeltvedt et al. [15] figure 2).

3.5. Variables Affecting Alumina Dissolution.

It has been previously established [11, 16, 17] that the variables that affect the rate of dissolution can be divided into two categories:

1. Operating variables (influenced by cell operation), including the bath composition.
2. Alumina powder properties (alumina quality).

Haverkamp [16] provides a useful summary of these factors:

Table 3.1 – The factors affecting alumina dissolution (After Haverkamp [16] Tables 7.27 and 7.28).

Parameter	Effect on dissolution time
Cell Conditions	
Stirring Speed	Important – faster stirring speed gives faster dissolution
Superheat	Important – higher superheat gives faster dissolution
Size of alumina addition	Larger alumina additions cause greater temperature depression with consequent slower dissolution
Electrolyte alumina concentration	Longer dissolution times are observed at high bath alumina concentrations (with some variability)
Alumina Properties	
Particle size	None observed for size fractions
Adsorbed Water	Strong effect – high MOI gives shorter dissolution times
Adsorbed HF	Small decrease in dissolution time
Adsorbed $NaAlF_4$	None with laboratory prepared samples

3.5.1. Operating Conditions.

Dissolution time decreases with increasing *electrolyte velocity* [11, 16, 17]. Most researchers agree that the electrolyte flow velocities generated in a commercial operating cell are an important factor in the dispersion and the subsequent dissolution rate of alumina in that cell. Therefore at higher electrolyte velocities greater contact between the alumina grain surfaces and the electrolyte occurs, with a minimum electrolyte freezing around the grains. Hence vigorous stirring reduces the degree of agglomeration. This effect is likely to be more important at low stirring speeds where the effect of the stirring is to avoid clumping of alumina. At higher stirrer speeds the effects would be expected to be less marked.

All this shows that the rate of *turbulent* transport in the electrolyte is of importance. Turbulence affects the supply of heat to the feeder zone, the transport of undissolved alumina away from it and the extent to which concentration gradients of undissolved alumina are present in the cell. Lui *et al.* [18] found that as turbulence increases from 0 to 0.1 m^2/s^2, the percentage of alumina feed which dissolves in the electrolyte increases from 25% to 49% of the feed mass. The proportion would probably increase even more steeply if the impact of local turbulence intensity on the rate of dissolution itself was taken into account.

Turbulence and the accompanying *bath movement* is a result of two main mechanisms:

- Bubble driven flow from the gas evolved at the anodes
- Magnetohydrodynamics – from the magnetic fluxes inherent in the cell.

All present research (for example [19, 20]) states that the bubble driven flow is more significant than magnetohydrodynamics. Chensonic *et al.* [19] found that the time to reach a steady state concentration for the gas driven flow was half that required for the electromagnetic flow (30 versus 65 minutes). Combining the two flows reduced the time to reach a steady state concentration to less than that required for either flow alone. This indicates that gas-driven is particularly important to the distribution of the feed material. They also suggested that the gas driven flow will have a much larger vertical component than a flow driven by electromagnetic forces, which are generally largest in the plane of the anode. In addition, the pulsing of the gas bubbles as they move over the face of the anode into the anode gap creates oscillations in the bath flow, which increase the level of mixing and facilitate both dissolution and distribution. It was concluded that the center aisle is the main distributor for alumina. The distance between individual anodes is not critical. Point feeders should be located at the anode gaps. This is all confirmed by Moxnes *et al.* [21] who found feeder holes could be kept open by directing the anode gas towards them.

On dissolution effects, Kobbeltvedt *et al.* [15] found that gas bubbling enhanced the dissolution rate by increasing the quantity which dissolved initially (stage 1 in figure 2.1) and an increase in the dissolution of the remainder of the batch, a turbulence effect. Chensonic *et al.* [19] showed that a larger ACD causes smaller wave heights in the ACD (more turbulence).

Clumping is also a factor determined by *alumina addition size*. The dissolution time increases with increasing alumina addition size [16, 17]. The maximum temperature drop of the electrolyte as a result of the alumina being added also increases with the size of the alumina addition. Haverkamp [16] found that the temperature drop to be directly proportional to the size of the alumina addition as would be predicted by the heat flow calculations in the absence of electrolyte freezing. With larger alumina additions the thermal effect will be greater, so that more freezing of electrolyte onto alumina is likely to occur resulting in a longer dissolution time. This could mean that the balance of the reaction control will be more towards heat transfer control rather than diffusion control.

The *bath alumina concentration* also has an effect. Increasing the initial alumina concentration in the electrolyte causes an increase in the dissolution time, though the change has been found to be slight in the low alumina concentration range. Haverkamp [16]expected this decrease because at high alumina concentrations the driving force for diffusion of the dissolved alumina, containing complex species, away from the dissolving particles is less as the concentration approaches the saturation concentration for alumina.

Superheat, has a large influence on the heat transfer rate associated with the dissolution of alumina. At low superheat, electrolyte is more likely to freeze around the added alumina and heat transfer becomes the rate controlling step. At higher superheat less electrolyte freezing will occur and a sufficient heat flux will be available for the dissolution process to proceed at a rate such that diffusion control becomes more important. Here less electrolyte freezing occurs so that the other factors such as chemical reaction or diffusion control become more important. Haverkamp [16] found for larger additions of alumina, electrolyte freezing occurs even at 15^{O}C superheat, so that a marked decrease in dissolution time is not observed with increasing superheat.

3.5.2. Alumina Properties.

Alumina properties have a marked effect on the dissolution of alumina. By far the biggest effect (and the one of interest to this project) is the effect of *alumina moisture content*. Most research show that when the both the LOI 300 and LOI 1000 are increased the dissolution of alumina rises markedly. Haverkamp [16] found the dissolution time decreased 44% (on average) by increasing the LOI 1000 from 1 to 2.5% . This is consistent with the results found by Kuschel and Welch [17]. Similar results are seen for an LOI 300 increase. To explain this effect Haverkamp [16]speculated that the rapidly evolved water may reduce the dissolution time by fragmenting the agglomerated alumina particles, resulting in better dispersion of the alumina. Lui et al. [22] found a similar effect when comparing gamma alumina dissolution with alpha alumina. They found gamma alumina shatters into fine fragments upon heating in the electrolyte. Shattering increases the interfacial area needed for chemical dissolution. Haverkamp also suggests that local agitation might be generated by the propulsion effect of the released gases, resulting in decreased dissolution time also. Both observations are the result of different moisture contents demonstrating that the alumina water has a strong influence on the dissolution rate of alumina.

Adsorbed HF and the *adsorbed bath vapour* have been found to have little effect on the dissolution rate. Haverkamp [16] found the dissolution time for the laboratory fluorinated aluminas show only a small decrease from the times for standard alumina. This decrease in the dissolution times can be attributed to the increased moisture content of the alumina which is a consequence of the fluorination procedure. The fluoride does not appear to enhance the dissolution rate even though the process of fluorination does. Similar results were found with the presence of $NaAlF_4$ on alumina. Haverkamp [16] found that $NaAlF_4$ does not lead to significantly better wetting of the alumina by the molten cryolite. Therefore, of the changes that take place to the alumina with dry scrubbing treatment, $NaAlF_4$ adsorption is not an important component in reducing the dissolution time by an enhanced wetting mechanism.

Hence it is not all that surprising that researchers [16, 17] have found on average the dissolution time decreases about 40% as a result of *dryscrubbing treatment.* The literature reviewed point to increased moisture content significantly affecting the dissolution rate. Hence it is likely that the increased moisture retention of s-alumina from, for example, the fine bath particulates result in better adsorption of water from the pot fumes, resulting in better dissolution characteristics.

4. Fluoride Emission from Aluminium Cells.

4.1. Introduction.

The importance of identifying the sources of hydrogen fluoride (HF) emissions in the aluminium smelting process has been proposed for many years. In the past there have been a limited amount of contribution studies, which have revealed a limited breadth of understanding. Henry's [2] foundation study in 1963 highlighted the major sources and approximate contributions. Grjotheim et al. [4] then published a comprehensive review of the fundamental theory and studies in 1971. Further studies in the 1970's, most notably by Wahnsiedler et al. [5] in 1978, added to this understanding. All these studies identified the main sources of generation of HF being from the moisture of the alumina, the hydrogen content of the anode and a particulate hydrolysis content. However this data and the relative contributions of these sources differ for the present smelting technology, as most of these studies were prior to the widespread introduction of dry scrubbing technology and the use of much less acidic electrolytes. Even the raw material specifications for alumina have changed significantly. Furthermore, all these past studies presented overall generation results without a detailed consideration of some of the underlying formation sources. Only a general view was taken, with some contributions overlooked, or worse ignored. The following is a summary of the literature published to date.

4.2. The composition of the fume gases.

The gaseous phase before coming into contact with air consists principally of carbon dioxide and carbon monoxide, which are formed by the consumption of carbon anodes during electrolysis [2]. The volume ratio of the two gases varies during the normal cycle of cell operation, with it decreasing when the cell temperature is abnormally high and during anode effect. However on average the carbon dioxide content of the unburnt gas is between 60 to 85%, and the balance is largely carbon monoxide. Contact of these hot gases with air at vents (cracks and open feeder holes) in the crust results in a substantial decrease in the carbon monoxide content through combustion.

Other gases are found in small amounts during normal cell operations. These include sulfur dioxide (SO_2), hydrogen sulfide (H_2S), carbonyl sulfide (COS), carbon disulphide (CS_2), silicon tetrafluoride (SiF_4), hydrogen fluoride (HF) and water vapour. During

anode effect, fluorocarbons are formed, mainly carbon tetrafluoride (CF_4) together with small amounts of hexafluoroethane (C_2F_6). Although these compounds contain a high percentage of fluoride, they do not constitute a serious material loss because the period of anode effect is relatively short and they are not formed during normal cell operation [2]. Particulate material from vaporisation and entrainment is also found in the fume, with a substantial part of the fluoride loss residing in such a particulate form. This fluoride content, inparticularily the hydrogen fluoride content, is the focus of the rest of this chapter.

4.3. Composition of Fluoride Emissions.

Typical prebake cell fluoride emission rates are 5 – 10 kg/tonneAl HF and 18 – 60 kg/tonneAl dust. The scrubber then reduces this to 0.1 to 1 kg/tonne Al HF and 0.5 to 5 kg/tonneAl dust [9] [23]. Overall fluoride emissions from most cell designs consist of typically half of a particulate form and half as a gaseous phase [8]. This is confirmed by Less and Waddington [24] who found the proportions were approximately:

Table 4.1 - The proportions of fluoride emissions from cells (After [24]).

	Percentage of total fluoride emissions	
	Prebake	Vertical Stud Söderberg
Coarse particulate	20%	1.5%
Fine particulate	35%	7.5%
HF	45%	91.0%

Therefore for prebake cells there is approximately an equal amount of particulates and gaseous fluorides. However Henry [2] found that the ratio of gaseous to particulate fluoride in reduction cell fumes varies over a range of about 0.5 to 1.3. These values were derived from the analysis of fumes which have burned in contact with air at openings in the crust. Pure unburnt fumes usually show a lower ratio of about 0.3. This imbalance is explained by hydrolysis of some of the particulates to HF. Burning of the hot gas-particulate mixture when it contacts air results in thermal hydrolysis of some of the particulate fluorides, with the formation of additional hydrogen fluoride.

In compositional terms, the *particulate phase* typically consists of carbon dust, cryolite, chiolite ($Na_5Al_3F_{14}$), aluminium fluoride, calcium fluoride, and condensed hydrocarbons. The *gaseous constituent* is mainly hydrogen fluoride although carbon tetrafluoride, di-carbon hexa-fluoride and silicon tetrafluoride have also been identified. The levels of emissions vary with the type of cell and is influenced daily by operating conditions such

as metal tapping, anode changing and setting, alumina feeding, humidity of the ambient air, bath composition and alumina properties.

However from an emissions viewpoint and due to the focus of this study only the particulate fluorides and gaseous hydrogen fluoride are of interest and will henceforth be concentrated upon.

4.4. Mechanisms of Formation of Fluoride Emissions.

The following emission breakdown will be used for the remainder of this thesis. All the individual contributors have been identified and confirmed by many past researchers [2, 4, 5, 8]. However the classifications have been defined for this thesis. Overall the total fluoride content can be identified to be formed by three processes:

1. **Particulate fluoride generation**.
   A. Entrainment of particulate materials during evolution of gases.
   B. Vaporisation from the electrolyte.
2. **Primary generation** of hydrogen fluoride by a hydrogen species reaction at the electrodes and in the electrolyte of the cell. There are three main sources:
   A. Alumina water.
   B. Hydrogen in the anodes.
   C. Dissolved water content in the electrolyte.
3. **Secondary generation** of hydrogen fluoride gases by reactions <u>not</u> in the electrolyte. This content mainly results from:
   A. Thermal hydrolysis of the particulate fluoride content.
   B. Fluoride desorbed from the surface of secondary alumina.

These major fluoride generation sources are illustrated in figure 4.1:

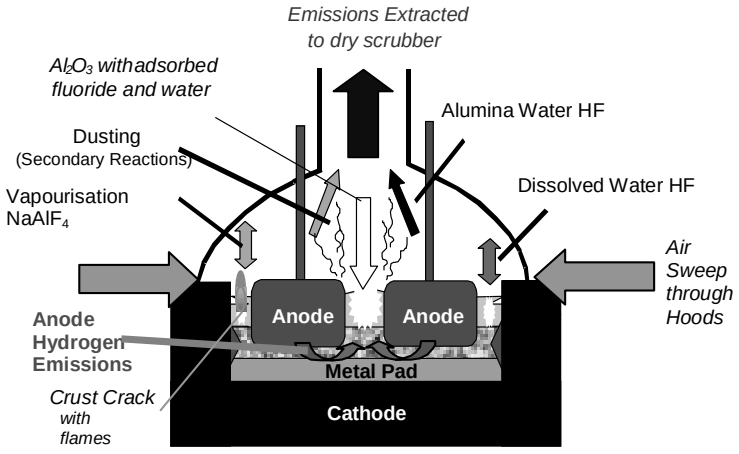

Figure 4.1 – The major fluoride emission sources from a prebake aluminium cell.

The first two sources are mainly particulate fluoride generation. This content has not been studied in this thesis. The last two are the hydrogen fluoride generation sources. Secondary generation of HF links these two contents. This is outlined in section 4.6.

4.5. Primary Generation of Hydrogen Fluoride.

Primary generation of hydrogen fluoride is electrochemical evolution of HF from within the electrolyte of an aluminium reduction cell. In essence this involves a hydrogen containing species reacting with a fluoride constituent of the bath to produce HF. The most favoured reactions explaining the formation of hydrogen fluoride by reaction at the electrodes within the cell are as follows [8]:

Table 4.2 – Potential reactions for primary HF generation.

Reaction	@ 970^{O}C*	
	ΔG (kJ)	logK
$2Na_3AlF_{6(s)} + 3H_2O \Leftrightarrow Al_2O_{3(s)} + 2NaF + 6HF_{(g)}$ (4.1)	*166.4*	*-6.99*
$Na_3AlF_{6(l)} + \frac{3}{2}H_2 \Leftrightarrow Al_{(l)} + 3NaF_{(l)} + 3HF_{(g)}$ (4.2)	454.8	-19.11
$AlF_{3(sol)} + 3H_2O \Leftrightarrow Al_2O_{3(sol)} + 6HF_{(g)}$ (4.3)	-44.8	1.88

**Results calculated using HSC thermodynamic package*

Because the equilibrium constant is over a thousand fold higher for aluminium fluoride than for any other species, *reaction 4.1* is unlikely to occur. The moisture will preferentially react with aluminium fluoride in the bath rather than cryolite or any other component [6].

However *reaction 4.2* may occur as it requires a cell potential of 1.53V compared to the normal operating potential of 1.8V. This method of HF generation is supported experimentally. When studied the observed generation and calculated emission closely correspond. Sources of hydrogen can be from the anode carbon (from baking), entrainment of water in air or alumina [8]. Depending on moisture content, part of the water in alumina will be vapourised while the alumina rests on the crust, but some of the water is more tightly bound and will follow it into the melt [4]. Note that in practice air has a limited access beneath the crust. This suggests that anode hydrogen and alumina moisture are the major contributors to primary HF formation.

Overall, the most favoured reaction is *reaction 4.3*. Here the source of water is from that content entrained in air or alumina or from electrochemical generation at the anode.

Both the equilibrium constant and free energy are favourable for this reaction to occur at cell temperatures.

4.5.1. Alumina Hydrogen Fluoride Generation.

Two major studies have been conducted investigating the emissions generated from the alumina content. It must be noted that while both studies are still used as the basis of modern models they are more than 20 years old. Hence historical technological limitations makes the results of any of these studies questionable in relation to modern smelting techniques.

Henry [2] in 1963 investigated the contributions of various hydrogen (H_2, H_2O) sources on the on the generation of gaseous fluoride emissions. He found that there was little relationship between atmospheric humidity and fluoride emissions. Here Henry introduced small samples of alumina at varying moisture contents and took gas samples before and after introduction. He found an average of 1/20 of the water content reacted to HF, irrespective of the initial water content. In other long term (4 weeks) experiments cells were fed alumina which in one test period had a water content as high as 2.0wt% and as low as 0.1 wt%. In all cases (as figure 4.2 illustrates) no significant difference in HF levels were found during these periods. The only difference found in the emission was when the alumina was preheated to 1000^{O}C. Here the average emission was reduced from 5% of the total alumina water reacting to less than 3%. This suggests that the adsorbed water does not react with the electrolyte, but is desorbed before entering the melt. Henry concluded that relatively little hydrogen fluoride could be attributed to the reaction with moisture contained in the alumina fed to the cells.

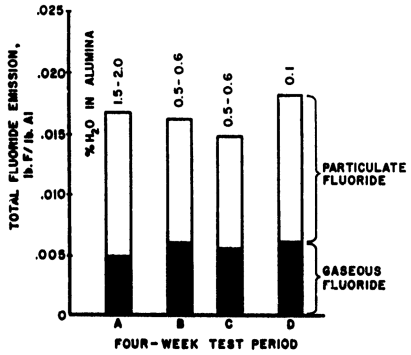

Figure 4.2 – Gaseous and particulate fluoride emissions as influenced by moisture content of the alumina. (After [2] figure 6, pg. 78).

Henrys results have caused great debate among researchers [4] because studies (for example [12]) have shown that aluminas hydration is profoundly affected by its environment relative humidity at ambient conditions. Grjotheim et al. [4] reports that as the crust temperature is in the range 400 - 600^{O}C. Hence from moisture loss curves of Bayer alumina the corresponding water content of alumina would be 0.2-0.5wt% at 600^{O}C, giving a fluoride emission of 6 to 9 kg F/ton Al if it reacted completely. This is ample to explain all the HF produced. However what Grjotheim et al. misses is that

not all the adsorbed could be added as the moisture content could be reduced to 0.1wt % or less during operations prior to emergence in the bath due to differential conditions or prior heating.

Wahnsiedler [5] presents a more realistic estimate of the contributions of primary HF formation using a 170kA prebake cell. Here factors affecting total emission where measured and a regression equation fitted for their variations.

Table 4.3 - Sources of Hydrogen converted to HF (After [5] table V and VII pg 419).

Source	Total (H)	Fraction Converted (%)	Evolution Rate (kgF/tonne Al)
Alumina Water	46 g/min	8.6	9.63
Anode Hydrogen	0.093%	8.7	0.76
Air Sweep	871 g/min	0.26	5.47

According to table 4.3, 91.4% of the alumina water and 91.3% of the anode hydrogen is not converted to HF. This agrees well with Henrys results. The 8.6% reaction efficiency suggests that not all the alumina water (adsorbed and structural) is reacted in the electrolyte and that other processes are occurring to the alumina before addition to prevent the water entering the system.

As Grjotheim et al [4] suggests the unreacted water content may be used in other generation processes also. Here a content may also be dissolved in the melt as hydroxyl ions allowing subsequent reactions to take place more slowly.

4.5.2. Hydrogen Fluoride from Dissolved Water.

Dissolved water is an undocumented but widely accepted constituent of the electrolyte. There is wide ranging evidence for its presence in the bath, the foremost being the hydrogen impurity in the electrolyte Grjotheim et al. [25]. With the modern low alpha aluminas which contain a hydrate or structural content, an equivalent water concentration is feasibly present dissolved in the electrolyte. Such *dissolved water* could undergo a hydrolysis reaction with the aluminium fluoride (or more correctly, $NaAlF_4$) constituent of the electrolyte according to equation 4.4:

$$NaAlF_{4(sol)} + 3H_2O_{(diss)} \Leftrightarrow Al_2O_{3(sol)} + 3Na_3AlF_{6(sol)} + 6HF_{(g)} \quad (4.4).$$

The only mention in the literature of this contribution comes from Grjotheim et al. review paper. Here he tries to explain Henrys seemingly erroneous results with this possible content:

> "the water content {of the alumina} is initially dissolved in the melt, and subsequent hydrolysis reactions take place more slowly. The water dissolved in the melt is most likely present as hydroxyl ions….Hydroxide and fluoride ions have a close resemblance with respect to size, charge and polarizability, and be substituted for in many compounds. Hence a certain solubility of water in the fluoride bath would not be unexpected."

This theory was never proven or disproved since its publication.

4.5.3. Hydrogen fluoride from Hydrogen in the Anodes.

Henry [2] demonstrated that the hydrogen of the anode gives rise to a significant amount of hydrogen fluoride in less acidic electrolytes. There is also undocumented but widely accepted evidence that the HF emission in Söderberg cells is higher due to this content [25]. This residual anode hydrogen content is thermodynamically fairly stable, since the anode has been baked to cell temperatures earlier. However since the anode has a potential of at least 1.5V, there are several possible oxidation reactions that this hydrogen can undergo. Grjotheim et al. [4] states that a thermodynamic calculation shows that hydrogen will not produce hydrogen fluoride by direct reaction with the electrolyte. He proposes that hydrogen may be oxidised by either CO_2 (reaction 4.5):

$$H_2(g) + CO_2(g) = H_2O(g) + CO(g);\ E^O_{1300K} = -1.361 \text{ kcal} \quad (4.5).$$

Or by electrochemical formation (reaction 4.6) - choosing aluminium as the reference electrode with $E^O=0$ - in the form of:

$$(\text{Oxide ion}) + H_2(g) = H_2O + 2e;\quad E^O_{1300K} = 1.270 \text{ V} \quad (4.6).$$
$$(\text{Oxide ion}) + C(g) = CO_2(g) + 4e;\ E^O_{1300K} = 1.155 \text{ V} \quad (4.7).$$

All these can be represented by the overall electrochemical HF formation reaction (4.8) which requires a voltage of ~ 1.28V:

$$Na_3AlF_{6(l)} + \frac{3}{2}H_2 \Leftrightarrow Al_{(l)} + 3NaF_{(l)} + 3HF_{(g)} \quad (4.8).$$

Previously Grjotheim et al. [4] suggested that the hydrogen was initially oxidised by the anode carbon dioxide to form water, and this water subsequently hydrolysed the sodium tetrafluoroaluminate to form gaseous hydrogen fluoride. However one can not distinguish between any of the proposed mechanisms, because the anode is at a potential that enables both electrochemical oxidation of the hydrogen to water and the direct formation of hydrogen fluoride. While parallel reactions can occur (resulting in a low fraction of hydrogen being converted to hydrogen fluoride) kinetically and mechanistically direct formation is a more feasible mechanism, since the concentration of the fluoride ions far exceeds those of oxide ions.

The first significant study by Henry [2] in 1963 perhaps reveals the best information on the amount of fluoride evolved from the anode. Here a 10000 ampere experimental prebake anode reduction cell was used to generate the cell gases. Three different anodes were used. A graphite anode containing 0.01 wt% H, one under-baked at 960^{O}C (0.08% H) and one baked at 1069^{O}C (0.06% H). With respect to current technology the bath composition (a much lower AlF_3 content) and alumina used were quite different, with a different alpha content and structural water. Emissions were analysed from batch samples using chemical analysis of the emission extracted from below the crust, using a purpose built vent hole. The results are summarised in table 4.4. Here the gaseous emissions increase, with a corresponding increase in the particulate emission with increasing anode hydrogen content.

Table 4.4 – Henrys anode hydrogen HF evolution results (After table VII [4]).

Type	Anode H (wt%)	Bath Ratio	Al_2O_3 (wt%)	Calc*	Temp (^{O}C)	Fluoride Emission (kg/tonne Al)		
						Gaseous	Particulate	Total
Carbon	0.06 – 0.08	1.48	4.23	4.3 – 5.7	976	3.9	15.1	19.0
Carbon	0.06 – 0.08	1.49	2.13	4.3 – 5.7	975	4.4	14.1	18.5
Graphite	0.01	1.46	3.09	0.72	971	2.0	10.4	12.4

**Calculated using equation 1 for the stated anode hydrogen contents.*

Henry concluded the anode hydrogen fluoride emission was a significant HF generation source. He did not explain his results in terms of its overall contribution or give a qualifying mechanism scheme. However Grjotheim et al. [4] noted that if the graphite generation is taken as a zero basis, then it can be calculated that hydrogen in the anode is responsible for approximately 48 to 52% of the HF emission or 10 to 12 % of the overall generation. Using the theoretical reacted amounts (in the calculated column of table I) this amounts to approximately 50% of the H in the anode reacting.

Again Wahnsiedler et al. [5] provides a useful study of the factors affecting fluoride evolution from a 170kA prebake cell. The prebaked anodes had a hydrogen content of 0.093%. Here a factors affecting total emission where measured and a regression equation fitted for their variations. Hydrogen fluoride was measured using the Alcoa gaseous fluoride analyser (a semi continuous insitu chemical analysis method) above the crust. Among the factors studied was the effect of anode hydrogen on both gaseous and total fluoride evolution. Using the regression coefficients and a few assumptions, the breakdown of the hydrogen sources generation were presented in table 4.3.

Hyland et al. [26] proposed that if equation 4.8 is used for a calculation basis then theoretically, an anode containing 0.08wt% hydrogen could generate 5.7 kg/tonne Al of HF. However the data of both Henry and Wahnsiedler disagree, showing only a fraction of this hydrogen content reacts. Neither provide a clear reason to why all this hydrogen does not react. Wahnsiedler does point out that the poor conversion could be attributed to sluggish kinetics when compared to the rate of removal by anode gas and air sweep. This does seem to support Grjotheim et al. [4] assumption that the hydrogen must first be converted to a hydroxide species before reaction.

4.6. Secondary Generation of Hydrogen Fluoride.

The *particulates* are generated via vapourisation processes from exposed electrolyte and also entrainment of particulate materials from the bath, fed alumina and crust during evolution of the gases. A significant portion of these leave with the cell gases (CO, CO_2) and burning of this hot gas-particulate mixture when it contacts air can results in thermal hydrolysis of some of the particulate fluoride with the formation of hydrogen fluoride. This source has been defined as *secondary generation* of hydrogen fluoride. This is HF generation outside the cell electrolyte.

4.6.1. Total Particulates.

The *particulate solids* produced by both vaporisation and entrainment can be divided into two fractions as illustrated by figure 4.3.

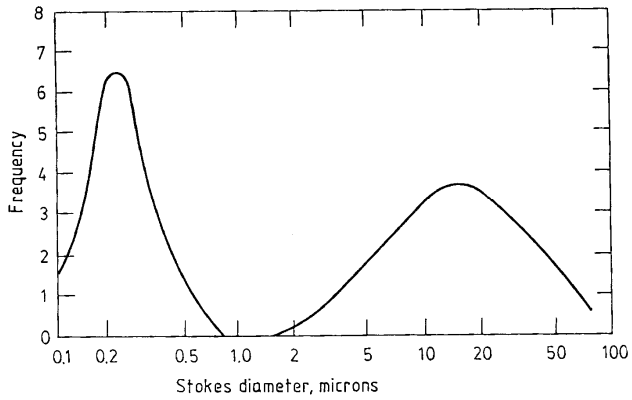

Figure 4.3 - Typical particle distribution of dust evolved form primary aluminium cells. (After [8] figure 7.4 pg. 202)

The *coarse fraction* (which typically contains 10 to 20% mass fluorine) are agglomerations as well as fluorides entrained or adsorbed on carbon dust or alumina. It principally consists of cryolite, α-alumina and carbon probably from entrained particles with little change in composition on cooling.

In contrast the *finer material* contains 30 - 40% mass fluorine. This is thought to evolve from the decomposition reaction of $NaAlF_4$. However X-ray analysis indicates the absence of the expected aluminium fluoride indicating it is likely to have been hydrolysed. The most likely reactions are the hydrolysis of aluminium fluoride containing species as shown:

$$2AlF_{3(s)} + 3H_2O_{(g)} \Leftrightarrow Al_2O_{3(s)} + 6HF_{(g)} \quad (4.9)$$

The absence of chiolite and presence of cryolite (apart from the amount entrained) in burnt gases is likely due to the following hydrolysis reaction, or that sodium teterafluoroaluminate directly hydrolyses to the incumbent products:

$$3Na_5Al_3F_{14(g)} + 6H_2O_{(g)} \Leftrightarrow 5Na_3AlF_{6(s)} + 2Al_2O_{3(s)} + 12HF_{(g)} \quad (4.10)$$

$$3NaAlF_{4(g)} + 3H_2O_{(g)} \Leftrightarrow Na_3AlF_{6(s)} + Al_2O_{3(s)} + 6HF_{(g)} \quad (4.11)$$

The amount of these particles tend to increase with decreasing electrolyte ratio (or higher levels of excess aluminium fluoride) [4].

4.6.2. Particulate Generation - Vaporisation from the electrolyte.

Vaporisation accounts for most of the particulate material evolved during cell operation. Bath appears to achieve its equilibrium partial pressure in the anode gas. Bath vapour then condenses as it cools to form particulate fluoride [6]. This is mainly due to the decomposition of $NaAlF_4$ (though Na_2AlF_5, NaF and $Na_2Al_2F_8$ contribute). Briefly tetrafluoroaluminate $NaAlF_4$ is not a stable solid, although quenching of the vapour phase produces a metastable solid phase. Normally the vapour undergoes rapid decomposition on cooling below $700^{O}C$ to two more structural solids, driven by the constant evolution of CO_2 and CO from the cell and air intake at the hoods. The main reaction proposed is as follows:

$$5NaAlF_{4(g)} \Leftrightarrow Na_5Al_3F_{14(s)} + 2AlF_{3(s)} \quad (4.12).$$

The particulate solids formed have their size further reduced via thermal hydrolysis reactions. This occurs as the fumes come in contact with oxygen and moisture from the air and layers of primary alumina through which the emissions must pass.

The vapour pressure of the electrolyte is dependant on the composition of the bath as following figure illustrates:

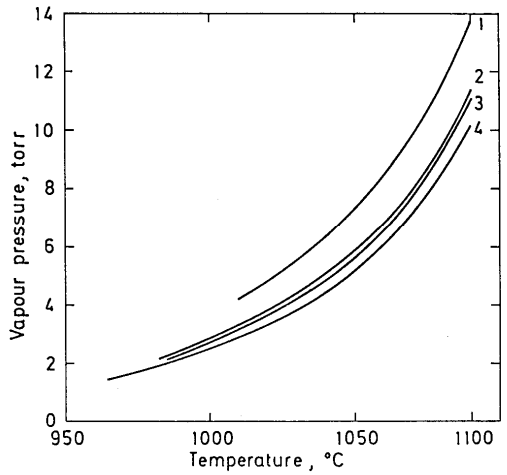

Figure 4.4 - Total Vapour pressure of the System Na_3AlF_6-Al_2O_3-CaF_2 versus temperature (compositions in Mass%). (1)100% cryolite (C). (2)90% C, 5%Al_2O_3, 5%CaF_2. (3)85% C, 5% Al_2O_3, 10% CaF_2. (4)85% C, 10% Al_2O_3, 5% CaF_2. (After [8], figure 7.2).

Obviously vaporisation can be suppressed by adding alumina and calcium fluoride or by going to higher ratios. Lithium fluoride also suppresses the vapour pressure because of

its lesser tendency to form tetrafluoroaluminate. However lowering the operating temperature is probably the most efficient way of reducing vapour pressure [8].

4.6.3. Particulate Generation - Entrained Bath.

Haupin and Kvande [6] provide a concise summary of this mechanism. When a bubble reaches the surface, its dome breaks producing tiny droplets that will be carried away if the gas velocity is sufficient. The liquid rushing in to fill the cavity formed by breaking bubble ejects a single larger droplet. Since these droplets are larger, a higher gas velocity is needed for entrainment. It has been shown that entrainment varies directly with gas velocity and the ratio (gas velocity)/(liquid density – gas density) and inversely with surface tension of the liquid. The crust acts both as a filter to remove entrained liquid and a long exit path giving more time for the entrained particles to settle out [6]. More simply, liquid bath in the pot gas freezes and becomes particulate as the gas cools.

Early measurement indicate 20 to 40% of the particulate came from [4, 24] based upon microscopic examination of the particles. However Wahnsiedler et al [5] using CaF_2 content as a trace found that only 5 to 9% of the particles were entrained bath.

4.6.4. Secondary HF Generation - Particulate Hydrolysis.

Most fluoride literature mentions the effects of hydrolysis on the total emissions fluoride content, though most past studies have found ways of side-stepping its effects. For instance Wahnsiedler et al. [5] considered only total fluoride evolution to avoid the exchange reactions, while Henry [2] simply attempted to negate the effect by sampling sufficiently close to the hot electrolyte (i.e. at the crust) so that he could assume little hydrolysis took place. However Wahnsiedler et al. [5] did express this hydrolysis content in his work, mistakenly identified as direct air primary generation (refer to table 4.5). Given that most cells (even in 1978) operated with some form of crust and that the electrolyte constantly emits a vapour and reaction gas, this 19% generation fraction (4.7 g/min of a total evolution of 13.69 g/min F) is more likely from vapour hydrolysis than direct electrolyte primary HF generation. The earliest concerted attempt at incorporating the hydrolysis content into a study was presented by Haupin [27] in his 1984 fluoride evolution model. As with the later and greater 1993 model [6] it predicts the hydrolysis content using a factor based on experimental data.

However Henry [2] proposes that hydrolysis does not occur to any significant degree in the duct nor above the crust in the superstructure because the temperature of the moisture containing air is not high enough. Instead he noted that "thermal hydrolysis or reaction of solid or vaporised fluorides with water vapour at elevated temperatures takes place primarily at the point where the hot gases escape through vents in the crust". Henry compared gases sampled under the crust and just above the crust after vent-burn. He found significantly different HF contents, with a large increase in HF from 23% to 33-57% above the crust. Similarly, Less and Waddington [24] found that while investigating the size distribution and chemical composition of dust in cell emissions before and after the CO conversion to CO_2 at the crust (or vent burning), found that the proportion of the total fluoride content present as hydrogen fluoride in Soderberg cell gas doubled from 45% in the unburnt fumes to 91% once the emissions was burnt. As with Henrys findings, it all provides evidence that hydrolysis occurs during vent burning.

Greenwood [28] also suggest that secondary emission is a function of the liquid electrolyte area accessible to air and the volume of gas drawn out of the cell. He also suggests that the hydrogen fluoride emission is also partially dependant on the cell air flow as the air contains moisture which can react with the vapours. Basically the crust condition of the cell and the amount of air inflow through the cell play an important role in fluoride evolution.

As for lower temperature hydrolysis, Heiberg et al. [29] and in 1999 found that there were minor emissions in his experimental range (70^{O}C to 170^{O}C) but these emissions (0.8 mg/Nm^3 at 130^{O}C) are not significant in the generation order of magnitude (10 to 200 mg/Nm^3). Here dust particulates collected at an aluminium smelter were exposed to hot, humid air in laboratory controlled conditions. The HF concentration was measured in the exit gas at frequent intervals over a period of several hours. Both pure fume dust and a mixture of alumina and fume dust was tested. With gas temperature and humidity kept at relevant levels a noticeable HF emission (referred to as chemical HF emission) was detected. They concluded that particulate fluorides may be a significant source of HF in clean gas and that the humidity was a more significant factor in the emission than ambient temperature. Figure 4.5 shows the results of one of the tests of the fume dust and mixed dust at 20g water/kg dry air and 100^{O}C.

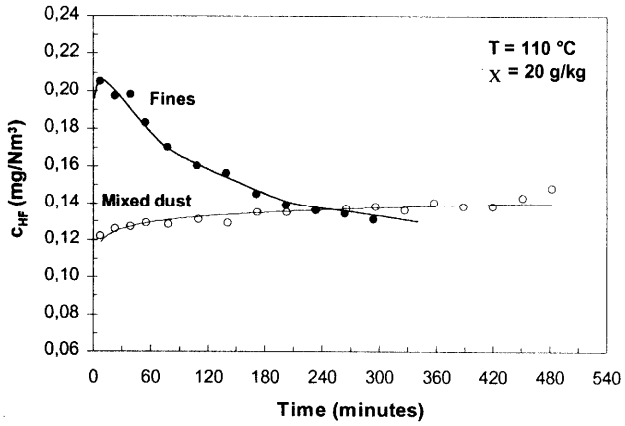

Figure 4.5 - Emission of HF from mixed dust (filter cake) and fines at T=110^{O}C, X=20g/kg. (After [29] figure 1).

The fines have a gradual decrease in HF emission due to a steady decline in the concentration of reactive fluorides in the dust. In the mixed dust the concentration stays constant, indicating the depletion of reactive fluorides is insignificant in this case and also indicating that reactive fluorides are not the only source of fluorides. The additional fluorides were thought to be the result of agglomerated fume. In one mixed sample it was estimated that the agglomerated fume contained up to seven times as much fluoride as the fine fraction.

Further runs were made on filter bag alumina to find this products emission potential at various humidities and temperatures. The results are summarised in figure 4.6:

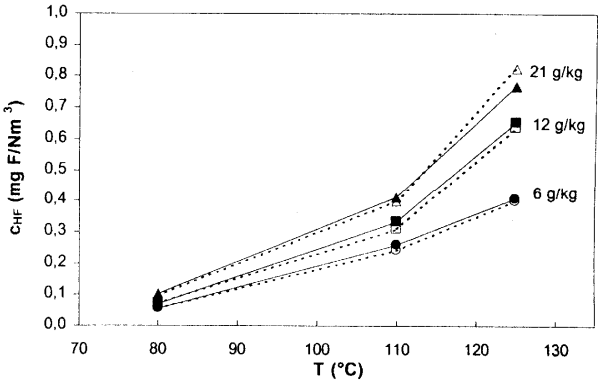

Figure 4.6 - HF emission from filter bags. Effect of temperature at different humidities levels. Dashed lines represent calculated concentrations. (After[29] figure 2).

The figure shows that HF emissions increase exponentially with temperature. The emission also rises with increased humidity. They did however note that the filter bags under investigation had been exposed to temperatures in the middle to low range only. The amount of "intact" reactive fluorides in the filter dust at the time the bags were

removed from the scrubber therefore may have been too high in relation to the high-temperature situation leading to increased emission.

Wahnsiedler et al [5] presented more realistic plant data. Here the emission was measured for variations in among other factors, changes in air humidity. Hence for the cell parameters in table 4.5 the following contributions can be predicted:

Table 4.5 - Average raw material requirements for P155A cell studied (After [5] table IV).

Parameter	Value
Current	170 kA
Alumina	1640 g/min
Anode Carbon	435 g/min
Air Sweep	85 m^3/min at 30^oC
Alumina (LOI + Moisture)	2.8%
Alumina Water	46g/min F equivalent 97 g/min
Anode Hydrogen content	0.093%
Anode Hydrogen as Water	3.6 g/min F equivalent 7.6 g/min
Pressure of water in air	1.41 kPa
Weight of air sweep	98.8 kg/min
Weight of water in air sweep	871 g/min F equivalent 1839 g/min
Anode gas volume produced	2.47 m^3/min at 950^oC, 0.6 m^3/min at 25^oC

From this the following can be gauged:

Table 4.6 - Sources of HF (After [5] table VII, pg 419).

Mechanism No.	Source	Evolution Rate (gF/min)	Fraction (%)
1	Vaporisation	10.00	41
2	Bath Entrainment	0.6	2.5
3a	Alumina Hydrolysis	8.3	34
3b	Anode Hydrolysis	0.7	2.9
3c	Air Hydrolysis	4.7	19

It can be calculated that $NaAlF_4$ is vaporised at a rate of 9.25 g/min, equivalent to 5.58 g F/min in saturated anode gas. This is a difference of 4.42 g F/min from the measured 10 gF/min. The difference is likely to be connected with the amount of direct contact between air and the sweep bath. At any rate, the air hydrolysis content was found to be a significant emission contributor, being the third most important HF generation source for this particular cell technology (which includes alumina analysis, crust cover and cell heat balance).

Overall the thermal hydrolysis content has been identified as a potentially significant emission contributor.

4.6.5. Secondary HF Generation - Desorbed Fluoride.

Essentially the dry scrubbing system in a smelter is a closed fluoride cycle, with the captured fluoride emissions being fed back to the cell via the secondary alumina. Only a minor amount of additional fluoride required to maintain the mass balance. However within this system there is the potential for this *adsorbed* fluoride being desorbed during the feeding procedures due to the high temperatures it experiences. It has been suggested [30] that if significant amounts are lost then a fluoride recycle load within the extraction system may occur. Past studies into the heating of this surface fluoride content [16, 31, 32] have shown that given the correct conditions, the surface fluoride may be desorbed off the reacted alumina.

Fluoride Adsorption.

In the last 30 years the adsorption of Hydrogen Fluoride onto alumina has been the focus of numerous laboratory and in plant studies. The following reaction scheme has been used to describe the process:

$$nHF_{(g)} + Al_2O_3 \rightarrow Al_2O_3 \cdot nHF_{(ads)} \qquad (4.13)$$

$$\frac{6}{n} Al_2O_3 \cdot nHF_{(ads)} \xrightarrow{HEAT} 2AlF_3 + 3H_2O + \frac{6-n}{n} Al_2O_3 \qquad (4.14)$$

It is now recognised that the process is nowhere as simple as is represented by these equations [8]. Gillespie [31] proposes that rather than the HF being adsorbed on the alumina surface as all the previous studies fundamentally assumed, it undergoes an irreversible reaction (i.e. in dry scrubber conditions adsorption of HF is independent of the partial pressure of gaseous HF) aided by water to bind the reacted fluoride on the surface. Moreover he showed that adsorption capacity was proportional to specific surface area and adsorption humidity. Both factors indicate that HF adsorption is a surface process.

From that study [31, 33] it was found that the most likely product of the reaction is a thin layer of structural aluminium hydroxyfluoride, $AlF_x(OH)_{3-x}.6H_2O$, formed in an aqueous reaction at the alumina surface. Two mechanisms where prevalent at low

relative humidities - below 35% termed RH_{low} and at higher relative humidities - above 35% or Rh_{high}. The effects of water vapour is dramatic as illustrated by figure 4.7.

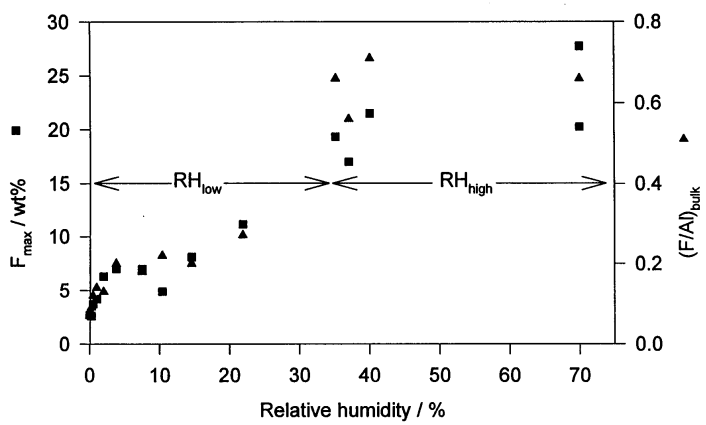

Figure 4.7 - The adsorption capacity of smelter grade alumina versus relative humidity in the range 0 to 70%. (After [31] figure 5.3, pg 64).

The change between RH_{low} and RH_{high} is dramatic as would be expected due to the two mechanisms. Under RH_{low} conditions the relationship between adsorption capacity and humidity is similar to that of reversible water adsorption as found by Lamb [34] also.

(A). RH_{low} Mechanism.

Here the maximum HF capacity of the alumina is dependant on the partial pressure of water, specifically the relative humidity of the reaction zone. This is indicative of an adsorption mechanism in which the reversible adsorption of water is an important step in product formation.

Under these conditions it is postulated that *structural aluminium hydroxyfluoride*, $AlF_x(OH)_{3-x}.6H_2O$ is formed in a thin layer not anhydrous AlF_3 as predicted by thermodynamics. This appears amorphous to x-ray powder diffraction and can not be detected. The adsorption capacity was found to be similar to aluminium hydroxide, aluminium oxide hydroxide, transition alumina and α-alumina at 0.4 - 1.7 mg/m^2. Similar reactivity suggests similar surfaces.

The reaction mechanism proposed involves the following steps:

1. H_2O adsorption to form an aqueous layer on the aluminium surface, whose thickness is determined by the relative humidity;

2. Sodium species which are present on the alumina surface may be released into the aqueous layer, causing the local pH to increase and the alumina surface to dissolve as AlO_2^- or $Al(OH)_4^-$ ions.
3. As HF is adsorbed acidifying the surface water layer, a small amount of $Al(OH)_3$ precipitates;
4. HF adsorption continues reducing the pH below neutrality. Dissolution of the alumina surface to form AlO_2^- and AlO^{2-} occurs;
5. Reaction of AlO_2^- and AlO^{2-} with fluoride ions to be precipitated as $AlF_x(OH)_{3-x}.6H_2O$.
6. The water layer constantly reequilibriates to replace water which is incorporated in to the $AlF_x(OH)_{3-x}$ lattice. Eventually the water layer becomes saturated with reaction product and the reaction stops.

As the relative humidity is increased, the quantity of reaction product which is required in order to saturate the aqueous layers increases, and therefore the ultimate fluoride capacity increases.

The overall adsorption rate appears to be controlled by the rate of reaction of the surface chemicals rather than transport phenomena such as fluid phase mass transfer and intraparticle diffusion.

(B). RH_{high} Mechanism.

At relative humidities greater than 35% the adsorption capacity of smelter grade alumina increases dramatically and small crystallites of $AlF_x(OH)_{3-x}.6H_2O$ and $AlF_3.3H_2O$ are formed. Here the average adsorption capacity of smelter grade alumina was 3.6 mg/m^2 and was independent of relative humidity.

Under these conditions the reaction mechanism is similar, except that water-filled pores provide an environment which is conducive to the formation of larger crystallites of product. Basically:

1. Due to capillary condensation effects, water condenses rapidly within the pores of the alumina to form aqueous pools.
2. Adsorption of HF into aqueous pools results in dissolution of the alumina surface and precipitation of fluoride bearing solid phases in a similar manner to RH_{low} adsorption.

3. The water filled pores provide significantly larger volume within than in RH_{low} , in which the dissolved species are less restricted and therefore more able to form distinct crystallites.

(C). Ageing.

Gillespie [31] found that samples produced under dryscrubbing conditions and aged under ambient conditions are indefinitely stable. However when aged at high humidity the product layer is transformed into distinct crystallites of aluminium hydroxyfluoride by a dissolution/re-precipitation mechanism involving water filled pores. Samples which are hydrofluorinated at greater than 35% humidity show continued growth of $AlF_x(OH)_{3-x}.6H_2O$ and $AlF_3.3H_2O$ under all storage conditions due to residual water condensed within the alumina pores.

Fluoride Loss Mechanisms.

Gillespie [31] indicates two mechanisms of dehydration and HF evolution for the surface products in his two regimes.

The RH_{low} regime:

Here the aluminium hydrofluoride hydrate phase dehydrates at temperatures below 450^{O}C. At temperatures above 450^{O}C hydrolysis of aluminium hydroxyfluoride results in the release of HF. Here as the temperature is increased, desorption of H_2O and HF occurred in distinct events due to $AlF_x(OH)_{3-x}.3H_2O$ dehydration and hydrolysis of $AlF_x(OH)_{3-x}$. The average enthalpy of desorption was approximately 45.0 kJ. This can be seen in the following diagram:

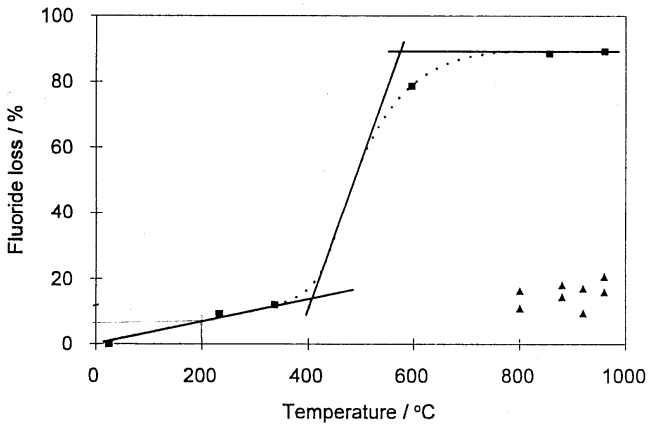

Figure 4.8 - Fluoride loss vs temperature for shock (triangles) and static (squares) heating of RH_{low} alumina. Initial fluoride content 7.13%, static heating time 125 minutes.

(After [31] figure 6.7, pg 100).

The RH_{high} regime:

Here the two reaction products under go the following reactions on heating:

- $AlF_x(OH)_{3-x}.6H_2O$ dehydrated at less than 120^OC and decomposed above 195^OC
- $AlF_3.3H_2O$ (stable at 70^OC) dehydrated to amorphous AlF_3 below 100^OC and probably transformed to β-AlF_3 above 300^OC.

This is supported by the results of Hyland et al [35] and Gillespie [31] heating investigations. The results of these are presented below. Note that Gillespies results have been extrapolated from the data of a 7% fluoride content sample dehydrated in RH_{low} conditions. The sodium content is unknown.

Table 4.7 - XPS surface atomic compositions (After [35] table 2, pg 1326).

Temperature, Time	Na:F:Al	% F loss	
		Hyland [35]	Gillespie [31]
Laboratory HF/Al_2O_3			
Unheated	0.06 : 0.72 : 1		
200°C, 3h	0.09 : 0.73 : 1	0	6
500°C, 1h	0.07 : 0.48 : 1	33	60
700°C, 1h	0.08 : 0.20 : 1	72	90
Dry Scrubber HF/Al_2O_3			
Unheated	0.36 : 0.90 : 1		
200°C, 3h	0.31 : 0.75 : 1	18	---
500°C, 1h	0.20 : 0.29 : 1	68	---
700°C, 1h	0.16 : 0.17 : 1	82	---

The heating profile for dry-scrubber alumina differs from that of its laboratory prepared counterpart in Hylands study, as more fluorine is lost at lower temperature. Gillespies results show some resemblance. This difference may be accounted for by the increased sodium content present in the dry scrubber sample and the dissociation of this Na-F bond. Figure 4.9 compares the dry scrubber unheated and heated to 700^OC samples.

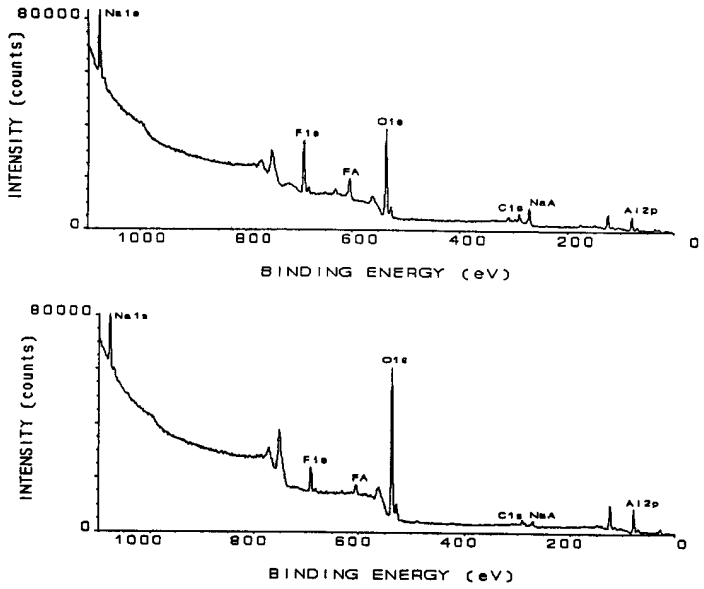

Figure 4.9 -XPS wide scans of dry scrubber alumina (a) Unheated. (b)Heated to 700^{O}C. (After [35], figure 1, pg 1324)

Clearly less than 20% of the original F remains. However without knowledge of the adsorption humidities little else quantitative can be determined from the study. Further studies require stricter control and recording of all parameters. However considering that crust temperatures are around 500 - 600^{O}C it can be concluded (as Hyland et al [35] did) that most of the adsorbed fluorides will simply be released when the secondary alumina is added to the reduction pot. The exact mechanism of return is not known or whether much of this in fact is recycled back to the extraction system. However Salt [36] states that plant evidence suggests that some product must be reacted, as the AlF_3 content added is reduced by 14 to 15% (not as great as the 99% reacted alumina recycle suggests). This is indicated in figure 4.10. This is further confirmed by Cochran *et al.* [3] study which found that only a minor amount of fluoride was lost (<20% of the surface F, attributed to a physisorbed layer) with the remainder (said to be in the form of a chemisorbed layer) forming AlF_3 upon heating. A thermograph of heating the products quite clearly shows these results:

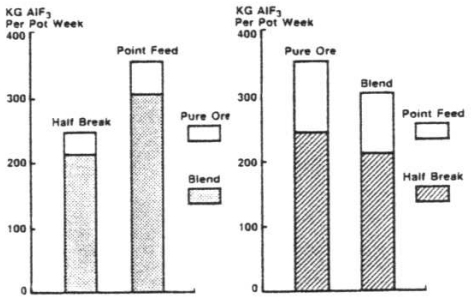

Figure 4.10 - Aluminium Fluoride usage by feed type. (After [36], figure 5 pg 301).

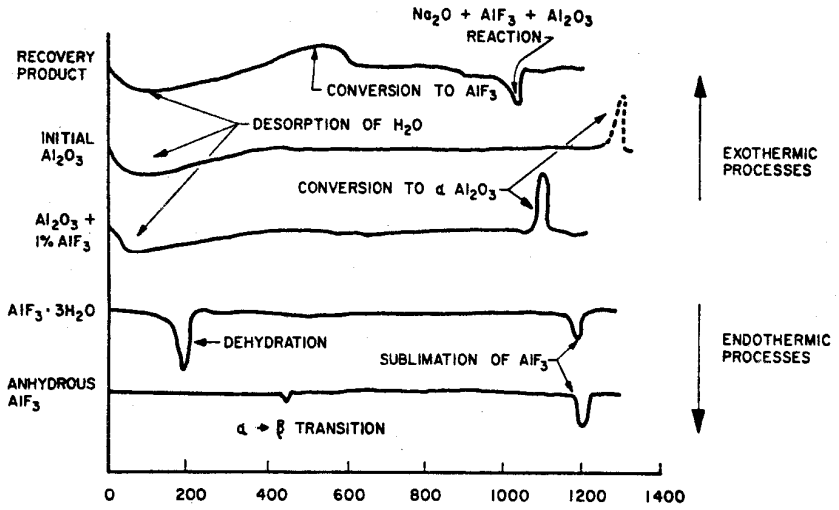

Figure 4.11 – Thermographs for Al_2O_3 recovery products and possible recovery compounds. (After [3] figure 1, pg 56).

Clearly two distinct results have been found in past studies.

4.7. Combined Contribution Effects.

4.7.1. Electrolyte Compositional Effects.

There is a clear dependence between *emission rate* and *electrolyte temperature* as shown by Franke et al [37] in figure 4.12. Here a reduction of 20^{O}C (975 to 955^{O}C) results in a reduction of 4 kgF/tonne Al (7.6 to 3.6 kgF/tonne Al).

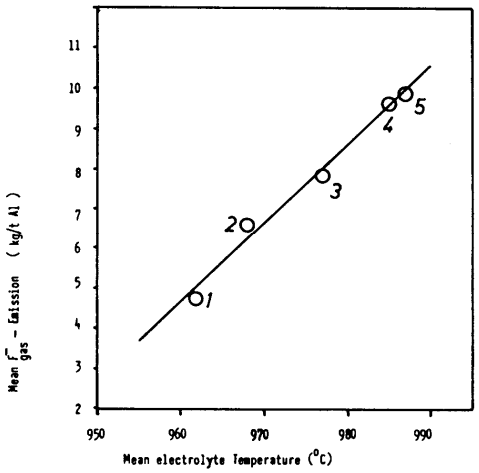

Figure 4.12 - The temperature dependence of the fluoride emission. (After [37], figure 1, pg 370).

However the compositional and temperature factors were not separated by the investigator, hence the compositional contributions to this emission reduction can not be ascertained (the liquidus temperature being reduced by changing the amounts of additives in the electrolyte). This illustrates the inter-relationship of the effects. Other studies have been more successful in decoupling the factors however.

Henry [2] presents the first detailed study into understanding the separate factors affecting fluoride emission from Aluminium cells. Note that here the fluoride content is considered as the total content, with no differentiation between the particulate and gaseous components. The major conclusion he found was that the primary factors are cell temperature, bath ratio and alumina concentration on the emission rate. The fluoride emission is increased by increased temperature, decreased bath ratio, and decreased alumina concentration. The relationships found are illustrated in the following figure:

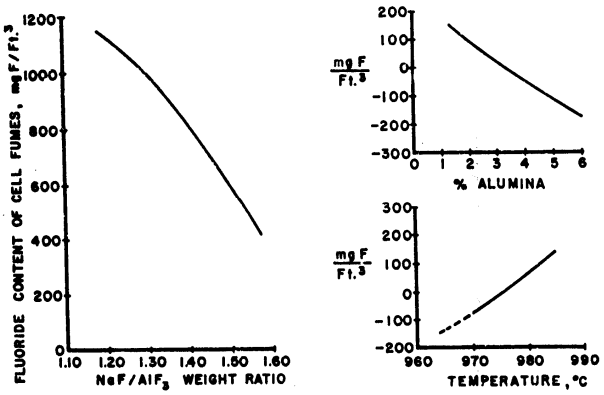

Figure 4.13 - The Relationships found by Henry [2] for (1)Bath Ratio. (2)Alumina Content. (3)Temperature. (After [2] figure 1 pg 73).

Volatility (weight loss) measurements of pure cryolite and mixed alumina bath show good agreement with the experimental cell emissions.

He however notes that the large number of variables in aluminium cell operation make it difficult to establish with a high degree of certainty the correlation of operating factors with fluoride emission. This difficulty exists even with small-scale experimental reduction cells operated by research personnel.

Wahnsiedler et al [5] produced an interesting comparison of studies into the correlations for fluoride emissions derived up to 1978. Average curves for fluoride emissions from Solntsev and Henry [37] are shown with the data from that study [5] for different bath ratios at a fixed superheat ($15^{O}C$). Extrapolations had been made for a direct comparison.

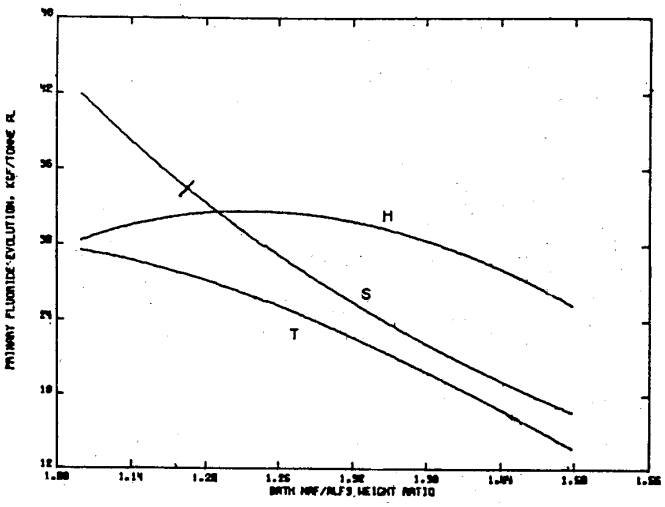

Figure 4.14 - Fluoride evolution predictions vs bath ratio for a 15^{O}C superheat. S= Solntsev, H =Henry, T= Wahnsiedler. (After [5], figure 1, pg 409).

As shown there are significant differences between all the curves in the areas of the amount of particulate fluoride generation, overall evolution level, amount of entrainment, and influence of bath ratio, bath temperature, and hydrogen source on evolution. It is increasingly evident that disparity in the results is not that uncommon in the in the fluoride adsorption-generation area. Given the age of the studies, the results are once again questionable in relation to modern smelting techniques and technology.

Lid et al [7] also presents such correlations for a primary alumina fed, point feed prebake, 230kA cell. His results (figure 4.15) follow the trends established by the researchers discussed above.

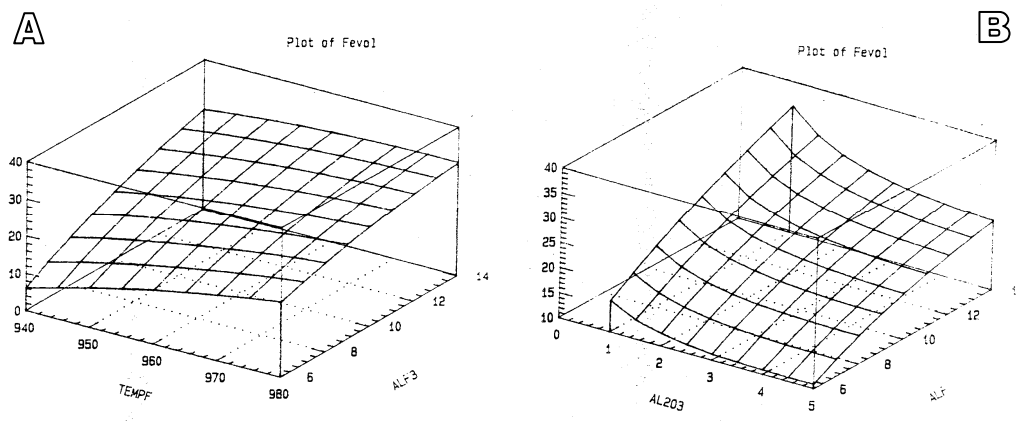

Figure 4.15 – Lid et al[7] total fluoride evolution results. (A)Variations in F with cell temperature and AlF_3 concentration. (B)Variation in F evolution with Al_2O_3 and AlF_3 concentration.

Overall from all these studies it can be concluded that decreasing the electrolyte temperature, AlF_3 concentration and/or increasing the Al_2O_3 concentration will reduce the overall fluoride emission. However the extent of this emission reduction is

technology dependant, with crusting practices, raw material specifications and cell condition influencing the overall emitted fluoride generation.

4.7.2. Modelling Combined Contribution Effects.

Haupin and Kvande [6] present a much more applied study of the factors affecting the overall emission using a predictive model. The most reliable model is based updating the modelling work of Haupin [27] with further research and greater detail of the separate particulate and HF generation processes. Again this resulted in different results to past studies. However this derived model agrees well with current plant measurements (circa 2000). Quite simply, unlike the data presented above, the fluoride measurements that this model is based on is similar to the current smelting technology.

The model is quite versatile. Factors accounted for in the model were volatisation of the bath, entrained bath, primary formation of HF, hydrolysis in the fume, activities of alumina and aluminium fluoride. The model only predicts fluoride emission for normal equilibrium cell conditions with good ore coverage though. As Welch [8] and Wahnsiedler [5] both show, normal cell operations such as feeding, anode change, tapping and anode effects will affect the fluoride emission, no provision for this has been made. The best advice was to use the Wahnsiedler correlation (eq. 4.16).

For explicit details on the model refer to [6]. The model predicts the following parameters for a constant superheat a flat maximum at a bath ratio of 1.07. With the inclusion of the hydrolysis of the bath the following relations can be found for emissions.

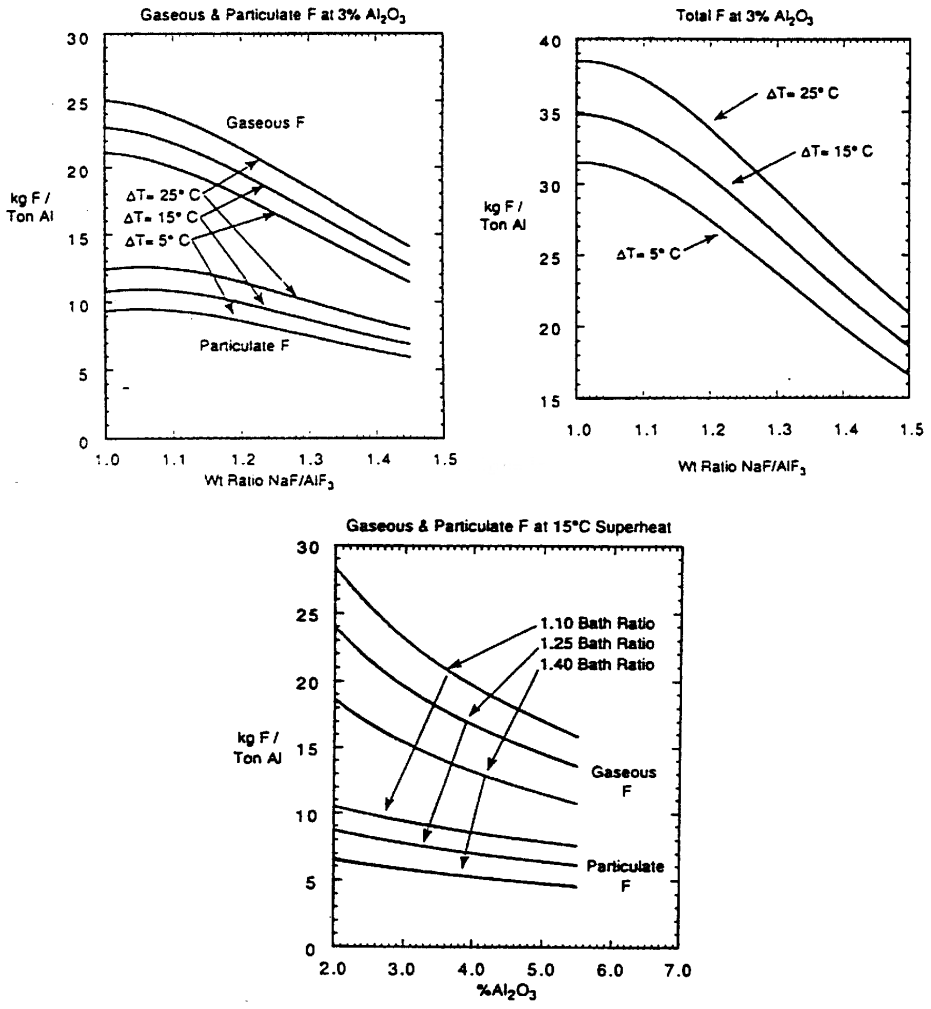

Figure 4.16 - The relations found by Haupin and Kvande.
(1)Total Fluoride vs bath ratio. (2)Particulate and gaseous emissions vs bath ratio.
(3)Gaseous and particulate emissions vs alumina content.
(After [6] figures 1a, 1b, 2, pg 8-40).

4.7.3. Correlations for Fluoride Emissions.

Solntsev [4] presents an empirical relationship for the *total fluoride evolution* (W in kg F/ton aluminium produced) from an aluminium cell. He assumed the majority of the total fluoride emission results from vaporisation and primary generation, ignoring the entrainment mechanism. The correlation derived is:

$$W = \frac{279}{(CR)^2} + 0.047T_b - 61 \quad (4.15)$$

Where:

CR is the molar ratio of NaF to AlF_3
T_b is the cell temperature in degrees Celsius.

Note, this correlation is a non-condition specific derivation and will not account for cell dynamics or variations in separate mechanisms. For any detail a more rigorous method should be used.

To obtain a more accurate account of the mechanisms contributions, Wahnsiedler et al [5] in 1978 conducted a plant study measuring the predicted factors affecting fluoride emission on two smelting cells over a nine month period. The fluoride values were correlated with measured ambient air conditions, bath composition, alumina LOI(300) and LOI (1000), anode hydrogen content, bath temperature, and unusual events (anode effects and tracking - feeding amount changes), and additions of hydrogen fluoride by hand. It was found ambient air had little effect on evolution so was not included in the analysis.

From this the following equations (4.16) was derived for specific evolution in a cell:

$$F = -158.5 - 54W + 0.244T_b + 3.77p_{H2O} + 3.62AW - 1.29BA + 0.35CF + 13.5AE - 2.6TR + 3.79AF + 9.64HC \quad (4.16)$$

F = Total primary fluoride evolution (kg/tonne Al)
W = Bath weight ratio.
T_b = Bath Temperature (^{O}C).
P_{H2O} = Ambient partial pressure of water (kPa).
AW= Alumina water content (%).
BA = Bath Alumina content (%).
CF = Bath calcium fluoride content (%).
AE = Anode effect – 1 if present, 0 if not.
TR = Track – 1 if present, 0 if not.
AF = Hand fluoride addition.
HC = Average hydrogen content of the anodes (%).

This is only an approximation, since the duration of each event as well as its frequency must be important [6].

5. Primary Generation of Hydrogen Fluoride.

Primary generation of hydrogen fluoride is electrochemical evolution of HF from within the electrolyte of an aluminium reduction cell. In essence this involves a hydrogen containing species reacting with a fluoride constituent of the bath to produce HF. There are three identified sources of hydrogen for primary HF generation:

- from a hydrogen content of the anode,
- from a dissolved water species in the bath,
- from water associated with the fed alumina.

However the applied anodic potential is sufficient for several concurrent reactions to occur. It is the aim of this section to measure the extent that this HF is produced from each source and from that make generalisations on the exact mechanism of primary generation.

The following experimental chapters detail both laboratory studies and industrial data which were conducted to achieve this overall aim. Whilst laboratory experiments and simulations are useful in understanding selected reactions, studies of operating aluminium smelting cells have shown that the former approach has limitations due to the complexity of the situation. However a comparison of real industry data and controlled laboratory experiments can lead to a more consistent view of the generation process. Hence this study has contained both situations, with the controlled idealistic data gathered in the laboratory compared to the real situation measured in industry.

Trials in industry were conducted on three different cell technologies. All cells are hooded center point fed prebake cells with a cell voltage around 4.10 to 4.20V. The alumina feeding system are different for cell technology I and technologies II and III. Apart from aluminium production, cell technology II and III are similar and hence share similar emission characteristics. The comparative details are listed in table 5.1:

Table 5.1 – Comparing the three studied cell technologies.

Property	Cell Technology I	Cell Technology II	Cell Technology III
Orientation	Side by Side	End on End	End on End
Production (tonne Al/day)	1.3	2	1.5
Line Current (kA)	171	265	205
Number of Anodes	18	26	20
Number of Feeder Holes	3	4	4
Duct Flow Rate (Nm^3/h)	6500	10000	6000

5.1. Hydrogen in the Anode.

Of all the sources investigated by past researchers, the influence of the residual hydrogen content of prebaked carbon anodes is one of the least understood. As the literature review showed (section 4.5.2), only limited studies have been made into the effect of this content on the total emissions. Of the studies of consequence [2, 5] the conclusions on the exact amount that reacts differ significantly. This study aimed to clarify this inconsistency. It also aims to address some of the questions raised about the significance of this source, and how it affects the overall emissions reduction scheme of an aluminium smelter.

5.1.1. Experimental Methodology.

Laboratory studies of the anode HF generation potential were performed using a laboratory scale electrolysis cell. A FTIR spectrometer was used to monitor the hydrogen fluoride emissions generated from electrolysis (refer to figure 5.1). The IR adsorption peak at 4073.9 cm^{-1} was monitored. For the trials, the cell with bath composition 10% excess AlF_3, 5% CaF_2 and 3% or greater alumina was heated to 962^{O}C. The flow rate of the nitrogen cover gas was monitored to gauge the duct gas

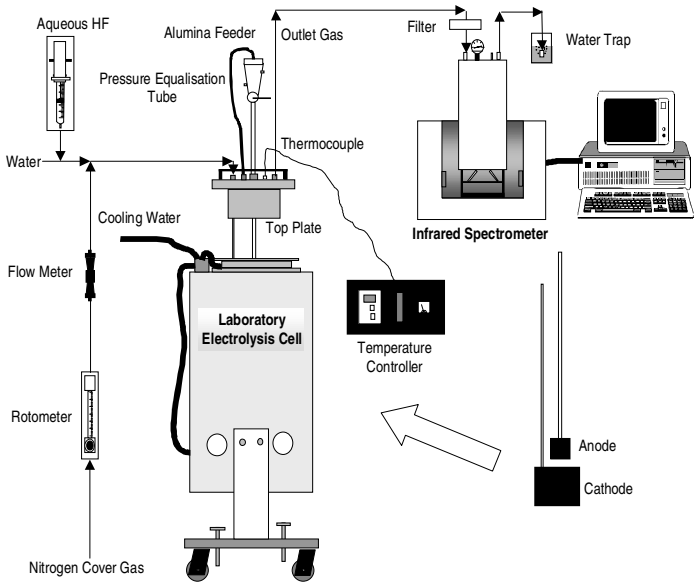

Figure 5.1 - The experimental laboratory apparatus.

velocity.

Three different anodes were used in electrolysis (0.8 A/cm^2 current density):

- Low hydrogen anode – baked at 1200^{O}C
- High hydrogen anode – baked at 900^{O}C
- Graphite anode

The hydrogen content of each anode is presented in table 5.2:

Table 5.2 - Anode hydrogen contents.

Anode	Bake Temp (^{O}C)	Hydrogen Content (%)
High Hydrogen	900	0.094
Low Hydrogen	1200	0.042
Graphite	---	0.003

Over the trial period 10 g of alumina was fed per hour to replenish the alumina content of the bath. Alpha alumina was fed for the first two cycles, followed by a single feed of smelter grade alumina. All responses were recorded.

5.1.2. FTIR Calibration.

The signal intensity response from the FTIR was calibrated against standard fluoride solution concentrations injected into the inlet gas stream. The resulting calibration curve (figure 5.2) is the combined results of several runs. Due to the water content of the dilute solutions exact results have a large margin of error (±30% at best). This makes the calibrated results more qualitative rather than quantitative. Hence all results will be presented in the raw signal intensity format, with the significant results converted using this calibration.

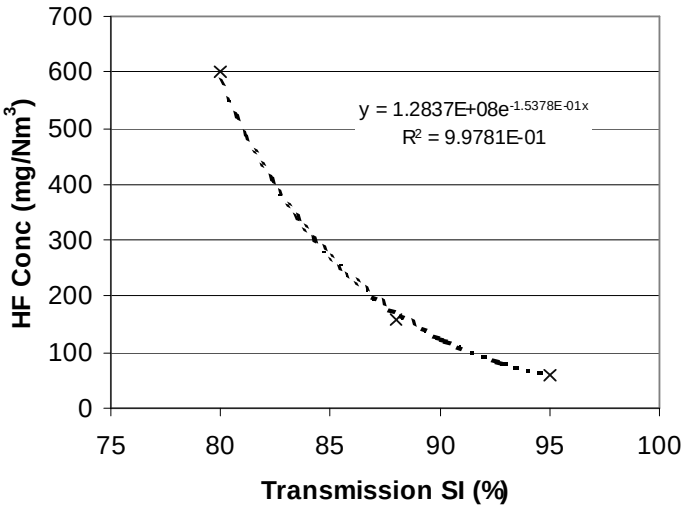

Figure 5.2 – The calibration curve for the FTIR fluoride signal intensity peaks.

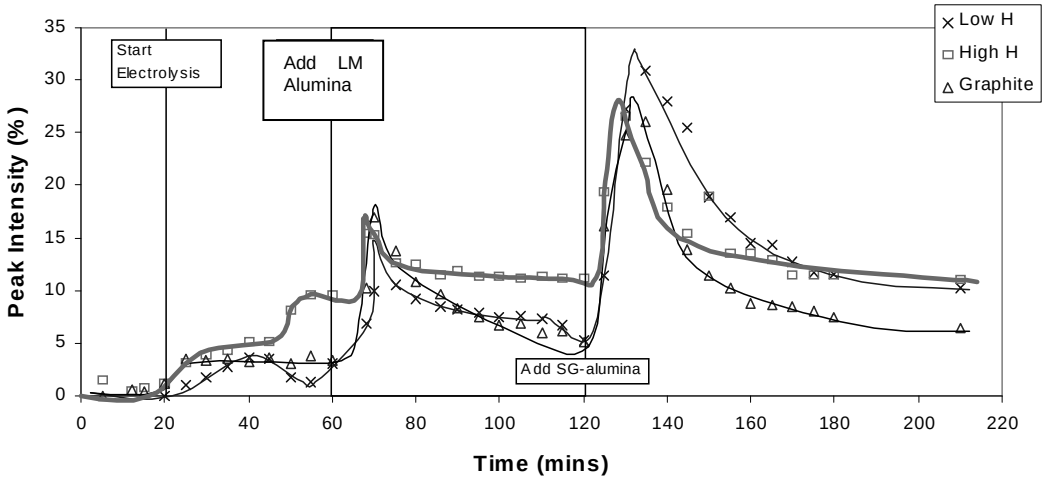

Figure 5.3 - Emissions from different anode materials used during laboratory electrolysis.

5.1.3. Results.

Figure 5.3 compares the three representative emission results for the three different anode types. Further results can be found in appendix 5. The high hydrogen emission shows the typical profile changes. During bath heating (0<t<20min) virtually zero emission was observed. The anode was then immersed into the bath and electrolysis started. This caused a slow rise in the HF emission as gas generation begins and the anode starts to be consumed. This will eventually reach a steady state emission level (here SI= 9.5% at 45 minutes).

Alpha alumina was added after 40 minutes of electrolysis to prevent anode effect. Here a slight rise in emissions is seen due to the residual water content of the alumina, and possibly some hydrolysis effects from the feed air moisture. This then decays back to a second steady state level (SI = 10.9%). SG-alumina (smelter grade) was then added after 2 hours. This has a higher peak due to the higher water content of this alumina. Due to experimental limitations the peak of this curve was not recorded. It is likely that the actual maximum is higher due to this. After maximum emission the HF level decays back to the final steady state emission level (SI = 12.0%). For each run the three steady state levels and their calibrated emission levels (using an approximate calibration curve for the signal intensities) are presented in table 5.3.

Table 5.3 - Measured non alumina HF emissions levels.

Anode	Emission (mg/m^3)		
	SI	Emission	Difference
High Hydrogen			
Steady State 1	9.5	116.0	0
Steady State 2	10.9	143.8	27.8
Steady State 3	12.0	170.3	26.5
Low Hydrogen			
Steady State 1	5.0	58.1	0
Steady State 2	7.5	85.3	27.0
Steady State 3	9.4	114.2	28.9
Graphite			
Steady State 1	2.9	42.0	0
Steady State 2	6	67.7	25.7
Steady State 3	8.3	96.4	28.7

Clearly all three runs have an obvious difference in each steady state level generation (refer to table 5.3). Here the high hydrogen anode has higher HF emission, than the low hydrogen anode, which has a higher emission than the graphite anode. It is proposed that the difference in steady state levels is an alumina effect related to the alumina equilibrium with a dissolved water content in the bath (refer to equation 4.8). Hence the greater the alumina concentration in the bath the greater the amount of dissolved water associated with this content (i.e. it is in equilibrium with this content).

Hence when more alumina is added, the steady state level the emission decays to will be higher. This is seen in the difference between the steady state levels in table 5.3. This difference for the 10g addition is consistently 27 mg/m^3. This equates to an emission contribution of 11 mg/m^3 per alumina wt% in the bath. Hence for this trial this makes the graphite emission effectively measuring the dissolved water emission, as its anode hydrogen content is negligible (in light of the proceeding results). This will be explored in more detail in section 5.3.

From this assumption the average H in the anode emission for the high and low anode emissions can be calculated using the graphite run as a basis. This can be converted to an approximate reaction efficiency using equation 4.8 to calculate the possible generation amount of HF from each hydrogen content (refer to table 5.4).

Table 5.4 - Calculated and measured HF emissions.

Anode	Emission (mg/m^3)		
	Ave HF	Calculated	% Reacted
High Hydrogen	75	510	14.7
Low Hydrogen	17	230	7.4

Note that the difference in the values is due to the assumption that the dissolved water content at the start of all three runs is the same. Due to possible differences in heating conditions and dissolved water retention on start up, this may not be the case.

Overall an average hydrogen conversion factor of 10% can be estimated. These are approximate values as there were calibration difficulties encountered for the FTIR instrument. However looking at the rough estimates of the percentage of H reacted shows that these values agree with the previous figure published by Wahnsiedler et al. ~8% [5]. It does not agrees with the 50% reaction value calculated by Grjotheim et al.[4] from Henrys results. It must be noted again that the conditions used by Henry vastly differ from those studied here.

This partial reaction of the anode hydrogen follows the trends proposed by the other past studies. As Wahnsiedler et al. [5] suspected, this is likely due to the rate at which CO and CO_2 are produced and emitted. The conversion of C to these species is an order of magnitude greater than that of H to HF. This results in a large amount of gas being evolved from the same surface as the HF reaction is initiated. Hence, not all of the hydrogen in the carbon will contact the electrolyte and not all will react with this either, given the reaction kinetics. Obviously the higher the hydrogen content, the greater the probability that some will react. Interestingly the remainder of this H is likely to either form part of the dissolved water content of the bath (refer to [4]), or if swept away in the anode gases it could be carried to the extraction system with the other fumes through the crust. Depending on the crust integrity this content will contribute to secondary HF generation - thermal hydrolysis of the particulates at the vents in the crust.

5.1.4. Conclusions.

This study has shown that the Wahnsiedler [5] low Hydrogen reaction figure to be accurate, with approximately 10% of the hydrogen in the anode reacting to form HF. This makes up around 5% of the total emission of the studied industrial cell (refer to

chapter 8). The remainder of the unreacted hydrogen either forms part of the dissolved water content in the bath or is transported to the extraction system via the crust vents where it could aid in secondary HF generation (refer to chapters 6 and 7). Hence, in an emission reduction scheme the effectiveness of the anode baking process contributes to a portion of the total HF emissions.

5.2. Dissolved Water.

Electrolytic dissolved water is a widely accepted constituent of the electrolyte within the aluminium smelting research area. However this is based more on circumstantial evidence, rather than quantitative evidence. Here the dissolved water of the electrolyte has been linked to producing the hydrogen impurities in the molten metal [25]. Typically the H content ranges between 0.2 to 0.5 ppm in the melt. It is agreed by researchers [25, 38] that this theory is a reasonable explanation for this impurity. This is because it is quite feasible for an concentration of dissolved water to reacts according to the following equation (5.1).

$$2Al_{(l)} + 3H_2O_{(diss)} = Al_2O_3 + 3H_{2(g)} \qquad (5.1)$$

This suggests that the dissolved water content is in equilibrium with the alumina content of the bath for this reaction to occur.

The following experiments use this as a basis. Based on reaction 5.1, laboratory and industrial experiments should be able to measure the effect of the dissolved water on the HF emission during a change in the alumina concentration of the bath.

5.2.1. Experimental Methodology.

The experimental apparatus used is illustrated in figure 5.1. The set up follows that used for the hydrogen in the anode trials. Electrolysis was conducted with a graphite anode to neglect the effects of the anode hydrogen HF generation. Here changes in alumina concentration were made by batch additions at planned periods during the experiment.

Here 20g of alpha alumina (with LOI(300) = 0.46 wt% and negligible LOI(1000)) was added to a standard bath composition 10% excess AlF_3, 5% CaF_2. After 110 minutes 10g of smelter grade alumina (refer to table 5.6 for properties) was added to the bath.

Finally after 210 minutes 10g of sodium hydroxide was added to the bath and its effect on the emission measured. For each addition period electrolysis was run for 40 minutes, stopped for 20 and recommenced for 30 minutes. This aimed to measure any residual emissions with no electrochemical potential.

5.2.2. Experimental Results.

Figure 5.4 illustrates a representative run for the dissolved water trial.

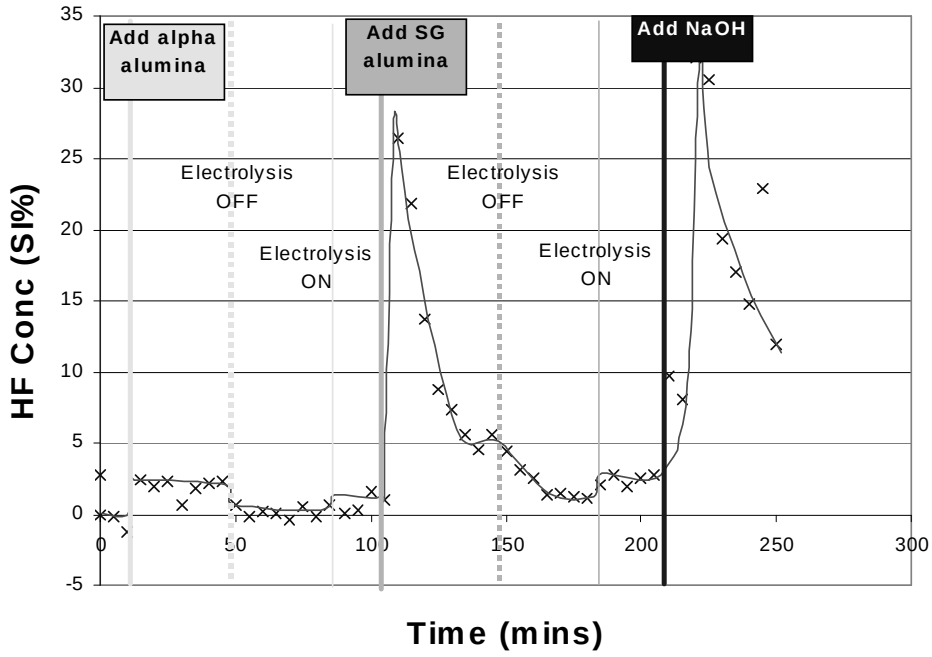

Figure 5.4 – The emission content from the dissolved water run.

Here we see the effects of dissolved water on alumina generation. On addition of the first amount of alumina to the bath a minor HF emission is detected (SI=2.5%= 39.5 mg/Nm^3). The bath alumina content from the 20g addition is around 2.7 wt%. As the α-alumina would have introduced only a minor amount of water, the emission is proposed to come from the dissolved water content residual in the additives to the bath (cryolite, aluminium fluoride and calcium fluoride) before electrolysis started.

Once electrolysis stops the emission reduces to virtually zero. This indicates that electrolysis is required to maintain emission from this source, not surprising as the water

reaction requires a anodic potential to occur [4]. Once electrolysis recommences, the emission generation starts again.

Adding 10 g of SG alumina produces a spike in the emission from the alumina water added (refer to section 5.3), which decays down to a steady state value of SI=5.5% (=62.7 mg/Nm^3). This level is higher due to the greater alumina content present. Hence for a 10g addition the emission difference is ~23 mg/Nm^3. Again stopping and starting electrolysis has an effect on the emission.

The same effects were seen during the anode hydrogen trials (section 5.1). As shown in table 5.3, the steady state emission changes with each alumina addition during the anode hydrogen experiments. Here for a 10g addition of SG alumina, a 27 mg/Nm^3 emission change is measured in the steady state emission. This is consistent with the results found for this experiment. As discussed above, this was concluded to be the result of the dissolved water emission.

The difference between the anode hydrogen runs and this run is the hydroxide addition. Here adding 10g of sodium hydroxide directly to the bath shows a dramatic increase in the emission. The emission increases 2 orders of magnitude to SI=33% or 4300 mg/Nm^3. The emission then decays back to the steady state value dictated by the equilibrium shown in equation 5.1. This suggests that the hydroxide ions (and potentially some of the adsorbed water) reacts to form HF. This source of hydrogen can also react to form HF in the electrolyte. It is proposed that the actual form of

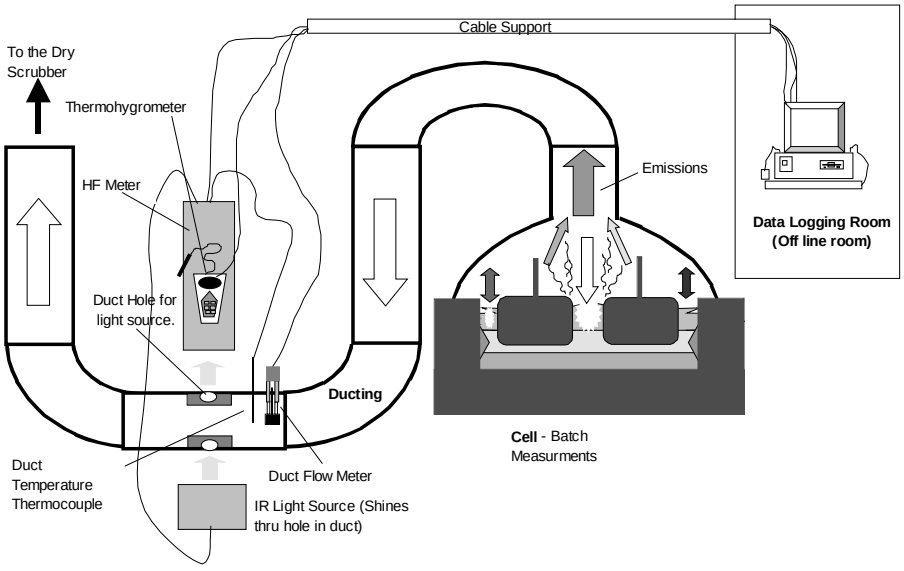

Figure 5.5 - The in-plant study equipment for cell technology I.

dissolved water in the melt is hydroxide ions. This is due to their potential similarity

with fluoride and apparent stability with the bath constituents. Note that this is simply a theory, further studies would have to be conducted to prove this point.

5.2.3. Industrial Methodology.

In-plant fluoride measurements in the cell duct were recorded using an infrared based adsorption HF meter (refer to [39] for details) in the configuration shown in figure 5.5.

Here the outlet (duct) HF concentration of a point fed electrolysis cell (with an average anode hydrogen content of 0.044 wt%) was measured continuously and was correlated with continuous measurements of ambient temperature, humidity, duct gas flow, duct temperature, feeder hole state, crust integrity and amount of alumina fed.

To establish the effect of dissolved water generation the cell was set to a track or zero alumina feed state. Here no alumina is fed to the cell. Hence the HF emissions can be measured without a constant alumina water input, or uncontrolled change in the alumina concentration. This negates the alumina water emission source. It also allows the alumina concentration to electrochemically decay during the period of the track. Thus the HF emission change associated with this alumina concentration decay can be measured.

5.2.4. Industrial Results.

Figure 5.6 illustrates two track periods from cell technologies I and II. Both show typical emission response to the zero fed (track) conditions (refer to chapter 7).

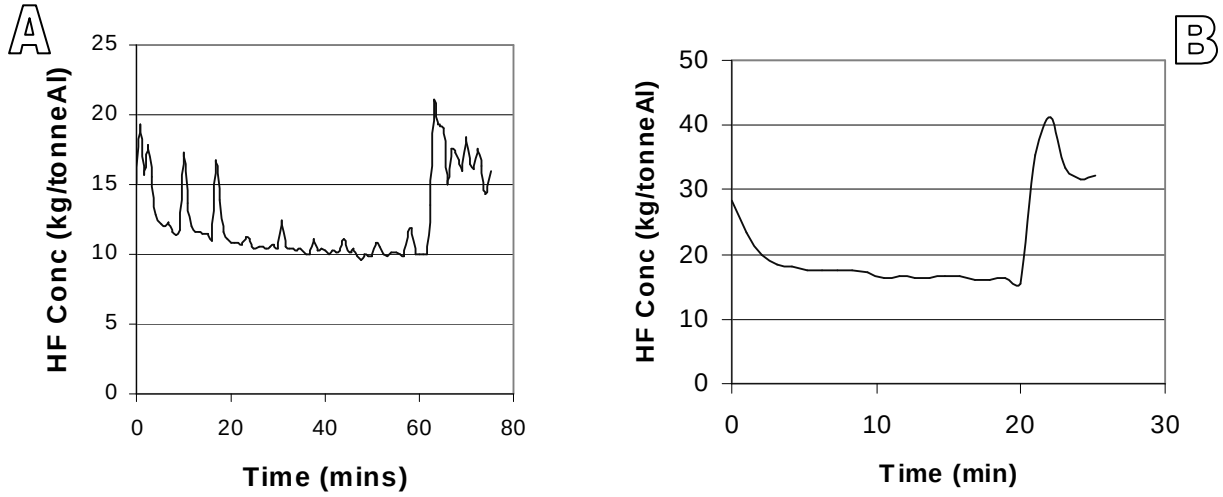

Figure 5.6 – HF emission response to zero alumina feeding conditions.
(A)Cell Technology I. (B)Cell Technology II.

Due to air mixing, alumina dissolution and other effects which affect the response time of the measured emissions the true studied track period is that period after the initial decay. The fitted decays lines are shown in figure 5.7.

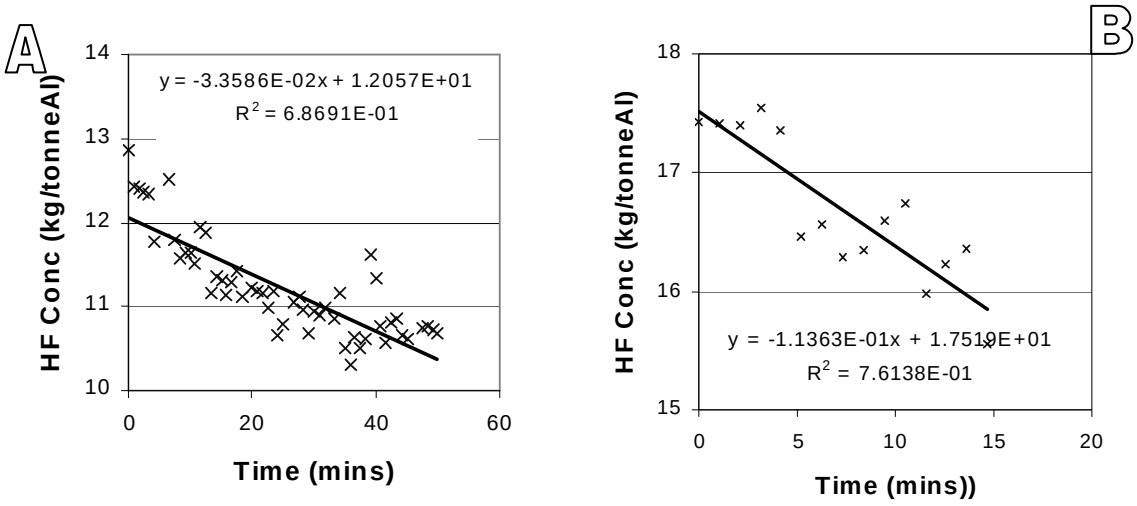

Figure 5.7 – Fitted decay lines for the zero feed emission responses.
(A)Cell Technology I. (B)Cell Technology II.

Cell technology II also had the alumina concentration modelled during the time of track. This is illustrated in figure 5.8.

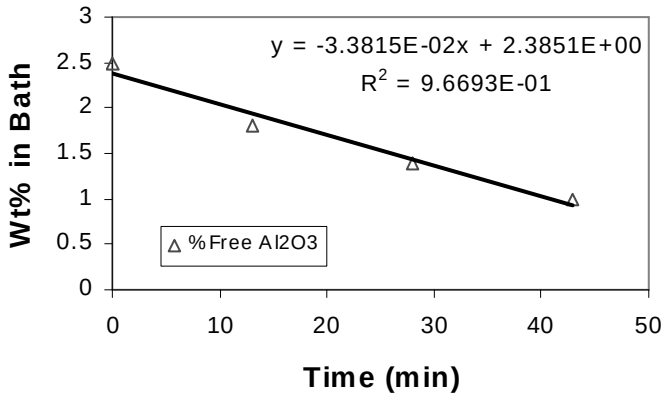

Figure 5.8 – The measured alumina concentrations in the bath during zero feed period for cell technology II.

As figure 5.7 clearly illustrates, the HF emission does follow the decreasing alumina content (refer to figure 5.7). If this is assumed to be the result of HF generation from

the equilibrium shown by equation 5.1, then the dissolved water HF generation content can be approximated.

Using Al_2O_3 consumption of 1.9 kg/kgAl produced it can be calculated that the Al_2O_3 usage is approximately 2.6 kg/min. This is reasonably close to the measured usage of 3.4 wt%/min.(=2 kg/min for a 6 tonne bath mass) shown for cell technology II in figure 5.8. Note that this figure depends on cell condition [40, 41] and heat balance.

At any rate, for cell technology I the predicted alumina consumption is 1.7 kg/min with a dissolved water emission decay rate of $3.35x10^{-2}$ kgF/tonneAl/min. For cell technology II the predicted alumina consumption is 2.6 kg/min with a dissolved water emission decay rate of $1.14x10^{-1}$ kgF/tonneAl/min. Taking into account the equilibrium shown in equation 5.1, this results in the emissions detailed in table 5.5.

Table 5.5 – The dissolved water emission rates for cell technology I and II for 3wt% alumina.

Cell Technology	Alumina Usage (kg/min)	Emission Decay Rate (kgF/tonneAl/min)	Emission (kgF/tonneAl)
I	1.7	3.35×10^{-2}	8.3
II	2.6	$1.14x10^{-1}$	2.8

The differences in the emission is thought to be the result of different alumina feeding technologies and these effects on alumina dissolution in the bath. This would affect the equilibrium shown in equation 5.1. Here depending on the path taken during dissolution (refer to section 3.5) differing amounts of alumina water may react with the electrolyte. This would affect the water content from the alumina that forms the dissolved water also. This will be discussed in more detail in chapter 8.

5.2.5. Conclusions.

The dissolved water content is a significant emissions contributor for a cell technology with good feeding technology (and hence ideal alumina dissolution). Both the laboratory and industrial results show that the dissolve water content of the electrolyte to produce significant amounts of HF dependant on the cell potential, feeding technology and bath alumina content. This is due to the equilibrium of this dissolved water content with the alumina content in the bath. It is also proposed that the dissolved water species in the bath is in a hydroxide ion form. Overall this contributor can account for up to 8 kg/tonneAl HF.

5.3. Alumina Water Generation.

Hydrogen fluoride generation from the water content of alumina has been long regarded as a major emission source. From Henrys [2] early study to this most recent investigation, both forms of alumina water – surface adsorbed and structural – have been regarded as the major source of the fluoride emission. There has been contention over the exact amount and source of the water that reacts. Henry found that very little of the adsorbed water reacts. This was disputed by Grjotheim et al. [4] suggesting that other mechanisms were at work. The results of the dissolved water emission generation suggest that there is some weight to this argument. Any unreacted moisture could in fact become part of the dissolved water content in the bath and react on a much slower time scale to that measured by Henry. However in the context of this investigation these two sources are treated separately.

Therefore the alumina water emission the emission generated immediately after alumina addition. The residual water then goes on to be used in other emission sources such as dissolved water and secondary HF emission generation.

5.3.1. Experimental Methodology.

The experimental set up follows that detailed in section 5.1.1. Here three 10 g amounts of alumina were fed per hour to replenish the alumina content of the bath. Low water content alumina (LM alumina) was fed for the first two cycles, followed by a single feed of smelter grade alumina (SG alumina). All responses were recorded. The LOI(300) and LOI(1000) contents of the alumina are detailed in table 5.6.

Table 5.6 – The LOI(300) and LOI(1000) analysis for the fed alumina(wt%).

Property	α alumina	LM alumina	SG alumina
LOI(300)	0.46%	1.50%	1.25 %
LOI(1000)	0.00%	0.09%	0.76%

5.3.2. Experimental Results.

Figure 5.3 demonstrates the significant effect that alumina water has on HF generation when added to an electrolysis cell. Here a spike response in the emission is seen on the addition of alumina with a water content. Referring to figure 5.3, the high hydrogen anode the addition of SG-alumina results in approximately 5000 mg/Nm^3 extra HF generation at the peak. This results from rapid primary generation of the evolved alumina water. It will be shown later that this is likely caused by the structural water in the alumina. Here 10g of alumina was added. It has approximately 0.8% wt structural water, which is equivalent to ~1600mg HF total (if AlF_3 is assumed to react with H_2O to form Al_2O_3 and HF). This suggests like the results of past studies [5, 30], that only a fraction of the structural water reacts. Here approximately 20% of the structural water (~320 mg) could be calculated to react over the 50min SG-alumina emission period. Once this water has reacted, the response decays down to the steady state level. Again the unreacted water could provide moisture for secondary HF generation at the crust/air interface.

The difference in generation from differing structural water contents is apparent in figure 5.4. Here preheated (@100^{O}C) alpha alumina is added to the bath initially. As there is no structural water (LOI(1000)~0), no spike response is recorded. However when the smelter grade alumina is added (LOI(1000)=0.76wt%), a large spike response is measured. The spike height also differs between, the low moisture content alumina and the smelter grade alumina in figure 5.3. This can be seen comparing the peak heights in table 5.7.

Table 5.7 – The HF peak heights for the different LOI alumina.

Alumina	LOI(300) (wt%)	LOI(1000) (wt%)	Peak Conc.* (mg/Nm^3)
Alpha (α)	0.46	0.0	~0
Low Moisture (LM)	1.50	0.09	~380
Smelter grade (SG)	1.25	0.76	~4800

**Concentration calculated minus steady state emission. Approximate as actual peak height not recorded.*

There is a difference in adsorbed water, between these alumina, however as the industrial measurements will show, the differential temperature between the bath and feeder are sufficient to desorb most of this content before it enters the bath. Due to the uncertainty in the peak heights these values can not be quantitatively compared. It is certain however that the major factor behind the differences in generation here is the structural water content of the alumina seen in the LOI(1000) values.

This all suggests that the greater the structural water content, the higher the spike is and hence the greater the HF generation. This is seen comparing the three different aluminas responses in figures 5.3 and 5.4. This follows Henrys [2] findings, where preheating the alumina to $1000^{O}C$ altered the structural water content and hence the amount of HF generated from the alumina. Here the spike heights should be directly proportional to the structural water content and fraction of the water reacted with the bath. It all suggests that of the two forms of water on the alumina, the form which causes the majority of the emission is the structural water. The adsorbed water is likely lost during feeding due to the temperature changes experienced on its journey.

This is an additive effect, where the alumina water HF emission adds on top of a constant non alumina steady state emission (here attributed to anode hydrogen and dissolved water content). This is also seen in the industrial measurements. This fact is used for a decoupling calculation, which simplifies emission analysis (refer to chapter 7 for the Δ correlation).

5.3.3. Industrial Methodology.

The set up of the equipment used for measuring the HF emissions from an industrial aluminium electrolysis cell is illustrated in figure 5.5. The trials were conducted on cell technology I.

The emission from both the water blended primary and secondary alumina were compared to normal emission from the unaltered alumina counterparts The blended aluminas were mixed with approximately 3% water. The properties of the resultant mix was then analysed and the LOI(300) and LOI(1000) determined. The comparative properties of the alumina used in the trial is listed in table 5.8.

Table 5.8 – The average properties of the alumina for the hydrated alumina trials.

Property	Primary	Wet Primary	Secondary	Wet Secondary
LOI(300) (wt%)	1.58	4.46	1.79	3.54
LOI(1000) (wt%)	0.67	0.72	2.28	2.77

Both batch HF sampling and continuous monitoring (using the HF meter illustrated in figure 5.5) was conducted. Batch HF emission involves measuring the duct flow rate using a pitot probe and manometer. The probe is inserted into the duct at several predetermined positions. From this the average of the pressures the flow can be

determined. Gas samples are collected using a dry duel filter system. [42]. The first membrane pre-filter collects the particulate, the second bubbles the remaining fluoride gas through a sodium hydroxide(/glycerol) solution, which reacts with the HF. The solution is analysed in a laboratory by *wet methods* (refer to Danchik et al [43]).

From these the concentration and mass emission can be found from the following simple relations:

$$\text{Concentration} = \frac{\text{Mass of Fluoride}}{\text{Volume of Sample}} \quad (5.2).$$

$$\text{Mass Emission} = \text{Concentration} \otimes \text{velocity} \otimes \text{Area of Duct} \quad (5.3).$$

5.3.4. Industrial Results.

All the data collected show that the fluoride emissions clearly follows the alumina feeding periods. Figure 5.9 illustrates the similarity between the overfeeding and underfeeding periods and the overall amount of fluoride generated. The cause of this effect is the reaction of the water content of the alumina with the electrolyte (refer to equations 4.1, 4.2 and 4.3. The lack of a time delay between addition and HF generation also points to an immediate reaction. Note however that the "Tracking" or zero alumina feeding procedure after anode change illustrates that this is not the only contributor to the HF emission. As the dissolved water emission section illustrated a residual HF concentration attributable to other emission sources is still recorded. This fact leads to a simplification in the industrial emission analysis. As will be explained in Chapter 8, there are two separable contributions – a one associated with alumina feeding and one independent from alumina feeding. The emission sources can then be seen to vary within these two semi independent contributions.

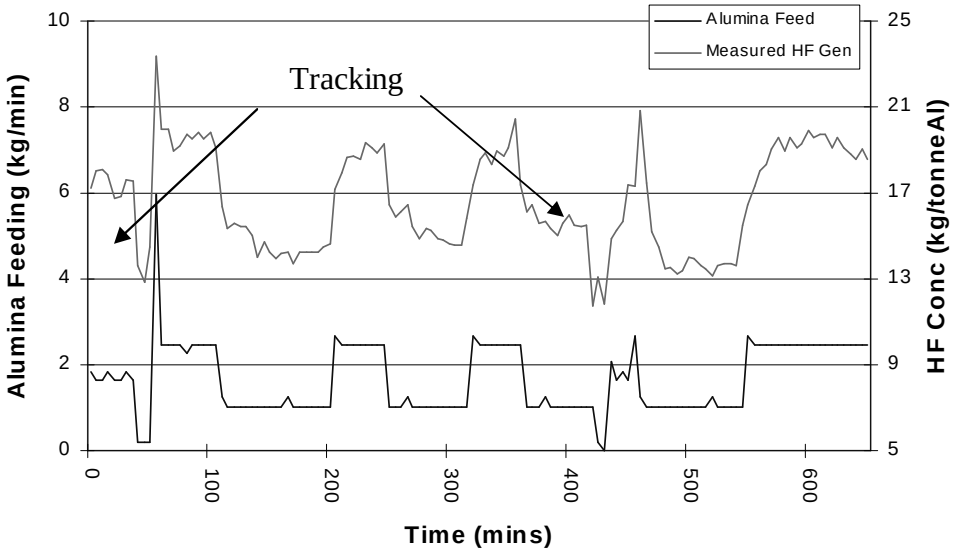

Figure 5.9 – Continuous emission data from cell technology I.

Three wet alumina trials were conducted to see the effect of surface water on the HF emissions from cell technology I. If little or no effect could be seen from adding significantly more adsorbed water to the bath, then this water source on the alumina must play a minor role in primary generation of HF. As with the laboratory trials this would point to the structural water content of the bath to be the important water source in alumina primary HF generation.

Table 5.9 presents the results of the only run with the particulate and HF measured with the duel filter batch instruments.

Table 5.9 - Comparing wet alumina runs with normal condition results

Type	**Secondary**	**Secondary**	**Wet Secondary**
Test	I	II	III
Daily Cell Temp (^{o}C)	958	963	974
Average Duct Temp (^{o}C)	93.3	116	110
LOI 300 (wt%)	1.63	1.95	3.54
LOI 1000 (wt%)	2.38	2.18	2.77
Gas Flow (Nm^3/h)	5 777	5675.12	5687.38
Particulate F (mg/Nm^3)	84.89	121.56	150.55
HF (mg/Nm^3)	198.7	311.31	321.27
HF (kg/h)	1.15	1.77	1.83
HF Percent (%)	70.1	71.9	68.1

This single result is within the established baseline concentration limits (0.8 - 1.5 kg/h) for the normal condition of cell technology I (refer to chapter 7). The overall generation depends on cell condition, bath composition and ambient conditions. With these considerations the three runs compare within the established limits. This suggests that the surface water has little effect on the overall primary generation of HF.

Figure 5.10 - Dusting resulting from adding wetted alumina to cell technology I. (A)Before. (B)After.

Figure 5.11 – A volcano resulting from adding wetted alumina to cell technology I. (A)Before. (B)After.

It is interesting that the particulate measurement has increased for the wet secondary alumina. It must be noted that the alumina used in the last two measurements had more fines than the first run, but as figures 5.10 and 5.11 illustrate, the excess water produces exaggerated dusting and volcano features on the feed alumina, especially in closed feeder holes. This is the result of the violent desorption of the water when entering the high temperature bath. Yet another indicator of the loss of the adsorbed moisture. This

should increase the amount of particulates from increased entrained bath. However without flames, the HF content from secondary HF generation should not be expected to increase as this relies on thermal hydrolysis (refer to chapter 6). This is the result measured, as illustrated in table 5.8.

The continuous HF data from the HF meter (refer to figure 5.4), of the transition from normal alumina to the hydrated counterpart supports the conviction that that the adsorbed or surface water on alumina has little effect on HF generation (refer to figure 5.12 and figure 5.13).

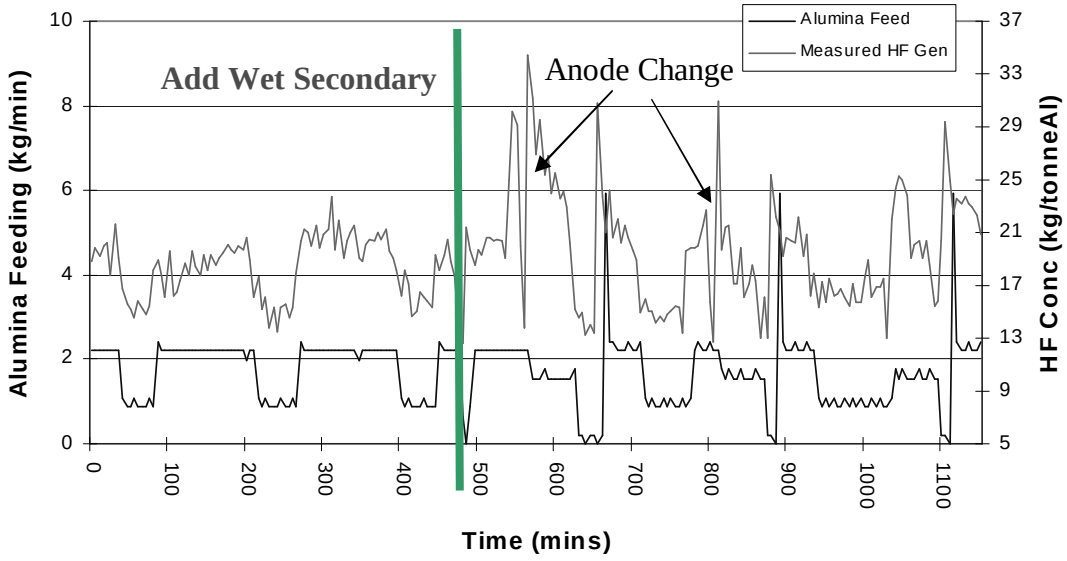

Figure 5.12 - Continuous HF concentrations for adding hydrated secondary alumina to cell technology I.

Neglecting the heat balance effect of anode change in figure 5.12 (a bad anode – assumed to caused by a metal spike was found after one hour of the trial and the anode

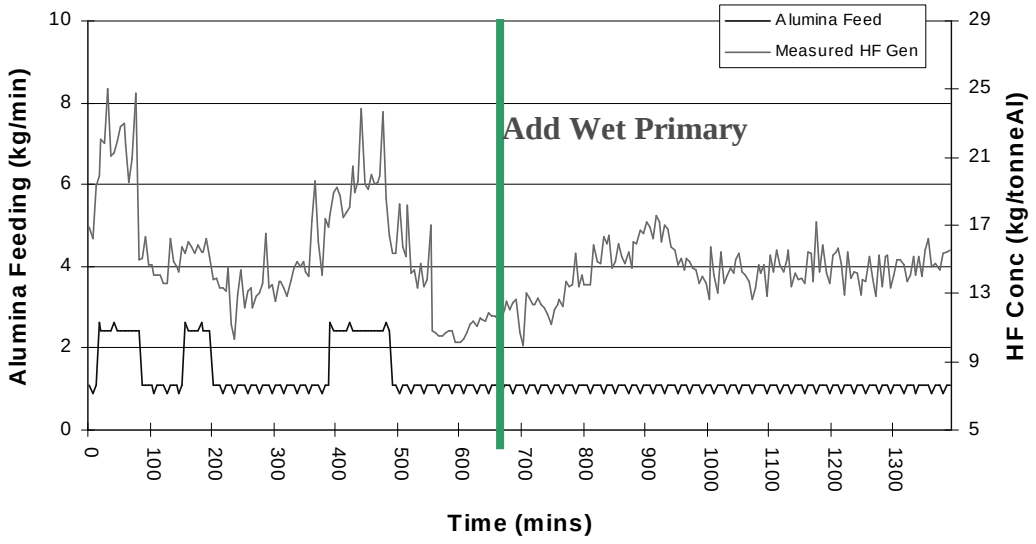

Figure 5.13 - Continuous HF concentrations for adding hydrated primary alumina to cell technology I.

lifted, the resulting in an altered crust integrity - this markedly changes the measure HF concentrations – refer to chapter 7) it can be clearly seen that little change appears in the measured HF concentrations after the wet alumina is fed, once the heat balance effects have subsided (refer to chapter 8 for details on the effects of heat balance changes on the HF emission). The same result is seen for the wet primary addition. Here the steady state emission level (the average emission) remains unaltered once the wet alumina was added. In each case the HF concentration levels before and after addition remain relatively the same. Clearly the absorbed water content of the alumina has *little effect* primary HF generation.

As later analysis of the non alumina feeding emission effects (refer to chapter 7 for the theory on calculating the non alumina feeding emission) will show, this similarity can also be seen when comparing the $D_{feeding}$ and calculated non alumina feeding emission values B, of the wet alumina trials. Note that an anode change has occurred between these periods hence the slight difference in B and $D_{feeding}$ as the later value is calculated about 5 hours after the change once the normal condition was re-established.

Table 5.10 - $D_{feeding}$ and calculated non alumina feeding emission B for hydrated secondary trial.

Description	Ave HF (kg/tAl)	Ave Temp. (°C)	$D_{feeding}$ (kg/tAl)	Δ	Non Alumina B (kg/tAl)
Before wet alumina addition	17.98	112.0	5.20	0.3674	11.41
After Wet alumina addition	17.73	121.6	5.59	0.3072	10.09

All these results agree with the findings of Henry [2] who found that even immersing wet alumina in foil did not significantly affect the emission. He also found that a lot of the water was desorbed before entering the cell, condensing on the equipment. Here it produces the volcano effects seen on feeding (figure 5.11). Overall it likely that none of the adsorbed water and only some of the structural water reacted to form the measured HF concentration. This is quite consistent with the shock heating mechanism proposed in chapter 6. Here the temperature difference encountered by the alumina on addition to the bath is so great (approximately 900^{O}C temperature change in 5 seconds) that the relatively loosely bound surface water is flashed off. This surface water thus never reaches the electrolyte. This is also consistent with studies into alumina surface water properties [12]. Here it was found that the surface water was loosely bound, dependant on temperature an relative humidity of the surrounding atmosphere.

The unlikely reaction of the alumina surface water with the electrolyte can be further illustrated if a water balance is conducted on the cells input and outputs.

5.3.5. Alumina Water balance.

For further understanding of the generation contributions a mass balance was made for water addition to the bath (table 5.10). Calculations from the alumina moisture content show that if all the water was to react with the electrolyte, a significantly higher HF concentration would be recorded (refer to table 5.10). The water data was calculated using the simple stoicheometric relationship from the following reaction (5.4), for a secondary alumina with a LOI(300)=1.63 wt%, and LOI(1000)=2.65 wt%:

$$2AlF_{3(sol)} + 3H_2O_{(sol)} = Al_2O_{3(sol)} + 6HF_{(g)} \quad (5.4)$$

It is possible that HF could result from desorbed fluoride – a secondary generation source. For this analysis it is sufficient to assume that this source is negligible. This will be proven in detail in a later section (refer to chapter 6).

The water balance in table 5.11 predicts that little HF generation is likely from the adsorbed moisture on the alumina (a major part of the other water content) for cell technology I. Furthermore if HF emission is compared to all possible water generation sources it is likely that the generation results from only a small proportion (<24%) of the alumina's structural water content. This is consistent with Henrys [2] results, where he found the only change in emission came when he preheated the alumina to 1000^{O}C. This altered the structural water content. Both unreacted moisture contents are likely form part of the dissolved water content or may be entrained in the anode gases, to exit via the crust vents.

Table 5.11 - Water mass balance for 24h period for cell technology I.

			Water Data	% of Gen
Total HF Generation (24h)	0.9106 kg/h HF	**Reacted Water Equivalent**	0.5058 kg/h	100%
Alumina Added	100.30 kg/h	**Water added via alumina**	3.9918 kg/h	789%
		Structural Water	0.8531 kg/h	169%
		Other Water content	3.1386 kg/h	621%
Predicted Water HF Gen	0.3082 kg/h HF	**Reacted Water Equivalent**	0.1717 kg/h	33.9%
Predicted Non Alumina Gen	0.6024 kg/h HF	**Reacted Water Equivalent**	0.3341 kg/h	66.1%

In fact for a consistent background generation to be calculated from the Δ correlation (refer to chapter 7), only 20% of the structural water is predicted take part in alumina HF generation. As the alumina's structural water is thought responsible for this effect, it is likely that a large content is lost without reacting with the electrolyte. For several days data, the generation balance predicts that only a maximum of 24% of the structural

water reacts. Using the mass balance presented in table 5.9 this equates to only 4.3% of the water reacting which enters the cell via the secondary alumina. This agrees with the 8.6% figure proposed by Wahnsiedler *et al.* [5] and Henry's [2] alumina moisture study, bearing in mind the differing feeding methods and aluminas used in each study.

This reaction figure differs for different cell technologies. For cell technology II the calculated reaction figure is quite different. For a secondary alumina with LOI(300)= 2.31wt% and LOI(1000)= 2.89wt% we find the reaction figure to significantly higher – 40%. This equates to 6.6% of the total alumina water reacting (refer to table 5.12). This makes the alumina water reaction efficiency a technology related factor.

Table 5.12 - Water mass balance for 24h period for cell technology II.

			Water Data	% of Gen
Total HF Generation (24h)	2.0700 kg/h HF	**Reacted Water Equivalent**	1.1500 kg/h	100%
Alumina Added	132.92 kg/h	**Water added via alumina**	6.9117 kg/h	601%
		Structural Water	1.1436 kg/h	99.5%
		Other Water content	5.7681 kg/h	501%
Predicted Water HF Gen	0.8250 kg/h HF	**Reacted Water Equivalent**	0.4583 kg/h	44.6%
Predicted Non Alumina Gen	1.2451 kg/h HF	**Reacted Water Equivalent**	0.6917 kg/h	55.3%

As reviewed in section 3.4 and 3.5 alumina dissolution can follow three separate path ways, depending on the alumina properties and feeding mechanism. The point feed mechanisms and cell design different significantly in both cases. It can be said that cell technology I is a retrofit technology and hence its feeding design is not a full design but an idealised one for the existing structure. Cell technology II is a total design, in that its feeding system, center channel flow and alumina dissolution was designed to complement each other for greatest efficiency. As a the response study in chapter 8 will show, it is likely that the alumina dissolution in cell technology I is not as ideal as that in cell technology II, resulting is a much longer dissolution time. If Haverkamp [16] and Lui et al. [22] alumina fragmentation dissolution scheme is valid (section 3.5.2), then different dissolution routes would dictate how rapidly the evolved water would be expelled. In a less ideal feeding method the agglomerations and clumping of the alumina would prevent this rapid release of alumina and have a slower response on HF emission once the alumina was added. Conversely an ideal feeding method would have a rapid response as the individual alumina particles would fragment rapidly, releasing the structural water. It is likely that this is the difference between these two technologies.

Overall only a small amount of the total alumina water reacts – around 5 to 8%. This does agree with the 8.6% figure proposed by Wahnsiedler *et al.* in both cases. Note that the remainder of this water forms part of the dissolved water emission and some may be dispelled into the emission recycle system.

5.3.6. Conclusions.

Primary HF generation from alumina has been concluded to result from a fractional reaction of the structural water within the bath after addition. Laboratory experiments with differing structural water contents (LOI(1000)) show that varying the amount of structural water changes the amount of HF generation. The greater the amount of structural water, the higher the HF generation measured. Industrial trials show that little extra HF emission results from extra surface water, only an increase in the amount of entrained particulates generated. Essentially the adsorbed water is lost before entering the bath due to the large change in temperature experienced upon feeding to the high temperature electrolyte. The majority of the emission results from the structural water of the alumina.

This agrees with the results of Henrys study [2] into adsorbed water generation. Following the alumina shattering theory presented in the literature, once added to the bath the alumina agglomerated shatter rapidly releasing the internal structural water, dispersing it in the electrolyte. This water is then able to react with the electrolyte. As this process depends on the size of the feed alumina and the mechanism of feeding, by first approximation the structural water reaction should be dependant on the mechanism of dissolution. This is dependent on the feed technology. Overall only a fractional amount of the total alumina water reacts (4 – 8 wt%) to undergo primary HF generation. The remainder is either:

- Lost on addition to the bath due to the temperature change experienced – the surface water.
- Forms part of the dissolved water content of the electrolyte – possibility for the unreacted structural water.
- Exits the electrolyte entrained in the anode gases.

6. Secondary Generation of Hydrogen Fluoride.

Secondary generation of hydrogen fluoride from an aluminium reduction cell is defined as that HF generated outside the electrolyte of the cell. This includes hydrolysis of the generated fluoride particulates within and above the crust, and fluoride desorbed off secondary alumina. The following section investigates the significance of both these sources.

6.1. Particulate Hydrolysis.

It has been widely speculated in the past that a significant proportion of the fluorides are hydrolysed above the cell. Henry [2] suggested that this only occurred at the crust-air interface, while Heiberg et al. [29] demonstrated small amounts of hydrolysis within the dry scrubbing system. Therefore most past studies have the classification into particulate and gaseous is arbitrary since the relative amounts depend upon the sampling technique, sampling location and analytical procedure due to the hydrolysis reaction. It has been suggested that particulate materials may react with water vapour in the air and form HF while HF may sorb on non-fluoride particulates and be reported as particulate [6]. The extent of this is unknown and the exact mechanism has not been conclusively shown. It is the aim of this section to show where and when it is possible for these hydrolysis reactions to take place.

6.1.1. Thermodynamic Analysis.

A thermodynamic analysis of the possible equilibrium species has been conducted using HSC© thermodynamics package to identify the possible products pathways of the hydrolysis reactions. It must be noted that HSC is a predictive tool and has several limitations. It ignores the kinetics of a reaction, and its reaction path predictions are limited to the species in the database. As Gillespies [31] results indicate, alumina surface reactions are much more complex than simple species reaction systems predict. HSC does not predict the intermediate species, nor complex hydrolysis products which occur on the hydrated surface and pores. However as the following analysis shows, the mechanisms proposed in the literature [4, 26] fit the predicted equilibrium products with surprising accuracy.

As the total particulate simulations in figures 6.8 and 6.9 demonstrate, it is difficult to de-couple the individual reactions occurring during heating particulate. Hence it is

more informative to compare the thermal dissociation characteristics of the individual components compared to the hydrolysis reactions. From these the predicted relative effects can be gauged.

However before investigating the individual species a few generalities can be made by comparing all the reactions:

- Very little interesting happens to any of the individual components HF generation wise without the presence of water. Once water is presence, HF is generated to the detriment of mainly Na_3AlF_6 and $Na_5Al_3F_{14}$. An exception is AlF_3 which has little reaction both below 700^{O}C in both hydrolysis and simple thermal heating conditions as predicted by HSC. However with $NaAlF_4$ and Na_3AlF_6, the differences with the introduction of water are marked. As all past research has indicated, these products have the potential to react significantly with any environmental water source.
- In all cases little changes with hydrolysis, simply an amount of the initial species and the dissociation products react with the water to form HF.

(A). Sodium Tetrafluoroaluminate.

Figure 6.1 and 6.2 present the predicted results of heating sodium tetrafluoroaluminate in dry and hydrolysis induced conditions:

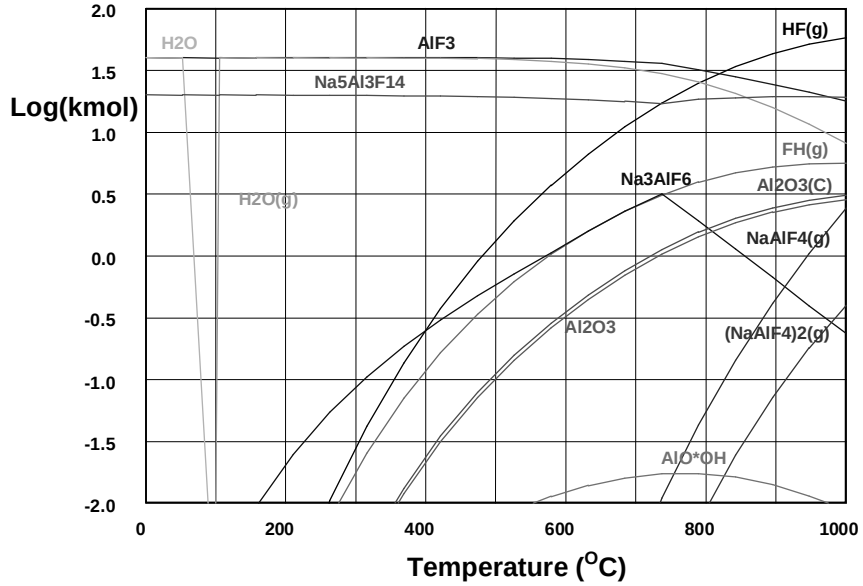

Figure 6.1 – Heating $NaAlF_4$ (100 mol $NaAlF_4$).

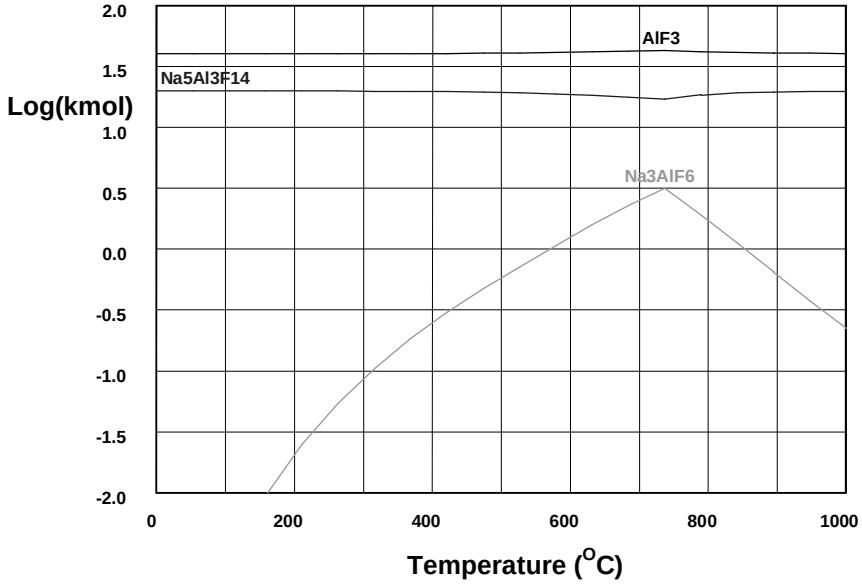

Figure 6.2 – The hydrolysis of $NaAlF_4$ (100 mol $NaAlF_4$, 20 mol H_2O).

Figures 6.1 and 6.2 show that sodium tetrafluoroaluminate is an unstable species. This fact is widely published [4]. As the thermal decomposition prediction illustrates the following reaction occurs at most temperatures:

$$5\mathrm{NaAlF}_{4(g)} \Leftrightarrow \mathrm{Na}_5\mathrm{Al}_3\mathrm{F}_{14(s)} + 2\mathrm{AlF}_{3(s)} \quad (6.1).$$

At higher temperatures a minor amount of the chiolite decomposes to aluminium fluoride and cryolite, though this is not a very significant reaction. Hydrolysis above 600^{O}C though changes the thermal decomposition reactions completely.

$$3NaAlF_{4(g)} + 3H_2O_{(g)} \Leftrightarrow Na_3AlF_{6(s)} + Al_2O_{3(s)} + 6HF_{(g)} \quad (6.2)$$

Here the aluminium fluoride and chiolite products are consumed to form the ever vigilant hydrogen fluoride and other aluminium oxide species. HF production becomes important (greater than 0.1 kmols) above 350^{O}C, becoming significant above 600^{O}C with the more favourable hydrolysis conditions of the decomposition products.

(B). Cryolite.

Cryolite is predicted to form alumina and HF from the following reaction (6.3) *[4]*. However HSC predictions suggest an alternative reaction this as the following figures illustrate:

$$2Na_3AlF_{6(s)} + 3H_2O \Leftrightarrow Al_2O_{3(s)} + 2NaF + 6HF_{(g)} \quad (6.3)$$

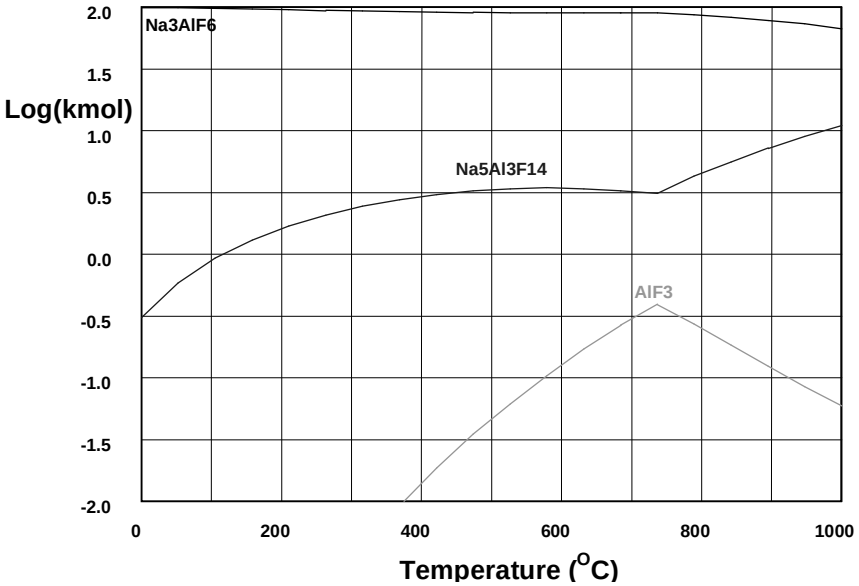

Figure 6.3 – Heating Na_3AlF_6 (100 mol Na_3AlF_6).

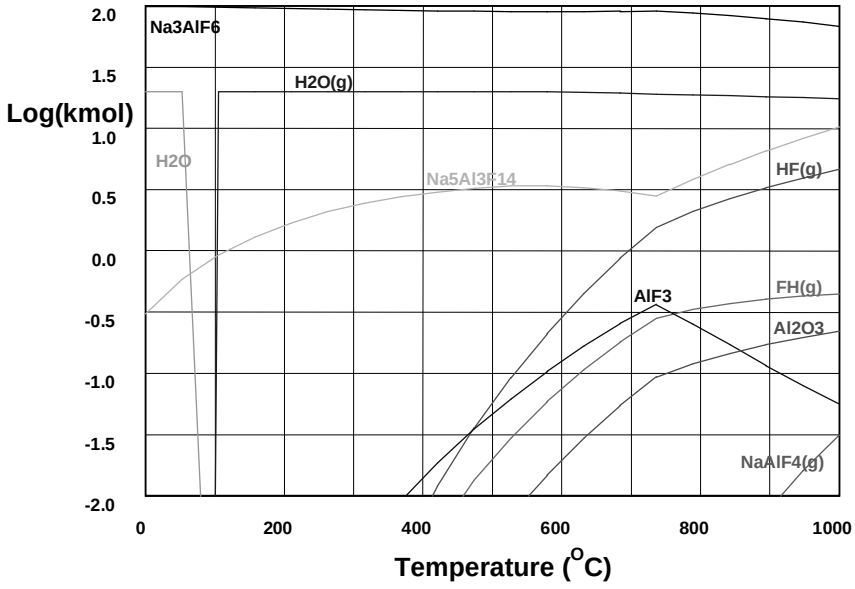

Figure 6.4 – The Hydrolysis of Na_3AlF_6 (100 mol Na_3AlF_6, 20 mol H_2O).

Even in the presence of moisture HSC predicts cryolite to be quite unreactive. At higher temperatures HSC predicts that the dissociation products (chiolite and aluminium fluoride) react with the water to form HF.

(C). Aluminium Fluoride.

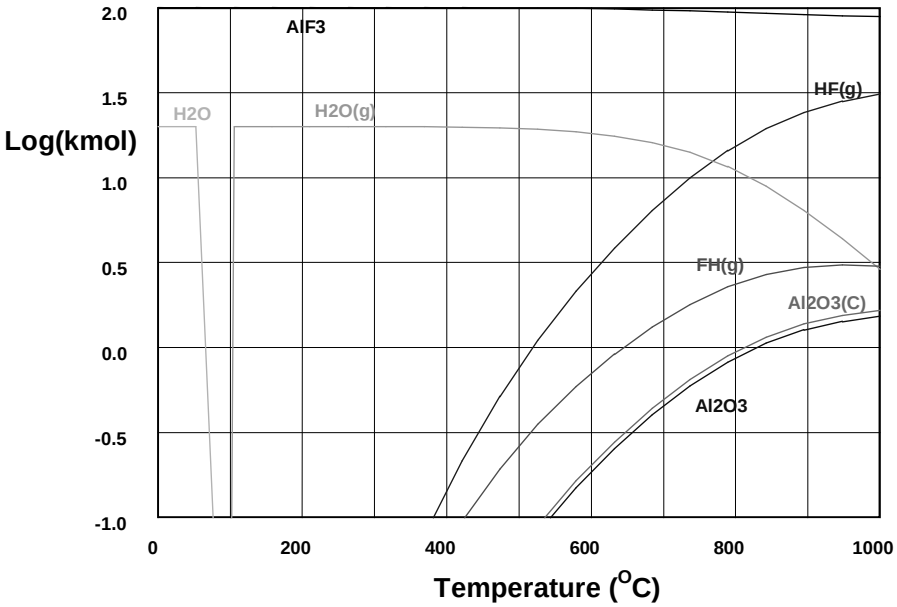

Figure 6.5 – AlF_3 Hydrolysis (100 Mol AlF_3, 20 mol H_2O).

As indicated by the predicted reaction schemes for sodium aluminium fluoride and cryolite, aluminium fluoride (as chiolite will show) is an important species in the hydrolysis reactions. With hydrolysis, HF becomes important above 350^{O}C and significant above 600^{O}C. It is this product which causes much of the hydrolysis HF in the fumes according to the following reaction:

$$AlF_{3(sol)} + 3H_2O \Leftrightarrow Al_2O_{3(sol)} + 6HF_{(g)} \quad (6.4)$$

(D). Chiolite.

As predicted chiolite is quite reactive with water above 400^{O}C, with HF becoming important above 400^{O}C and significant above 600^{O}C. Chiolite hydrolysis is responsible for much of the HF in the cell fumes according to:

$$3Na_5Al_3F_{14(g)} + 6H_2O_{(g)} \Leftrightarrow 5Na_3AlF_{6(s)} + 2Al_2O_{3(s)} + 12HF_{(g)} \quad (6.5)$$

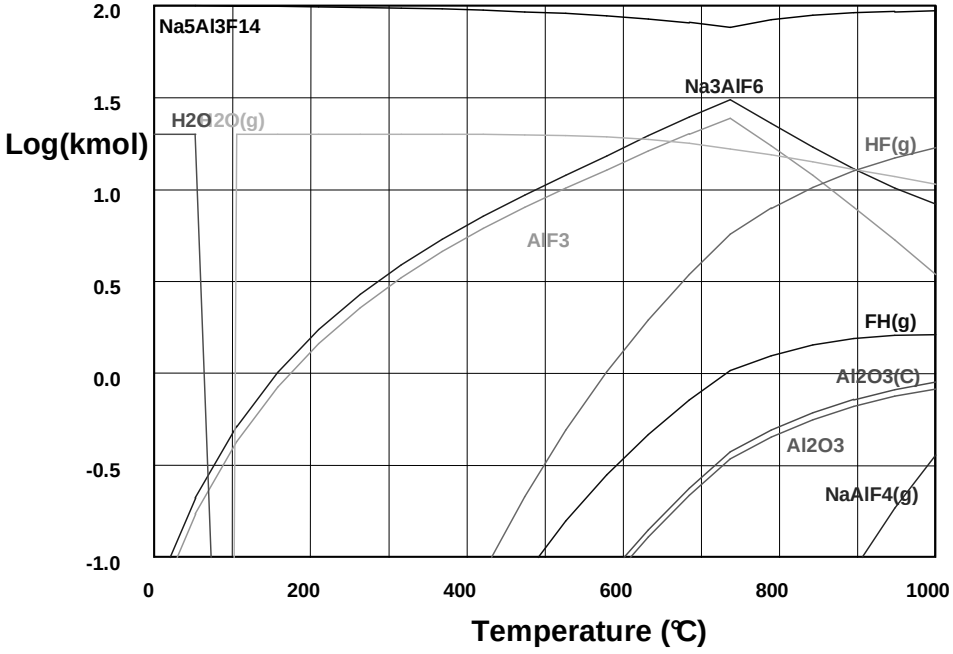

Figure 6.6 – The hydrolysis of $Na_5Al_3F_{14}$ (100 mol $Na_5Al_3F_{14}$, 20 mol H_2O).

(E). Particulate Decomposition.

Figures 6.8 and 6.9 present the possible equilibrium products from firstly a simple heat treated sample of bath particulate (figure 6.7), and then a thermally hydrated sample of bath particulates (figure 6.8). The bath particulate composition has been approximated as 100 mol $NaAlF_4$, 20 mol Na_3AlF_6, 20 mol AlF_3.

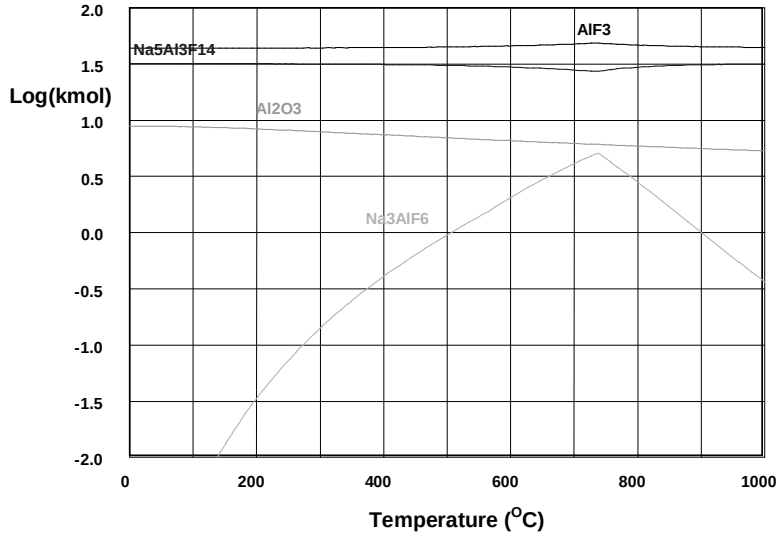

Figure 6.7 – Thermal decomposition of particulates
(100 mol $NaAlF_4$, 20 mol Na_3AlF_6, 20 mol AlF_3, 20 mol Al_2O_3)

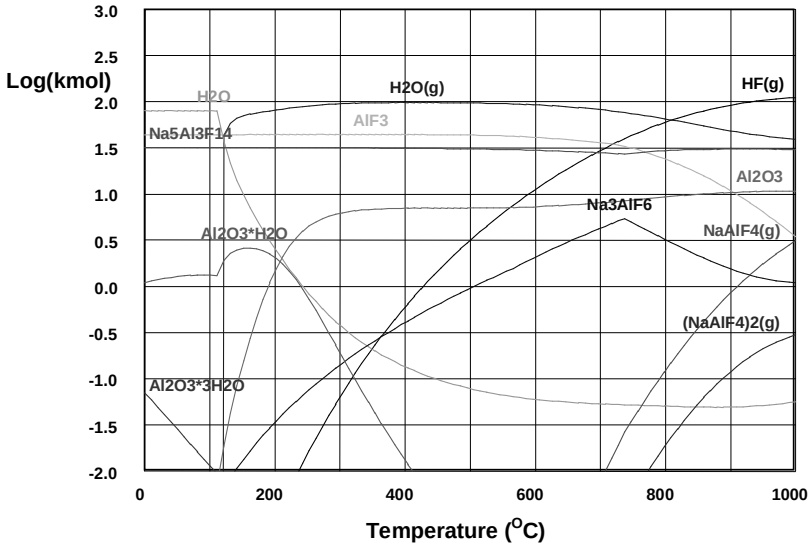

Figure 6.8 – Thermal hydrolysis of particulates
(100 mol of H_2O, 100 mol $NaAlF_4$, 20 mol Na_3AlF_6, 20 mol AlF_3, 20 mol Al_2O_3).

As stated at the beginning of the individual component hydrolysis the combined process are complex and requires decoupling as several competing formation, dissociation and hydrolysis reactions are occurring. For instance sodium tetrafluroaluminate decomposes forming other source species which in turn undergo dissociation and hydrolysis reactions. From the reactions of the individual components it is obvious that all the hydrolysis reactions occur to some extent in both cases. In the thermal decomposition case the water is provided by dehydration reactions of the alumina combined with hydrogen fluoride reaction with alumina:

$$6HF_{(g)} + Al_2O_3 \xrightarrow{HEAT} 2AlF_3 + 3H_2O \qquad (6.6)$$

This reaction (as are many of the others) is not as simple as the HSC package implies, though it is only a predictive tool. In both cases the decomposition and subsequent hydrolysis of the sodium tetrafluroaluminate species plays a significant role in the HF reaction, as the similarity in results (compare figures 6.1 and 6.2 with figures 6.8 and 6.9). Its widely published decomposition characteristics are fully predicted in the simulated particulates. As shown by the individual hydrolysis results, further HF generation relies on the presence of hydrolysis water.

(F). Conclusions.

Further generalities gleamed from the calculations are:

- No significant hydrogen fluoride generation occurs below 300^{O}C in the hydrolysis case.
- Hydrolysis promotes HF generation.
- HF production becomes significant (0.01 kmol) at a lower temperature with hydrolysis (300^{O}C compared to 350^{O}C by pure heating).
- $NaAlF_4$ is the species affected most by hydrolysis (see below).

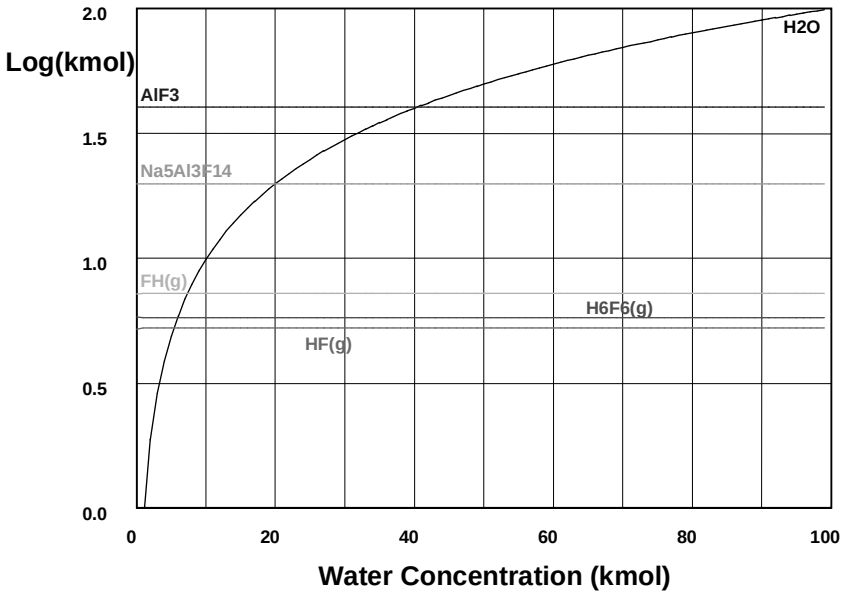

Figure 6.9 – Heating particulate simulation with changing water content at 400^{O}C.

The lack of kinetic considerations in the HSC calculations is obvious when changing moisture content is considered. Figure 6.9 shows the simulated particulate content in figure 6.7 and 6.8 heated at 400^{O}C undergoing hydrolysis under changing moisture content conditions. No change in HF levels occurs over the range. As the next section will show, this is not what occurs experimentally. Due to the rate of the volatilisation reaction, hydrolysis aids in removing HF at this temperature. Hence HSC helps in predicting the actual reactions, but the exact mechanisms are not predicted. It also lacks considerations of particle size and mixing. Within the particulate mixture particles of chiolite, and cryolite will not be homogenous, rather mixed. Agglomerations and particle size distribution lead to varying surface areas and reaction rates. Overall HSC is a useful tool in the correct context.

6.1.2. Experimental Methodology.

Here the fluoride loss of the bath particulate component of the total fluoride emission was measured. Hydrolysis reactions are forced by passing humid air over a representative material at various temperatures and residence times. The experimental set up is illustrated in figure 6.10:

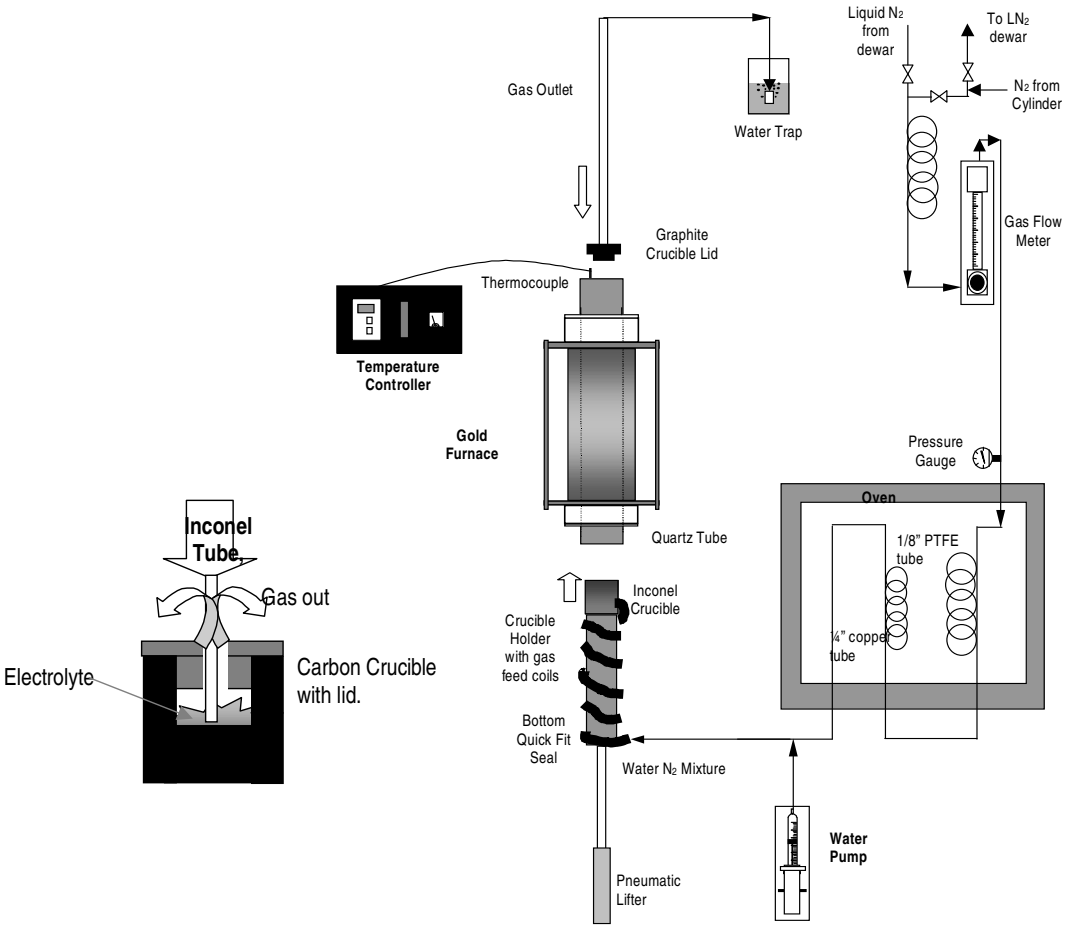

Figure 6.10 – The Humidity Trials Set Up.

Nitrogen cover gas is heated to 150^{O}C in an oven and water is injected into the heated outlet flow using a syringe pump. The humid flow is then feed into a furnace containing the bath particulate material in a sealed inconel crucible for a fixed residence time. Emissions are then scrubbed through a water container. The fluoride content before and after is determined using XRF. Filter alumina (a high bath species content material (i.e. $Na_aAl_bF_c$ derivatives – mainly chiolite and cryolite) sampled from a dry scrubber filter residue) was used to simulate the bath particulate component. Here the simulated particulates fines was heated in different moisture content environments for 4 and 8 hours trials. Hydrolysis reactions were accelerated by passing humid air over and through a heated electrolyte at various humidities.

The normal condition for the trials were heating a normal bath composition (4% CaF_2, 10% excess AlF_3, 0% initial Al_2O_3), with a 2L/min dry N_2 cover gas. All relative humidities quoted refer to a ideal RH% calculated at 25^{O}C. The trials conducted were as follows:

Table 6.1 – The bath vapour hydrolysis trials conditions.

Temperature (^{O}C)	Residence Time (h)	Humidity (%RH_{25})
300	4	0, 50,100,200
300	8	0, 50,100,200
500	8	0, 50,100,200
600	4	0, 50,100,200
600	8	50
800	4	0, 50

6.1.3. Experimental Results.

The experimental results follow the HSC predicted trends reasonable well. The results for all the comparable hydrolysis trials in the study are presented in figure 6.11. These are then compared by temperature and humidity in figure 6.12.

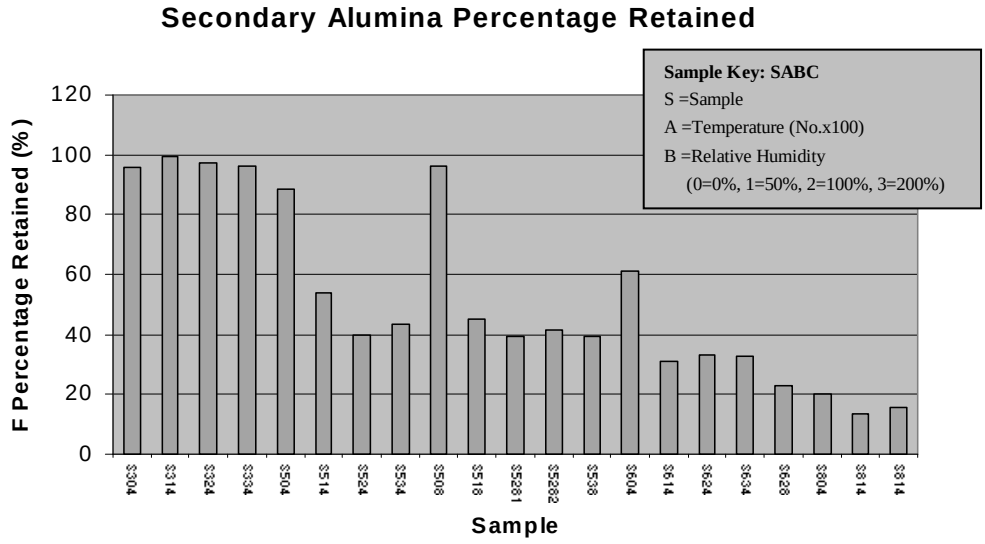

Figure 6.11 - Percentage retained of bath materials hydrolysed under different humidities.

As described by the HSC data, the expected trends on temperature decomposition and humidity hydrolysis are evident. Here (refer to figure 6.11) important amounts of HF are not released until after 300^{O}C, with a significant amount not evolved until past 600^{O}C. By comparing these results to the HSC results for the individual component hydrolysis and heating analysis it can be concluded that at high temperatures (here

represented by the results at 800^{O}C) the fluoride product is released by simple volatilisation reactions with minor stripping improvements with extra moisture in the cover gas. At lower temperatures (here represented by the results at 500^{O}C) the effects of the extra moisture are more marked. Very little fluoride is lost with no moisture in the cover gas, but around half is lost once moisture is introduced (50% RH_{25}). Further stripping improvements are made with increased moisture content. This is seen clearly when results for simple heating (volatilisation) and thermal hydrolysis (with residence time of 4h) are compared in figure 6.12:

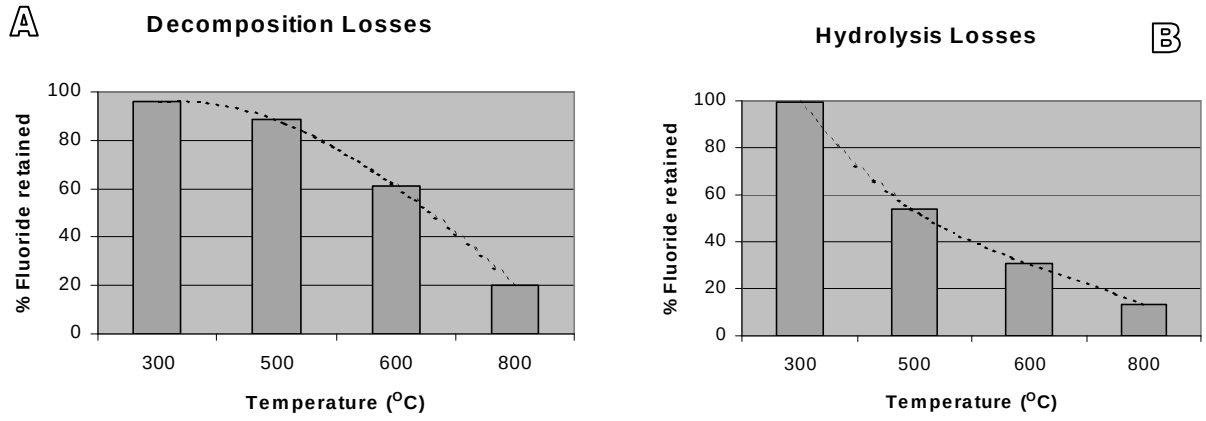

Figure 6.12 – Comparing simple heating with hydrolysis heating of the simulated particulate material. (A)Volatilisation (RH=0%@25^{O}C, 4h). (B)Hydrolysis (RH=50%@25^{O}C, 4h).

Figure 6.12(A) illustrates that the decomposition losses are very minor until past 600^{O}C. Heating in the presence of moisture (figure 6.12(B)) strips the fluoride at a much lower temperature. Certainly hydrolysis promotes HF generation, especially at high temperatures. This is similar to the results for the HSC simulated particulates. However unlike the trends predicted in the thermodynamic analysis there is some fluoride loss during heating above 600^{O}C. This is likely to be a decomposition reaction though moisture could be evolved at the higher temperatures from either the alumina etc. It is more likely that fine particulates are formed which escaped with the cover gas to reduce the fluoride content of the tested material. However this is a further example of the limitation of the HSC predictions.

6.1.4. Industrial implications.

As Henry [2] proposed, hydrolysis does not occur to any significant degree in the duct nor above the crust in the superstructure because the temperature of the moisture

containing air is not high enough. Instead he noted that "thermal hydrolysis or reaction of solid or vaporised fluorides with water vapour at elevated temperatures takes place primarily at the point where the hot gases escape through vents in the crust". As for lower temperature hydrolysis, Wedde [44] and found that there were minor emissions in his experimental temperature range (70^{O}C to 170^{O}C). These emissions (0.8 mg/Nm^3 at 130^{O}C) are not significant in the generation order of magnitude (10 to 200 mg/Nm^3). Hence the HSC results, Wedde's results and this study findings show that low temperature hydrolysis is not a significant HF generation source. This means that insignificant secondary hydrogen fluoride generation occurs above the cells crust.

All the thermal hydrolysis results are verified by both the HSC calculations and experimental results. These illustrate that a temperature above at least 300^{O}C is required before even a minor amount of HF is stripped from the particulates. The gases in both the extraction system ducts and above the cell rarely reach temperatures above 200^{O}C. It is thus unlikely that any particulate hydrolysis occurs within this realm. However these temperatures are reached within the gases escaping through crust cracks and open feeder holes (in point fed cells). Here, especially with flaming (caused by the gas burning reaction of $2CO + O_2 = 2CO_2$) hydrolysis is very likely due to the thermal energy provided by this reaction. Hence thermal (crack with flame) hydrolysis has been shown by these experimental results to be quite feasible. Here the moisture would be provided by either humid air (provided from the ambient air through the extraction system) or electrolyte water (water either evolved from an electrolytic reaction, from the anode or lost off the fed alumina). In either case this study shows even a minor amount of water at temperature above 400^{O}C can cause a significant amount of hydrolysis.

This has implications on the feeder hole state also. During the industrial investigations it was observed that the open feeder holes, especially the center holes, had a tendency to flame. Once the feeder hole was closed both HF levels and duct temperature dropped. The loss in duct temperature and HF levels has in the past been attributed to simple mass and heat transfer resistance increases from the alumina filling the hole. However the lack in thermal hydrolysis from this open feeder hole will also contribute to this effect. Given this and the effect of effective covering reducing both vapourisation and thermal hydrolysis suggests that crust integrity as the important factor of the background emission, and a easily controllable factor in reducing the overall HF emission.

Overall, depending on the crust integrity and feeder hole state, a large proportion of the overall HF particulate emission undergoes thermal hydrolysis. This will depend on flame temperature, alumina moisture content and ambient air moisture content. This makes this hydrolysis content difficult to predict, but an easily controllable content due to its dependence on crust integrity. This will be further illustrated when analysing the industrial emission data.

6.1.5. Conclusions.

These laboratory results compared with the thermodynamic analysis and with past research lead to the conclusion that little hydrolysis occurs above the cell due to the temperature of the duct gases (90 to 130^{O}C). Particulate hydrolysis is only significant at temperatures above 400^{O}C. Hence the most likely mechanism for the hydrolysis of the particulates is thermal hydrolysis at the crust-air interface, where flame hydrolysis could provide sufficient energy for these reactions to take place This is consistent with past literature [2]. Moisture is most likely provided from the added alumina, unreacted anode hydrogen and ambient air.

From all the past research results (both literature and this study) it was proposed that depending on the crust integrity and feeder hole state, a large proportion of the overall HF particulate emission undergoes thermal hydrolysis. This will depend on flame temperature, alumina moisture content and ambient air moisture content. This makes this hydrolysis content difficult to predict, but a controllable content due to its dependence on crust integrity.

6.2. Desorbed Fluoride.

It was established in section 2.2 that the generated fluoride emissions are extracted from the enclosed smelting cell to a dry scrubbing process which utilises primary (unfluorinated) alumina as the adsorbant. However within this system there is the potential for this *adsorbed* fluoride being desorbed during the feeding procedures due to the high temperatures it experiences entering the bath. It has been suggested (refer to [30]) that if significant amounts are lost then a fluoride recycle load within this extraction system may occur. This secondary emission source will be referred to as desorbed fluoride. It was the aim of this section to establish the extent of this fluoride generation source.

6.2.1. Laboratory Methodology.

EQUIPMENT.

Alumina saturated with fluoride using the fluorination method established by Gillespie [31] (refer to Appendix 1) was fed to a purpose built furnace. The final design used during the duration of the investigation is illustrated in figure 6.13. The reactor consists of the gold furnace with an internal 60mm OD x 53mm ID x 650mm long quartz tube. The bottom tube has been designed to be removable and is sealed using a pneumatic cylinder/lifter. Cover gas (a fixed mixture of nitrogen and humid air depending on the trial) enters from the bottom and fluorinated air exits through the top vent. These off gases then pass through a teflon tee which splits the flow approximately 1:10. The majority of the flow passes to the TISAB solution for fluoride detection using an ion selective electrode. The remainder of the split passes through a MgO fluidised bed reactor to remove the HF, through a flow meter to measure the outlet flow, then to a thermocouple and humidity sensor to determine the water content of the outlet stream.

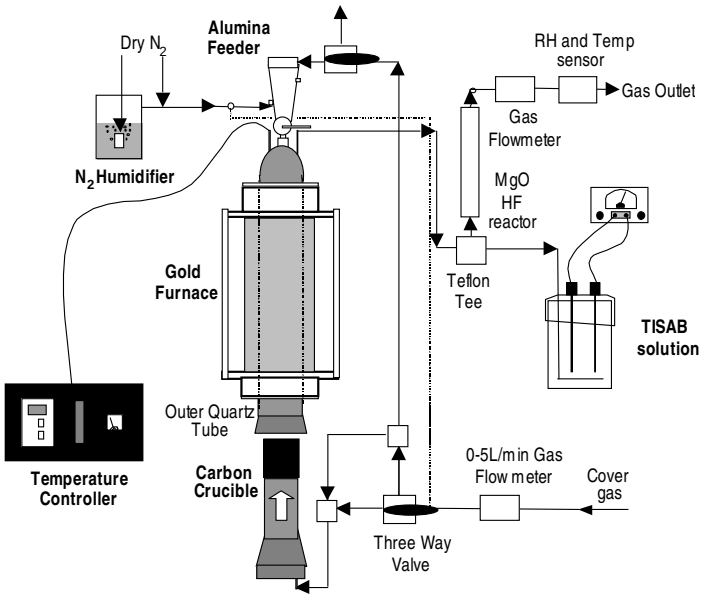

Figure 6.13 – The Emissions Reduction Rig Set Up.

An integrated moisture content value is determined for comparison using $CaCl_2$ to adsorb the water after it passes through the thermohygrometer.

A constant humidity flow was achieved by mixing saturated N_2 flow with a dry N_2 flow. Humidity is varied by changing the flow ratio (and hence the H_2O partial pressure in the outlet stream). The N_2 stream is saturated (100%RH) by bubbling the flow through water at a controlled temperature (usually 30 – 35^{O}C). The relative humidity is monitored using a thermohygrometer.

The N_2 flow in, H_2O flow stream, furnace temperature, TISAB temperature, ion selective electrode readings, outlet humidity and humidity temperature are all logged.

PROCEDURE.

In situ heating.

10 grams of fluorinated alumina was placed in a graphite crucible and inserted into the furnace at 25^{O}C. The furnace was sealed, ion selective electrode set up and data logger started. The furnace was heated at 70^{O}C/hr to 100, 300, 500^{O}C in separate trials. A ramped temperature trial at all these temperatures was conducted also.

Shock heating.

10g of fluorinated alumina was added to the emissions rig preheated to 100, 300, 400, 500 ^{O}C respectively, via the alumina feeder.

Air Sample.

Shock heating the samples in air rather than nitrogen.

Control Samples.

Control samples were heated in a muffle furnace in replicate conditions to those used in

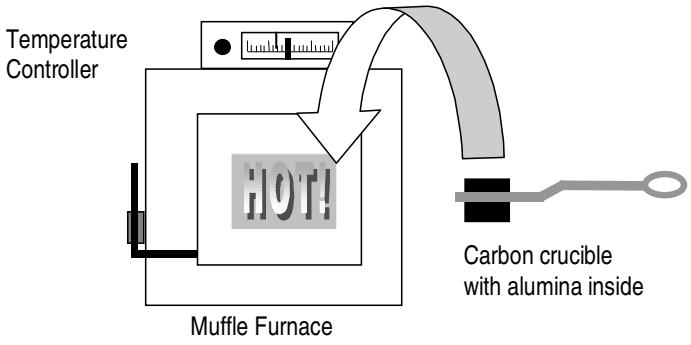

Figure 6.14 – The emissions control set up.

the simultaneous emissions run. Sample were heated for approximately 3 hours. The set up is illustrated in figure 6.14:

6.2.2. Alumina Properties.

The alumina used for the fluorination and desorption experiments fit the standard smelter grade properties outline in section 3.1 well. As expected the fines component was below 5% and the alumina had a BET surface area of ~67.5 m2/g. Both are within acceptable limits. However if the XRD scan of the alumina is examined (figure 6.19), the alpha content of the alumina is found to be lower than a standard alumina. LOI(300) = 3.0 wt% is high for a smelter grade alumina as is the LOI(1000)= 1.3 wt%. This is due to the high gamma content of the alumina.

6.2.3. Laboratory Desorption Results.

Figure 6.15 illustrates the major findings of the heating fluorinated alumina study. As with previous literature (for example Hyland *et al.* [32]) this study confirms that the reaction layer on the alumina surface dehydrates when it encounters a conventional thermal gradient (i.e. not sharp) at temperatures below 350^{O}C with little release in HF, and releases more significant amounts of HF when heated to temperatures above 350^{O}C. In this respect the run illustrated in figure 6.15a is the most interesting, as the alumina was held at progressively higher temperatures and the fluoride emissions measured. Looking at the results it is quite obvious a there is a rapid evolution of fluoride once the temperature passes ~380^{O}C.

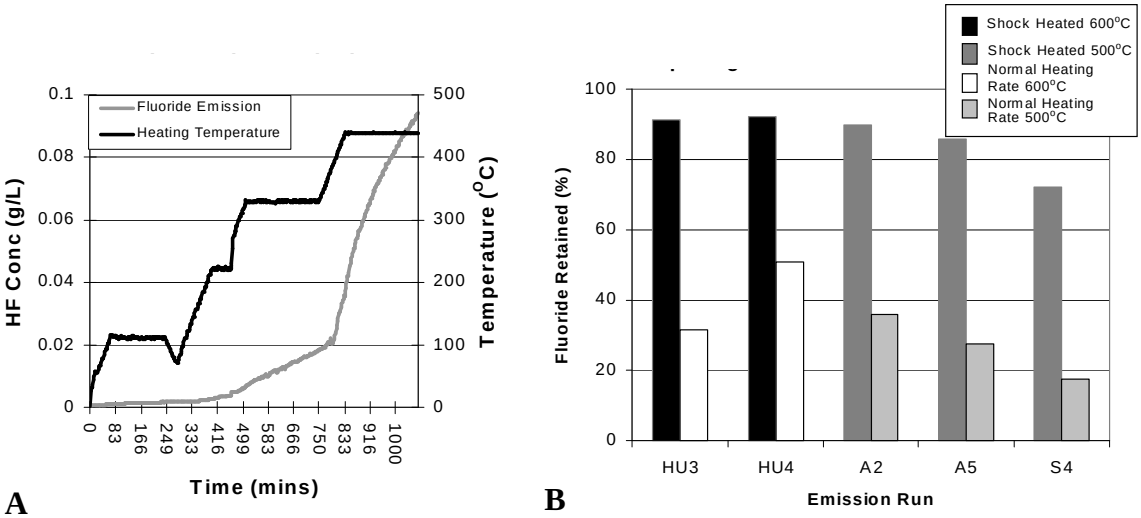

Figure 6.15 - Heating fluorinated alumina. (A)Insitu heating. (B)Comparing surface fluoride retention.

The XRF results for such comparison trials (HUC) compared with the equivalent emission runs (HUE) are listed in table 6.2.

However if the surface fluoride retention results in figure 6.15b and table 4.2 are examined the insitu and shock heating aluminas have retention results which are not consistent with the published literature results, and are quite different to the furnace heated control results. Haverkamp [45], Hyland [32] and Gillespie [31] report less than 50% fluoride retention above 500^{O}C (refer to section 4.6.5). Clearly this is not the case for the emission rig heated samples.

Table 6.2 – Comparison of the XRF results for the relevant emissions runs.

Sample	Ad Run	F (%)	E Run	Temp (^{O}C)	F (%)	F Loss (%)	% Retained (%)
***Insitu Heating** – All Emission Rig*							
1	-	-	EM9A	100	8.333	1.5x10^{-4}	100.00
2	AD13	6.518	EM11	500	6.667	-0.148	102.269
3	AD16	7.975	EM12	500	7.844	0.131	98.357
***Shock Heating** – All Emission Rig*							
4	AD17	7.654	EM13	300	7.987	-0.3326	104.345
5	AD18	7.970	EM14	400	7.915	0.0549	99.311
6	AD19	8.257	EM15	500	8.726	-0.469	105.674
***Control Samples** – HUE – emission rig, HUC - Control*							
1	AD22	7.844	HUE3	600	7.157	0.687	91.242
			HUC3	600	2.464	5.380	31.416
2	AD23	12.068	HUE4	600	11.145	0.923	92.347
			HUC4	600	6.132	5.936	50.810
3	AD24	8.165	HUE5	700	7.749	0.416	94.905
			HUC5	700	1.591	6.574	19.486
4	AD25	6.937	HUE7	700	7.029	-0.092	101.326
			HUC7	700	1.477	5.460	21.291
5	AD26	8.394	HUE8	500	7.418	0.976	88.373
			HUC8	500	2.425	5.969	28.890
6	AD27	8.571	HUE11	500	8.110	0.461	94.621
			HUC11	500	6.045	2.526	70.529
7	AD29	8.081	HUE9	500	8.283	-0.202	102.500
			HUC9	500	5.051	3.030	62.504
8	AD30	8.185	HUE10	500	7.914	0.271	96.689
			HUC10	500	6.045	2.140	73.854
***Air Samples** – AE – Emission Rig, AC - Control*							
1	AD33	7.525	AC1	500	6.410	1.115	85.783
			AE1	500	7.174	0.350	95.344
2	AD32	7.976	AC2	500	2.877	5.099	36.074
			AE2	500	8.053	-0.077	100.970
3	AD34	8.525	AC3	500	7.911	0.6141	92.796
			AE3	500	3.460	5.065	40.588

Peripherals Reversed

The control samples show a different result The measured fluoride retention follow the trends in the published literature. Clearly there must be a difference in the fluoride evolution process between the furnace heated samples and the emission rig heated samples. It is proposed that the amount of fluoride evolved differs depending on the rate of heating of the alumina. Here the rapid heating of the emission rig (labelled **"shock heating"**) may not allow the conventional fluoride loss mechanism to occur. Instead the surface fluoride and water are retained with the rapid temperature change. This large influx of heat may provide the activation energy to initiate these reactions. Hence

the surface products dissociate differently when heated at different rates. This can be established by examining the surface product.

6.2.4. Surface Analysis.

The following sections will illustrate, the phases formed on by shock heating the sample differ considerably from those on the furnace heated control samples and hence dissociate differently when heated.

6.2.5. SEM Investigation

Figure 6.16 compares the surface morphology of two alumina surfaces. The first is a plain unfluorinated sample compared to a fluorinated sample (surface fluoride content ~8%). The second compared an adsorption run and the two resultant surfaces from the emission rig shock heating and the conventional furnace heated samples. From both sets of images significant differences in the surface morphologies of each sample can be seen. However it must be noted that some crystal growth has occurred after adsorption and heat treatment of the specimens in figure 6.17 (the second investigation). Such ageing is expected and corresponds to known behaviour for alumina and has been reported by Gillespie [31]. These crystals are the results of hydration of the surface product aluminium hydroxyfluoride, $AlF_x(OH)_{3-x}.6H_2O$. It must be noted that EDAX surface analysis proved inconclusive due to the elemental limitations[2] imposed by the SEM construction. XPS analysis however (detailed below) is a applicable substitute for this.

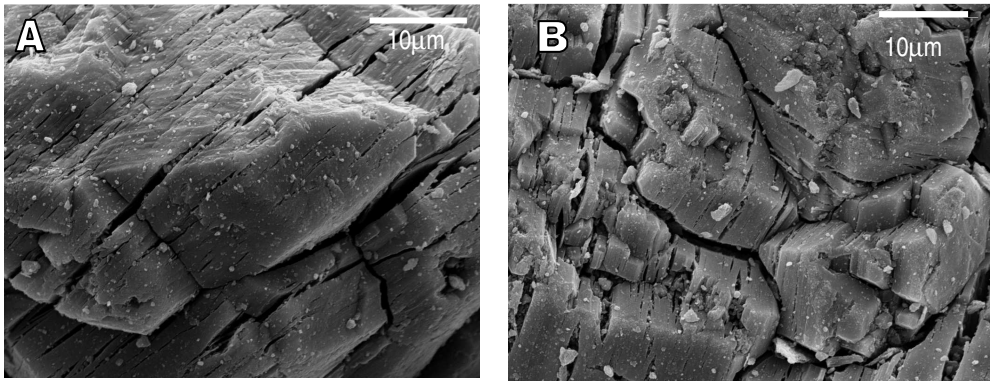

Figure 6.16 – Comparison of alumina particles at 2500x.
(A)Unfluorinated. (B) Complete Fluorination.

[2] This investigations SEM EDAX instrument can only detect elements greater than Na.

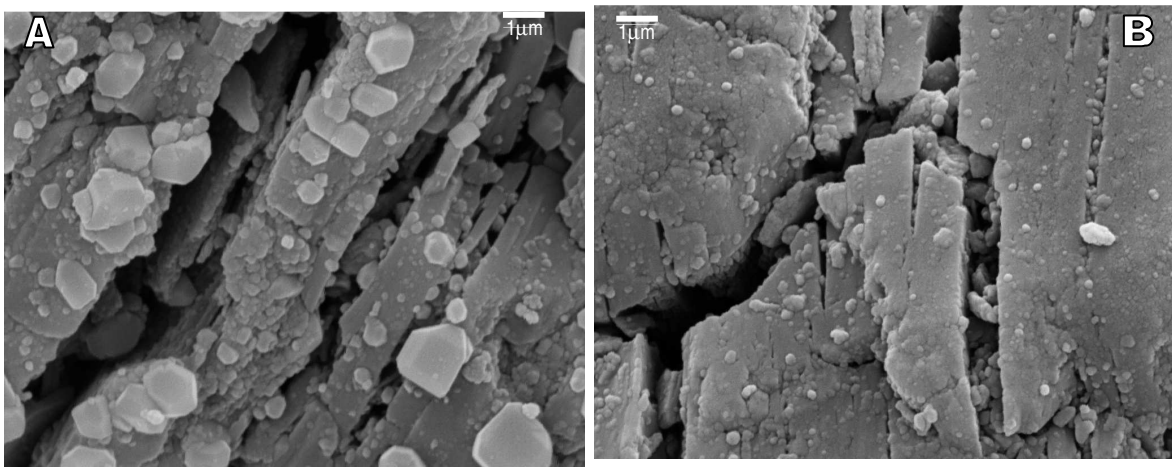

Figure 6.17 – Comparison of 600^{O}C alumina surface heating runs.
(A)Emission Heated Sample. (B)Control Heated Sample.

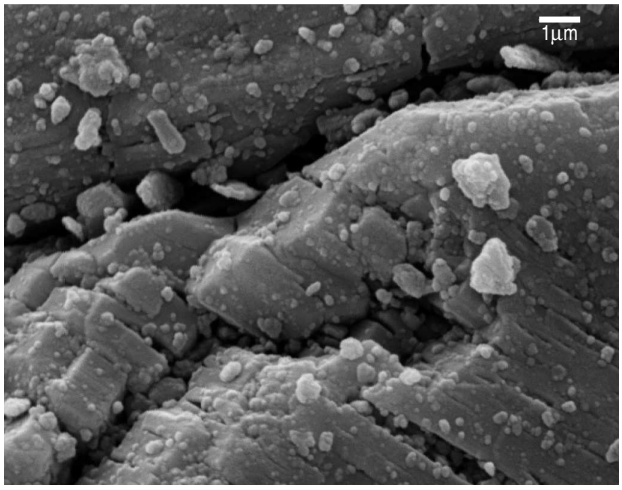

Figure 6.18 – Aged Adsorption Run (AD13) – 6.5wt% fluoride on surface .

Comparing the surfaces of unfluorinated alumina and fluorinated alumina (figure 6.16) definite crystal growth is seen on the surface once the particle is fluorinated. These crystals are sites of fluoride growth. As Gillespie [31] found, a thin layer of structural aluminium hydroxyfluoride, $AlF_x(OH)_{3-x}.6H_2O$, was formed in an aqueous reaction at the alumina surface. At low relative humidities (here fluorination was conducted at RH=4% so is in the RH_{low} regime) little crystal growth is seen in an un-aged sample (figure 6.16b) with the fluoride formed on a thin layer. Once aged with humidity (figure 6.17) the product layer is transformed into distinct crystallites of aluminium hydroxyfluoride by a dissolution/re-precipitation mechanism involving water filled pores. In the heat treated samples (figure 6.17) the crystals have grown significantly.

As explained above the crystals are the result of hydration of the surface fluoride product. However the surfaces of the emission samples and control are significantly different. Referring to table 6.2, there is a vast difference in the fluoride lost in both

humid emission samples. The emission lost around 10wt% of its surface fluoride compared to 70% in the control sample. This is reflected in the surface morphology. The distinct reduction in the crystal size and forms, points to vastly different mechanisms occurring during heat treatment. Note that the surface of the second control sample show evidence of similar crystal growth as the first. Again this sample has lost only 50% of its surface fluoride, giving it a distinctly different surface to the first control surface. Clearly the surface product of the furnace heated sample is lost while that of the emission rig is retained. Mechanistically there must be a difference in the process.

6.2.6. Adsorption Ageing.

XRD analysis also distinguishes the changes on adsorption ageing. There are significant differences between the traces of a freshly fluoride adsorbed specimen and one that has been left to age for weeks (even months). Presented in figure 6.19 is a comparison of the same adsorption sample (adrun21) analysed using XRD when freshly adsorbed (B) and then three months later (C) having aged in the sample container. As before, the freshly adsorbed sample differs little from the unadsorbed alumina. This is seen in the hydro primary adsorption samples also. However there are significant difference in the fresh sample (B) and aged sample (C) traces as marked out by points a. A comparative analysis of standard traces identifies these new peaks as two aluminium hydroxyfluoride phases $Al(OH,F)_3.0.375H_2O$ and $AlF_{1.65}(OH)_{1.35}.xH_2O$. These findings are consistent with that found in previous studies [31].

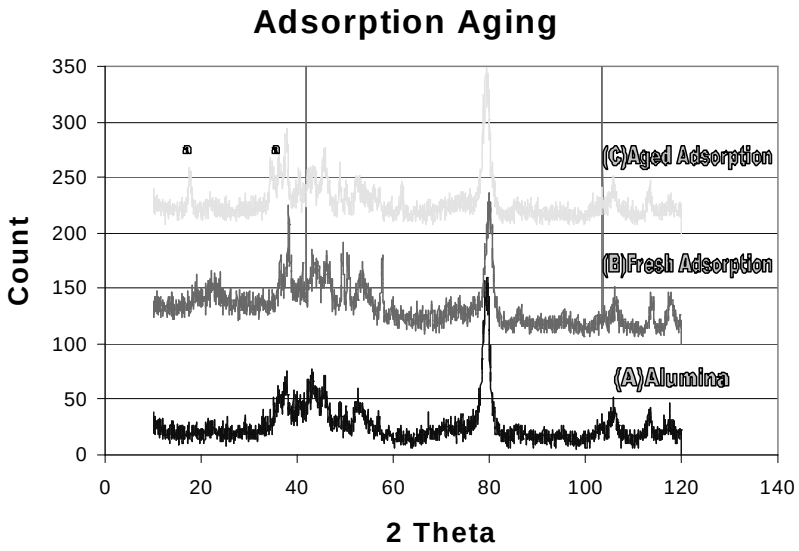

Figure 6.19 – Adsorption Ageing. (A)Adsorption Alumina. (B)Fresh Adsorption Sample 21. (C)Adsorption Run 21 aged three months.
Characteristic Peaks: (a)Aluminium Hydroxyfluoride.

6.2.7. Surface Comparison.

Surface analysis using X ray diffraction (XRD), X ray photoelectron spectroscopy (XPS) and a scanning electron microscope (SEM) was conducted on an adsorption and Emission sample to confirm and expand on the findings. However it was found that the other techniques provided little extra information and as with previous studies [16] [31] XRD provides the most valuable information with regard to the surface structure. What the investigation does show, are comparable data on surface composition and in the SEM case, an idea of the morphology changes occurring on the surface.

Adsorption Sample (Run 32).

Presented in figure 6.20 are the collected results from XPS, XRD and SEM analysis of adsorption run 32. The XRD scan indicates that the sample has aged (note the peak at 18 2θ) though the SEM images do not show the characteristic crystal growth. The two XPS deconvoluted fluoride peak positions (685.38 and 686.67) are more uncertain. One of the peaks is likely to be $AlF_3.3H_2O$ (686.3), though the other does not match any recorded data. What is known is that it is not NaF (684.5), it is likely an aluminium hydroxy fluoride species. This can not be confirmed by the aluminium 2p peak scan as the Al_2O_3 peaks dominate the positions, as illustrated in figure 6.22.

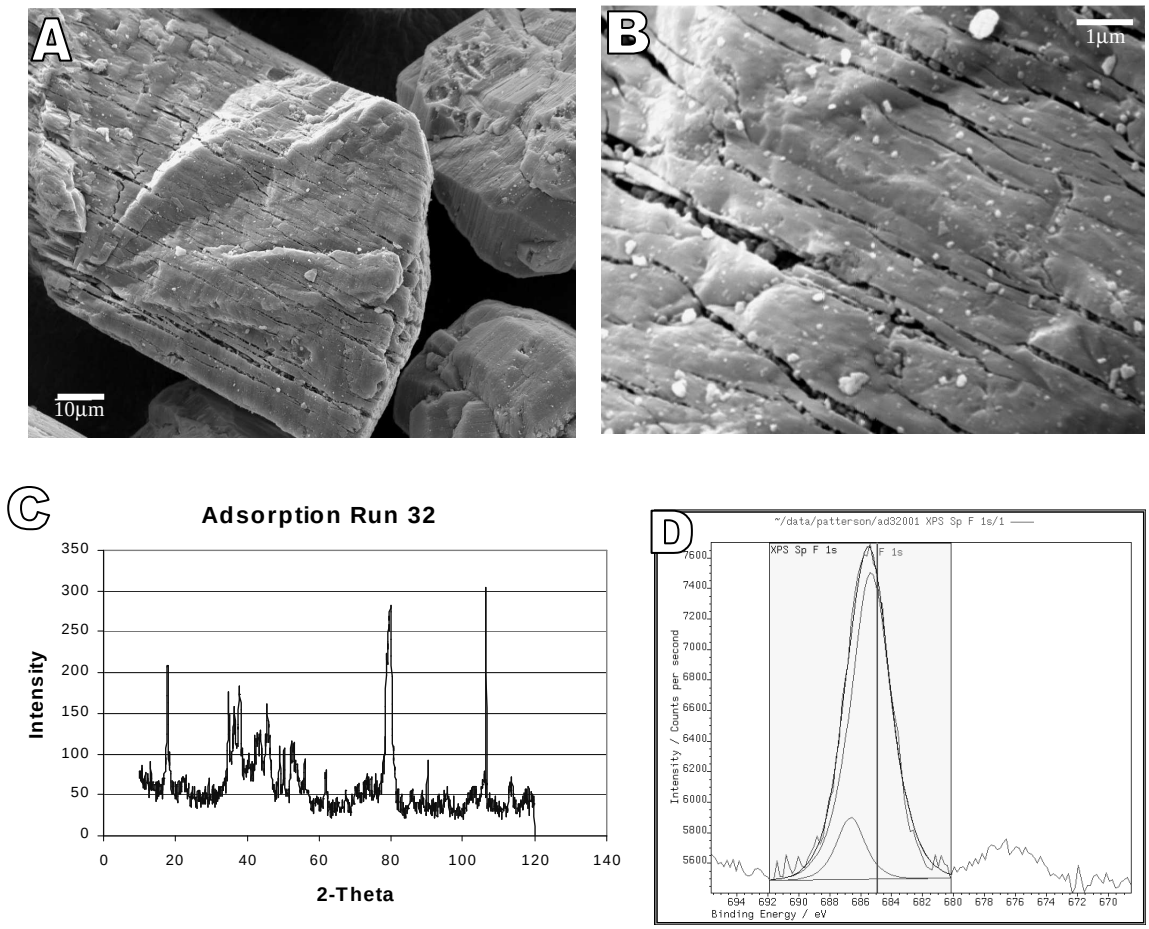

Figure 6.20 – Surface Analysis results for Sample Ad32. (A)SEM Image at 1050x. (B)SEM Image at 8400x. (C)XRD Scan. (D)Fluoride XPS Peak.

Emission Rig Heated (Run A2).

As previously figure 6.21 presents the collected results from XPS, XRD and SEM analysis of adsorption run 32. Unlike adsorption 32, the SEM and XPS results indicate that little ageing has occurred to this sample. Again the XPS deconvoluted fluoride peak positions (at 686.1 and 687.81) have uncertain results. Notably the entire peak has been shifted differently to that shown by the adsorption sample. This indicates that different surface fluoride species occurs on each sample. However it is likely that one of the peaks is $AlF_3.3H_2O$ (686.3), though the other does not match any recorded data. This peak position differs from that found on the adsorption sample, inferring a species change may have occurred on heat treatment (likely dehydration). However it is likely to be another aluminium hydroxy fluoride species. The aluminium peak for the emission sample does help the analysis as it contains a peak not corresponding to the oxide. This is discussed in the next section.

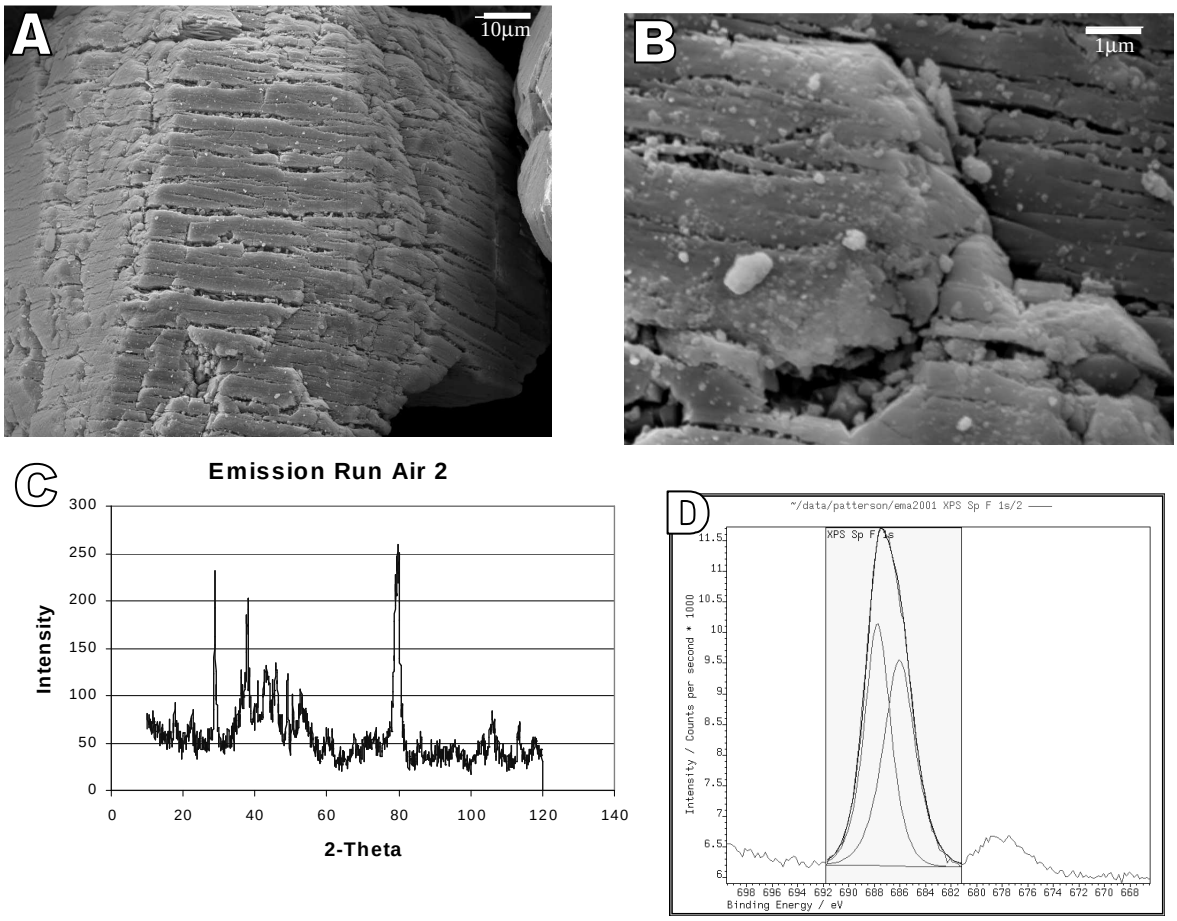

Figure 6.21 – Surface Analysis results for Sample EmissA2. (A)SEM Image at 1050x. (B)SEM Image at 8400x. (C)XRD Scan. (D)Fluoride XPS Peak.

6.2.8. XPS Surface Analysis.

The XPS also gives data on the surface composition of the samples. Table 6.3 compares the qualitative results gained.

Table 6.3 – Comparing Surface Compositions of Ad 32 and EmissA2.

Peak	Adsorption Run 32		Emission Run A2	
	Atomic Conc %	Mass Conc %	Atomic Conc %	Mass Conc %
F 1s	5.41	5.67	15.39	15.90
O 1s	47.37	41.77	37.91	32.99
C 1s	21.01	13.90	20.39	13.30
Al 2p	25.71	38.26	23.43	34.40
Na 1s	0.06	0.08	2.47	3.09
N1s (Adsorbed)	0.43	0.33	0.42	0.32

As expected [31] the sodium (Na) concentration is minimal in the emission sample. It is speculated that NaF is evolved at quite low temperatures. However the fluoride concentration on the surface of the emission sample is unexpectedly high. This compares to the XRF analysis which shows Ad 32 to have 7.92% F and EmissA2 to have 8.053% (i.e. around 8% for both samples). This indicates the fluoride is more concentrated on the surface of the emission sample than the adsorption sample, due to another species. An explanation for the higher fluoride concentration is evident in the binding energy positions (BE) of the emissions aluminium spectrum. Figure 6.22 shows the scans of each species is quite different.

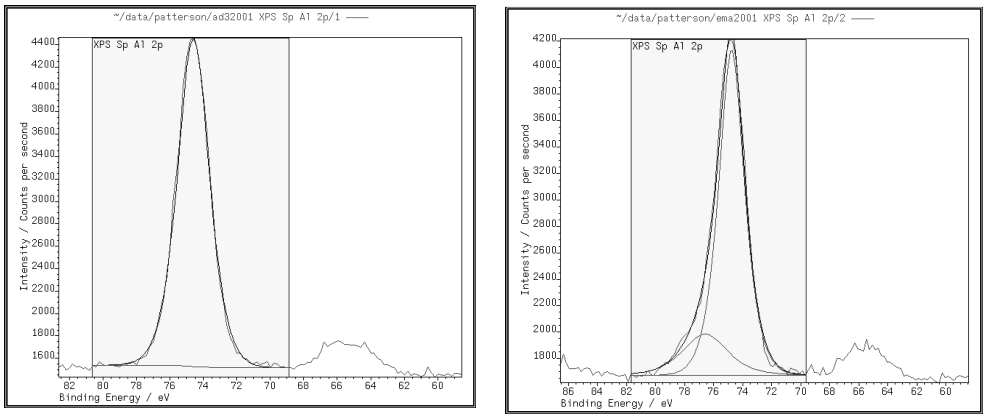

Figure 6.22 – Comparing the Aluminium XPS detailed Scans.
(A)Adsorption Run 32. (B)Emission Run Air 2.

By deconvoluting the peaks, it can be seen that a similar peak at BE~74.7 (74.629 for Ad32 and 74.856 for EmissA2) corresponds to the Al_2O_3 species. However the higher binding energy shoulder on the emission sample (at BE 77.505) indicates another aluminium species (likely a Al-F bond) occurs on the surface. This is perhaps responsible for the higher surface fluoride concentrations. This has to be substantiated with further XPS analysis.

6.2.9. Emissions Stages.

Illustrated in figure 6.23 are representative XRD plots of the stages in an emission reduction trial, containing the XRD traces of unadsorbed alumina, adsorbed alumina and control and shock heated emission samples. Initially the alumina (A) has no fluoride adsorbed on the surface so this can be treated as the base scan. Little difference can be seen between the adsorbed alumina (B) and control heated sample (C). However the shock heated emission specimens trace (D) has two points of differences highlighted (characteristic points a and b). Analysis of these peaks with reference to XRD standard

traces have identified the species as aluminium fluoride AlF_3 (but not the β and γ phases) and aluminium hydroxide $Al(OH)_3$. Previous studies [33] have postulated that *structural aluminium hydroxyfluoride*, $AlF_x(OH)_{3-x}.6H_2O$ is formed in a thin layer, which appears amorphous to x-ray powder diffraction and can not be detected. This study confirms this layer dehydrates when it encounters a conventional thermal gradient (i.e. not sharp) at temperatures below 450^OC with little release in HF and releases more

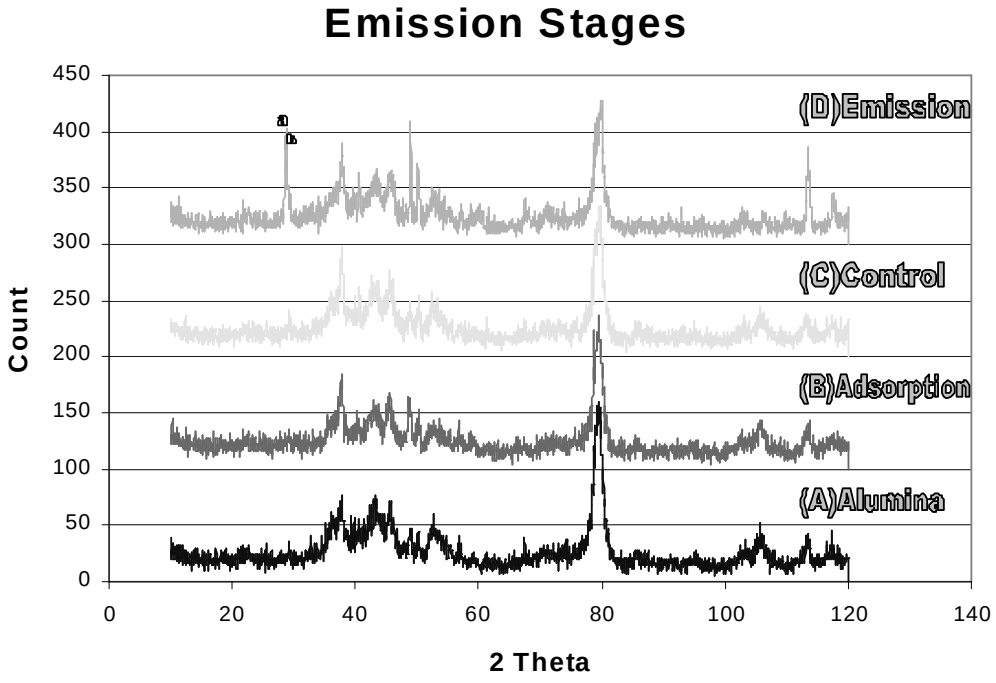

Figure 6.23 – The stages in an emission trial. (A)Adsorption Alumina. (B)Adsorption Run 35 (Fresh). (C)Emission Run 4 – Control. (D) Emission Run 4 – Emission. Characteristic Peaks: (a)AlF_3 Peak. (b)$Al(OH)_3$ Peak.

significant amounts of HF when heated to temperatures above 450^OC.

The shock heating mechanism is obviously different to this, in that it results in little HF being released at any temperature due to a surface reaction causing the aluminium hydroxyfluoride to be converted to aluminium fluoride and aluminium hydroxide. The hydroxide are likely the crystals found on the surface of the emission specimens shown in figure 6.17 and 6.18. Furthermore, it is speculated from these initial results that the temperature gradient is so great that once dissociated the water and fluoride (likely in the form of HF) do not have time to escape from the crystal structure but rather have sufficient energy to react with the alumina to form aluminum fluoride and hydroxide, much in the same way aluminium fluoride is formed in industry [46] as shown in the following reaction.

$$6HF + Al_2O_3 \xrightarrow{400-600^O C} 2AlF_3 + 3H_2O \quad (6.7)$$

It is interesting that similar results as these were found in 1967 by Russian researchers Bulgakov and Antipina [47]. They found by reacting alumina with aqueous HF (for an unspecified time period – assumed to be short though) "leads to the formation of basic aluminium fluoride hydrates, which are converted on heating (at 500^{O}C) into basic aluminium fluorides". The proposed reaction was:

$$Al_2O_3 + H_2O \longrightarrow Al(OH)_3 \xrightarrow{HFsoln} Al(OH)_2F \xrightarrow{HFsdn} Al(OH)F_2 \xrightarrow{HFSdn} AlF_3 \quad (6.8)$$

Certainly the form of the water is more likely to be adsorbed, but the hydroxyfluoride species is along similar lines to those found in previous studies. The fact that aluminium fluoride was formed at the end may have resulted from the high fluoride concentration on the surface.

Given all this, if this is applied to an industrial situation, the age of the alumina, the temperature it is heated to while sitting in the feeder bin and how fast it is added to the crust, will determine the amount of fluoride lost before the secondary alumina reaches the bath. In theory a point fed cell, with a large bulk of secondary alumina should not lose much of the adsorbed fluoride as it is fed quite quickly to the cell. However secondary alumina has other fluoride components other than adsorbed fluoride, and it may be these which produce significant amounts of HF before bath reaction. The question is which mechanism – shock heating or conventional heating occurs in industrial point fed electrolysis cells.

6.2.10.Modelling Alumina Hydrolysis.

A thermodynamic analysis using HSC© thermodynamics package to identify the possible products pathways for alumina in an HF environment has been conducted. Figures 6.24 and 6.25 illustrate the effect of simply heating the alumina (simply Al_2O_3 with no separate phases) with HF compared with thermal hydrolysis conditions. As with predicted results for conventional heating of alumina, HF generation is only important above 350^{O}C and significant above 600^{O}C. The shock heating route is not predicted.

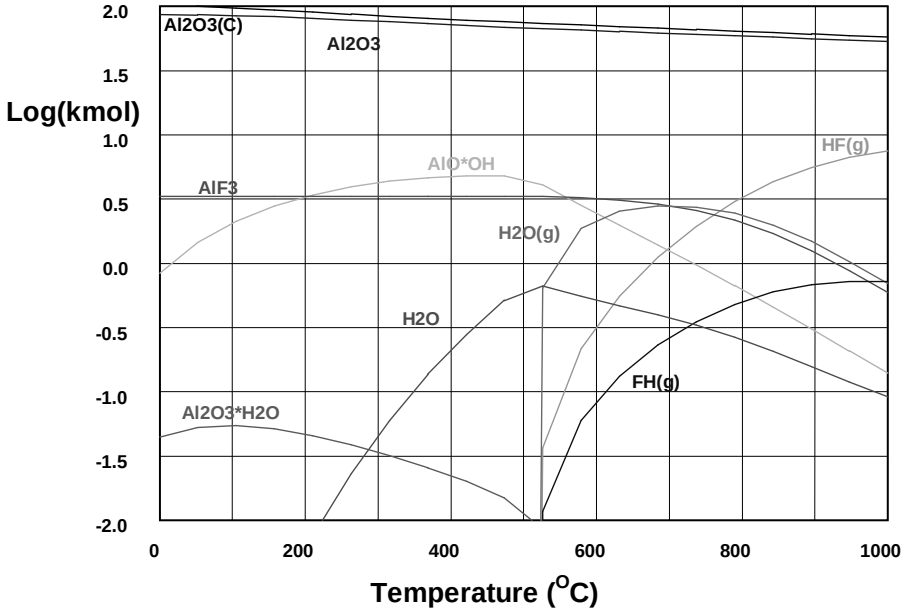

Figure 6.24 - Possible species upon heating alumina in an HF environment (10 mol HF, 200 mol Al_2O_3).

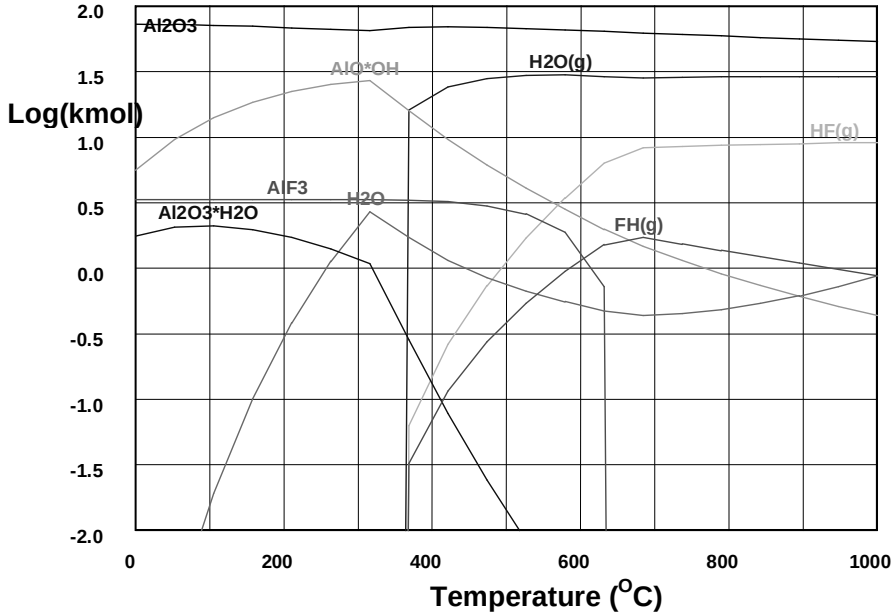

Figure 6.25 - Possible species upon heating alumina in an HF environment (10 mol HF, 200 mol Al_2O_3, 30 mol H_2O).

Here the thermodynamics predict that at lower temperatures AlF_3 is the stable phase with HF reacting with Al_2O_3 to form AlF_3, and at higher temperatures HF and Al_2O_3 are the stable phases (AlF_3 decomposes to form these). This is contrary to the XPS and XRD results in section 1.16 and 1.17 and Gillespies [31] results. Instead a complex hydrated species has been found to form, which has differing decomposition paths

depending on the heating rate. Here HSC treats the composition purely as a mixture, ignoring kinetic processes (such as shock heating), and species not included in its database. Hence it is not surprising that the reactions describe the normal heating reactions quite accurately, but fail to show the possibility of irreversible reactions on the surface due to extreme conditions. As stated in the introduction to this section, Gillespies model of fluoride adsorption [31, 33] contradicts all this, suggesting a reaction products other than AlF_3 forms on the surface. Regardless of any of this, the findings of this investigation indicate that the reactions are far more complicated than are simply indicated by the thermodynamic analysis.

6.2.11.Industrial Methodology.

Comparative testing of feeding primary (no reacted fluoride) and secondary alumina (contains reacted fluoride) should indicate whether adsorbed fluoride has any role in fluoride generation. It can be calculated by assuming an average s-alumina bath particulate species Na_2AlF_5, from the total fluoride content of 1.64% the amount of adsorbed fluoride is only 0.276%. This is a relatively small proportion of the real F content. As any comparison of the Na and F weight percentages shows (refer to figure 3.0), the F and Na trends are identical. This shows that most of the fluoride in the s-alumina is contained in the bath particulates which re-enter the bath upon feeding.

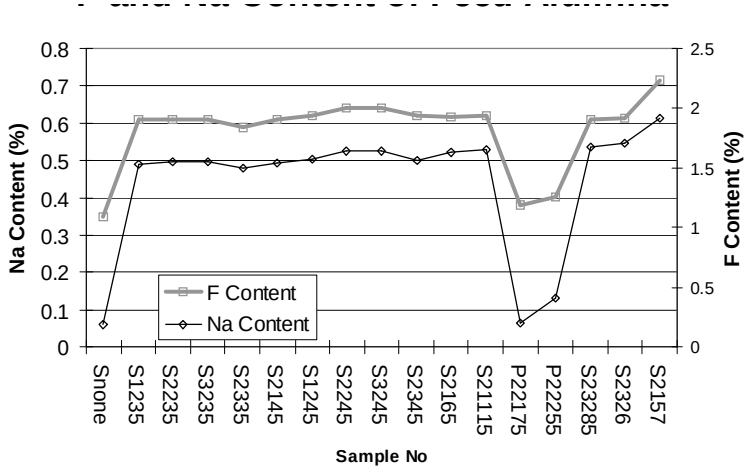

Figure 6.26 – Comparison of the F% and Na% of s-alumina analysis.

In emissions terms if this adsorbed content is all lost this equates to 0.4619 kg/h HF (assuming an average feeding rate of 2.65 kg/min alumina). This should show a detectable change if a significant amount of fluoride is desorbed.

Two separate trials on two different cell technologies were conducted. These are detailed below.

6.2.12.Primary vs Secondary Results.

Figure 6.27 illustrates the change from primary to secondary alumina feeding on a point fed, 200kA reduction cell. The primary alumina was fed after tapping around 21.30 and is definitely being fed after 03.00. As observed there is no significant change in the emission after adding primary alumina.

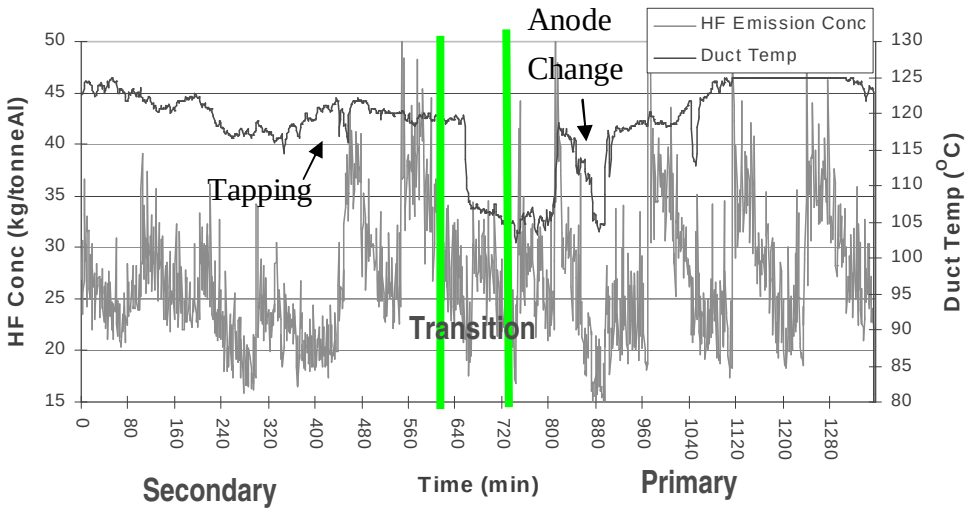

Figure 6.27 – The logged base emissions and temperatures followed by the transition from secondary to primary alumina fed for cell technology III.

Even though there is a significant difference between the alumina properties (refer to table 6.4), this does not effect the emission.

Table 6.4 – Comparing the properties of the cell technology 3 primary and secondary alumina.

Property	Primary	Secondary
%F (wt%)	~0	0.61
%Na (wt%)	0.42	2.09
LOI 300 (%)	0.98	2.31
LOI 1000 (%)	0.88	2.89

This means that the fluoride in secondary alumina is not lost before entering the bath, and that the extra moisture does not go into HF generation. This suggested that the additional fluoride on s-alumina was not a significant contributor to the fluoride emissions.

This result was also seen when comparing the emissions for similar humidity and operation schedules for cell technology I. Table 6.5 shows the average HF and particulate fluoride contents of the emission for feeding primary and secondary alumina.

Table 6.5 - Comparing batch measured fluoride generation contents for cell technology 1.

Type	Secondary	Secondary	Secondary	Primary	Primary	Primary
Date	5/5/99	6/5/99	9/7/99	19/5/99	25/5/99	27/7/99
Daily Cell Temp (^oC)	958	963	963	972	958	973
Average Duct Temp (^oC)	93.3	92.9	116	112	110	114
Gas Flow (Nm^3/h)	5 777	5 806	5675.12	5 541	5 677	5660.753
Particulate F (mg/Nm^3)	84.89	112.01	121.56	72.16	97.69	130.64
HF (mg/Nm^3)	198.7	240.4	311.31	163.0	216.5	310.02
HF (kg/h)	1.15	1.40	1.77	0.90	1.23	1.75
HF Percent (%)	70.1	68.2	71.9	69.3	68.9	70.4

Little change in both hydrogen fluoride and particulate generation is seen with the two different feeds. This suggests that very little of the fluoride is lost on feeding (up to 10% max is likely depending on feeder hole condition) due to the environment it experiences in the present point feeding technology. Given that the primary HF generation values are within the established baseline concentration limits (0.8 - 1.5 kg/h), it is easy to conclude that adsorbed fluoride is not an important factor in HF generation in these cells. Again when the continuous emission graph is examined, little change is seen in the emission once the transition from secondary to primary feed is made.

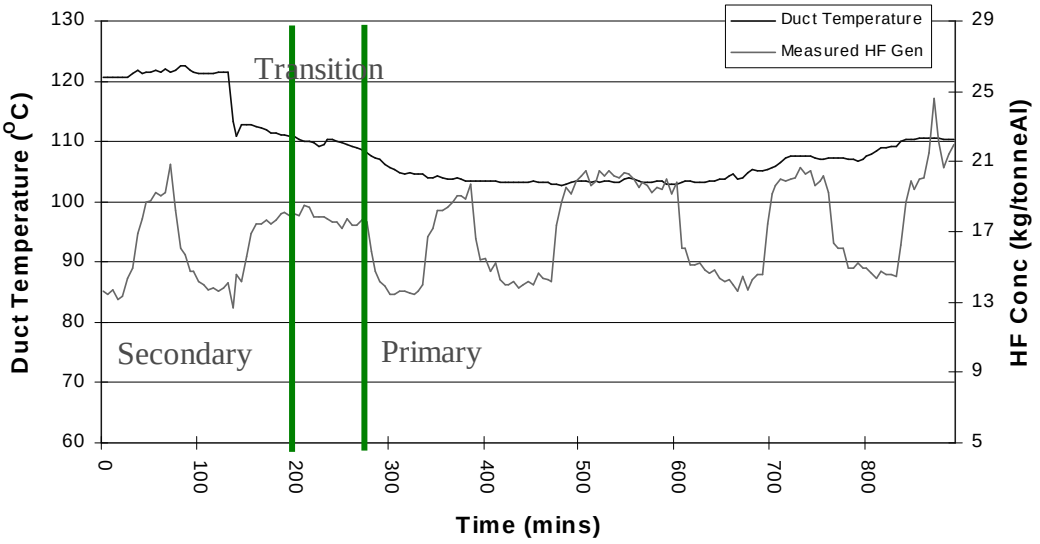

Figure 6.28 – The transition from primary to secondary alumina from cell technology I.

Again there is little change between primary and secondary alumina. Furthermore, unlike the feed technology dependance of the alumina feeding emission, the fact that the

fluoride does not desorb on feeding is not design related. As suggested previously it is mechanistic, related to the temperature change experienced on addition to the bath.

Due to the similarity in emissions between primary and secondary alumina emission it is likely that fluoride desorption from these industrial measurements follow the proposed shock heating scheme. The laboratory trials have shown that if the alumina is heated quickly little fluoride is lost, otherwise for significant fluoride generation to occur the alumina has to be heated above $350^{O}C$. When fed in a point fed cell the alumina undergoes a temperature change of almost $900^{O}C$ under 5 secs. This simulates the shock heating conditions of the laboratory trials. It is very likely that the reactions observed in the laboratory take place in point fed cells and this results in the similarity of primary and secondary emissions.

This also establishes the fact that the fluoride recycle load is not significant in these point fed cells. If no fluoride is desorbed from the fed secondary alumina then the speculated recycle load within the dryscrubbing cycle will not occur. Therefore in the context of an emission reduction program, this suggests that adsorbed fluoride is not an important contribution in HF generation in these cells and hence can be treated as a minor factor in emission control schemes.

6.2.13.Conclusions.

It is proposed that the amount of fluoride evolved when heated was dependant on the rate of heating of the alumina. In both the control heating samples and literature emission data the rate of heating is slow (heated in a static furnace and cold crucible) allowing the surface fluoride species to dehydrate and dissociate into HF, H_2O and Al_2O_3. However XRD studies of the shock heated alumina produced from rapid heating in the emissions rig (the alumina is added via a feeder to a preheated crucible) produces AlF_3 and $Al(OH)_3$ reaction products which retain almost 100% of the surface fluoride. XPS analysis shows differences in the surface products also, with a much higher surface concentration of fluoride on the shock heated samples.

It is proposed that the rapid heating does not allow the former mechanism to occur but traps both the fluoride and water with the rapid temperature change providing the activation energy to initiate these reactions. This traps the fluoride on the surface in the form of AlF_3 and $Al(OH)_3$, with a surface morphology much like that of an aged adsorption sample.

Applying this information to an industrial situation, it was postulated that the age of the alumina, the temperature it is heated to while sitting in the feeder bin and how fast it is added to the crust, would determine the amount of fluoride lost before the secondary alumina reaches the bath. In theory a point fed cell, with a large bulk of secondary alumina should not lose much of the adsorbed fluoride as it is fed quite quickly to the cell. This was seen in the industrial trials when comparing primary and secondary emission. No difference in emission was recorded for two independent reduction technologies when the alumina with reacted alumina was fed to the cell. It is likely due to the alumina being shock heated upon feeding (a $900^{O}C$ temperature change is experienced in a 5 second period) and retaining the fluoride before addition to the cell. This shows that adsorbed fluoride is not a significant contributor to an industrial cell emission and that the speculated fluoride recycle load with in the dryscrubbing cycle does not occur.

7. Industrial Emission Data.

As mentioned in chapter 5, three different cell technologies have been studied during the course of this investigation. The major differences were outlined in table 5.1. The following section aims to explore all the factors which affect the previously outlines emission contributors within a industrial hooded center point fed prebake aluminium cell. Comparisons from all three cell technologies will be used to illustrate the major factors which cause hydrogen fluoride emission changes.

7.1. Definitions.

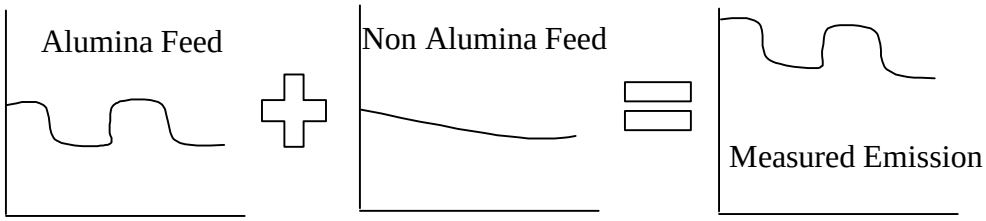

Figure 7.1 – The separated emission components.

Past emission studies [5, 6, 27] have used regression factors to find the relative amounts of the HF emission contributions. These have given numerical approximations to the contributions, but not fitted the mechanisms to complete satisfaction. This study has taken a different approach to simplify the analysis. Here a distinction has been drawn between the *alumina feeding contribution* and a *non alumina feeding contribution*. These are treated as two separate (but not mutually exclusive) components of the measured industrial emission data:

1). *Feed generated HF* – defined as those emissions generated from adding alumina to the electrolyte. This generation is considered to arise from the primary HF generation associated with the water content of alumina reacting with the electrolyte. The best characterisation technique of this content in the real emission data was found to be from the $D_{feeding}$ content (= the difference between the overfeeding (O) and underfeeding (U) generation content). It will be shown that little difference can be found in its value, when comparing various values of this factor during periods where no heat balance disturbances were affecting the cell.

2). *Non alumina generation content* – The contribution left once the alumina feed response is subtracted out of the measured emission. This contribution is thought to consist of secondary HF generation (thermal hydrolysis component at the crust vents), the dissolved water emission component and a constant amount of HF generated from the primary generation reaction of the hydrogen in the anodes. These seem to be the most likely sources of the HF emission present during zero feed conditions (during the tracking process). If these assumptions hold true, then this non alumina level is not affected by any repetitive process (unlike the under and over feeding steps of the alumina feeding cycle). This makes it a constant emission for a fixed alumina cell atmosphere and chemistry. The Δ correlation derived from these studies directly calculates the idealised non alumina levels (refer to section 7.2).

7.2. The Δ Correlation.

The derived Δ correlation is based on the assumption that the measured HF emission can be broken into two separate independent HF sources – non alumina and alumina feeding emission. It is assumed that cell factors affect both these contributions independently.

If this is true then:

$$\Delta = \frac{O}{A} - \frac{U}{\alpha} = \frac{-Bd}{(\alpha + d)\alpha} \qquad \therefore B = -\frac{\Delta A \alpha}{d} \tag{7.1}$$

Where:

U = Underfeed HF emission (kg/h). α = UF alumina feed rate (kg/min).
O = Overfeed HF Emission (kg/h). A = OF alumina feed rate (kg/min).
B = Non alumina emission (kg/h). D = U – O. d = A - α.

7.2.1. Derivation.

Ideal Scenario.

Here we assume that the HF generation is solely dependant on the alumina feeding rate (i.e. the non alumina feeding contribution does not exist). Hence:

$$\frac{O}{A}-\frac{U}{\alpha}=\frac{U+D}{\alpha+d}-\frac{U}{\alpha}=\frac{D\alpha-Ud}{\alpha(\alpha+d)}=0$$

$$\text{if } \frac{O}{A}=\frac{U}{\alpha}=\text{Constant}$$

Actual Scenario.

Here the non alumina feeding emission is actually part of the emission scheme and must be included in the factors.

$$\frac{O+B}{A}-\frac{U+B}{\alpha}$$

$$=\frac{D\alpha-Bd-Ud}{\alpha(\alpha+d)} \text{ as O = U + D}$$

$$=\frac{D\alpha-Ud}{\alpha(\alpha+d)}-\frac{Bd}{\alpha(\alpha+d)}$$

$$\propto -\frac{Bd}{\alpha(\alpha+d)} \text{ if the ideal case is thought to hold true.}$$

Hence if the alumina component is assumed to follow the ideal case (a gross simplification) with an independent non alumina feeding component, then this non alumina feeding contributor can be quantitatively calculated.

7.2.2. The Validity of the Δ Correlation.

As established above, this correlation can be used to calculate the constant non alumina feeding emission. Figure 7.2 illustrates a representative measurement of the HF emission during a forced zero feed period. Here the fed goes from an underfeed period to zero alumina fed. Hence the primary HF generation contribution of the alumina is removed and the emission quickly decays to the non alumina emission level. Once alumina feeding was re-established at an overfeed level, the emission rises. Effectively the alumina water HF generation contribution adds to the HF emission once again.

The emission levels at zero fed serve as a cross check for the validity of the Δ correlation. The value calculated from it should match the non alumina fed value of 0.557, and 0.540 kg/min. Therefore from the Δ correlation (with an overfeed of 2.65 kg/min and underfeed of 1.15 kg/min) the non alumina HF generation can be calculated

as 0.543 kg/min. This compares well with the measured average zero feed HF values. This gives a non alumina HF content of 0.602 kg/tonne Al for that cell.

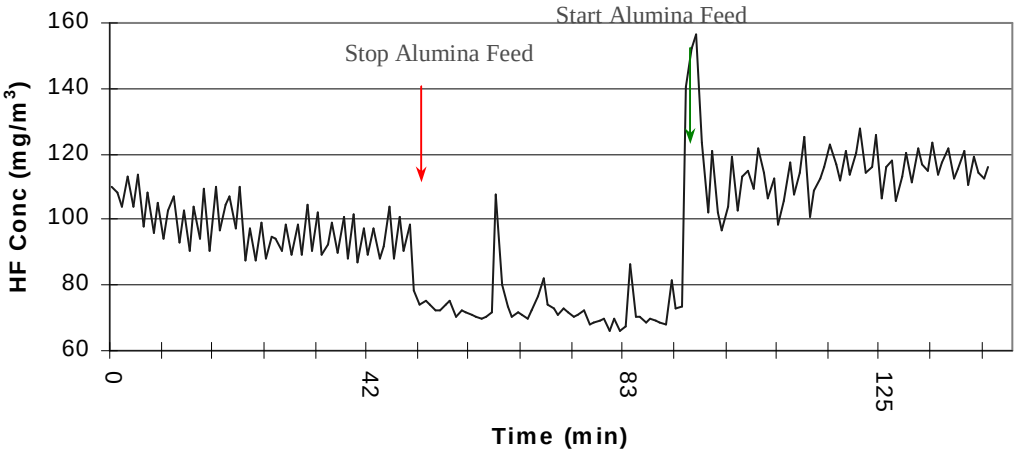

Figure 7.2 - HF response during an a zero feeding period for cell technology I.

7.3. Experimental Procedure.

The equipment set up in the in plant measurements was based on the arrangement of instruments as outlined in section 5.2.3. Here an infrared HF meter was installed to measure the emission of a single cell by measuring a pathlength through the outlet duct. The set up of the HF monitor and other logging equipment used for the industrial trials is illustrated in figure 7.3:

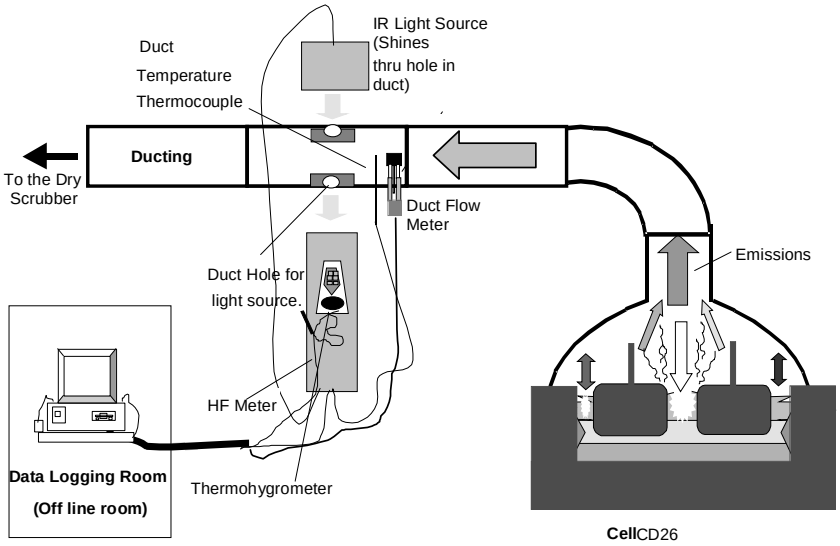

Figure 7.3 – Equipment set up for cell technology II and III.

Here the ducts exit above the cell. The arrangement of the HF monitor used on overhead ducting technology (cell technology II and III) is illustrated in figure 7.4:

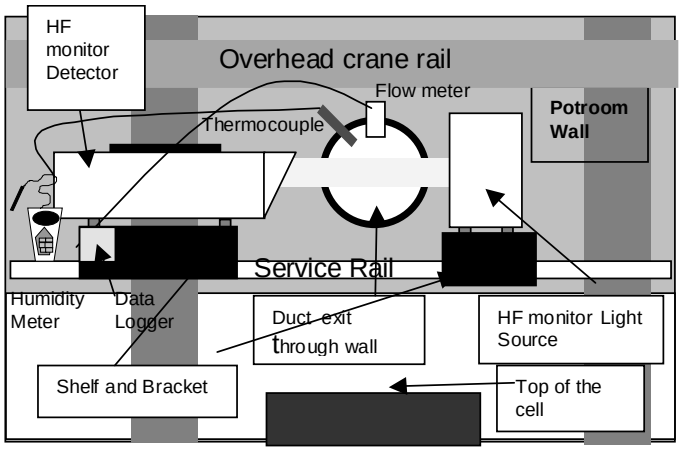

Figure 7.4 – HF monitor duct set up on overhead cells for cells technology II and III.

During each industrial investigation the following factors were monitored:

Continuously.

- Hydrogen Fluoride Concentration – Using the Norsk HF monitor.
- Duct Temperature – Using a thermocouple in the duct.
- Duct Flow Rate – Using a pressure differential velocity meter.
- Ambient humidity and Temperature – Using a thermohygrometer.
- Alumina feeding rate.

Batch Wise.

- Cell temperature.
- AlF_3 additions.
- Metal tapped, bath height and metal height.

7.4. Base line emission characteristics.

The base measurements are effectively measurements of the cells emission during the normal operation of the cell (i.e. without any changes in routine operations). It develops a baseline measurement of the typical emission from the cell, the characteristic response to changes in alumina feed rate, and the variations of emission with ambient conditions.

Figure 7.5 compares a typical emission response for cell technology I and II. In both cases the typical response to alumina feeding and ambient conditions was observed. The emission rate follows alumina feeding rate closely – a trait attributed to the alumina water (structural) reaction of the feeding contribution (refer to Section 5.3).

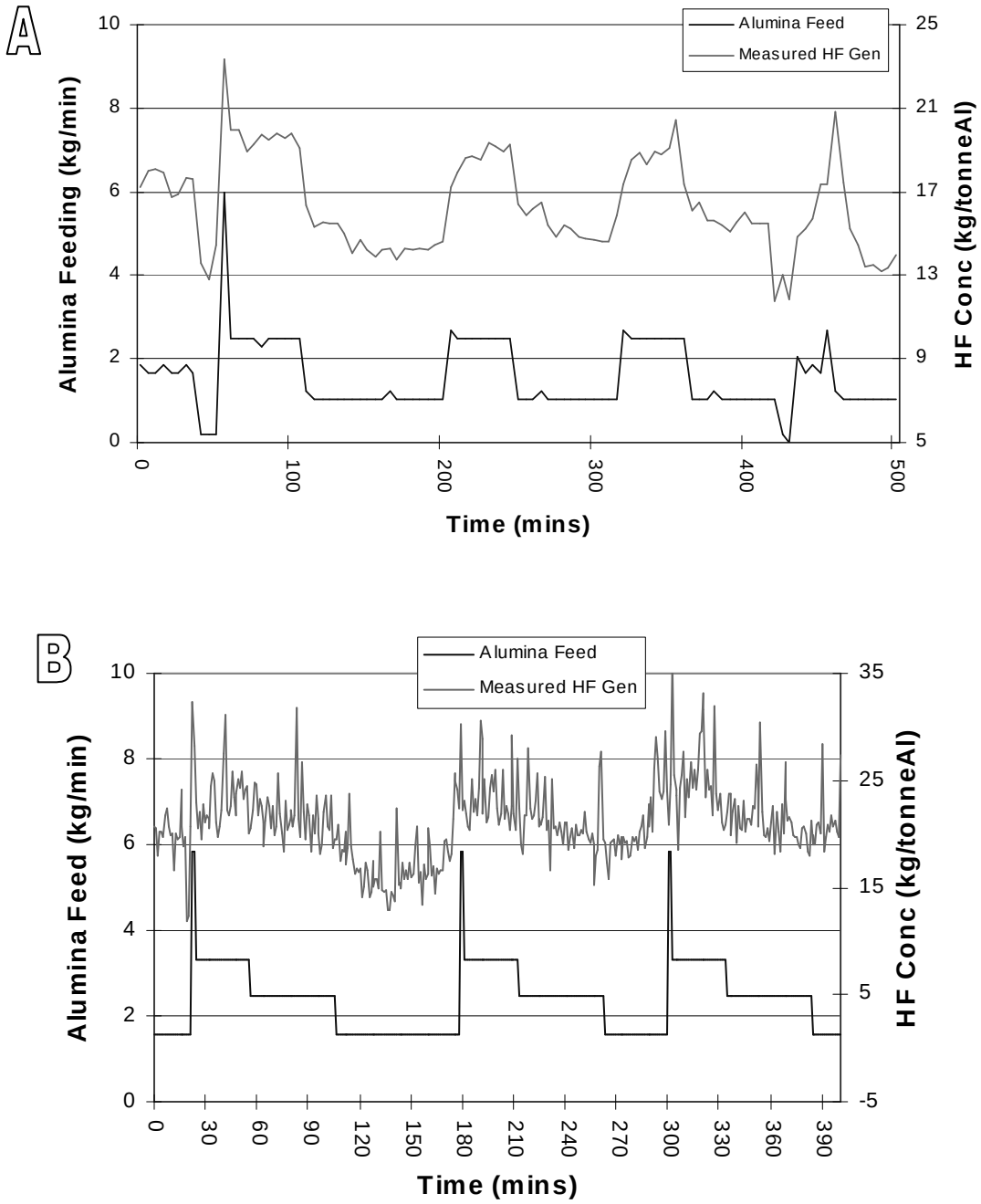

Figure 7.5 – The base measurements for (A)Cell Technology I. (B)Cell Technology II.

Overall the emission for cell technology II is much greater than that recorded for cell technology I. This is mainly due to humidity effects. For cell technology I the overall

emission was 15 to 25 kg/tonne Al for an average humidity of (pH_2O) 0.4 to 2 kPa. This compares to cell technology II which had an average emission ranging between 20 to 30 kg/tonne Al with a much higher humidity – this varied between 1.5 to 4 kPa. Hence the differences in these emission rates is likely due to the amount of moisture entering the cell. This is due to both the humidity of the ambient air and the duct flow rate. As established section 6, this will affect the secondary emissions thermal hydrolysis component, but not much of the primary generation component. This will be explored in more detail in a later section (section 7.5).

Table 7.1 compares the basic emission characteristics for each cell technology.

Table 7.1 – Comparing the base emission characteristics of the three cell technologies.

Contribution	Cell Technology I	Cell Technology II	Cell Technology III
Alumina Contribution	Constant* D=5.5 to 7.4 average at 6.5 kgF/tAl *Approximately 6.5 kgF/tonneAl*	Constant* D=9 to 10 average at 9.5 kgF/tAl Approximately 9.5 kgF/tonneAl	Constant* D=9.5 to 11.2 average at 10.5 kgF/h Approximately 10.5 kgF/tonneAl
Non alumina feeding	*Varies with pH_2O, duct flow and crust* 10 to 15 kgF/tonneAl 60 to 70% of the emission	*Varies with pH_2O, duct flow and crust* 10 to 17 kgF/tonneAl 45 to 65% of the emission	*Varies with pH_2O, duct flow and crust* 5 to 12 kgF/tonneAl 30 to 50% of the emission
Crust Integrity	*Poor. Constant covering.* 1 of the 3 feeder holes always open	*Very Good. Constant covering.* 1 of the 4 feeder holes always open.	*Very Good. Constant covering.* 1 of the 4 feeder holes always open.
Humidity variations	*pH_2O = 0.4 – 2 kPa. Ave = 1.2 kPa*	*pH_2O = 1.5 – 4 kPa. Ave = 3 kPa*	*pH_2O = 1.5 – 4 kPa. Ave = 3 kPa*

** for a fixed feeder hole state.*

As table 7.1 illustrates, the major difference in emission contribution terms result from changes in non alumina emission. This is likely to mainly result from ambient humidity variations. This occurs as the anode emission should be approximately constant, when averaged over the total number of anodes. This results in humidity being the major variable in this cell (in fact any cells) emission for a fixed crust integrity.

The greater alumina emission for cell technology II compared to I is thought to be technology dependant. From analysis of the emission data this value has been found to be constant for any single cell design, fixed feeder hole state and constant crust integrity.

These points will be explained in the following sections.

7.5. Humidity Effects.

7.5.1. The Overall Emission.

The best effect of humidity on an industrial cell emission was recorded for cell technology II. The geographic location of this smelter allowed the measurement of the emissions with large daily absolute humidity variations. Here the overall emission could quite easily be seen to vary with humidity. This is illustrated in the representative HF emission in figure 7.6a.

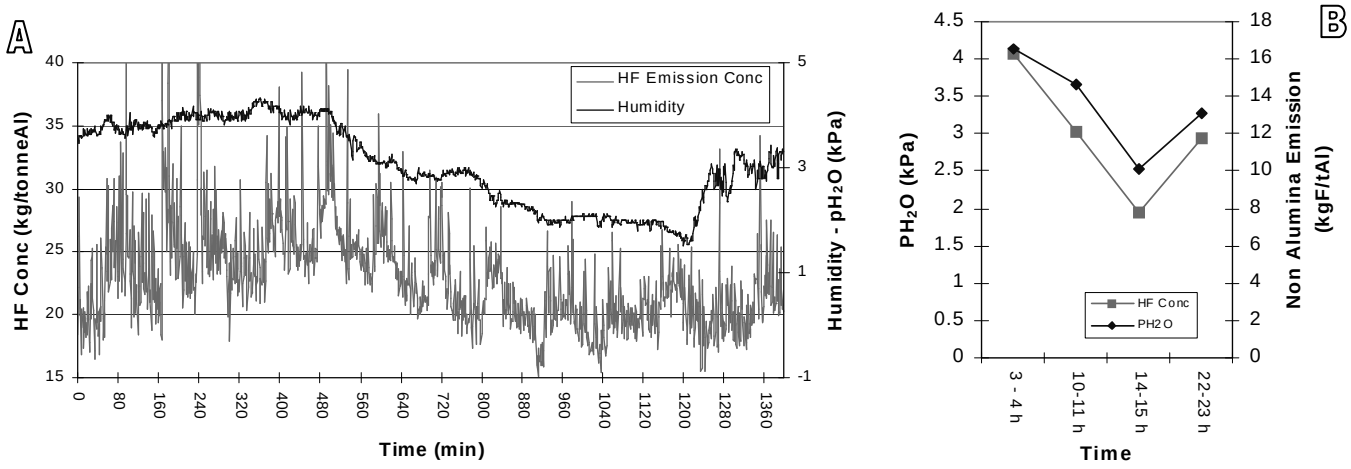

Figure 7.6 – Changes in the emission with changes in humidity for cell technology III.
(A). Total Emission. (B). Calculated non alumina feeding emission.

This trend is expected due to the large thermal hydrolysis emission contribution to the non alumina feeding emission. The similarity in non alumina feeding and humidity (pH_2O) in figure 7.6b illustrates this point. The effects on the alumina feeding emission is very limited. The D values for the time periods are all very similar also, averaging around 0.52. This shows that the humidity had little effect on the alumina emission component. The only variation that occurs with changes in humidity was in the non alumina feeding emission.

The changes in the non alumina feeding with humidity can also be seen in figure 7.7. This plots two trends for the calculated non alumina feeding versus the humidity in the air (pH_2O) for cell technology II. Both plots are for a cell condition with a similar crust integrity and two open feeder holes (hence the small amount of points). The difference between figures is the time period of the comparison. For each period the crust integrity differs, with new anode positions etc..

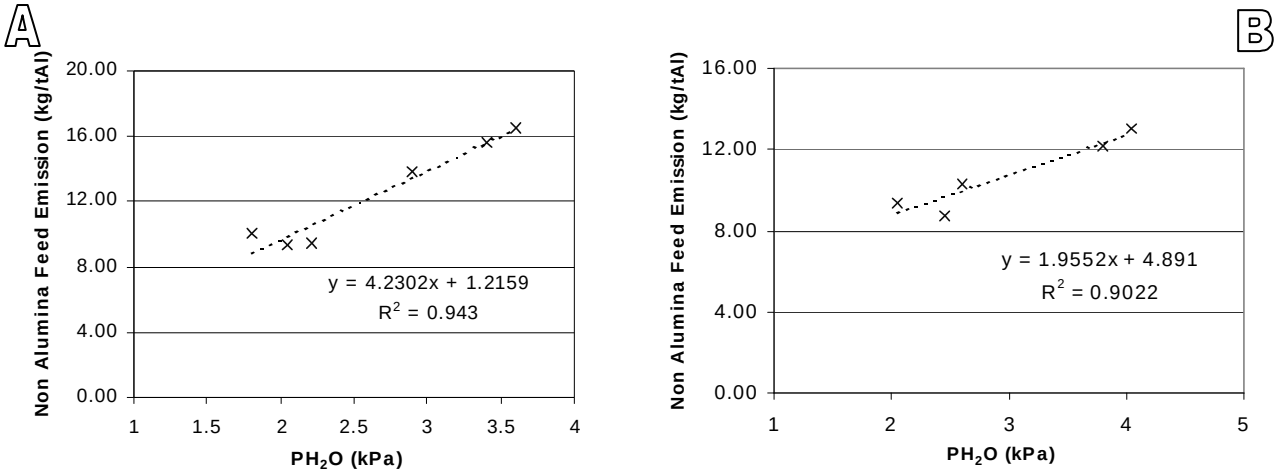

Figure 7.7 – The non alumina feeding emission vs. ambient humidity (pH_2O).
(A)First set of base measurements. (B)Second set of base measurements.

For any given day, even with good crust cover, the crust integrity influence is not exactly the same. This should explain the spread in these results (refer to section 7.7). Regardless, in each case there is an upwards trend, though the slopes of the two fits do not agree. This trend is hard to calculate due heat balance effects and other comparison problems. This was seen in the results for cell technology I. Here humidity correlation results could not be compiled due to the poor crust condition of the cell. Due to this, any operation affecting the crust condition (tapping, anode change and crust addition) affected the non alumina feeding emission (refer to section 7.6). This makes separating out the crust integrity effects and air moisture effects impossible for this cells measured emission data. As the crust integrity was more or less ideal for cell technology II, assuming an independence of effects for similar crust and feeder hole states was possible.

7.5.2. Humidity Effects on Anode Change.

Anode change exposes a large amount of bath area to the duct air. Both the time periods and different humidity conditions during different anode changes are compared in this section to study the effects of humidity on emission generation.

(A). Typical Anode Change Emission Responses.

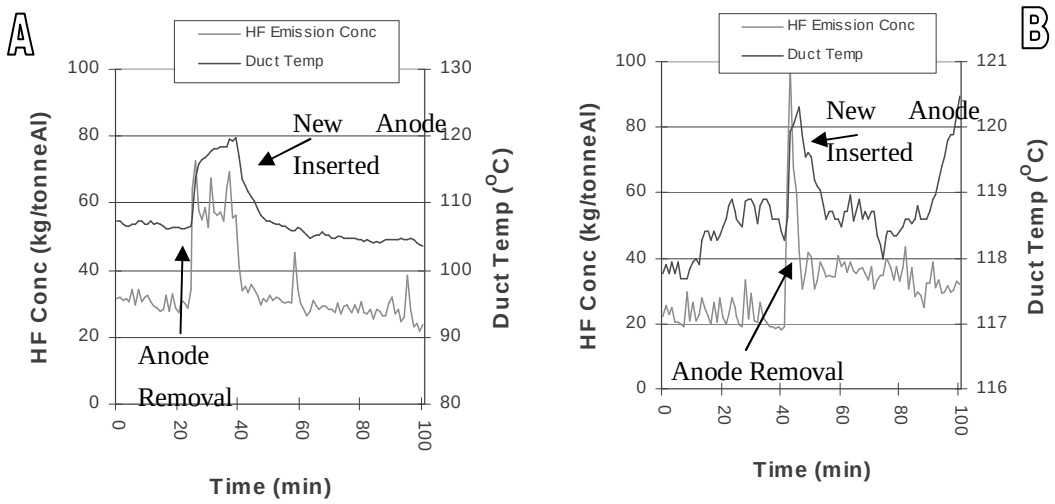

Figure 7.8 – A typical anode change emission profile (A)Cell Technology II (B)Cell Technology III.

Anode change has the biggest thermal impact on the cell of any operation [48], and has the largest impact on the HF emissions of any routine potroom operation. Comparing the two anode change profiles in figure 7.8 it can be seen that cell technology II has a much more wide spread emission profile and heat balance effect than that for cell technology III. This is due to the length of time the anode is out of the bath. Here the anode remains out of the bath for at least 12 to 17 minutes according to the typical profile (refer to figure 7.8, anode is out of the bath for 15 minutes). A more typical anode change profile is presented for cell technology III. This effect is more instantaneous as the anode remains out of the bath for a much shorter period – on average around 4 minute. This is the same profile seen for cell technology I.

Regardless of the open bath exposure time, the rise in temperature is a result of the removal of the anode and replacement. The most important fact is that it has an instantaneous effect upon anode removal. Here the HF level spikes once the anode is removed and stops just as quickly once bath freezes around the cold anode. The greater emission results from the period when the anode is removed and the bath is exposed to the cell air. It is speculated that the non alumina feeding emission increases due to greater vaporisation emission generation and simultaneous thermal hydrolysis. The simultaneous rise in duct temperature results from greater radiation heat losses from the exposed electrolyte [48]. The end state (temperature and emissions) is dependant on how much electrolyte is left exposed after anode change. Any duct temperature and HF concentration rise can be caused (refer to figure 7.8b) if a hole is left in the crust. Usually the cold anode freezes the bath around it, preventing this.

(B). Variation in Anode Change Time.

To study the effect of humidity on anode change, the anode change time periods were varied. A much longer time was used between extracting the old anode and placing the new anode back in the bath, here 20 minutes. This time was also shortened to 8 minutes. As figure 7.9 shows, this simply resulted in an extended and shortened period of increase emission and duct heat loss proportional to the time the bath is exposed to the atmosphere. Again simple heat losses (radiative and convective) coupled with extra vaporisation and hydrolysis explain the rise in both the emission and duct temperature. Note that the initial emission increase in figure 7.9b is due to crust addition before the anode change operation. The anode change begins once the duct temperature rises.

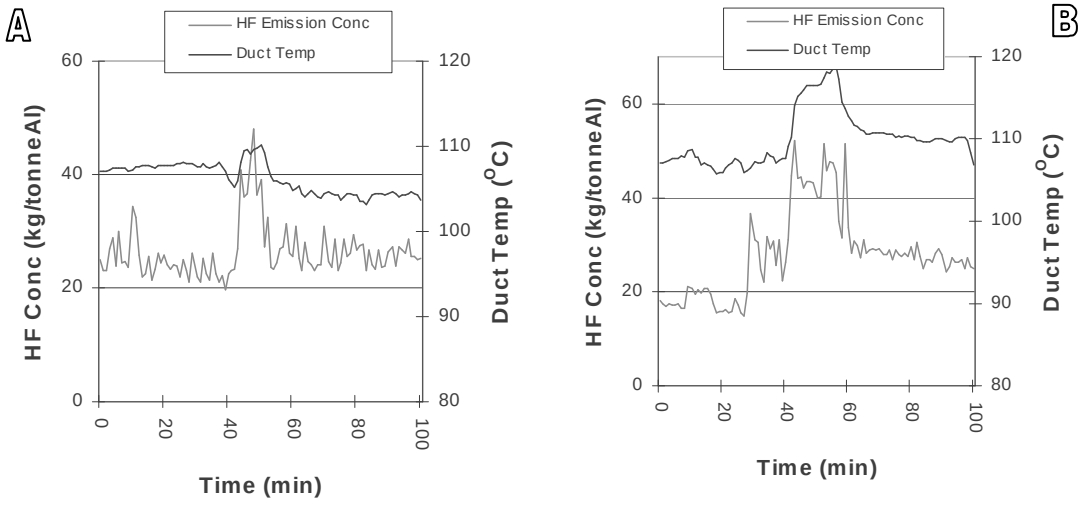

Figure 7.9 – Cell Technology II Emission profile differences from: (A)Shorter anode change. (B)Longer anode change.

(C). Variations in Anode Change Ambient Humidity.

An analysis of the hydrolysis effects during the anode change period can be estimated if it is assumed that a constant area of bath is being exposed for each anode change. This is idealised and will vary with each operation and anode position. However if it is approximated that an anode exposes its length and width, and an average emission value is taken before and during each anode change, the following correlation with humidity can be derived (refer to figure 7.10):

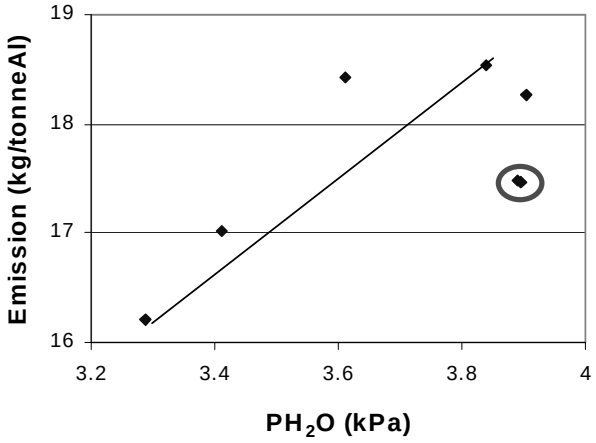

Figure 7.10 – The hydrolysis correlation for anode changes for cell technology II.

There is a straight line trend similar to that found for the non alumina effects (refer to figure 7.7). Note that this effect includes both the impact of opening two covers and the extra ambient air this includes at this point (though this mainly impacts on the duct temperature not the actual HF emission) and also the effects of the reduced crust integrity. Highlighted in figure 7.10 are the results of the anode change trials (as illustrated in figure 7.8). Both have values that do not fit the trend. It is likely that the abnormal operation procedures with reduced hooding (more than 2 covers removed) due to the extra attention paid to these trials have biased the results. They can be (cautiously) ignored due to this fact. All other values follow the upwards pattern expected of increased hydrolysis.

7.5.3. Humidity effects from varying the Duct Flow.

The aim of this trial was to investigate the effects of changing the duct flow rate (or suction) on the emission. Cell technology II had the ability to increase the duct flow to the cell from 6000 Nm^3/h to 11000 Nm^3/h. Therefore a trial was devised to measure the HF emission at 6000, 7800, 9000 and 11000 Nm^3/h. It must be noted that the adjustment of the duct flow changes the heat balance of the cell quite dramatically, with more heat being lost from the anode stubs and bars at the higher flow rates. For this reason the changes in the flow rate were minimised to 40 minute intervals. While not giving a clear idea of the differences in feeding rates (as the feeding windows at each level are longer than 40 minutes in most) it does give relative levels of contributions. An average level of HF emission for comparison has been taken depending on the feed window. These results can be seen in figure 7.11 and table 7.2.

Table 7.2 – The Results of the Duct Flow Investigation.

Base Flow (Nm^3/h)	Flow Temp (^OC)	Emission (kg/tAl)	% less (kg/tAl)	Amount of water (kg/h)	%less
11000	106	36.96	0	298	0
11000	106	34.32	7.14	298	0
9000	113	34.56	6.49	243	18.18
7800	116	31.82	13.89	211	29.09
6000	116	29.52	20.12	162	45.45
6000	117	28.8	22.08	162	45.45

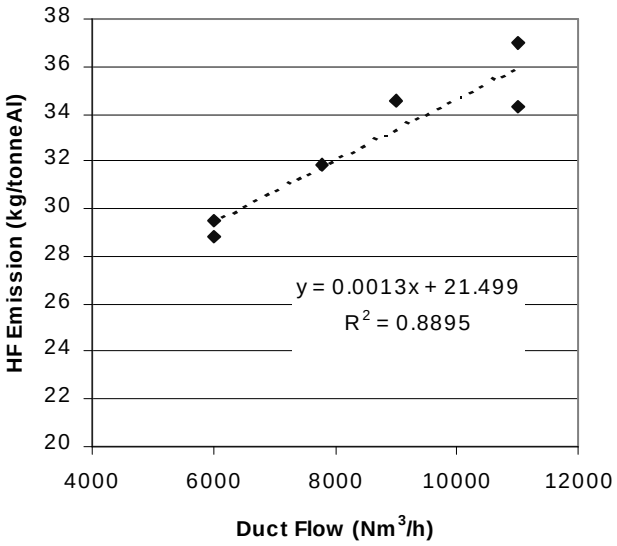

Figure 7.11 – Comparing the approximate emissions from the duct flow trial.

The results are clear. Increasing the flow increases the HF emission. There is a 20% increase in emission from 6000 Nm^3/h to 11000 Nm^3/h – about 4% per 1000 Nm^3/h. The reason is likely a greater thermal hydrolysis content of the cell. The base measurements reveal that the alumina contribution is reasonably constant (it still depends on feeder hole state, with a closed feeder hole reducing the emission due to alumina preheating and causing a mass transfer barrier for the emissions). As feeder hole state remained constant over the period of the trial and that duct flow does not impinge on the alumina feeding rate, the alumina emission is unaffected by duct flow. Hence this is a non alumina feeding effect, specifically a thermal hydrolysis effect. This can be established as the only other major contributor to the non alumina feeding is anode hydrogen generation. This contribution is a constant factor, therefore leaving thermal hydrolysis as the only significant emission variable. Table 7.3 illustrates this, showing the approximate changes in moisture content of the air flow for the estimated 40^OC, 40% relative humidity ambient conditions of that day. A corresponding change

in the emissions is seen. Hence increasing the duct flow increases the moisture content entering the cell. With a constant vaporisation rate (this would increase slightly with increased duct flow) more water vapour enters the cell and reacts via thermal hydrolysis in the vents – here mainly the open feeder holes.

Therefore the duct flow is a factor in the emission rate. Increasing the flow increases the amount of humid air entering the cell and hence the affects the thermal hydrolysis content.

7.5.4. Conclusions.

Ambient humidity has a very large affect on the overall emissions from an industrial cell. For cell technology II the ambient air humidity was found to effect the overall emission. An increase of humidity from 1.5 to 3.5 kPa shows a 100% increase in the baseline emission. This change is seen in the non alumina emission component and not in the alumina emission. The emission rate during anode change was also found to be dependant on humidity. This suggested that the increased emission is a result of thermal hydrolysis effects. This dependance was also seen when varying the duct flow rate also affected the HF emission. A 20% increase in the average emission was found between 6000 to 11000 Nm^3/h. This was attributed to a greater moisture content entering the cell with the ambient air.

Overall the difference between the emissions from cell technology I and II can be attributed to the greater humidity at technology II smelters location. Here the greater ambient humidity increases the thermal hydrolysis component of the non alumina feeding emission

7.6. Heat balance effects.

Normal process operations cause heat balance disturbances to the cell and hence make the normal monitoring readings invalid around these times. Therefore for contribution breakdown purposes, the areas of interest in the measured emission concentrations are the stable cell periods. These are at least 4 hour after anode shift and up to an hour after tapping. Adding crust also affects the emission. These characteristic are interesting never-the-less. While not being useful in identifying the exact compositions, they show how the emission is affected by routine operations to the cell.

7.6.1. Tapping.

Greenwood [28] found that emissions increase during the taping operation due to changes in crust condition from anode shifting. This is also seen in this study. Figure

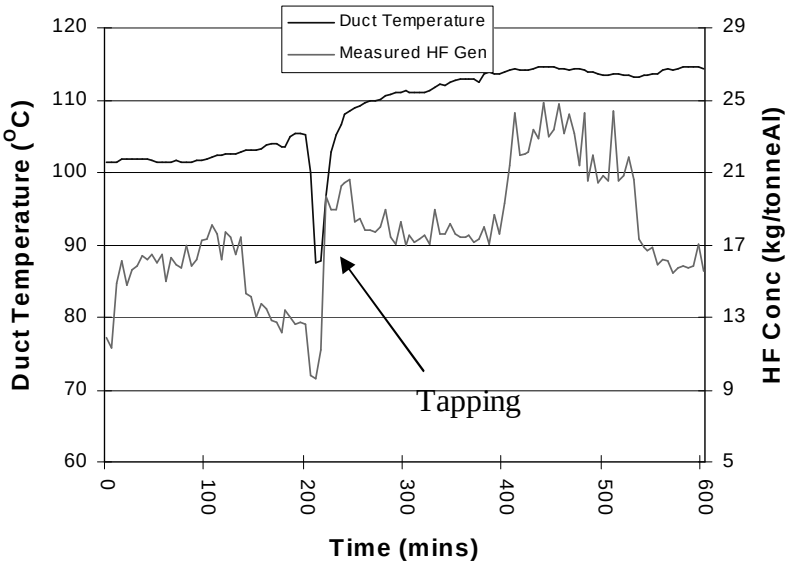

7.12 illustrates the HF emission and duct temperature response to tapping for cell technology I.

Figure 7.12 - The HF response curve upon tapping for cell technology I.

Here the effect is spread over a long period due to crust integrity changes when the anode height is adjusted. Measurements of the bath temperature during tapping show the temperature effects to be quite localised (figure 7.13) showing that the bath temperature effects are minimal and can not explain the long term changes in duct temperature and HF emission.

The step change with little effect on $D_{feeding}$ points to the cause of the effect. As established earlier $D_{feeding}$ is characteristic of the alumina feeding contribution of the real emission.

Table 7.3 –$D_{feeding}$ and calculated Non Alumina Feeding Emission B for cell technology I tapping.

Description	Ave HF (kg/tAl)	Ave Temp. (°C)	$D_{feeding}$ (kg/tAl)	Δ	B (kg/tAl)
Poor Crust - Before Tap	18.19	109.5	7.07	0.2638	9.90
Poor Crust – After Tap	25.26	118.1	8.61	0.3986	14.95
Good Crust – Before Tap	10.54	101.9	2.54	0.2287	7.45
Good Crust – After Tap	13.48	116.8	3.00	0.3018	9.83

Referring to table 7.3, the largest change calculated is in the non alumina feeding emission. It must be noted that there is a minor change in the $D_{feeding}$ value as this is not completely independent of non alumina feeding effects. Overall this suggests that the majority of the response must be secondary generation emission effect. This is because the dissolved water and hydrogen in the anode HF generation are unlikely to be affected. Observations of the crust integrity show significant change in the cracks around the anodes occur after tapping due to anode movement. In fact cracks become significant on a freshly covered anode after 2 to 3 tapping operations due to the ageing/sintering effect of the crust environment. Hence the overall response is likely to be a crust integrity effect. This will be explored in section 7.7.

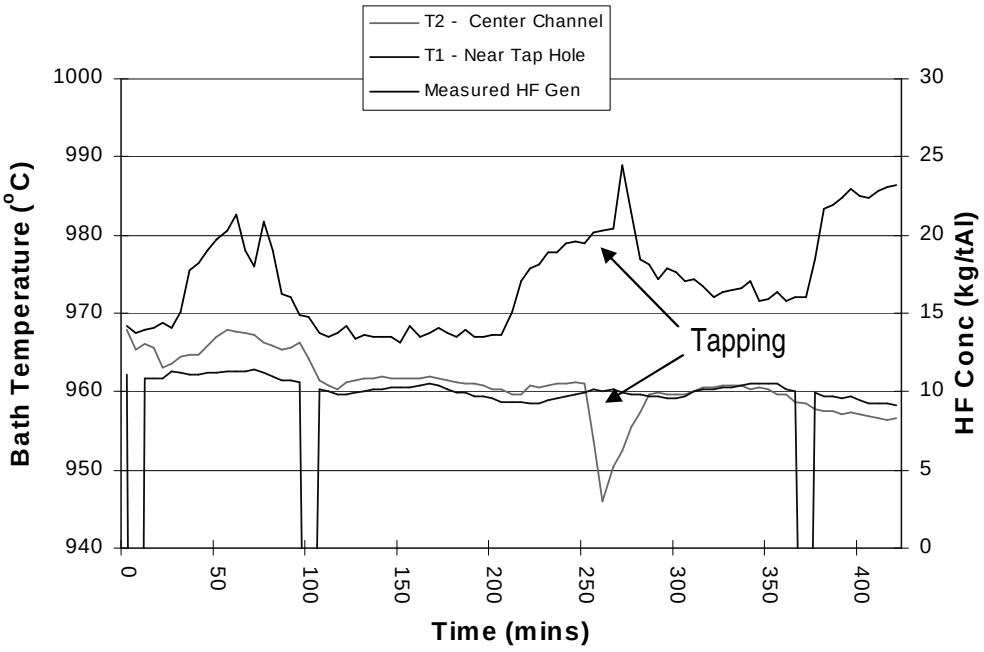

Figure 7.13 - Bath Temperature effects upon tapping.

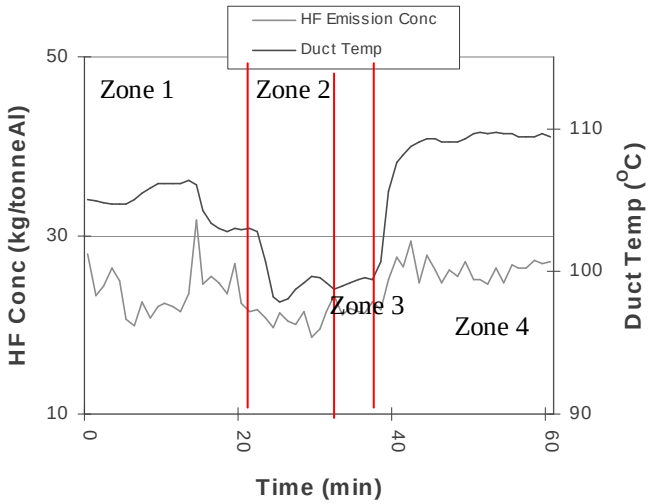

Figure 7.14 – A typical tapping emission profile.

Conversely tapping has a negligible response in the cell technology II HF emissions. Unlike the crust integrity driven effect seen above due to the poor crusting practices, the dominant effect here is a heat balance one from the open tap door as the crusting practices for this cell technology were much more ideal. Figure 7.14 illustrates a typical tapping profile.

Due to the good crust integrity, the classical top heat loss profile for tapping [48] was recorded in the duct temperature. The emission stays fairly constant due to the added effect of breaking the crust, balancing the effect of the extra air entering the cell. The duct temperature is reduced for the period the door is open. The heat losses follows the four zones proposed by Gadd [48]. Zone 1 is the normal duct temperature. Zone two occurs when the tap door is opened and ambient air mixes with the cell air, at the same time a tap hole is made exposing some electrolyte to the air. Zone three has a temperature rise as the tapping pipe is inserted into the open tap hole, reducing heat loss. Zone four occurs once the tap door is closed again. As Gadd explains, the duct temperature returns to a greater level due to the exposed electrolyte from the open tap hole. Emissions rise slightly also due to this. However not a significant effect in the overall HF generation scheme.

7.6.2. Anode Effect.

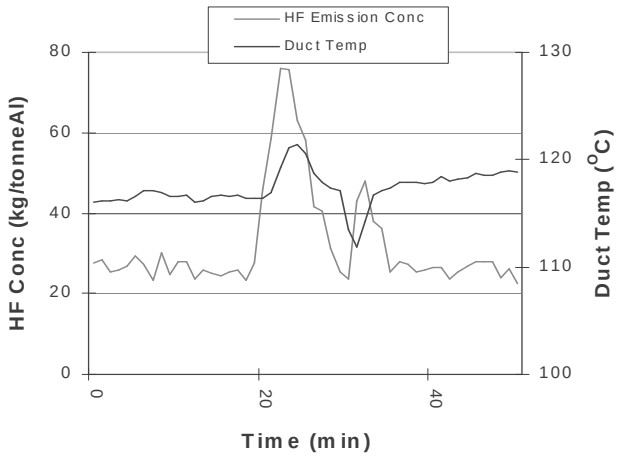

Figure 7.15 – A typical anode effect emission profile for cell technology II.

Figure 7.15 illustrates the typical profile during anode effect for cell technology II. The is a distinct temperature rise from the event with a sharp peak in HF emissions. Just as the resistance spikes, the emission reacts just as instantaneously. It is predicted that the CF_4 and C_2F_2 compounds are generated also. These would not be detected because the adsorption spectra are different to HF, and are not calibrated into the detection system.

Still the rise in emissions is interesting as it follows the same pattern measured in the laboratory, where emissions increase slowly as alumina is depleted in the test cell and spike at anode effect.

Obviously the effect was automatically terminated for a short while. The loss of duct temperature after the HF spike is due to covers being removed from the cell to manually terminate the effect. This is seen by the smaller second rise in HF concentration. The temperature profile follows that published by Gadd [48].

7.6.3. Crust Addition.

Crust addition has a great impact on the emissions recorded. Adding crust changes the crust integrity, and hence increases the mass transfer barrier of the air – bath interface. If this reduces the flaming at cracks in the crust, then the thermal hydrolysis component (secondary generation) will be seen to reduce. This was recorded for cell technology I and II.

For cell technology I every shift the flames are covered with crushed bath. This involves lifting all the covers and adding crushed bath on the areas where there are flames (usually between the side wall and anodes due to the anode movements upon tapping). This produces an excessive amount of dust in extraction system, reduces the duct temperature due to the open covers which dilutes the HF concentration in the duct also. Both these impacts can be seen in the following two diagrams in figure 7.16. The signal intensity is a measure of the amount of light passing from the light source to the HF meter. It is affected by the amount of particles in the duct, hence is reduced during covering due to the dusting incurred.

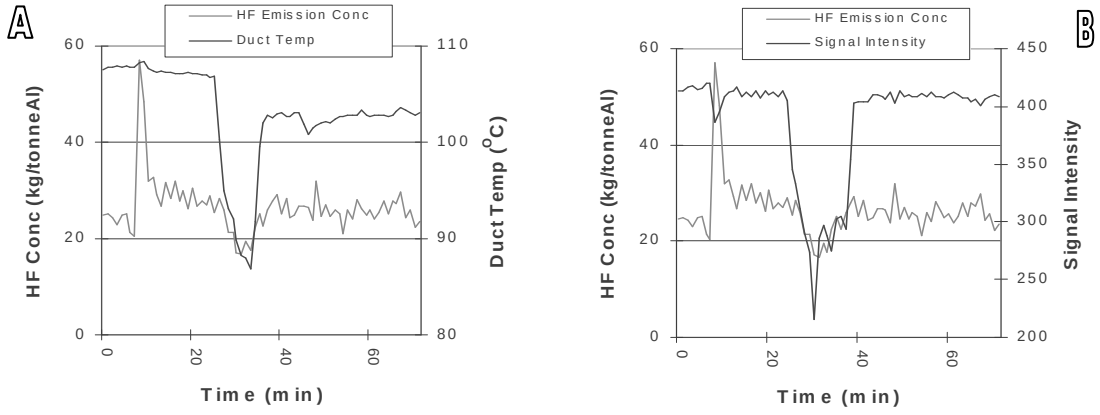

Figure 7.16 – A typical crust addition emission profile for cell technology II. (A)Emissions Profile. (B)Signal Intensity profile.

The profile differs to that for cell technology I. Here the crust integrity was non-ideal and covering was only applied to a new anode and its immediate surroundings 8 hours after each anode change. This resulted in a large effect on top heat loss due to the vast improvements in the thermal barrier on the new anode. This can be seen in figure 7.17.

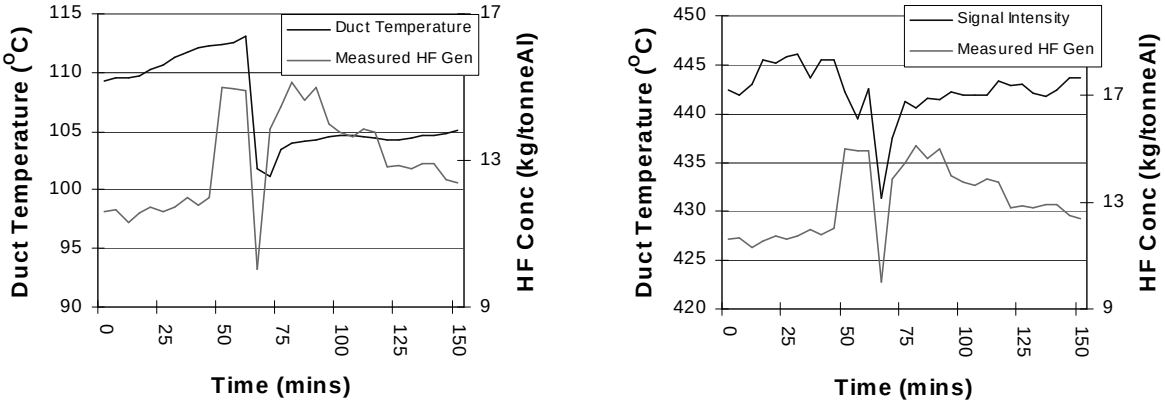

Figure 7.17 - A typical crust addition emission profile for cell technology I. (A)Emissions Profile. (B)Signal Intensity profile.

Hence with good covering duct thermal effects are dominated by the loss of covering efficiency rather than additions to crust integrity. Still a change in the duct temperature is evident from the reduction of flaming.

7.6.4. Conclusions.

Overall the heat balance effects are not that significant if the crust integrity is unaffected by the operation. Hence the only operation of significance is anode change as this changes the crust integrity significantly. However as emissions from cell technology I indicate, when the barrier this cover is non ideal then the emission is affected significantly any time the amount of moisture is varied entering the cell air. Effectively this is changing the thermal hydrolysis component of the cover. This points to the top barrier as being a significant factor in the overall HF emission contributors.

7.7. Crust Integrity Effects.

The top crust of an industrial aluminium electrolysis cell consists of a consolidated crust and a loose granular (alumina) layer above. A desirable crust should have a certain strength to hold itself above the molten bath, support the loose materials on top of it and resist disturbances during anode change and alumina feeding. It is also required to produce good thermal insulation and minimise gaseous fluoride emissions [49].

Most past research [5, 6, 28] agree that the crust integrity is an important factor in the evolution of hydrogen fluoride form the cell. Hyland et al. [26] suggests for fluoride emission reduction "that ensuring good crust integrity and cover would be the most practical solution with the smallest penalty to cell operations". The crust has been identified to act in two ways in reducing fluoride emissions from the cell.

Firstly it presents a mass transfer barrier for both the particulate vapours escaping the cell and also from moisture entering it into the hot electrolyte. In effect the efficiency or integrity of this crust dictates the amount that is released to the scrubbing system. Figure 7.18 illustrates the difference between a non ideal crust cover and a good crust. Effectively for good crust integrity there are only minor cracks in the surface and the crust has sufficient mechanical strength to prevent sections falling into the bath. Good routine crusting practices incorporated into cell manual operations, such as daily covering maintain a good crust.

Figure 7.18 – Two crust types. (A)Poor crust integrity. (B)Good Crust integrity.

The second method of fumes reduction of the crust is its possible scrubbing ability. Much like the alumina in the dry scrubber, it is thought that the mixed bath – alumina composition of the crust could adsorb the emissions while they pass through it to the

extraction system. This relies on the notion that the particles act like they do in the dry scrubber as a fluid bed with extensive exposed area. Other studies [49, 50] have shown the crust to in fact starts to consolidate into sintered agglomerates above 600^{O}C, with clear consolidation occurring above 700^{O}C. Furthermore the transformation of the γ alumina to α platelets which sinter to form an interlocking network [50, 51] due to the heat flux experienced. Penetration of the molten bath into this network also helps consolidate and densify the crust [52]. The longer the residence time the greater the effect [49]. All this suggests that the scrubbing ability would be effectively reduced as the crust ages.

The aim of the following section is to clarify the exact effect the crust has on the fluoride emissions of the cell.

7.7.1. Experimental Methodology.

Cell technology II was used to investigate the effect of improving the crust integrity of a test cell.

Here the original crushed bath crust used on the for cell technology II was replaced with a 5 cm layer of primary alumina. The original crust integrity of the cell was maintained at a high standard to reduce the effects of air bun on the black anodes. Effectively the only regions of high thermal hydrolysis were the tap hole, the region exposed in the center channel when an anode was replaced and between the duct and tap ends are exposed at any time. Cracks on the upstream and downstream side walls between the wall and the anodes were negligible.

7.7.2. Experimental Results.

As the following diagrams illustrates (figure 7.19), this has reduced both the top heat loss (different thermal barrier, though as this is already very good this reduction is minimal) and the HF emission.

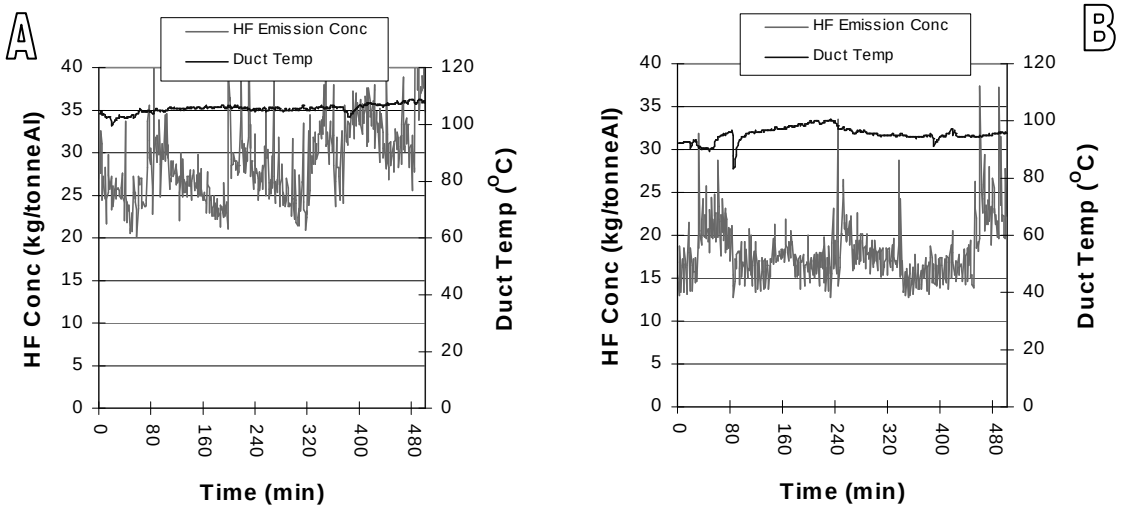

Figure 7.19 - Comparing the emission before and after crust addition for cell technology II. (A)Before crust addition. (B)After primary crust addition.

This dramatic reduction in emission may be due to two effects:

- Firstly the improvement could be the result of primary alumina scrubbing ability, adsorbing some of the emissions. Over time the alumina could reach its adsorption saturation limits, with the contamination effects of the bath progressively deteriorating the effectiveness of this barrier.
- However it could also be the result in improvements made improving the mass transfer barrier. Here the fresh alumina are free flowing individual particles which settle together on the surface and could provide a better barrier than the replaced aged cover. Over time this surface alumina sintering and general compositional changes at the crust temperature could allow permanent vents for the fume to be formed through the cover. This would reduce the covers effectiveness as a barrier.

Hence whatever combination of effects occur this crust ageing effect is clearly seen when comparing the three emissions (figure 7.20).

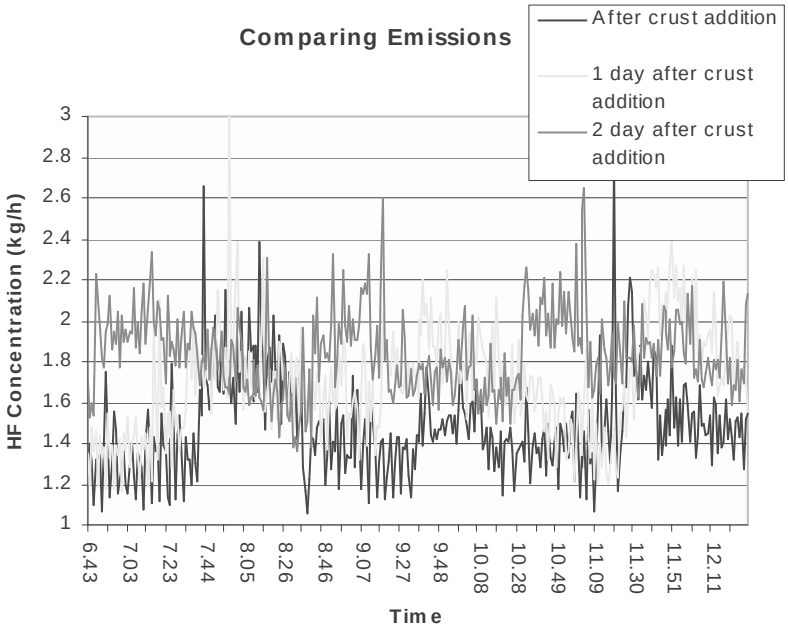

Figure 7.20 - Comparing HF emission between 6.43am and 12.30pm after crust addition, 1 day after crust addition, and 2 days after crust addition.

It is apparent though that the effects of the crust decay quite dramatically. The non alumina feeding emission has recovered significantly after the first day of cover, and is nearly back to the levels before the cover was changed by day 3. Laboratory analysis of the crust samples taken daily at 2pm show very little however (refer to table 7.4).

Table 7.4 - Laboratory results of the primary alumina cover over the 4 days of the crust trial.

Day	%Ca	%Na	%F
1	0.064	0.79	1.69
2	0.024	0.34	0.89
3	0.115	1.62	4.0
4	0.049	0.56	2.43

If the cover had a progressive rise in the fluoride and Na contents this would indicate that the crust was adsorbing the emission. The scatter suggests that this is not happening. However this is a cursory examination of this effect with a small selection of samples (4 days samples from 3 different positions mixed for 4 data points). Overall though the results do suggest that ageing of the covering is more likely the reason for increased emission rather than the covers scrubbing ability. This would seem to fit the crust consolidation mechanisms proposed by Lui et al. [51].

Note that this reduction and subsequent rise of emission is not entirely related to hydrolysis effects as improvements in crust integrity may suggest. If an analysis of the non alumina feeding is calculated using the Δ correlation it can be shown the alumina

contribution is also affected (refer to table 7.5). When the Δ correlation is used to separate out the non alumina feeding and alumina contribution it is found that both are reduced. From the discussion above the reduction in the non alumina feeding is due to a reduction in the thermal hydrolysis factor. Also from the evidence provided the new crust presents an improved barrier for the emissions, which essentially improves crust integrity (this includes feeder hole state). The question remains as to why the alumina feed emissions are reduced.

Table 7.5 – The calculated non alumina feeding emission (B) and D values for the crust trial.

Trial	Time	pH_2O	O	U	Δ	B	D	R.E.
		(kPa)	(kg/min)	(kg/min)		(kg/tAl)	(kg/tAl)	(%)
Base	5-7am		2.67	1.85	-0.37259	13.33	9.84	44.4
Crust Day 1	8-9am		1.88	1.1	-0.13313	4.76	9.36	42.2
	12-1pm	3.79	1.87	1.08	-0.12339	4.41	9.48	42.79
Crust Day 2	00-01am	2.83	2.18	1.5	-0.29752	10.64	8.16	36.8
	05-06am	2.13	1.92	1.34	-0.27409	9.81	6.96	31.42
	11-12am		2.14	1.45	-0.27773	9.94	8.28	37.3
Crust Day 3	01-02am		2.2	1.5	-0.29148	10.43	8.40	37.9
	05-06am		2.05	1.4	-0.27305	9.77	7.80	35.2
	11-12am	2.21	2.18	1.6	-0.3613	12.93	6.96	31.4
Crust Day 4	04-05am	2.52	2.36	1.65	-0.33877	12.12	8.52	38.4

From the general base emission analysis in table 7.1 it can be seen that cell technology II HF emissions alumina component is greater than cell technology I emissions alumina HF generation. This could be attributed to increased reaction efficiency due to the cell design parameters. This can be illustrated if the predicted amount of structural water reaction is calculated. Taking a base feed of 2.45 kg/min, average alumina emission of 1.1 kg/h and a structural water content of secondary alumina of 0.88wt% (the measured figure for the primary at the smelter), it can be calculated that the reaction efficiency is around 44% - more than the 20 to 33% figure found for cell technology I. For each of the daily readings a figure of 38 to 45% was constantly calculated for a cell state with **two** open feeder holes.

It will be shown in Chapter 8, the alumina dissolution process for cell technology II is quite different from that for cell technology I. Cell technology II have an alumina emission decay time constant of approximately 2 minutes, while the cell technology I had a time constant that averages around 12 minutes. Note that this figure is both technology dependant – alumina dissolution relies on the center channel flow, feeding techniques and thermal design of the cell – and feeder hole state dependant (this will be explained below). At any rate it is clear that alumina dissolution is more effective in the

technology II cell design and this likely results in a greater amount of the structural water reacting and hence a higher alumina component in the HF emission.

However to assume that the emission is only affected by the amount of structural water content is idealistic. In reality the emitted HF content is being measured, after it passed through several resistances (mass transfer barriers). These mass transfer barrier potentially retains some of the emission. This is most easily seen when the feeder hole is closed and the emission has to be released through the alumina which fills the hole. This makes the total emission a technology dependant figure, related to feeder technique, cell design, center channel flow, alumina dissolution and crust integrity.

Therefore the reason for the difference in figures is not as simple as reaction efficiency. It also depends on *feeder hole state*. This is seen in the results for cell technology II (table 7.6) where the reaction efficiency decreases with decreasing D.

Table 7.6 – The calculated non alumina feeding generation for cell technology II.

Reading	pH_2O	O (kg/h)	U (kg/h)	B (kg/h)	B (kg/tAl)	D (kg/tAl)	R.E. (%)
1	1.8	2.45	1.60	0.8338	10.01	10.2	46
2	3.6	2.86	2.08	1.3769	16.52	9.4	42
3	2.9	2.67	1.87	1.1489	13.77	9.6	43
4	3.4	2.77	2.00	1.3059	15.67	9.2	41
5	2.05	2.10	1.41	0.7831	9.40	8.3	38
6	2.45	2.05	1.357	0.7305	8.77	8.4	38

As previously stated a closed feeder hole has a completely different emission path due to the mass transfer barrier the mass of alumina in the hole presents. Conversely an open feeder hole allows the emission to be emitted directly. Hence feeder hole state will affect the emission. Here D (=O-U) was severely affected by the added cover and subsequent filling of the feeder holes. This will be explored in the next section.

7.7.3. Conclusion.

Crust integrity (which includes feeder hole state) is an important factor which affect the over generation of the HF emission. The crust acts as a barrier to both moisture entering the bath and causing HF generation and as a mass transfer barrier against emission evolution. Any reduction in the effectiveness of this barrier results in greater hydrogen fluoride generation. This is associated with a greater amount of thermal hydrolysis increasing the non alumina feeding emission contribution to the overall emission. Mechanisms to the cause of this effect are uncertain. However this preliminary

study points to the crust acting more as a mass transfer barrier rather than scrubbing effects. This seems to fit the crust consolidation mechanisms in the literature.

7.8. Feeder hole states.

7.8.1. Introduction.

It is proposed that the reduction in the alumina emissions contribution can be attributed to the state of the feeder holes. As explained by Moxnes [21], a feeder hole is described as open if the point fed alumina does fill the hole during feeding. It is closed then if the hole is filled with alumina during the feeding process. Due to the mass transfer barrier this presents for the escape path of the emissions the feeder hole state – closed, partially closed or open – will have an effect on the alumina emission. Effectively the feeder hole state is part of the crust integrity as it forms part of the effectiveness of the top cover barrier it preventing emission release and contact of the cell air with the electrolyte.

A closed feeder hole does not allow the emissions to directly escape, while the open feeder holes present no such hindrance. During the crust trial described in section 7.7.4 only 1 of the 4 feeder holes was open, compared to 2 of the 4 in the base measurements. This will affect the emission because it reduces both the hydrolysis component and alumina emission. It is likely that the emission reached normal levels again after two days due to feeder hole state, if the reduction from one extra feeder hole is factored in. This can be seen in table 7.6. This can be seen more clearly in the results for cell technology I which has poor crust integrity.

7.8.2. Feeder hole state and the Alumina Emission.

Feeder hole state affect the mass transfer barrier the generated emission have to pass through to enter the extraction system of the cell. The experimental evidence definitely suggests that only a proportion of the structural water reacts (section 5.3). And it has been shown that the crusts ability to scrub the emission is limited. Greenwood [28] asserts that open feeder holes give a greater emission (when compared to bar break cells) due to possible air sweep across the point feed holes causing a lower pressure via a venturi effect increasing evaporation.

So what exactly is the effect of the feeder hole state?

If the feeder hole state was an important factor in HF emission, a large differences in the levels of HF emission should be seen for each feeder hole. Here the feed rate windows (overfeed, base feed and underfeed) would not be distinguishable as a blocked feeder hole would give a low to zero emission when fed due to the mass transfer barrier, while alumina fed to a open feeder hole would give a high emission. What is observed however is a is reasonably constant emission in each feed window no matter which feeder hole is being fed (refer to figures 7.4 and 7.5). This suggests that the emission still escapes via other route during normal operation and is not escaping solely through the crust. However there is a noticeable change in this pattern occurs when there is extreme changes in covering.

Hence only a fraction of the structural water reacts. Alumina dissolution rates does explain some of the differences between the alumina reaction efficiency of certain cells (i.e the difference between the slow HF response for cell technology I and the faster HF response in cell technologies II and III – refer to chapter 8), but not the difference between different periods in the cell. Difference in the alumina emission contribution and the calculated reaction efficiency for a certain cell can be explained by differences in the crust cover, or more specifically the feeder hole states of the cell. The emissions from different feeder hole states are quite different. With an open feeder hole the alumina emission if localised is able to escape the hole directly. However with a closed feeder hole the alumina filling the hole acts as a mass transfer barrier against the loss of emission, scrubbing the gas if it manages to pass through the barrier (i.e. the case in a partially filled hole – refer to section 7.8.3). Hence the feeder hole state will dictate the amount of HF reaching the surface. This argument is best seen when the crust integrity of cell technology I was dramatically improved (refer to figure 7.21 and table 7.7).

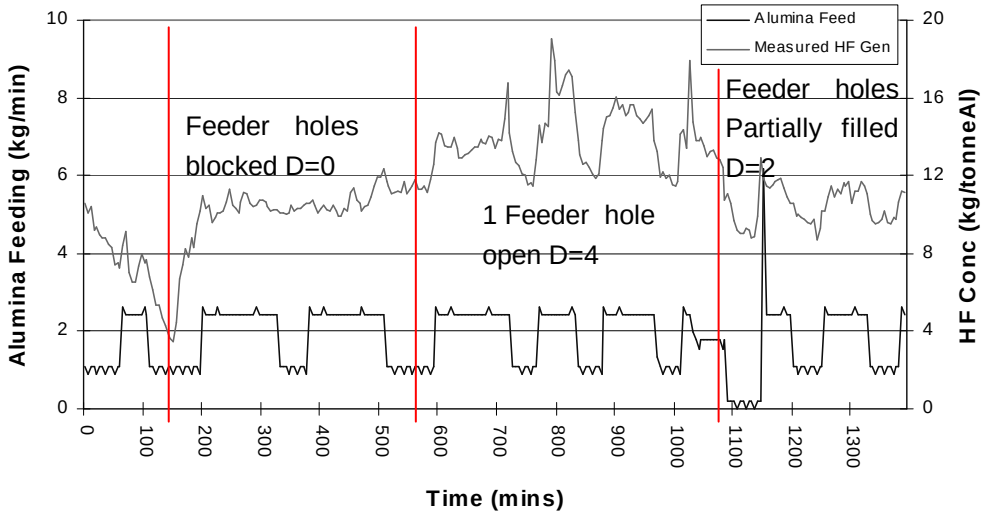

Figure 7.21 – Feeder hole state changes for extreme changes in crust for cell technology I.

Table 7.7 – Calculated Δ correlation data for extreme crust changes in cell technology I.

Trial	Time	pH_2O	O (kg/h)	U (kg/h)	B (kg/tAl)	D (kg/tAl)	R.E. (%)
Normal	5-6am	1.34	1.21	0.8526	10.24	6.60	24.56
Crust	02-03am	1.24	0.5615	0.5471	9.87	0.27	0.99
	13-14pm	1.31	0.8465	0.6259	8.16	4.07	15.16
	20-21pm	1.44	0.6325	0.5162	7.74	2.15	7.99
	Track @ 16.05	1.34	--	--	--	--	--

Here a primary alumina layer was put on top of the crust for the duration of the trial (4 days). As with the results seen for cell technology II (section 7.7.2) the layer progressively deteriorated, though the effects of scrubbing and degenerating crust integrity can not be separated due to the poor crust of cell type I at the time of the measurements. However if the emission trace (figure 7.21) and calculated non alumina feeding (table 7.7) for the first day of this trial are studied it can be seen that the emission varies considerably over the day. This is due to the changes in feeder hole state.

Before the trial began a single feeder hole was open, D was normal for this cell type (D~7) and the reaction efficiency was approximately 25%. When first added, the primary crust coverage completely fills in the feeder holes. This is seen in the crust integrity check sheet for that morning. For this period D~0 and the reaction efficiency is almost zero (02-03am in table 7.7), making the changes in the alumina emission indistinguishable. This is the stabilisation period of the cell cover where the gas vents are being established, gas bubbles through the covers, and little flame hydrolysis is seen.. During this period crust integrity is almost 100%. After a while a feeder hole becomes unblocked (13-14pm in table 7.7) and the alumina emission becomes identifiable once again. Here the reaction efficiency (R.E.) can be calculated using the Δ correlation as 15% - showing a feeder hole to be at least partially open. After the track (@16.05) the feeder hole become almost completely blocked, changing D to 2 and reaction efficiency to around 8. This suggests that the crust has now aged enough to have some permanent vents for the emissions and that the feeder holes are now partially allowing the emissions from the alumina to escape.

Obviously the alumina reaction efficiency is dependant on crust integrity (which encompasses feeder hole state). Note that without a clear difference between alumina emissions the non alumina feeding emission can not be accurately calculated. It is

affected by the crust integrity also, so during this trial the alumina emission and non alumina feeding are not independent. This makes the Δ correlation invalid for this region. Overall this shows that with some open feeder holes the alumina emission is probably emitted with little effect from the crust cover, especially with an aged cover. However once the crust integrity and feeder hole states reach a certain level (i.e. nearly fully blocked) then emission retention become a factor in the emitted alumina contribution which effects the amount of emission detected. This is seen in the $D_{feeding}$ value and calculated reaction efficiency.

CONCLUSION.

It is likely then that a fraction of the structural water reacts, and an amount is prevented from being emitted according to the number of open feeder holes and crust integrity. This all suggests that the reaction efficiency (and D as it is reduced proportionally with R.E.) is a measure of both the feeder hole state and a measure of the amount of amount of structural water reacted. Therefore crust integrity becomes an important factor in HF emissions. Both the non alumina feeding emission and alumina emission have part of their content retained in the crust due to its scrubbing ability.

7.8.3. Feeder Hole Mechanisms.

From the results of the results of the preceding sections mechanisms for the journey for secondary alumina (s-alumina) from a point feed shuffle to entry into the bath can be proposed.

Open Feeder Hole.

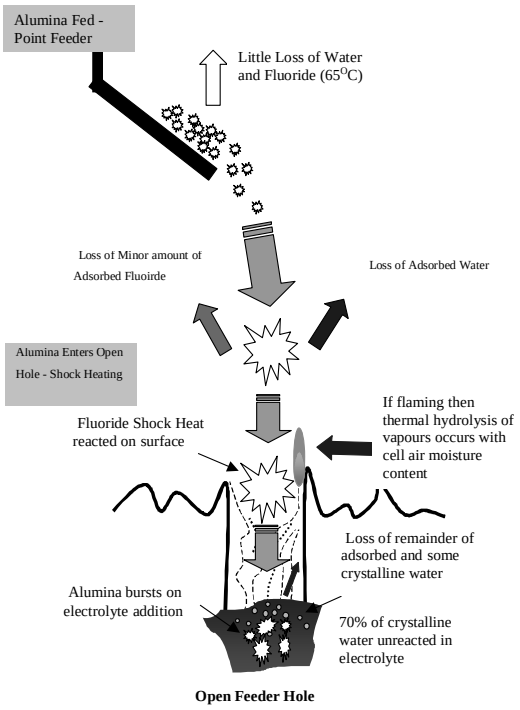

Figure 7.22 - The journey for s-alumina feeding to a open feeder hole.

The proposed mechanism is shown in figure 7.22. Here the alumina is heated to 55 to 70^{O}C in the shuffle before being fed. Little water and fluoride is lost from the bulk (neglecting surface losses) during this period. As the alumina is fed it undergoes a large temperature change due to the fumes being emitted from the open hole (the major source of fume from this type of hole) reaching bath temperature once immersed in the electrolyte. Effectively the alumina is shock heated with most of the water lost via rapid desorption/dehydration, but little of the adsorbed HF lost. The remainder of the water is lost once the alumina particles explode from the structural waters rapid expansion in the bath. A fraction of this water content reacts with the bath, the remainder either enters the bath as dissolved water or is lost as fumes escaping through the open hole. Here the alumina feed component is the greatest as there is no mass transfer barrier against the immediate release of the alumina water primary HF generation. Thermal hydrolysis is also promoted by the exposed bath. If the feeder hole flames (as is often the case for open feeder holes) then the non alumina feeding emission will be much greater for this feeder hole state.

Closed Feeder Hole.

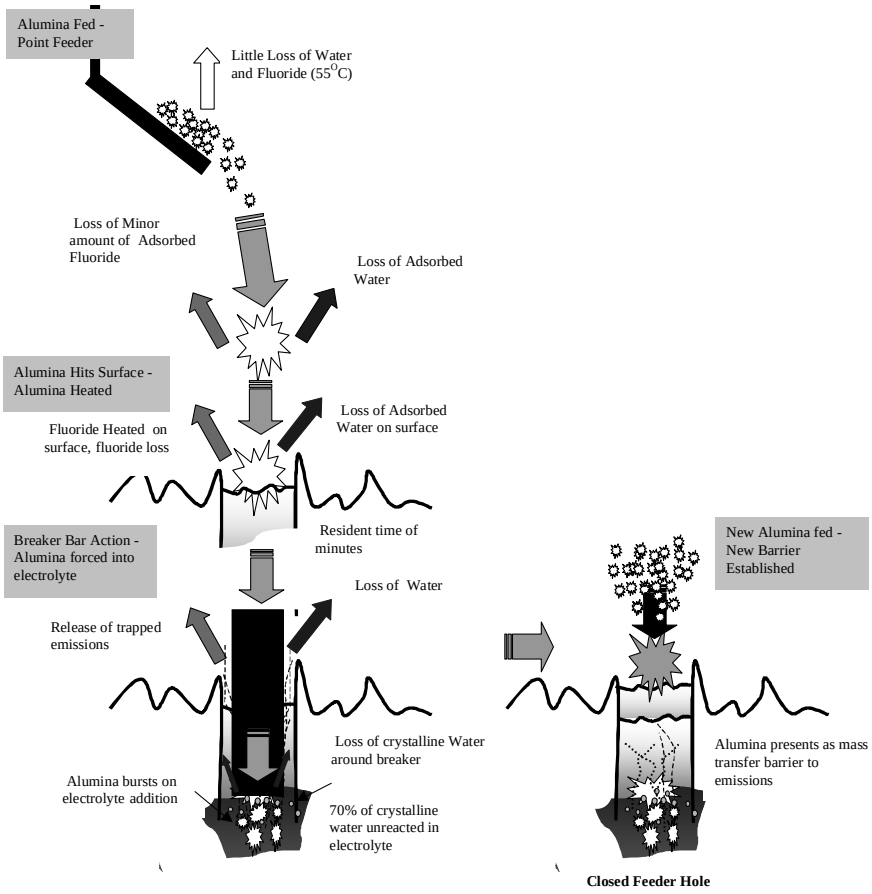

Figure 7.23 - The journey for s-alumina feeding to a closed feeder hole.

The proposed mechanism is shown in figure 7.23. A closed feeder hole has a smaller temperature difference between shuffle and surface due to the heat transfer barrier the extra alumina in the hole presents. This may lead to a smaller heating rate and not ensure the alumina is shock heated. Hence it is possible that once the alumina hits the surface after crust break, that it could lose some "adsorbed" HF during its time at the top of the hole. More importantly is the mass transfer barrier that the closed hole presents. A closed feeder hole does not allow any emissions to escape between shuffles (unlike a partially filled hole). It is speculated that the majority of the trapped gases escape on crust break (as shown in the wet alumina trial section). The added alumina then provides a formidable barrier, not allowing the gases to escape. Due to this barrier the thermal hydrolysis emission is significantly reduced compared to the open feeder hole state. This reduces the non alumina feeding emission as the overall crust integrity of the cell benefits from this feeder hole state.

Partially Filled Hole.

The results are in between the former mechanism. The basic difference to the closed feeder hole mechanism is that the alumina dump at the end is not sufficient to act as a mass transfer barrier and the emission escape via a volcano with dusting. The scrubbing behaviour of the fresh alumina is likely to have an effect on the composition of the emitted gases also, reducing the HF emitted to the ducts. Here though the bath is not exposed to the cell air so that thermal hydrolysis can not occur. Hence the non alumina feed emission will not increase with this feeder hole state. The major differences are shown in figure 7.24.

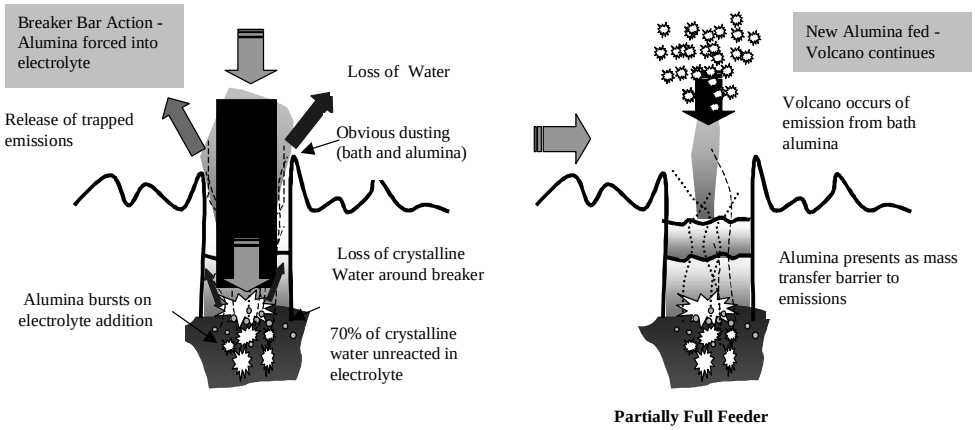

Figure 7.24 - The journey for s-alumina feeding to a partially filled feeder hole.

7.8.4. Conclusion.

Feeder hole state is an important hydrogen fluoride emission factor. The state of a feeder hole – open, closed or partially closed – form part of the effectiveness of the crust to act as a mass transfer barrier. These states are an important part of the crust integrity of a cell. An open feeder hole allows both emission to escape and moisture to enter the cell. When a feeder hole is open and flaming the thermal hydrolysis generation content is greater and the emissions from alumina feeding are greater as there is no mass transfer barrier to pass through once the alumina enters the bath. A closed feeder hole has the opposite effect. It is an effective barrier to both moisture and emissions from the electrolyte and both the alumina feeding and non alumina feeding emission are reduced by this feeder hole state. A partially filled feeder hole allows the alumina feed emission to escape but still forms a barrier to the cell air, and thus reduces the thermal hydrolysis component.

7.9. Duct Temperature Effects.

From the theory established duct temperature should not be a variable which directly affects the emission. This is because there are no significant HF generation processes occurring in the duct. Therefore any correlation that the emissions have with duct temperature will be the result of a factor which affects both the duct temperature and the emission generation. This can be seen for cell technology I and II.

7.9.1. Cell Technology I.

Figure 7.24 shows a obvious relationship between cell duct temperature and HF emissions for cell technology I.

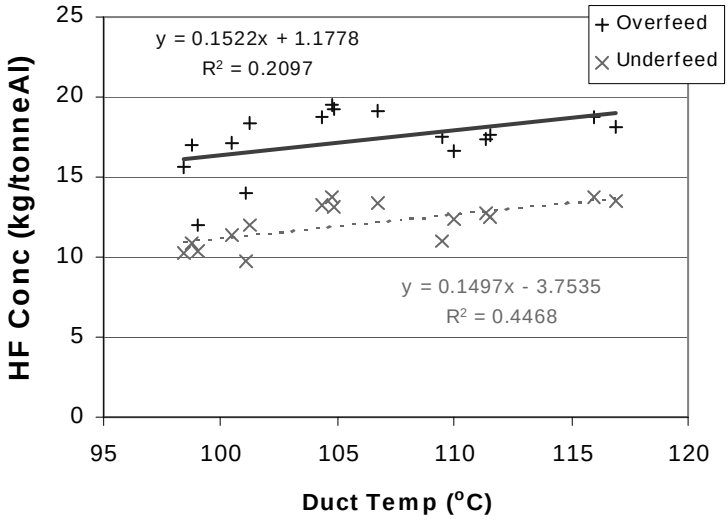

Figure 7.25 - HF conc/feeding vs duct temperature for cell technology I.

The slopes of the trend lines for the underfeed and overfeed emission (figure 7.25) show that the slopes are very similar. This reinforces the validity of the correlation.

However due to the variable crust integrity because of the poor crusting conditions of the normal cell condition there is no clear relationship between duct temperature and bath temperature (figure 7.26).

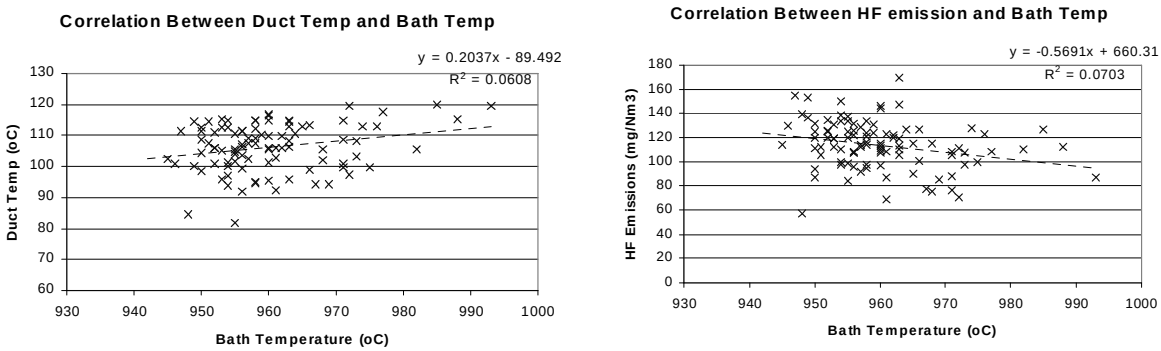

Figure 7.26 - Duct temperature vs bath temperature correlations for cell technology I.

The mechanism is in fact tied crust integrity. The worse the crust integrity the higher the heat loss from the top surface. Simultaneously the emission increases as there is a greater amount of the bath exposed and greater thermal hydrolysis potential.

For a cell with a better crust integrity this trend is not seen. This is illustrated by cell technology II.

7.9.2. Cell Technology II.

Unlike cell technology I, cell type II has idealistic crust integrity. Hence like the measurements of Gadd [53] the duct temperature follows the ambient temperature because there are little long term changes in the top heat loss with batch operations. The changes seen in figure 7.27 are all acute and subside once the heat balance effect is terminated (such as cover loss, anode change, tapping – refer to Gadds top heat loss study for more detail [48]). In general both temperature follow each other.

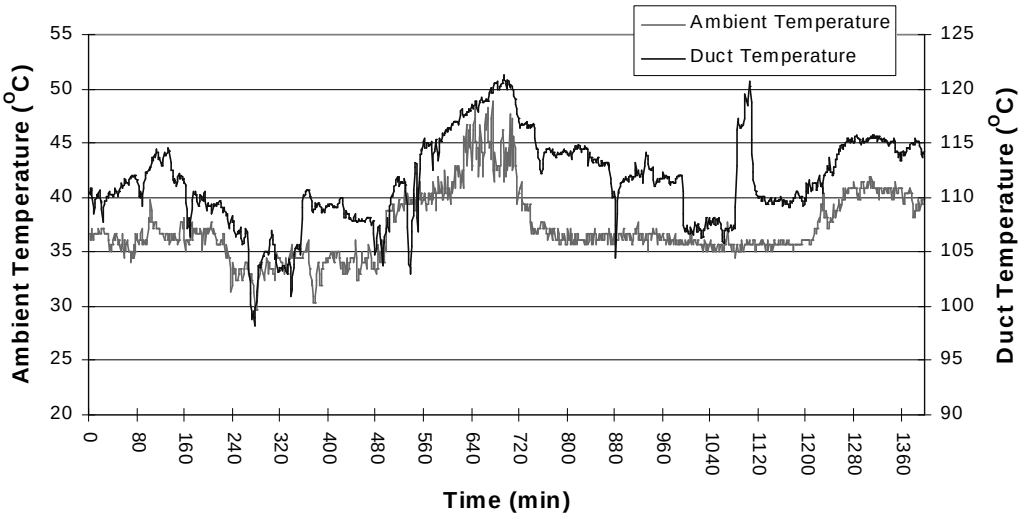

Figure 7.27 – Ambient and duct temperature trends for cell technology II.

This fact effects the duct temperature trends for this cell technology. Figure 7.28 shows that there is a correlation between emissions and duct temperature. Again this is due good crust integrity of cell technology II.

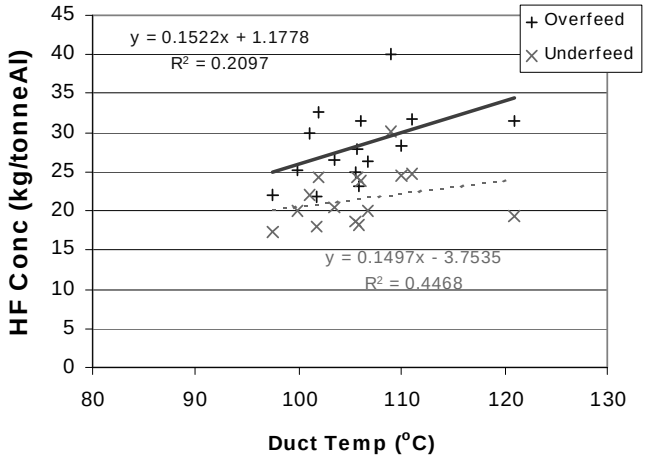

Figure 7.28 – The relationship between duct temperature and HF emissions for cell technology II.

The upwards trend is more likely the result of the ambient humidity dependance on the ambient temperature. As established by the base measurements in section 7.4, cell technology II experienced vast daily changes in the ambient humidity. As the thermal hydrolysis content varies with this (section 7.5), the duct temperature dependance is linked to this content and not a direct variable. This can be seen in figure 7.29, which plots the same data as figure 7.28 but with respect to the ambient humidity (pH_2O).

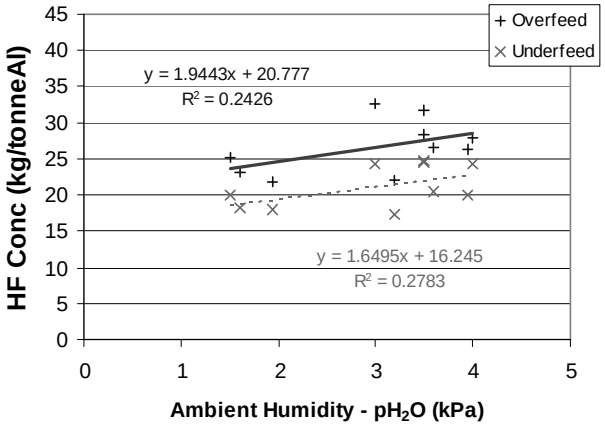

Figure 7.29 - The relationship between ambient humidity and HF emissions for cell technology II.

7.9.3. Conclusion.

Duct temperature does not directly affect the emissions. It is a secondary factor indicating the effect of another cell contributor. In the case of poor cell covering it indicates the changes in crust integrity and this effect on secondary HF generation. In the case of a cell with good crust cover the emission follow the humidity (again secondary HF generation) which is in turn affected by the ambient temperature. For this crust condition duct temperature has been shown to follow ambient humidity trends.

7.10. Bath Temperature.

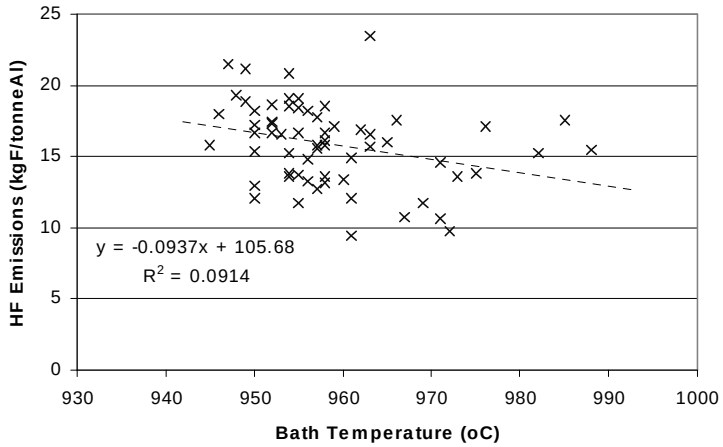

Figure 7.30 – The correlation between bath temperature and HF emissions for cell technology I.

As figure 7.30 shows, there is little correlation between the gaseous HF emissions and the bath temperature. The emission is rather scattered and the fitted trend line is has a very small correlation coefficient. This poor relationship can be also generalised to the excess AlF_3 composition. Any general text [8, 11] will show that this is the major factor affects the liquidus temperature of the bath in an industrial cell (refer to figure 7.31).

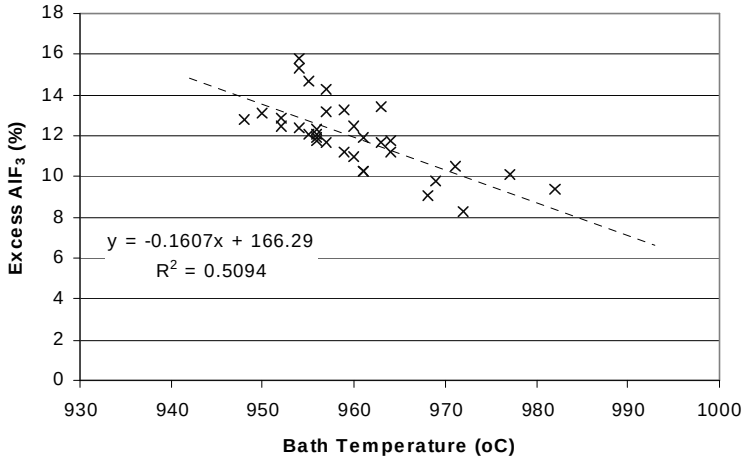

Figure 7.31 – The poor correlation between excess AlF_3 composition and bath liquidus temperature for cell technology I.

This poor agreement fits the findings that the alumina emission (characterised by $D_{feeding}$) is relatively unaffected by anything other than the crust integrity. However this

correlation is a little surprising as the reaction rate of alumina water and anode hydrogen in the bath should be temperature dependant. It is likely that for HF generation other factors such as crust integrity in cell technology I are dominating. For cell technology II a similar poor correlation can be found. As concluded (section7.5), humidity is the dominating factor for this cell technology. This can be seen in figure 7.32:

Figure 7.32 – The non-relationship between cell temperature and HF emissions for cell technology II.

In both cases the trend should show increasing emission with temperature due to

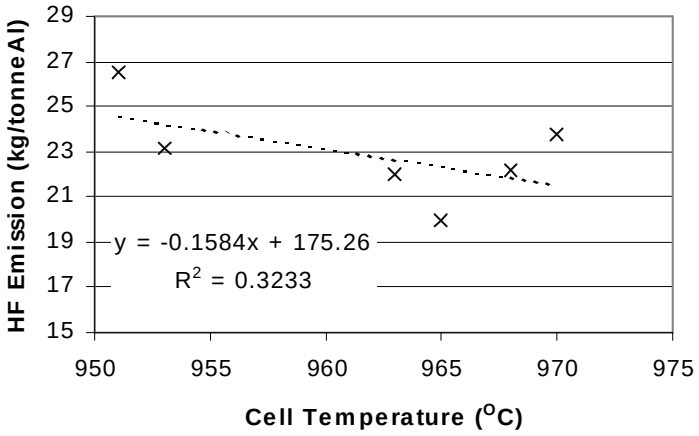

increased vapourisation [6] as shown by Franke [37] (figure 4.12) and Henry [2] (figure 4.13). As other factors dominate this, was not measured.

7.11. Overall Conclusions.

All emissions from the three studied cell technologies follow the same basic trends. Each emission was found to follow the alumina feeding pattern, and consisted of two separable components: The alumina emission and the non alumina feeding emission.

The alumina emission –Is thought to be generated from a percentage of structural water dependant on the dissolution process in the cell (cell technology dependant) with this generation content varying for an individual cell due to changes in the feeder hole state. Here the generated emission is thought to be partially retained during its exit pathway from the feeder holes. Thus overall this contribution depends on alumina feeding rate, alumina composition, crust integrity (of which feeder hole state is an important component) and cell technology. Bath temperature appears to have little affect on this composition.

The non alumina feeding emission – Found to consist of the anode hydrogen emission component and also a thermal hydrolysis component. Here it was found that the non alumina feeding emission is mainly affected by the absolute moisture content of the air (measured as the partial pressure of water in the air pH_2O). This was seen in the base measurements, when comparing changes in emission during anode shifts (at different pH_2O conditions over the trial period) and also when the duct velocity was changed. This brought more moisture into the cell and increased the hydrolysis component of the emission. It was found that the Δ correlation satisfactorily calculated the non alumina feeding emission for most cell conditions.

Crust integrity was found to be one of the most important factors in cell emissions. It acts as both a barrier against moisture entering the electrolyte causing hydrolysis and also a mass transfer barrier against emission evolution. Feeder hole state – open, closed or partially filled – affect the effectiveness of this barrier and hence play a major role in the crusts ability in emission reduction.

Duct temperature does not affect the emission directly. This fits the finding of the generation mechanisms which are not affected by the duct temperature directly. Effects seen in both the emission and the duct temperature are related to the dependance on both on a common factor such as ambient humidity and crust integrity.

8. Modelling Hydrogen Fluoride Emissions.

Based on the theory established in the previous sections, two separate types of modelling can be conducted. Firstly the alumina feeding emission response to changes in alumina feeding rate can be investigated and a model devised to explain this in terms of the water content of the alumina. Secondly an overall predictive model can be calculated. This would takes into account the different generation mechanisms common to the studied cell technologies. This predicted emission and the individual contributions can then be compared to the actual data for a particular set of conditions.

8.1. Dynamic Modelling.

8.1.1. Step Response Analysis.

Introduction.

It was established in section 5.3 that the emissions data from the industrial cells follows the feeding cycle of alumina. This was attributed to a primary generation reaction of the constituents of the electrolyte with mainly the structural water of the alumina. Closer inspection of the step (figure 8.1) shows the actual response of the HF emission is not immediate but follows a response curve.

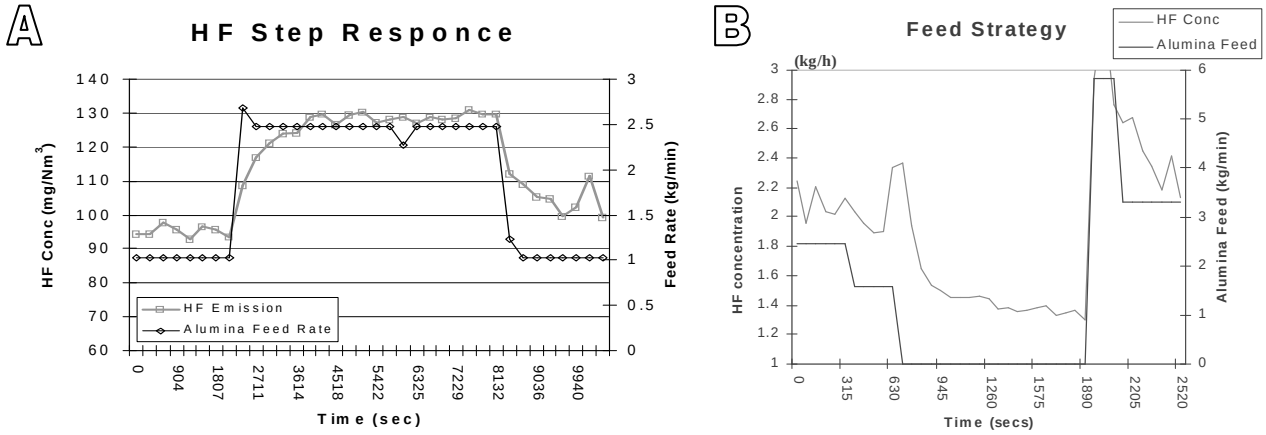

Figure 8.1 – Step response of HF emission to alumina feed for (A)Cell technology I. (B)Cell technology II.

As predicted the HF concentration follows the alumina concentration profile (figure 8.1). It is suggested that the response is mixture of both the alumina dissolution process

and the mixing effect of the gases within the cell extraction system. In the industrial investigations, the HF meter was situated in a down stream duct. Even though the flow rate was sufficiently high to allow little delay between events and readings, the analysis relies on the emissions travelling between generation and detection unchanged. This is not the actual situation. In reality the gases mix above the bath and will not be the ideal plug flow stream expected. This will add to the emission response characteristic.

The second factor will be alumina dissolution. Figure 8.2 illustrates the measured free alumina concentration in the bath during the tracking period illustrated in figure 8.1a.

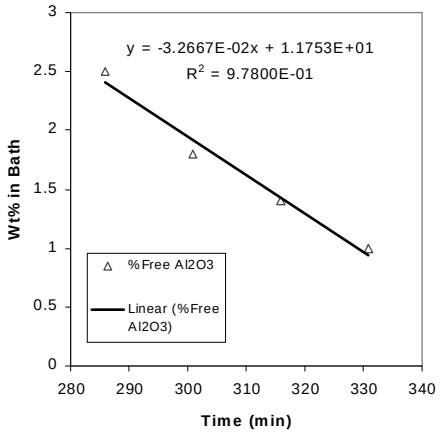

Figure 8.2 – The alumina concentration decay curve for track for cell technology II.

The decay is linear, as constant electrolysis dictates.

The difference between the track period in figure 8.1b and the alumina decay line in figure 8.2 is two fold. Here both the mixing effects and also the water release from alumina during alumina dissolution cause the decay response. While total alumina dissolution depends on both the stages in alumina dissolution and the final electrolysis process, HF emission results from only the water lost during this process. According to classical alumina dissolution process, this occurs at the start of the dissolution process. Here the structural water is lost after the alumina is fed during its conversion from gamma phases to alpha phase alumina.

This fits the proposed dissolution scheme of the alumina exploding in the bath and subsequent conversion to alpha alumina in the bath [16, 22]. If this is the case, in theory the HF response curve represents the first stages of the alumina dissolution process and any factors affecting this (i.e. feed distribution and alumina agglomerations – refer to section 3.5) will also affect this response curve. If this dissolution mechanism is followed, the alumina would release the water in the early conversion stages, and then

the further dissolution stages would not be seen in the emission. These stages would also be dependant on feeding technique as smaller additions would result in faster alpha conversion. Larger agglomerates would take longer for the total alumina to be converted and hence lead to a longer HF decay time constant in the emission response. This should be in the HF emission response.

Fitting the Model.

Simple step response theory [54] shows that this follows a classical first order step response:

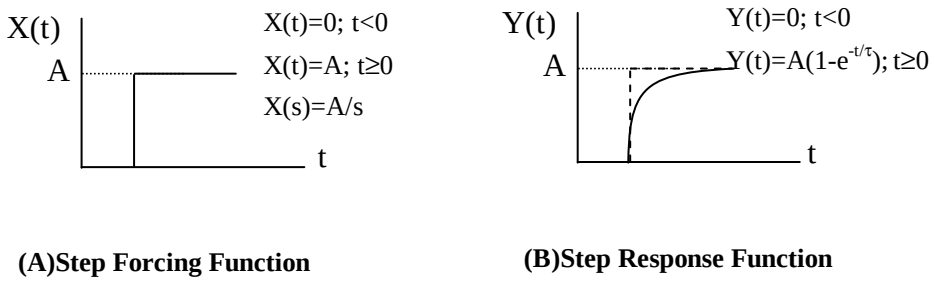

Figure 8.3 - The response theory for a step forcing function.

The negative step follows the same theory and results in a decay curve.

In the measured data the response curves differ as they have a constant starting value (x(t)=a) or non alumina feeding emission contribution. Hence the curves can be compared on a amplitude normalised basis as outlined in the following figure:

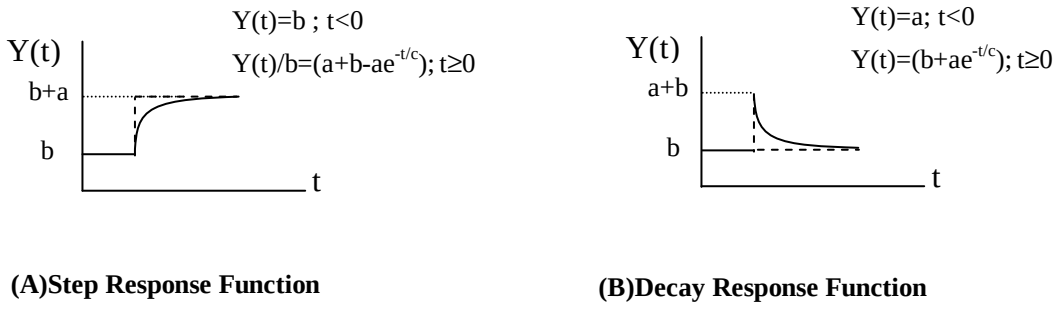

Figure 8.4 – The modified response curve containing a constant emission value.

By fitting a response function in the form shown in figure 8.4 then the time constant for structural water dissolution can be estimated. Figure 8.5 shows the average results for 20 fits of this step response model to emissions data for cell technology I.

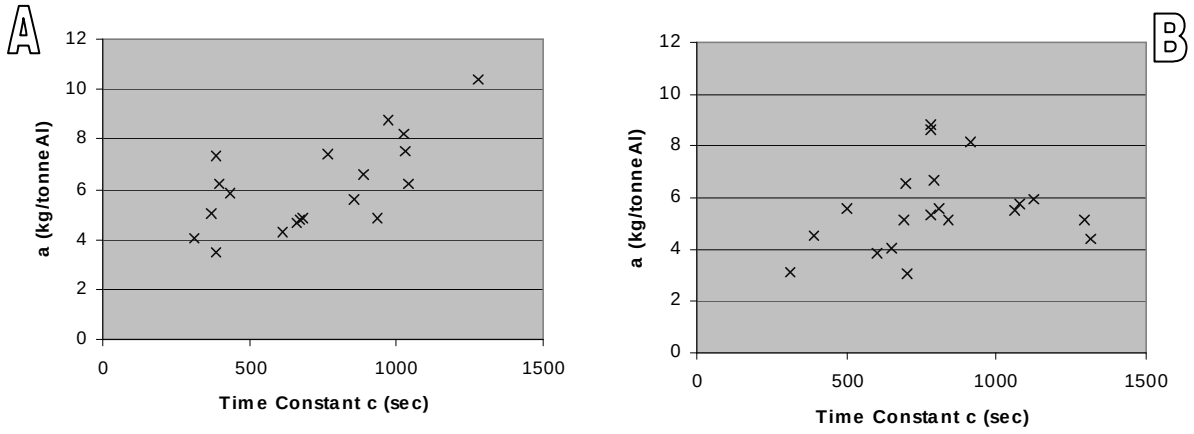

Figure 8.5 - The average results for the step response analysis for cell technology I. (A)Step rise average values. (B)Step decay average values.

Here it can be seen that the median fit for the step rise is a=6 kg/tonneAl with a time constant of c=780s and the decay step is a=5.5 kg/tonneAl with a time constant of c=682s. However the time constant in both cases ranges from 400 sec to 1200 secs. It must be noted that it is likely that this correlation is dependant on factors such as feeder hole condition (open, closed or partial) and cell condition (temperature and heat balance effects). The most obvious example is the variation in the non alumina feeding emission value (a) for each step as seen in figure 8.5. However due to the non ideal crust condition of cell technology I no quantitative analysis of these effects can be done due to the crust integrity variation.

This difference is also seen in the fits for cell technology II. Cell technology II has good crust cover, so the differences should be clearer. Here only the decay response from normal feed to zero feed was fitted to the model. This is due to the noise in the data. The transition from normal feed to zero feed (or tracking) gives the greatest change in emission compared to the noise in the data – effectively the signal to noise ratio is minimum here. The best data to model using decay response is the significant track periods (longer than 20 mins) where the HF concentration decays to the background level. Including the actual forced track periods of these feeding trials there are 3 other relevant track periods

Two different fits have been determined for cell technology II. On average the general fit has a time constant on average of ~2 minutes (the other parameters vary depending on cell condition). A representative curve is shown in figure 8.6. The other fit has a much longer time constant – two fits were found to have a time constant of 4 minutes and nearly 8 minutes respectively. These are shown in figure 8.7.

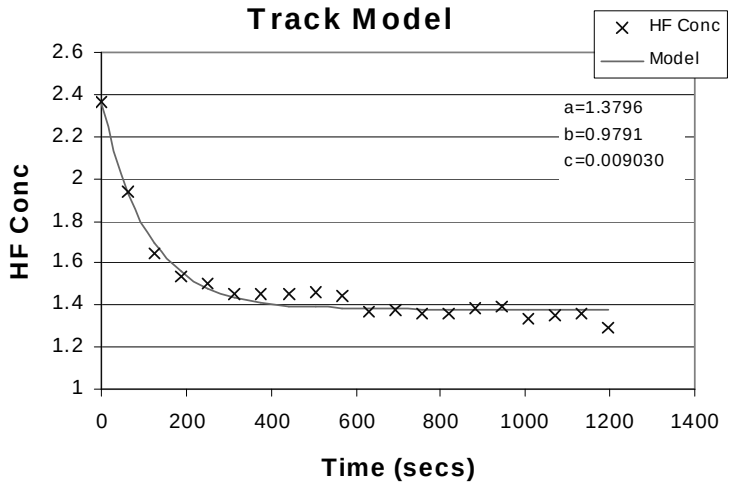

Figure 8.6 – A normal alumina response curve for cell technology II track.

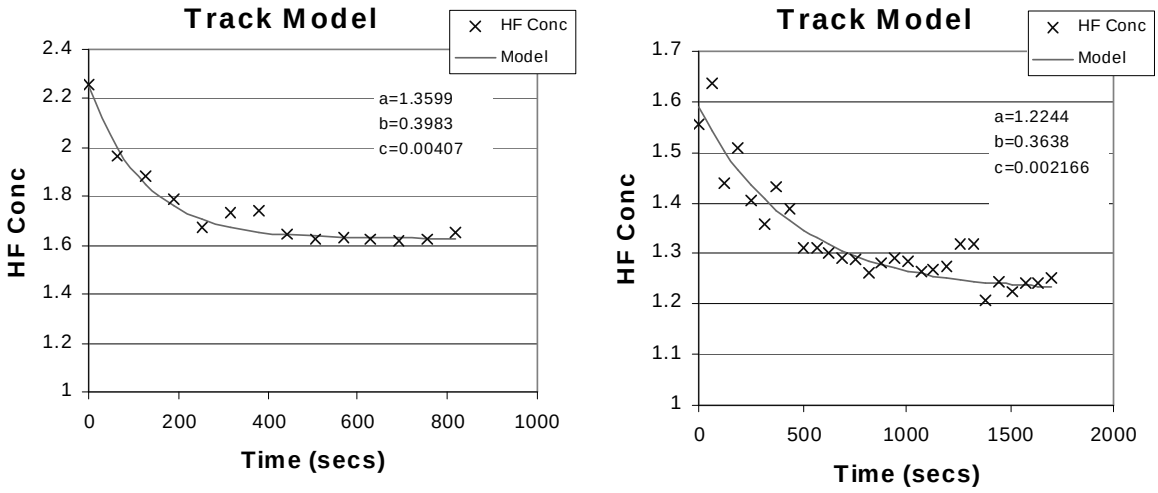

Figure 8.7 – Slower alumina response curves for cell technology II.
(A)Medium Response. (B)Slow Response.

Again the difference has been attributed to feeder hole state and cell condition. Here a is equivalent to $D_{feeding}$. For both the slower HF responses D=0.40 and 0.36. This is about half the $D_{feeding}$ of the normal response, which was found to be on average 0.65 to 0.7. A closed feeder hole does have a different emission and feeding process, and hence would affect the emission and response. In addition, the medium response track (figure 8.7(A)) is followed by an anode effect. Heat balance effects affects alumina dissolution also. The reasons for the different base generation values in figure 4.16 are the cells condition. As shown by the heat balance effects (tapping and anode change), a cells heat balance and condition influence the emission significantly.

Comparing these results, cell technology I average 12 minute time constant suggests that both feeding technology, cell technology, cell condition and feeder hole state differ substantially between these two cells. The response characteristic will be different for both cells. Cell technology II has a much faster flow rate than cell technology II, though it is unlikely that this is sufficiently higher to make a 10 minute response difference. This difference is more likely due to alumina dissolution differences.

Emission generation and hence stages of the alumina dissolution process are much slower for cell technology I, just by comparing the results with cell technology II. This connection may be the result of the aforementioned early stages of feeding, where less ideal alumina feeding (clumps) result in a slower alpha conversion than ideal (individual alumina particles) feeding. Both cell technologies have different point feeder designs. Cell technology I point feeders are a retro fit design which dumps rather than pours the alumina. It is likely from this observation that there are greater agglomerations in this technology compared to the fed alumina from technology II. It may also be due to better turbulent transport [18] down the center channel enhancing dissolution in cell technology II compared to I. However only a qualitative guess can be made as a detailed study of alumina dissolution and emissions generation was not conducted.

Conclusions.

The alumina feed response is a mixture of gas mixing in the extraction system and alumina dissolution properties. From the time constants derived from the step response analysis, it appears that cell technology II has a much faster dissolution time than cell technology I. This is likely related to the differences in the point feeding technology between the cells.

8.1.2. The Rate Model.

As shown in section 5.3 the main primary generation HF mechanism for the feed generated emission is a water reaction (alumina structural water) with the electrolyte as follows:

$$AlF_3 + 3/2H_2O = 1/2Al_2O_3 + 3HF \quad (8.1)$$

This is not the actual mechanistic reaction that occurs within the bath but the stiochiometric representation of the process. Even considering the results of this

investigation we can still only speculate about the actual mechanism of the reaction and the exact species that enter the bath. All that can be said for certain is that the water species are likely hydroxyl species in equilibrium with other molten ions. However a generalised rate law can be guessed at using the integration method [55] if the following assumptions are inferred to hold true:

- The aluminium fluoride concentration in the bath is constant at the feed area.
- The primary generation water concentration is proportional to the HF concentration measured.
- The rate of water dispersion in the bath is proportional to the rate of alumina dissolution.

As shown previously the last two are true for the initial stages of alumina dissolution. The first assumption however will have to be inferred to hold true.

If these are valid then a pseudo rate law of the following form can be used:

$$r_{HF}=k'[H_2O]^x \text{ where } k' = k[AlF_3] \text{ with } x = \text{order of the reaction} \quad (8.2)$$

Due to the complexity of the situation three orders were tested – first, second and 1.5 order, using the HF concentration data from the industrial runs for cell technology I. The data from this cell has the clearest correlation between feeding and generation and has the simplest feeding scheme. Twenty fits were made using a single step (rise and decay) from several selected days data. Three representative step decay fits are illustrated in figure 8.8.

Note that the first point in all fits is the most unreliable, due to the five minute averaging process used on the data. This point potentially includes data from minutes before the step change. This can lower its value. At any rate the second order model fits better than either the first or 1.5 order and this is the order that will be used in the final model, as shown in equation 8.3. In essence given the path the water takes to react with the bath (which differs to the alumina dissolution due to its reliance on alumina shattering etc.., though it can be said to be the same for a first approximation) and the diffusion barriers of the HF leaving the cell suggest a high order is quite likely.

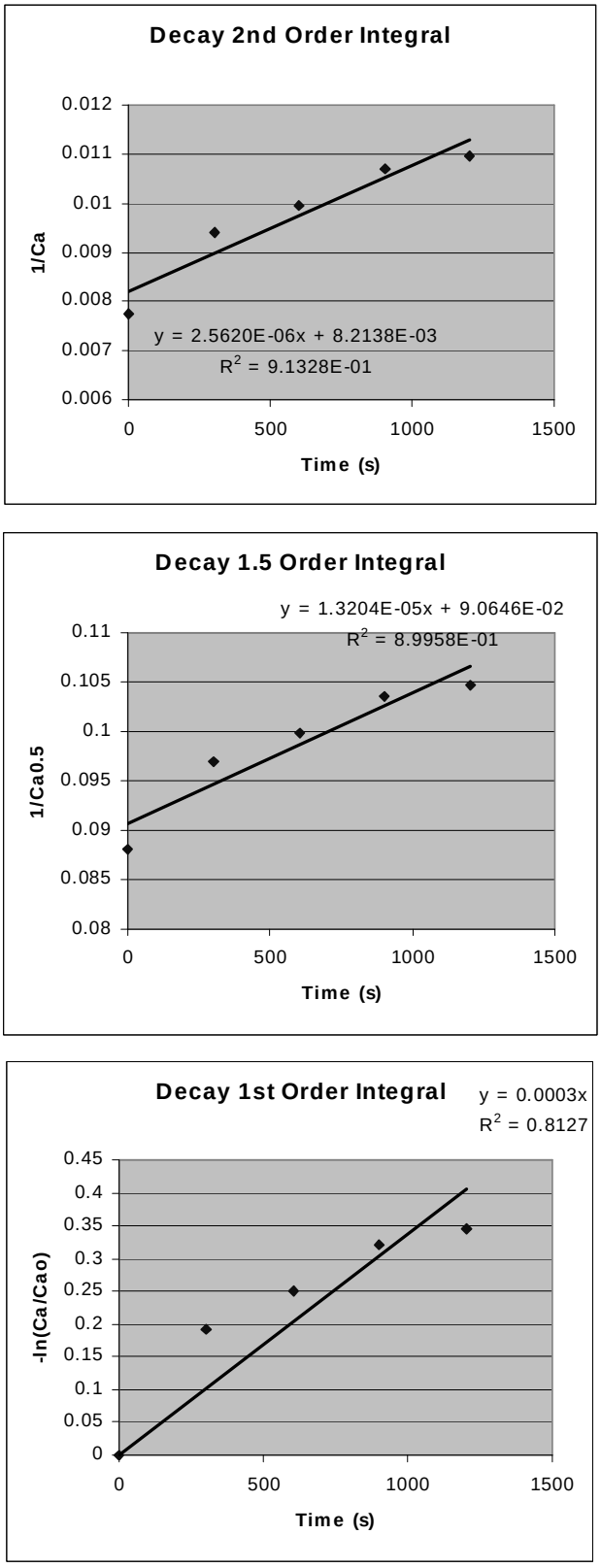

Figure 8.8 – Pseudo rate law fits for cell technology I: (A)Second Order. (B)1.5 Order. (C)First Order.

The same can be found for cell technology II (refer to figure 8.9).

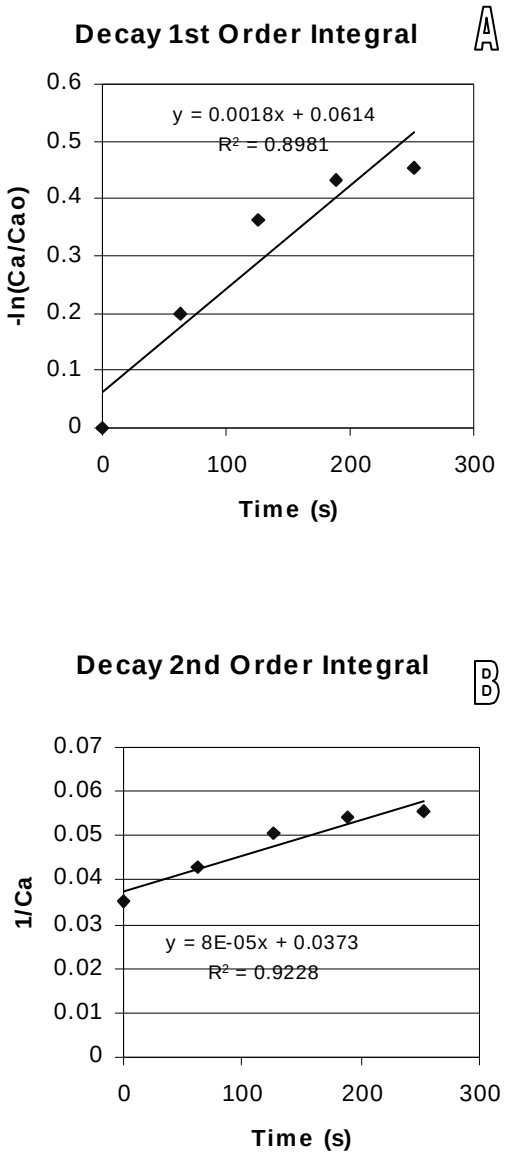

Figure 8.9 – Pseudo rate law fits for cell technology II: (A)First Order. (B)Second Order.

Hence the assumed rate law is of the form:

$$r_{HF}=k[AlF_3][H_2O]^2 \quad (8.3)$$

Values of k can then be found by plotting r_{HF} (measured in kg/h via the industrial results) versus an approximated reacted water concentration based on a 20% reaction conversion of structural water in the fed alumina as illustrated in figure 8.10.

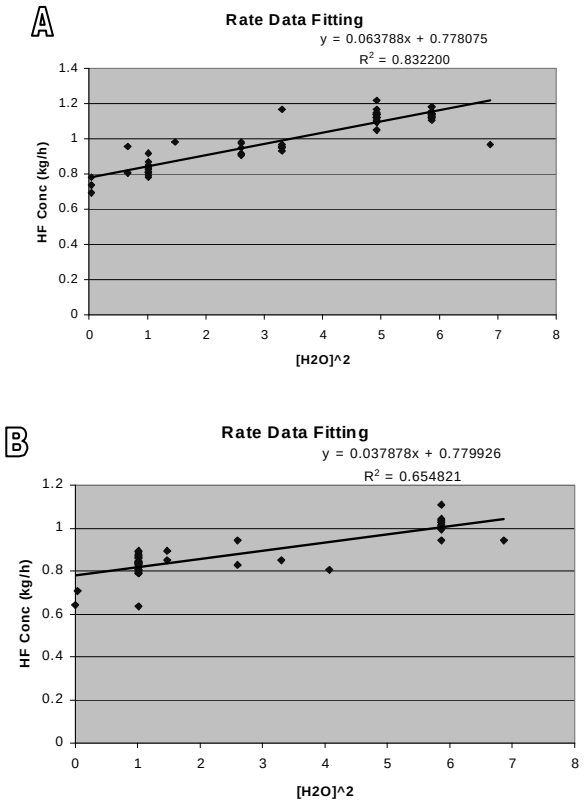

Figure 8.10 – Fitting the pseudo rate equation for cell technology I. (A)High k example. (B)Low k example.

Interestingly the average value found from several fits is $k=5x10^{-3}h^{1/2}wt\%^{-1}kg^{-1/2}$. However if all the runs are considered two distinct values of k are found. One is around $4.0x10^{-3}$ and the other averages about $7.0x10^{-3}$, though it varies slightly in some cases. This is seen quite clearly when the rate equation is fitted to some of the modelled days and a distinct change in the required rate constant is necessary.

This has also been found for cell technology II. Here the rate constant averages $k=1.0x10^{-2}h^{1/2}wt\%^{-1}kg^{-1/2}$. Though two distinct values of k are found. One is around $5x10^{-3}$ and the other averages about $1.2x10^{-2}$. These are illustrated in figure 8.11.

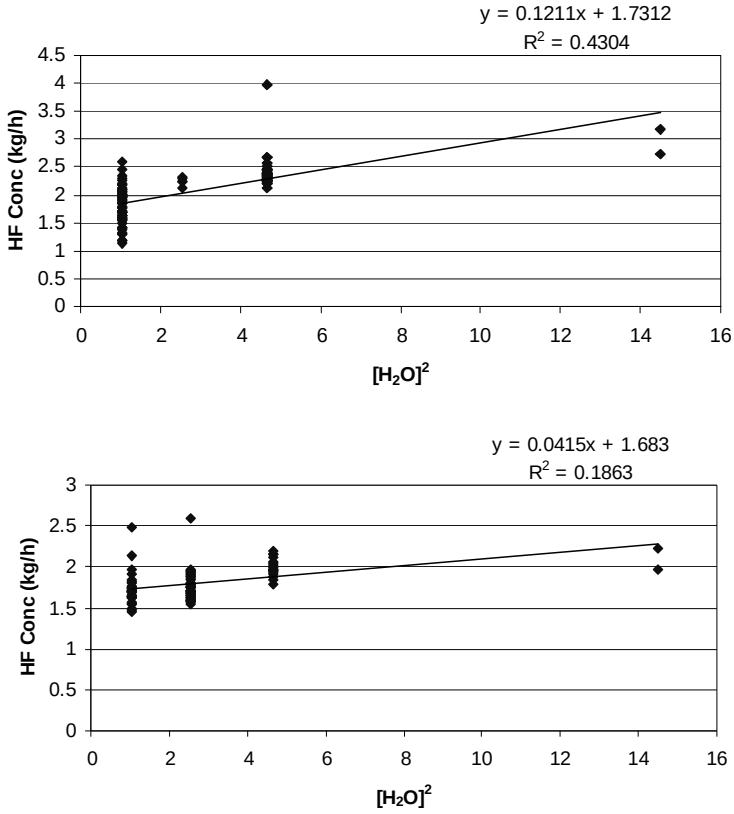

Figure 8.11 – Fitting the pseudo rate equation for cell technology II. (A)High k example. (B)Low k example.

This data can be fitted to the emissions breakdown shown in chapter 7:

1). The *alumina feeding* component – The contribution attempted to be modelled.
2). The *background* emission – A constant component dependant on humidity. Here the changes in the alumina feeding content is added.

For the purposes of this simple model the background emission was calculated using the dynamic model (check using the Δ calculation method) and replaced with a constant value appropriate to the period modelled. Hence the following model was used:

$$r_{HF} = B + k[AlF_3][H_2O]^2 \quad (8.4)$$

Where: B = the non alumina feeding emission.

The concentration of the water added to the bath [H_2O] was calculated as a fraction of the alumina added (~0.45wt% from the elemental analysis of the studied secondary alumina). As mentioned this relies on the assumption that the water reaction in the cell

is proportional to the amount of alumina added to the electrolyte. On a large scale this can be said to be true as a first approximation. However in reality the path the water takes to react with the bath is different due to the reliance on exposure from alumina shattering and reaction path through the electrolyte and crust. All this results in a fraction of unreacted water escaping the bath environment.

The rise and decay responses found in the step response analysis for cell technology I was also incorporated into the model for 5 ΔT intervals after a alumina feeding change. The approximate time constants (rise τ=780s, decay τ=682s) were used. The end results for a single run is illustrated in figure 8.12:

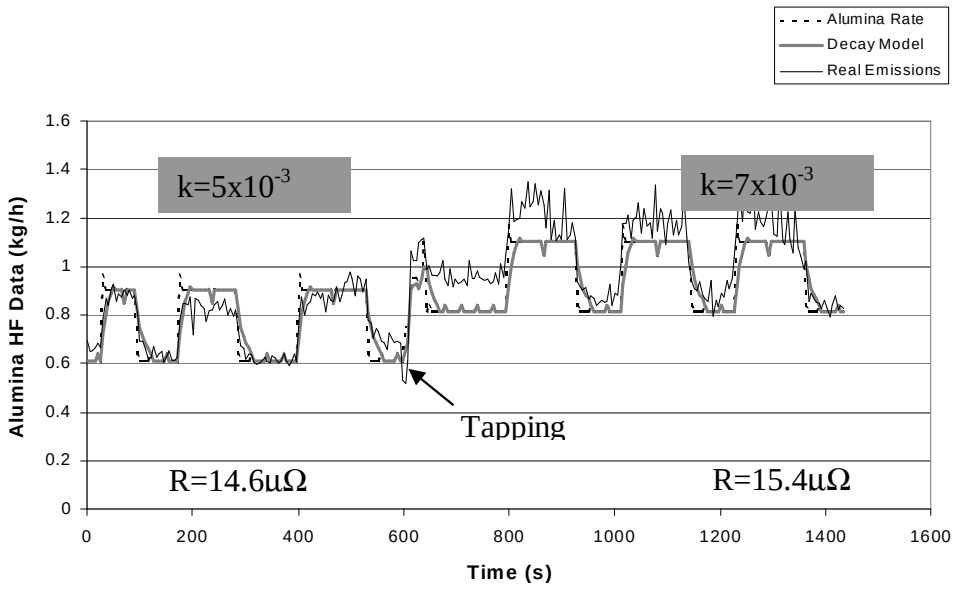

Figure 8.12 – The rate model for HF evolution rates for cell technology I. Model plotted has a k=5x10^{-3}.

It is obvious that the k used to model the data (k=5x10^{-3}) does not fit the entire run. Here the rate constants value changes from 5x10^{-3} to 7x10^{-3} after tapping occurs. These are the two distinct values found when k was initially evaluated. An examination of other days finds the same pattern - whenever there is a resistance change (almost always via anode movement) there is a change in the required k value to fit the model. The general pattern found is that around 14μΩ equates to k = 4 x10^{-3} and around 16μΩ equates to k =7x10^{-3}.

This change also corresponds with a change in $D_{feeding}$. As seen in chapter 7 this relates to crust integrity changes. Simply the resistance change for cell technology I occur from anode movement. This disturbs the crust increasing the non alumina feeding

emission. As crust integrity is also linked to the alumina feeding emission via mass transfer resistances, this is reflected in this emission also.

The same effect is seen when cell technology II is modelled (figure 8.13). Here an anode change changes the crust integrity and this affects the modelled k values. Here crust integrity changes change the emission profile with greater hydrolysis and worse alumina feed emission release.

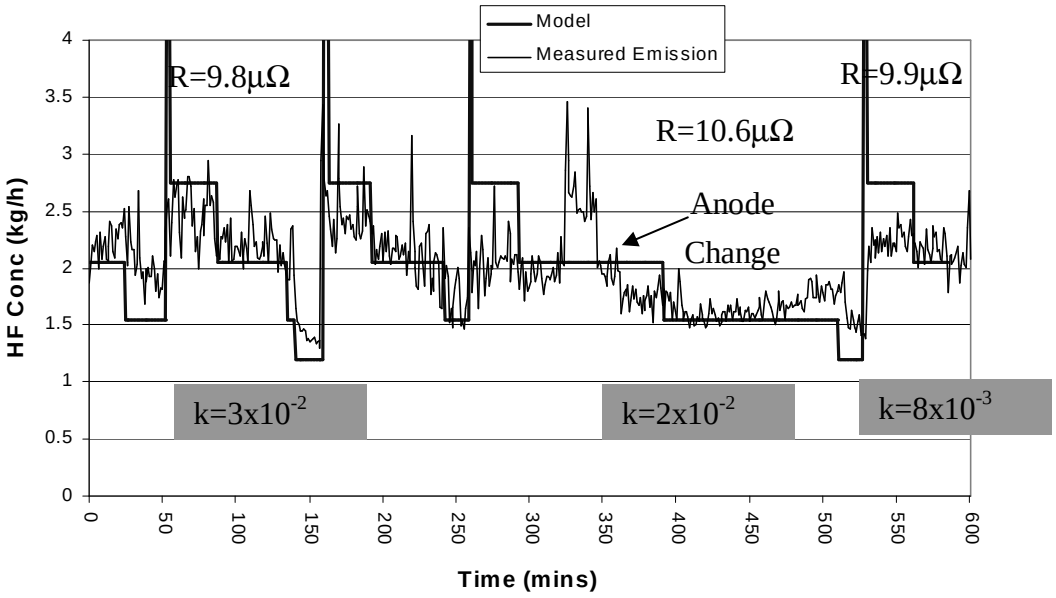

Figure 8.13 – The rate model for HF evolution rates for cell technology II. Model plotted has a $k=3x10^{-2}$.

Here the resistance has little correlation with the changes in k values. This suggests that changes in crust integrity are the most important contributor.

However it is also quite possible that the anode movement also increases the alumina dissolution rate temporally. This is best seen in cell technology I. Here a greater amount of water is reacted due to increased exposure rate and mixing. The only mention of ACD changes affecting turbulence in the literature is in Chensonic *et al.* [19] who only studied the effects between the anode and cathode. It is entirely possible that an unsteady state of bath transport occurs after extreme anode movements (e.g. after tapping) increasing dissolution.

All this can be seen when examining the Δ correlation for different periods shows that the crystalline water reaction efficiency increases from 25% to >35% once the resistance increases.

Table 8.1 – Resistance changes and Reaction efficiencies.

Sample		HF Emission (kgF/tAl)	Resistance (μΩ)	Feeder Holes open	RE (%)
1	A	14.7	14.4	0/3	24
	B	17.5	15.4	0/3	36
2	A	16.6	15.7	0/3	24
	B	16.4	15.4	0/3	20
3	A	16.6	14.4	1/3	20
	B	25.8	15.3	1/3	25
4	A	13.8	14.4	1/3	20
	B	19.4	15.3	1/3	25

As discussed in the section 3.5, the dissolution rate is affected increases in turbulence around the dissolution area. A visual interpretation of the data (refer to figure 8.10) supports this theory as the overfeeding fluctuations (which should be reasonably level) increases once the resistance increases. The literature suggests that turbulence is the major parameter affecting dissolution. From this two theories can then be proposed:

1). Anode movement increases bath turbulence down the center channel for a period of time after adjustment. This moves some of the fed alumina away from the feeder hole interrupting its escape path through the relatively low resistance feeder hole. Hence for random periods not all the gas escapes as it is trapped under crust away from the feeder hole (explaining the increased fluctuations).

2). Anode gas generation destabilisation once the anodes move. Bubble release should result from the initial movement which would have an immediate effect on the turbulence. Moreover as anode gas is the main source of emissions carrier and bath distribution source it is possible that this could effect the turbulence about the feeder holes.

It is likely a combination of both sources as bubble generation is linked to bath movement and crust integrity. As table 8.1 illustrates with a closed feeder hole (reading 1) the effects are exaggerated due to the greater relative decrease in crust integrity the anode movement makes as there are no significant cracks in the crust to start with. Hence the combined effect of crust integrity changes and short term changes in alumina dissolution are the likely cause of these changes.

8.2. Predictive Model.

To gain meaningful laboratory data a model which gives realistic values for HF generation is required. Haupin and Kvande (1993) [6] give the best estimate with quite realistic mechanistic correlations.

8.2.1. Haupin and Kvande Model.

The Haupin – Kvande emission model [6] published in 1993 is reputably the best emission model published in the available literature. It gives a realistic vapourisation model which predicts reasonable results for particulate generation. It also identifies the importance of the condition of the crust by incorporated in the catch factor for particulate entrainment. The problems with this model is its reliance on theoretical generation compared to the actual mechanisms. All primary generation mechanisms have been incorporated into a single calculation. This ignores the fact that each mechanism is affected differently by the cells state and ambient conditions.

This can be seen in the values the model outputs with cell technology I parameters inputted. Here the HF generation is under predicted. As discussed the fault lies in the bulk modelling of the hydrogen (anode hydrogen and alumina moisture) primary generation contribution. A separate model of each generation source must be used as the anode hydrogen is a background contributor, affected by crust integrity, while the alumina water content is more dependant on feeder hole condition. This has been attempted to be corrected within the limitations of the factors identified within this investigation. The following outlines the methods derived from the research detailed in this investigation to calculate the individual contributions.

8.2.2. Primary Generation Contributions.

Hydrogen in the Anode.

Hydrogen in the anode can be predicted using the findings from the experiments detailed in chapter 5. Here it was found that approximately 10% of the anode hydrogen content reacted to form HF with the electrolyte. If the carbon usage is known – calculated using the net carbon ratio and aluminium production – then the amount of HF produced can be calculated using:

$$HF_{anode} = 0.1 \times \text{Net Carbon} \times \text{Al production} \times \text{Anode H content} \quad (8.5)$$

Dissolved Water.

Dissolved water is the least understood contribution investigated in this study. Its prediction is based on plant data rather than mechanistic means. As calculated in Chapter 5 the contributions for the two studied cell technologies is:

Table 8.2 – The dissolved water contribution for the three cell technologies.

Cell Technology	Emission Decay Rate (kgF/tonneAl/min)	Emission (kgF/tonneAl/wt%Al_2O_3)
I	3.35×10^{-2}	0.050
II	1.14×10^{-1}	0.231
III	2.59×10^{-1}	0.404

Hence using the figures in table 8.2, the emission then depends on the alumina content of the bath.

Alumina Water.

Alumina water relies on a number of assumptions. These are as follows.

- The alumina is shock heated on addition to the feeder holes. Hence the majority of the surface water is lost with this rapid temperature change.
- The amount of water reacted with the electrolyte is dependant on the initial stages of alumina dissolution. Better alumina dissolution results in more water reacting with the electrolyte. This makes this generation process technology dependant.

- The amount of HF to reach the extraction system depends on the feeder hole state.

Using these assumptions the alumina HF generation can be calculated using the LOI analysis of the primary and secondary alumina. Here only a percentage of the structural water of the alumina content of the feed secondary alumina is assumed to react. If the LOI(300) result is assumed to represent the surface water and the LOI(1000) is assumed to represent the structural water content of the alumina (this is not the case as section 3.3 explains), then the total amount of reacting water can be calculated.

The calculated fraction depends on cell technology and feeder hole state. Results from cell technology I and II differ due to the design of the cells. Hence the overall reaction figure is based on industrial data from each cell. This figure also differs with feeder hole state due to the mass transfer barrier the different cell states present (refer to chapter 7). Using a percentage of open feeder holes the correlations for cell technology I and II is given in figure 8.14.

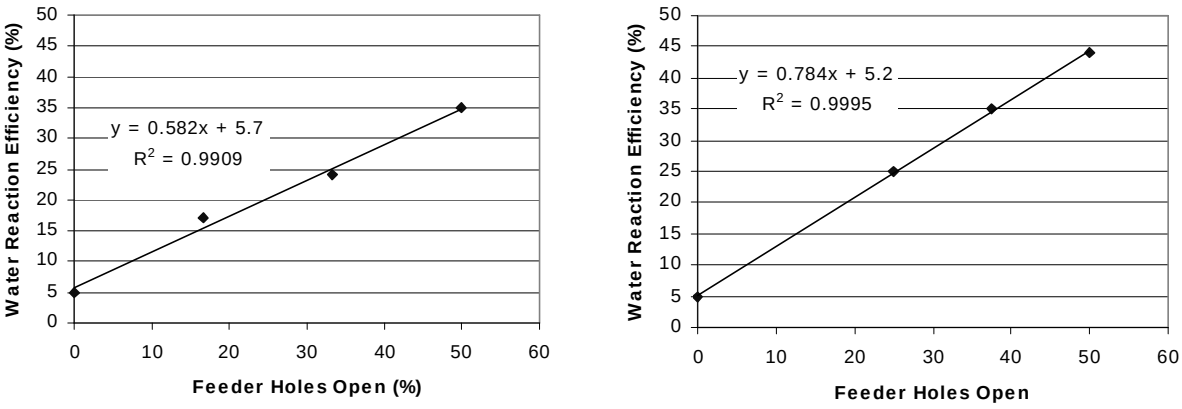

Figure 8.14 – The structural water reaction figures for (A)Cell Technology I. (B)Cell technology II.

This is then generalised by assigning the cell technology I gradient as a retrofit feeding technology = 1 and cell technology II as a total design feeding technology = 3. This gives a general water reaction correlation of:

$$\text{Water reaction (\%)} = (0.101*ftc + 0.481)*\%OFH + 5.7 \quad (8.6)$$

Where:

ftc = feeding technology coefficient (1=Retrofit, 2 = middle, 3=total design).

OFH = Open feeder hole percentage.

Using equation 4.3, the alumina analysis and the water reaction efficiency correlation 8.6, the amount of HF produced can then be calculated.

8.2.3. Secondary Generation Contributions.

Desorbed Fluoride.

As outlined in section 6.2 very little fluoride is desorbed if the alumina is shock heated during the feeding process. Hence emission source has been neglected in this model.

Particulates.

The particulates and thermal hydrolysis calculations are based on the original Haupin-Kvande 1993 model [6] calculations.

Entrained Bath: From Haupin and Kvande [6]:

$$F_{\text{entrained bath}} = 76000 \text{ x } (1\text{-catch})/\text{Surface Tension x Current Efficiency}) \quad (8.7)$$

$$\text{Surf T} = 270 - 0.137*T_b - 3.29*\%Al_2O_3 - 0.19*\%CaF_2 - 2\ln(\%Al_2O_3) + 0.00329*T_b*\%Al_2O_3 + 0.00056*\%CaF_2*T_b - xsAlF_3 \quad (8.8)$$

For the purposes of this model the catch term has been defined as a function of the crust integrity. The crust condition is a qualitative function for this model. No real quantitative research has been conducted on its real effects hence the following function has been used to try and give this term some meaning based on feeder hole state and relative crust state.

$$\text{Crust Integrity} = 0.9 \text{ x Crust Quality Ratio} + 0.1 \text{ x Feeder hole state} \quad (8.9)$$

The crust quality ratio is a the crust state number/3*100. And the crust state number is a relative number attributed to the observed or expected state of the crust. A poor crust has a suggested assigned crust state = 1, a good crust state = 2, and an excellent crust state = 3. The crust state is that relative condition of the top crust independent of the state of the feeder holes.

Vapourisation Particulate Generation: From Haupin and Kvande [6]:

$$F_{VP} = 5351000/ \%CE / P_b*(4*P_M+8*P_D+P_{NaF}) \quad (8.10)$$

Where:

%CE = Current Efficiency (%)

P_B = Ambient Pressure (kPa)

$P_M = (-K_p+(Kp^2+4K_p*(VP_b-P_{NaF}))^{1/2})/2$

$K_p = Exp((-21085/T)+15.45)$

$P_{NaF} = VP_b*(0.2073-182/T)*(-0.6366 + 1449*CR – 1.068*CR^2 + 0.2556*CR^3)$

$VP_b = Exp((-A/T) + B)$

$A = 21011 – 12235*R_b + 18862*R_b^2 - 6310.5R_b^3 + 116.7*\%LiF – 55*R_b*\%LiF – 151*\%MgF_2 + 1.466*\%MgF_2^2 - 6.7*\%Al_2O_3$

$B = 25.612 – 9.681R_b + 11.854R_b^2 – 3.8315R_b^3 + 0.025*\%LiF – 0.013*R_b*\%LiF – 0.0008*\%CaF_2 – 0.08696*\%MgF_2 + 0.001112*MgF_2^2 - 0.11*\%Al_2O_3/(1+0.193*\%Al_2O_3)$

R_b = Weight Ratio NaF/AlF_3 in bath

CR = Mol ratio $(NaF + LiF)/AlF_3$

T = Temperature (K)

Thermal Hydrolysis.

Again based on the model presented by Haupin and Kvande [6]:

$$F_{Hydrolysis} = \frac{380000(HBA)}{(\%CE)(P_B)} Exp\left(13.746 - \frac{14370}{T}\right) P_M^{1/2} \left(\frac{p_{H2O}}{102.9}\right)^{1/2} \quad (8.17)$$

Where :

p_{H2O} = Ambient Humidity of air (kPa).

HBA = Hydrolysis by air factor. Defined by Haupin and Kvande as 1 being average, 3 being excessive. It is an adjustable factor used to take into account for variations in the kinetics resulting from changes in ore covering. For the modified model both the crust integrity and feeder hole state have been taken into consideration:

$$HBA = 0.4*\text{Open Feeder Hole \%} + (100 – \text{Crust Integrity})*0.5 + 2 \quad (8.18)$$

The last constant recognises that there will always be a small percentage of thermal hydrolysis even with excellent crust integrity and no open feeder holes.

8.2.4. Modified Haupin-Kvande Model.

As asserted above, more realistic results are obtained by separating the primary generation contributions. At this point in time the vapourisation, entrainment and hydrolysis contributions are all calculated using the method outlined by Haupin-Kvande [6]. However in the primary generation portion the mechanisms have been separated. With these modifications the non alumina feeding emission can be calculated and the real emissions breakdown outlined in this report can be evaluated.

This model does not include the changes that occur due to alumina dissolution effects and heat balance effects. Such changes are dynamic and will not be explored. This is best dealt with using the Wahnsiedler correlation (equation 4.16) [5].

Validity of the Model:

Tables 8.3 and 8.4 compares the results from the modified model to that for cell technology I and II respectively.

Table 8.3 – Comparing the Model and measured results for cell technology I.

Parameter	Cell Technology I	Model
Cell Temperature (^{O}C)	963	
PH_2O (kPa)	1.6	
Open Feeder Holes	1	
Crust Integrity	1.5	
Particulate	6.156 kg/tonneAl 31.8%	5.850 kg/tonneAl 30.9%
HF	13.30 kg/tonneAl 68.2%	13.10 kg/tonneAl 69.1%
Alumina Emission	5.27 kg/tonneAl	5.27 kg/tonneAl
Non Alumina Feeding Emission	6.5 – 10 kg/tonneAl ~ Ave = 8	7.83 kg/tonneAl

Table 8.4 – Comparing the Model and measured results for cell technology II.

Parameter	Cell Technology II	Model
Cell Temperature (^{O}C)	962	
PH_2O (kPa)	2	
Open Feeder Holes	1	
Crust Integrity	2.5	
HF	21.0 kg/tonneAl	20.7 kg/tonneAl
Alumina Emission	8.4 kg/tonneAl	8.67 kg/tonneAl
Non Alumina Feeding Emission	12.6 kg/tonneAl	12.07 kg/tonneAl

The model agrees within acceptable limits (±10%). However as the results show that when comparing an average emission the results can be quite variable due to changes in the crust integrity for cell technology I and changes in the humidity for cell technology II. Overall if the crust integrity is predicted correctly, the results follow the trends seen in chapter 7. This will be shown in the following section.

8.2.5. Model Predictions.

The following section compares the results of the model and actual measurements for changes in environmental factors for the different cell technologies.

Changes in Bath Temperature.

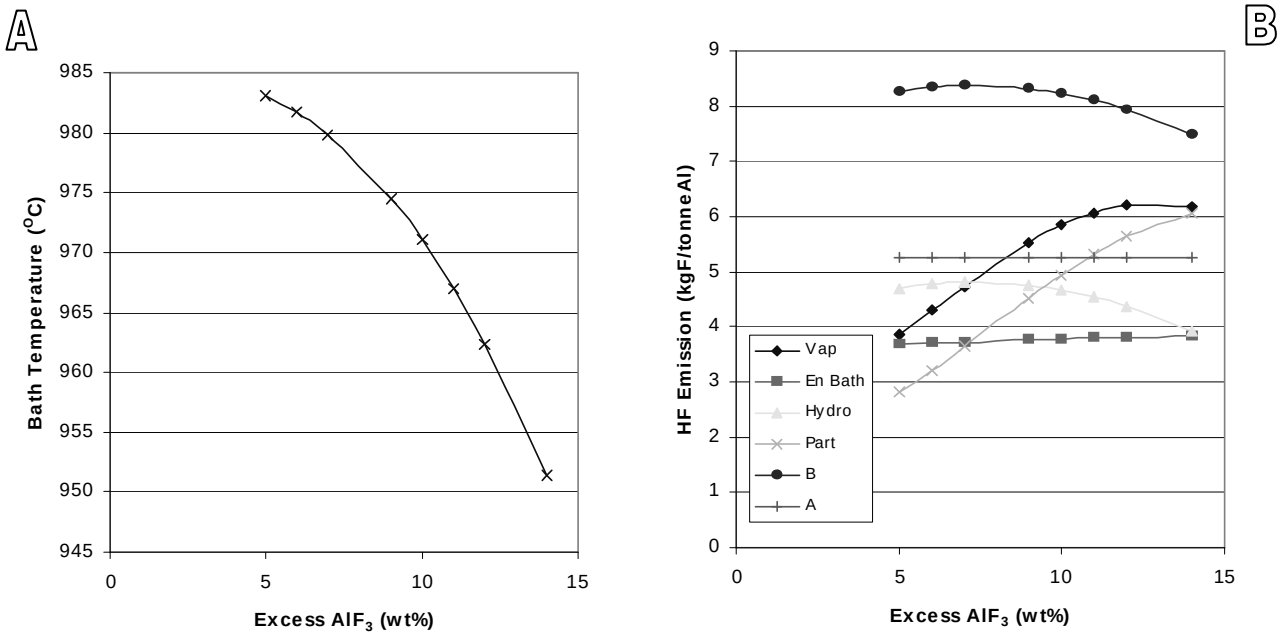

Figure 8.15 – The effect of excess AlF_3 on the emission (A)Bath Temperature. (B)Fluoride Emission. Vap = Vaporisation Emission, En Bath = Entrained Bath, Hydro = Hydrolysis, Part = Particulates, B = Non alumina feeding emission, A = alumina feeding emission.

The trends expected for changes in the bath temperature are seen in figure 8.15 when compared to past studies results (refer to section 4.7.1). The absolute values differ to that from Wahnsiedler [5] and Henry [2] due to the technology differences. The limitations of the model are seen however as the HF contributions are unaffected by the temperature variation. Chapter 7 does show little effect of the temperature on the $D_{feeding}$ value, though it is quite likely that the reaction temperature does have an effect on HF generation. However the bath temperature was found to have little effect on the

overall HF emission. However as no quantitative data has been gathered in the study for this specific contribution, the effect of temperature on the contributions can not be included in the data. It is sufficient to predict that they are reasonably constant given the findings of the industrial investigation. However due to this the changes of HF generation with temperature are not consistent with the previous model [6].

Changes in Humidity.

Figure 8.16 illustrates the effect of humidity on cell technology II as predicted by the modified model. Here the predictions are for 1.5 open feeder holes and a crust state of 2.5.

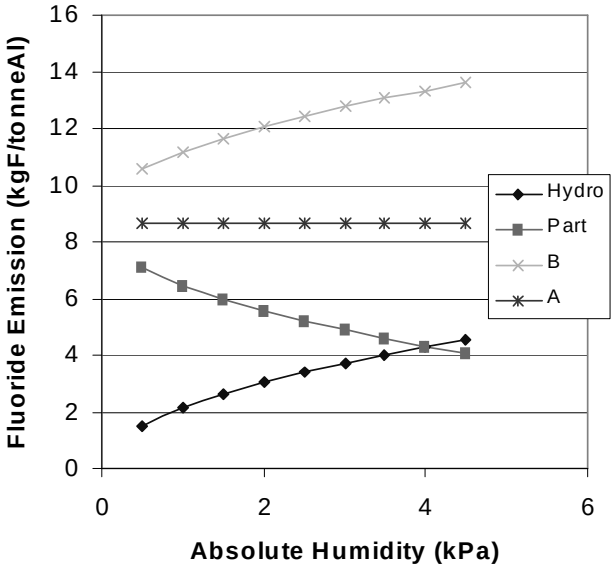

Figure 8.16 – The effects of Humidity on the Emission contributors for cell technology II.
Hydro = Hydrolysis, Part = Particulates,
B = Non alumina feeding emission, A = alumina feeding emission.

As detailed in chapter 5 and 7, with changing humidity the major effect is on the non alumina feeding emission (B in figure 8.16). Here the particulates are hydrolysed more to HF gas.

Changes in Crust Integrity.

Crust integrity for this model is made up of both feeder hole state and crust state. Hence the effects of both these factors on the hydrolysis emission are illustrated in figure 8.17.

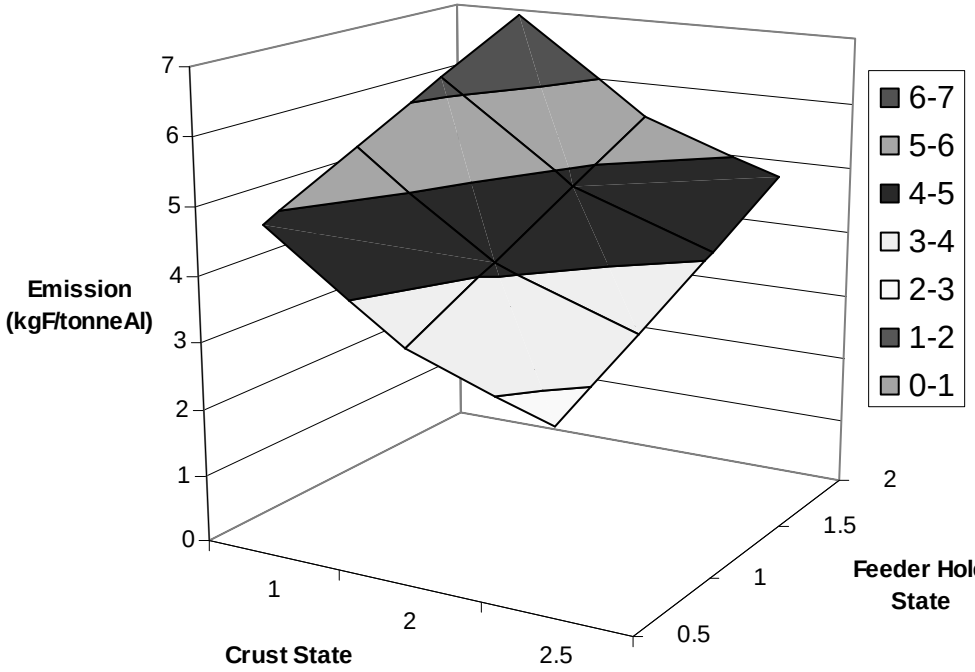

Figure 8.17 – The effects of crust state and feeder hole state on the hydrolysis emission for cell technology II.

As expected the hydrolysis emission reduces with a better crust integrity (or lower feeder hole state and greater crust state). The reverse is true for the entrained emissions. Overall the worse the crust integrity the greater the HF emission. This is illustrated in figure 8.18.

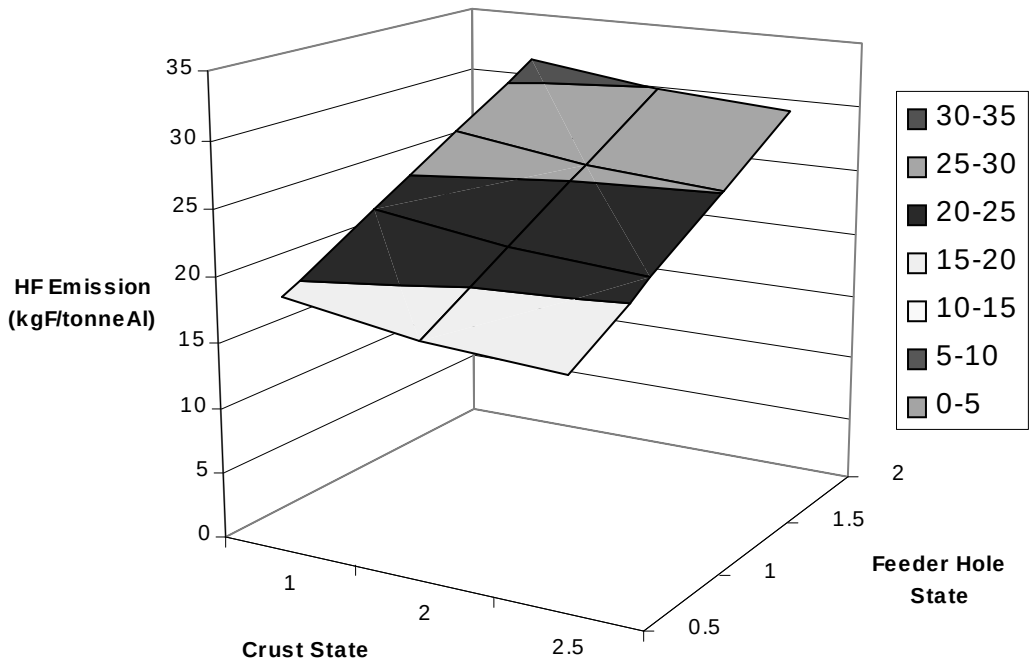

Figure 8.18 – The effects of crust state and feeder hole state on the overall HF emission for cell technology II.

Again the HF emission increases with a greater feeder hole state due to greater alumina water emission and a greater hydrolysis content, and decreases with a better crust state or mass transfer barrier.

8.2.6. Conclusions.

The HF emission can be reasonably predicted by the modified model if the dissolved water and alumina water reaction coefficients are known for a particular cell technology. There are limitations to the model however. The temperature reliance of the HF emission is now not factored into the model due to the breaking up of the contributions. This must be studied in further detail for this to be part of the model. However the data collected suggests this contribution is minor, hence allowing the model to be sufficiently accurate within the limits of the conditions studied in the industrial investigation.

9. Conclusions.

It was the overall aim of this investigation to gain a better understanding of the contributors to hydrogen fluoride generation from aluminium electrolysis cells. Past research is scarce, though it had identified the major fluoride generation sources. From this background the following results were concluded.

9.1. Primary Generation.

This was defined as electrolytic HF generation from within the electrolyte.

Numerous studies [2, 4, 5] had identified alumina water to be the major contributor to this generation source. This investigation confirms this finding, showing that this source is responsible for the measured short term variations in the overall HF emission. This is attributed to the changes in the rate of alumina feeding during the alumina feeding schedule. Here the more reaction water is added with a greater the alumina feeding rate. Furthermore it is likely that only a fraction of the structural water reacts to form HF. The remainder forms either part of the dissolved water content of the electrolyte and/or is entrained in the anode gases, being extracted to the fume treatment system. Both laboratory and industrial experiments showed the exact amount reacted depends on the feeding technology and crust integrity. For the cell technologies studied, the structural water reaction efficiency varied between 18 to 40% of the structural water reacting,. Generation from this source varies between 7 to 14 kgF/tonneAl. It is the biggest single generation source of HF in a modern electrolytic cell.

HF generation from hydrogen in the anode was also identified as a contributor to HF generation. From laboratory experiments, the low H reaction figure of Wahnsiedler [5] was confirmed. Approximately 10% of the hydrogen reacts. It is expected that the remainder is entrained in the anode gases and is extracted to the fume treatment system. Of all the HF sources this is the least significant. However its contribution is a constant one, hence always adds to the emission from a cell. It is estimated to contribute 2 to 5 kgF/tonneAl.

The dissolved water content of the electrolyte has also been found to provide a significant HF generation. This emission contributor has not been considered by the

majority of the past studies. The dissolved water content is proportional to the alumina content of the electrolyte during electrolysis. From both laboratory and industrial measurements it was found that this source gave a significant constant generation. Depending on feeding technology the emission can vary from 3 to 10 kgF/tonneAl. This makes it a significant emission contributor.

9.2. Secondary Generation.

This was defined as all the HF generation not generated in the electrolyte.

The most significant source of secondary generation is thermal hydrolysis of the particulates. Particulates mainly result from vapourisation of the fluoride based electrolyte into the fume extraction system. Past research [2] has suggested that this could only take place in the crust vents that have flames. These flames result from the CO content being converted to CO_2 at these crust cracks. Laboratory experiments have shown that hydrolysis only occurs to a significant degree above $600^{O}C$. This only occurs at these flaming vents in the cell. Industrial experiments also show the emission to be dependant on the ambient partial pressure of water in the air. This dependance is related to the thermal hydrolysis content. Again the laboratory experiments show the higher the partial pressure of water, the greater the hydrolysis particulate to HF conversion. This dependance on humidity results in the long term changes in an industrial cells emission. The crust integrity of the cell becomes important due to this content also. If there is a good crust cover then little vaporisation occurs, and there are few flaming cracks. The feeder hole state also has the same effect. An open feeder hole allows the vapours to escape. It is also an ideal path for the anode gases to escape from. This usually results in flaming and thus also increased thermal hydrolysis. A closed feeder hole presents a barrier which prevents these events from occurring. The thermal hydrolysis content can vary between 2 to 8 kgF/tonneAl.

Another identified source of secondary HF emission is the desorption of HF from secondary or fluorinated alumina. Both the laboratory and industrial experiments show that this content is minor. Rapid heating experiments in the laboratory found up to 95% of the fluoride was retained on heating. In an industrial cell there was little difference found between the emission from primary and secondary alumina. This leads to the conclusion that when compared to the other emission contributors, this source is insignificant. The reasons that this source does not produce significant emission is due to the a surface reaction which retains the fluoride on the surface. When the alumina is

fed to an industrial cell it experiences a rapid and large temperature change. The alumina is heated at approximately $180^{O}C$/sec heating. This does not allow the HF to escape but rather provides enough energy for the surface fluoride reaction product to be converted to AlF_3 and $Al(OH)_3$. This then enters the bath.

9.3. Cell emission Factors.

From the generation analysis it can be concluded that the emissions from a real cell vary on a short term basis, depending on the alumina feeding rate of the feeding schedule. It can also vary on a much long term basis based on the ambient air humidity. Other operations also affect the emission due to heat balance effects and changes in crust cover. The batch operation with the greatest effect is anode change. This is because it both exposes a large amount of bath to the humid ambient air and changes the crust integrity of the cell. Apart from the design of the cell, which dictates how well the alumina dissolves and thus the magnitude of the most significant emission contributor – the alumina water, there are three operational factors which are major contributors to the cell emission. The humidity of the air, the crust integrity, the feeder hole states and the efficiency of the batch operations will be the major factors affecting the HF emission. Duct temperature has no effect, and the effect of the cell temperature is masked by larger contributions.

Overall for a prebake point fed aluminium reduction cell the following emission contributor figures can be given (table 9.1). Both modelling and plant data show that the following figures to be reasonably accurate:

Table 9.1 – Summary of HF emission contributors.

Emission Contributor	Emission (kgF/tonneAl)	%HF Emission (%)	
Primary Generation.			
Alumina Water	7 - 14	40 – 60%	Alumina Feeding Contribution
Hydrogen in the Anodes	2 - 5	<10%	Non Alumina Feeding Contribution
Dissolved Water	3 – 10	10 – 30%	
Secondary Generation.			
Hydrolysis	2 – 8	10 – 30%	
Secondary F desorption	0.1 – 0.5	< 1%	

Hence in a modern prebake aluminium cell, the most significant factors affecting emission are alumina feeding and thermal hydrolysis. Experience show control of the crust integrity is the simplest method of reducing emission in the short term. This

relates both to normal operation and batch operations. A daily covering operation, filling in the flaming vents and blocking any crust cracks will significantly reduce this content. Reduction of all other sources of emission are a material composition problem. Simply reducing the water content (LOI(300) and LOI(1000)) and reducing the hydrogen content of the anodes will reduce the emission. However material considerations affect other aspects of cell operation and hence these factors are not as simple to adjust. This would have to form part of a long term strategy, where all considerations are taken into account. This would form the basis of an interesting future study.

10. References.

[1] B. J. Welch, "Impact of Changes in Cell Heat Balance and Operations on the Electrolyte Composition," presented at Proc 6th Australasian Aluminium Smelting Conference and Workshop, Queenstown, New Zealand, 1998.

[2] J. L. Henry, "A study of factors affecting fluoride emissions from 10,000 ampere experimental aluminium reduction cell.," in *Extractive Metallurgy of Aluminium.*, vol. 2, G. Gerard, Ed. Interscience, New York., 1963, pp. 67 - 81.

[3] C. N. Cochran, W. C. Sleepy, and W. B. Frank, "Fumes in aluminium smelting: Chemistry of evolution and recovery," *Journal of Metals*, vol. 22, pp. 54 - 57, 1970.

[4] K. Grjotheim, B. J. Welch, H. Kvande, and K. Motzfeldt, "The formation and Composition of the fluoride emissions from aluminium cells.," *Canadian Metallurgical Quarterly*, vol. 11, pp. 585 - 599, 1972.

[5] W. E. Wahnsiedler, R. S. Danchik, W. E. Haupin, D. L. Brackenstose, and J. W. Colpitts, "Factors affecting fluoride evolution from Hall-Heroult smelting cells.," presented at Light Metals 1978, 1978.

[6] W. E. Haupin and H. Kvande, "Mathematical model of fluoride evolution from Hall-Heroult cells," presented at Light Metals 1993, 1993.

[7] O. Lid, K. Nilsson, and S. Gjorven, "Strategy of pot operation related to fluoride emissions," presented at VI. Al Sympozium., 13 - 15/9/1988, Zbornik, 1988.

[8] K. Grjotheim and B. J. Welch, *Aluminium smelter technology.*, 2 ed: Aluminium - Verlag, Dusseldorf., 1988.

[9] E. Keul, "Emission control," presented at 13th International Course on Process Metallurgy of Aluminium., Trondheim, Norway, 1994.

[10] N. E. Richards, "Alumina in smelting," presented at 13th International Course on Process Metallurgy of Aluminium, Trondheim, Norway, 1994.

[11] K. Grjotheim and H. Kvande, *Introduction to aluminium electrolysis*: Aluminium-Verlag, Dusseldorf., 1993.

[12] M. M. Hyland, A. R. Gillespie, and J. B. Metson, "Predicting moisture content on smelter grade alumina from measurements of the water isotherm.," presented at Light Metals 1997, 1997.

[13] R. Desai, M. Hussian, and D. M. Ruthven, "Adsorption of water vapour on activated alumina. I - Equilibrium behaviour.," *The Canadian Journal of Chemical Engineering.*, vol. 70, pp. 699 - 706, 1992.

[14] M. A. Llavona, F. Blanco, P. Garcia, J. Sancho, and L. F. Verdeja, "Some new considerations on the measurement of humidity, M.O.I. and L.O.I..," presented at Light Metals 1988, 1988.

[15] O. Kobbeltvedt, S. Rolseth, and J. Thonstad, "On the mechanisms of alumina dissolution with relevance to point feeding aluminium cells.," presented at Light Metals 1996, 1996.

[16] R. G. Haverkamp, "Surface studies and dissolution studies of fluorinated alumina.," in *Chemistry*. Auckland: The University of Auckland, 1992.

[17] G. I. Kuschel and B. J. Welch, "On the mechanisms of alumina dissolution under conditions similar to cell operation.," presented at Light Metals 1993, 1991.

[18] X. Lui, J. M. Purdie, M. P. Taylor, and B. J. Welch, "Measurement and modelling of alumina mixing and dissolution for varying electrolyte heat and mass transfer conditions.," presented at Light Metals 1991, 1991.

[19] D. C. Chensonic and A. F. La Camera, "The influence of gas-driven circulation on alumina distribution and interface motion in a hall-heroult cell.," presented at Light Metals 1990, 1990.

[20] M. M. Bilek, W. D. Zang, and F. J. Stevens, "Modelling of electrolyte flow and its related transport processes in aluminium reduction cells.," presented at Light Metals 1994., 1994.

[21] B. P. Moxnes, B. E. Aga, and J. H. Skaar, "How to obtain open feeder holes by installing anodes with tracks," presented at Light Metals 1998, 1998.

[22] X. Lui, S. F. George, and V. A. Wills, "Effect of alumina phase structure on its dissolution in a cryolite melt," presented at Third alumina quality workshop, Hunter Valley, NSW, Australia, 1993.

[23] O. Lid, "Emission from modern pots with prebake anodes," presented at 5th Czech al sympozium., 1981.

[24] L. N. Less and J. Waddington, "The characterisation of aluminium reduction cell fume.," presented at Light Metals 1971, 1971.

[25] K. Grjotheim, C. Krohn, M. Malinovsky, K. Matiasovsky, and J. Thonstad, *Aluminium Electrolysis. Fundamentals of the Hall-Heroult Process*, I ed. Dusseldorf: Aluminium-Verlag, 1982.

[26] M. M. Hyland, B. J. Welch, and J. B. Metson, "Changing knowledge and practices towards minimising fluoride and sulphur emissions from aluminium reduction cells," presented at Light Metals 2000, 2000.

[27] W. E. Haupin, "Mathematical model of fluoride evolution from Hall-Heroult cells.," presented at Light Metals 1984, 1984.

[28] R. Greenwood, "Reducing fluoride emissions from electrolytic cells at New Zealand aluminium smelters," presented at Fourth Australasian Aluminium Smelter Technology Workshop, Sydney, Australia., 1992.

[29] A. B. Heiberg, G. Wedde, O. K. Bockman, and S. O. Strommen, "Pot gas fume as a source of HF emission from aluminium smelters - Laboratory and field investigations," presented at Light Metals 1999, 1999.

[30] E. C. Patterson, M. M. Hyland, V. Kielland, and B. J. Welch, "Gaining a realistic view of fluoride generation from aluminium electrolysis cells.," presented at Second Australasian environmental research event, Sydney, Australia., 1999.

[31] A. J. Gillespie, "Mechanistic studies of HF adsorption on alumina," in *Chemistry*. Auckland: University of Auckland, 1996.

[32] M. M. Hyland, J. B. Metson, and R. G. Haverkamp, "The adsorption of HF on alumina: A current understanding of the process.," presented at Fourth Australasian Aluminium Smelter Technology Workshop., Sydney, Australia., 1992.

[33] A. J. Gillespie, M. M. Hyland, and J. B. Metson, "The surface chemistry of secondary alumina from the dry scrubbing process," presented at Light Metals 2000, 2000.

[34] W. D. Lamb, "A study of the equilibrium adsorption of hydrogen fluoride on smelter grade aluminas.," presented at Light Metals 1978, 1978.

[35] M. M. Hyland, J. B. Metson, R. G. Haverkamp, and B. J. Welch, "Surface studies of hydrogen fluoride adsorption on alumina.," presented at Light Metals 1992, 1992.

[36] D. J. Salt, "Bath Chemistry Control System," presented at Light Metals 1990, 1993.

[37] A. Franke and W. Schmidt-Hatting, "The influence of bath composition on cell emission, bath temperature and alumina concentration.," presented at Light Metals 1977, 1977.

[38] E. R. Buckle and R. R. Finbow, "Solubility and chemical effects of water vapour and other gases in the molten salts of extractive metallurgy," *International Metals Reviews*, pp. 197 - 226, 1976.

[39] T. Foosnaes, V. Hjelle, and M. Karlsen, "Continuous monitoring of gaseous fluoride emissions," presented at Light Metals 1993, 1993.

[40] K. A. Rye, T. Eidet, and K. Torklep, "Dynamic ledge response in Hall-Heroult Cells," presented at Light Metals 1999, 1999.

[41] T. A. Utigard, "Why 'best' pots operate between 955 and 970oC," presented at Light Metals 1999, 1999.

[42] R. S. Danchik, H. F. Hillegass, and G. P. Tarcy, "The continuous measurement of gaseous fluoride in ambient air.," presented at Light Metals 1980, 1980.

[43] R. S. Danchik, R. C. Obbink, and G. F. Lenz, "Evaluation of sampling and analysis of potroom effluents for fluoride determinations.," presented at Light Metals 1978, 1978.

[44] G. Wedde, "Improved efficiencies in the dry scrubbing process," presented at Light Metals 1997, 1997.

[45] R. G. Haverkamp, M. M. Hyland, J. B. Metson, and B. J. Welch, "Adsorption of hydrogen fluoride on alumina," *Surface Interface Analysis*, vol. 19, pp. 139, 1992.

[46] A. L. McKenna, "Aluminium Compounds," in *Encyclopaedia of Chemical Technology*, vol. 2, M. Howe-Grant, Ed., Fourth ed. New York: Wiley-Interscience, 1992, pp. 265.

[47] O. V. Bulgakov and T. A. Antipina, "X-Ray diffraction analysis of the products of the reaction of hydrofluoric acid with alumina.," *Russian Journal of Physical Chemistry*, vol. 41, pp. 1680 - 1682, 1967.

[48] M. D. Gadd, B. J. Welch, and A. C. Ackland, "The effect of process operations on smelter cell top heat losses," presented at Light Metals 2000, 2000.

[49] N. Basmajian, "Consolidation in Aluminium Reduction Cell Cover," in *Chemical and Materials Engineering*. Auckland: University of Auckland, 2000, pp. 66.

[50] L. N. Less, "The Crusting Ability of Smelter Aluminas," *Met. Trans.*, vol. 8B, pp. 219 - 225, 1977.

[51] X. Lui, M. P. Taylor, and S. F. George, "Crust Formation and Deterioration in Industrial Cells," presented at Light Metals 1992, 1992.

[52] T. Eggen, S. Rolseth, K. A. Rye, and J. Thonstad, "Alumina Crusting in Cryolite Melts. Part I: Penetration of Molten Electrolyte into Alumina.," presented at Light Metals 1992, 1992.

[53] M. D. Gadd, B. J. Welch, and K. O. O'Brien, "Aspects of top heat loss in aluminium," presented at Chemica 99', Australia, 1999.

[54] D. R. Coughanowr, *Process Systems Analysis and Control*. Singapore: McGraw-Hill, Singapore., 1991.

[55] H. S. Fogler, *Elements of Chemical Reaction Engineering*. New Jersey, USA.: PTR Prentice Hall Inc., 1992.

[56] A. R. Gillespie, M. M. Hyland, and J. B. Metson, "Irreversible HF adsorption in the dry scrubbing process," *Journal of metals.*, vol. 51, pp. 30 - 32, 1999.

Appendix 1 – The Fluorination Rig.

The overall aim of the fluorination rig was to saturate the surface of the alumina at a constant humidity with reproducibility. Surface fluoride contents are quantified using X-ray fluorescence analysis. The major variables are summarised below.

Major Variables:

- N_2 flowrate.
- Aqueous HF concentration and flowrate.
- Moisture injected into the flow stream.
- Reactor Temperature.
- Humidity (Moisture content of the alumina). Controlled by varying the moisture content of the N_2 flow, the flow rate of the N_2 cover gas and the temperature of the fluorination reactor.

A1.1 Experimental Procedure.

The Equipment.

The equipment design is based on the rig outlined in Gillespie [31]. The rig as illustrated in figure A1.1 consisted of a heated nitrogen carrier gas into which hydrogen fluoride was vapourised from an aqueous solution and transported into a fluidised bed reactor. After reacting with the alumina the off gases were passed through a buffered solution (TISAB) in which the unreacted HF was captured. Using an ion selective electrode the fluoride content was continuously measured. The concentration in the gas streams was determined from known mass flows or from wet analysis methods [43].

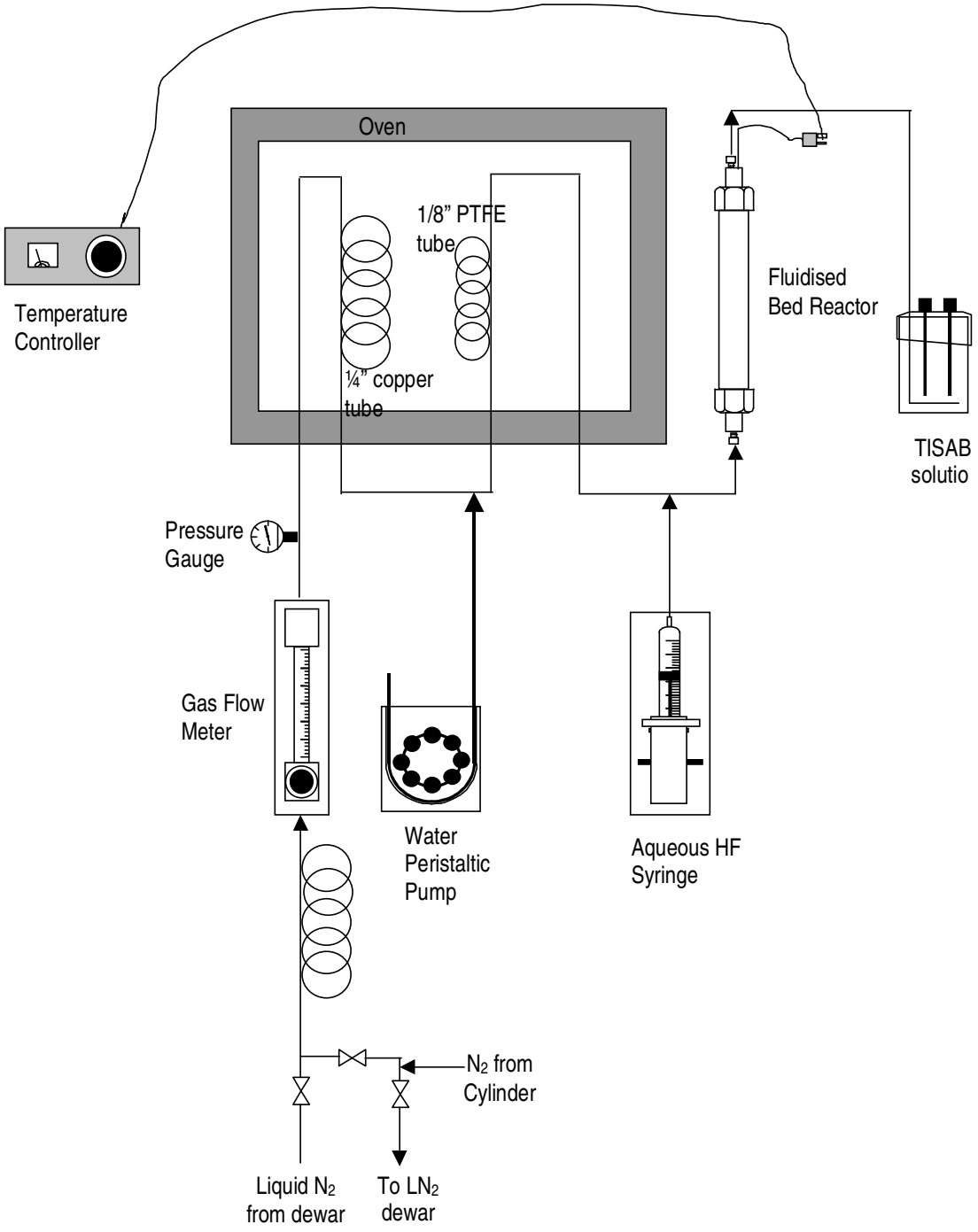

Figure A1.1 - The fluoride adsorption rig.(After [56])

The carrier gas was preheated in coils of ¼" copper tube while all tubes and fittings subsequent to HF injection were made of 1/8" PTFE or polyethylene for chemical resistance. A syringe pump was used to inject the aqueous HF as the flow rate (1.6 to 210 mL/min) is unaffected by back pressure. A peristaltic pump was used to inject water due to the relatively large amounts needed.

The reactor was a PTFE- copper lined tube with porous filters at either end to retain the alumina. The exhaust gas from the reactor was bubbled through a perforated ring of PTFE tubing into the TISAB solution in a PTFE beaker. The fluoride content was measured using a calibrated fluoride ion selective electrode and a suitable reference electrode.

Experimental Procedure.

5 g of alumina was added to the fluoride reactor between two porous polyethylene filters (frits). The reactor was sealed, connected to the data logging equipment and left for 10 minutes to heat up to 80^{O}C. Approximately 50 mL of 4 mol/L hydrofluoric acid was then added to the syringe pump. The N_2 gas flow was set to 1.5 L/min and allowed to flow for 10 minutes. After this time the data logging equipment was set and the hydrofluoric acid pumped through. The run was left to run for 10 to 24 hours, with need only to adjust the N_2 flow on occasion.

Once the run is complete, the alumina was collected and the rig run with humidified nitrogen (water injected into the hot N_2 flow) for 2 hours to collect any residual HF. All accessible surfaces are then flushed with water.

From the fluorinated sample, 0.5g is split for XRF analysis and the remainder used for the emissions trials.

A1.2 Experimental Results.

A representative run using these results is illustrated in figure A1.2. This is a break through curve. A breakthrough curve is a plot of the outlet fluoride concentration of the reactor vs time. The run is complete once the inlet and outlet values of fluoride are the same (in this case ~0.89 mg/L N_2). It can be seen that there is zero residual fluoride until approximately 300 minutes into the trial, indicating constant adsorption. Past this point the alumina surface is approaching saturation. The alumina is saturated at around 480 minutes when the residual fluoride detected becomes a straight line (representing constant addition). The tail at the end of the run is the point where fluoride addition terminates. Residual fluoride and evaporation of the TISAB causes a slight rise in the concentration over the remainder of the experiment. XRF analysis of the alumina quantifies the amount of fluoride adsorbed.

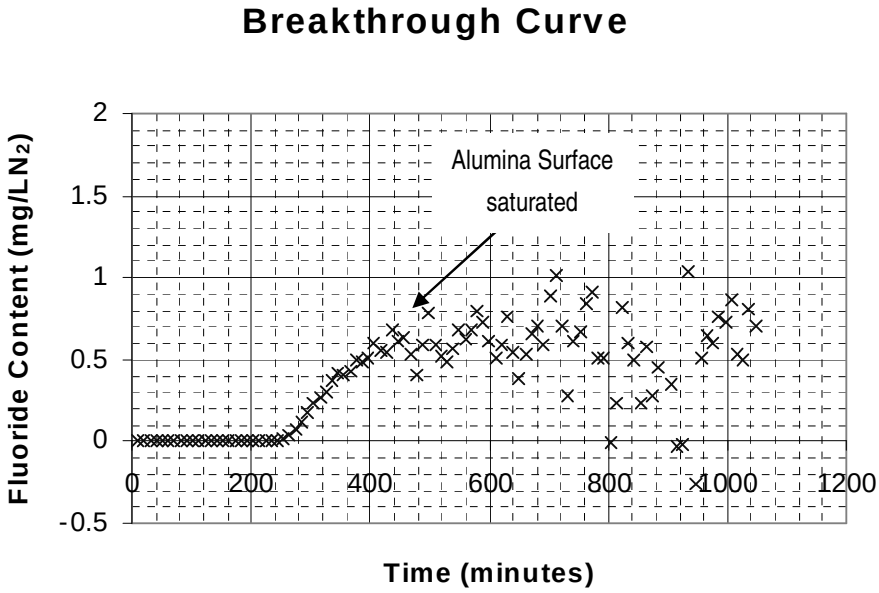

Figure A1.2 – Representative fluoride adsorption breakthrough curve.

The illustrated breakthrough curve shapes appear to be consistent with Lambs adsorption results [34] and Gillespies break through curves [31].

The *XRF analysis* shows that all the adsorption runs show between 5 to 8% fluoride adsorbed on the surface of alumina (refer to table A1.1).

Table A1.1 – XRF Analysis compared to Electrode Measurements

Sample	XRF Relative F%
Ad 5	6.83
Ad 6	6.70
Ad 7	6.28
Ad 11	5.26

Appendix 2 – Model Examples.

A2.1 – Haupin – Kvande.

Fluoride Evolution Model (Haupin and Kvande 1993). *Date Printed: 28/11/2000*

Constants *Cell Technology I*

Cell Data:

Current I =	170.9	kA				
V=	4.2	V				
Al Produced=	1300	kg/24hrs				
CE (%)=	93	%				
Bath Temp (T) =	1235.15	K				
=	962	oC				
Superheat =	4.61	oC	Mr	wt%/Mr	mol%	
Na3AlF6=	80.5	wt%	213	0.3779	62.85	
Excess AlF3 =	12	wt%	87	0.1379	22.94	
%CaF2=	4.5	wt%	78	0.0577	9.59	
% Al2O3=	3	wt%	108	0.0278	4.62	
%LiF=	0	wt%	26	0.0000	0.00	
%MgF2=	0	wt%	62.3	0.0000	0.00	
BR (WR)=	1.093					
CR=	2.186					
Phumid=	1.6	kPa	Absolute Humidity			
Pb =	101.3	kPa	Absolute Pressure			
Alumina H2O%=	4	wt%	Wore (secondary)			
%H in Anodes=	0.044	wt%	*(guess)*			

Particulates:

Catch=	0.416	(how good the covering is 1 is excellent)
HBA (Hydr by air)	1.485	(0 - 3, 3 is a lot, 1 is average)

Results Summary:

Type	kgF/tonAl	kgF/hr	%total	
FVP=	6.138	0.333	39.99	Volatisation
FEP=	3.812	0.206	24.83	Entrained bath
FGB=	5.398	0.292	35.17	Gaseous HF
FGP=	4.346	0.235	28.32	Hydrolysis
With Hydrolysis:				
Total Particulate Fp=	5.604	0.304	36.51	
Total Gaseous fluoride =	9.745	0.528	63.49	
Total Fluoride Ft=	15.349	0.831		

Liquidus temperature calculation:

TL=	957.39 oC	Equation from Røstum (1990)
Bath Temp=	962.00 oC	
Superheat=	4.61 oC	

Volatilization of Bath.

Vapour Pressure of Molten Cryolite:

VP=	511.3676	Pa
VPb (Na3AlF6) =	0.0051	bar
A=	21910.04	
B=	23.97586	
Gas Produced=	29.8890	kmol/tonAl

Partial Pressures:

PNaF=	2.97859E-05	bar
Kp=	0.1977	
PM (NaAlF4)=	4.9595E-03	bar
PD (Na2Al2Al8)=	1.2439E-04	bar

Volitilisation Fluoride Emission:

Fvp=	6.1385	kgF/tonAl

Entrained Bath.

Catch=	0.416	
SurfT=	125.2030	mN/m

Entrainment Fluoride Emission:

Fep=	3.8118	kgF/tonAl

HF Formation. Predicts 26.8% of water reacts from measurements.

1/3AlF3(in bath) +1/2H2O(g) = HF(g) + 1/6Al2O3(in bath)

Calculation Factors:

-ΔG/RT=	0.6924		
PH2O=	0.1319	bar	
%Al2O3*=	2.1641	wt%	Sat Al2O3
A=	0.920474		
B=	-3.75912		
aAl2O3=	2.4713		
aAlF3=	0.00018745		
MFC	0.05769231		
MFM	0		

Patial Pressure of HF in gas:

PHF=	0.03572443	bar

HF Fluoride Emission:

FGB=	5.3984	kgF/tonAl

Hydrolysis of Pot Fume.

1/2NaAlF4(g) + 1/2H2O(g) = 1/6Al2O3(s)+1/6Na3AlF6(s) + HF(g)

PHF=	look into	
HBA (hyd by	1.485	

Hydrolysis Fluoride Emission:

FGP=	4.3464	kgF/tonAl

Figure A2.1 – The spreadsheet calculations for the Haupin Kvande Model.

A2.2 – Cell Technology I.

Constants *Cell Technology I*

Cell Data:

Current I =	170.9	kA	
V=	4.2	V	
Al Produced=	1300	kg/24hrs	
CE (%)=	93	%	
Bath Temp (T) =	962.00	oC	
=	1235.15	K	
Net Carbon=	0.45	kg/kgAl	
Superheat =	4.61	oC	
Na_3AlF_6=	80.5	wt%	
Excess AlF_3 =	12	wt%	
%CaF_2=	4.5	wt%	
% Al_2O_3=	3	wt%	
%LiF=	0	wt%	
%MgF_2=	0	wt%	
Primary LOI 300 =	1.58	%	
Primary LOI 1000 =	0.47	%	
p-alumina Na% =	0.4	%	
p-alumina F% =	0.4	%	
Secondary LOI 300=	1.95	%	
Secondary LOI 1000=	2.68	%	
S-alumina Na% =	1.64	%	
S-alumina F% =	0.66	%	
Average Overfeeding Rate =	2.65	kg/min	
Average Underfeeding Rate =	1.15	kg/min	
Average Feeding Rate=	1.90	kg/min	
BR (WR)=	1.093		
CR=	2.186		

Mr	*wt%/Mr*	*mol%*
213	*0.3779*	*62.85*
87	*0.1379*	*22.94*
78	*0.0577*	*9.59*
108	*0.0278*	*4.62*
26	*0.0000*	*0.00*
62.3	*0.0000*	*0.00*

Mr	
Al	*26.982*
Na	*22.99*
F	*18.999*
HF	*20*
H_2O	*18*

Primary Generation Factors:

Open feeder holes	33.33	%	
Feeding Technology	1.00		1 Retrofit, 2 Middle, 3 Total Design
Overall Alumina Water R.E. =	24.9	%	~feeder hole states and technology
Dissolved Water Effect =	0.05	kg/h/wt% Al_2O_3	
%H in Anodes=	0.044	wt%	Experimental
Anode Reaction efficiency=	10	%	

Secondary Generation Factors:

Phumid=	1.6	kPa	Absolute Humidity
Pb =	101.3	kPa	Absolute Pressure

Particulates:

Crust Quality =	1.5	(1=poor, 2=medium, 3=good)
Crust Integrity	41.67	% (~Crust Quality and Feeder holes)
HBA (Hydr by air)	49.50	% (vapour converted by thermal hydrolysis)

Volatilization of Bath. (from Haupin and Kvande (1993)).

Vapour Pressure of Molten Cryolite:

VP=	511.3676	Pa
VPb (Na_3AlF_6) =	0.0051	bar
A=	21910.04	
B=	23.97586	
Anode Gas Produced=	29.8890	kmol/tonAl

Partial Pressures:

PNaF=	2.97859E-05	bar
Kp=	0.1977	
PM ($NaAlF_4$)=	4.9595E-03	bar
PD ($Na_2Al_2Al_8$)=	1.2439E-04	bar

Volitilisation Fluoride Emission:

Fvp=	6.1385	kgF/tonAl

Hydrolysis of Pot Fume.

1/2NaAlF4(g) + 1/2H2O(g) = 1/6Al2O3(s)+1/6Na3AlF6(s) + HF(g)

PHF=	look into		
HBA (hyd by air)	1.485	=hydrolysis %*3	(3 is lots, 1 is poor)

Hydrolysis Fluoride Emission:

FGP=	4.3464	kgF/tonAl

Results Summary:

Type	kgF/tonAl	kgF/hr	%total	
Vapourisation	6.138	0.333	32.78	Volatisation
Entrained Bath	3.807	0.206	20.33	Entrained bath
Hydrogen	0.786	0.043	4.20	Gaseous HF
Dissolved Water	2.769	0.150	14.79	Gaseous HF
Water	5.228	0.283	27.91	Gaseous HF
Hydrolysis	4.346	0.235	23.21	Hydrolysis
With Hydrolysis:				
Total Particulate Fp=	5.600	0.303	29.90	
Total Gaseous fluoride =	13.129	0.711	70.10	
Total Fluoride Ft=	18.729	1.014	100.00	
HF Breakdown: *Background =*	*7.901*	*0.428*		
Alumina Water =	*5.228*	*0.283*		

Liquidus temperature calculation:

TL=	957.39	oC	Equation from Røstum (1990)
Bath Temp=	962.00	oC	
Superheat=	4.61	oC	

Entrained Bath.

Catch=	0.416666667	=Crust Integrity/100 - how good the cover is, 1 is good
SurfT=	125.2030	mN/m

Entrainment Fluoride Emission:

Fep=	3.8074	kgF/tonAl

Water Primary Generation.

1/3AlF3(in bath) +1/2H2O(g) = HF(g) + 1/6Al2O3(in bath)

Na% with bath materials=	1.24	%
s-alumina Alumina %=	95.47049413	%
Crystalline Water=	0.448711322	%
Other Water=	4.63	%
Reaction Efficiency=	24.9	%

Assuming only a percentage of the crystalline water reacts:

					kg/h	kg/tonAl
HF produced:	Overfeed=	0.006584	kg/min	=	0.395039	7.29303
	Underfeed=	0.002855	kg/min	=	0.171318	3.162794
	Average=	0.00472	kg/min	=	0.283179	5.227912

Dissolved Water

Emission Rate=	0.15	kg/h	=	2.7692 kg/tonneAl

Hydrogen Primary Generation

Na3AlF6(l)+3/2H2 = Al(l)+3HF(g)+3NaF(l) (1)

AlF3(l)+3/2H2=Al+3HF (2)

Aluminium Production=	1300	kg/day	
Carbon used=	585	kg/day	
Anode Hydrogen %=	0.044	%	
Hydrogen Produced=	0.2574	kg/day	
=	10.63988095	mol/hr	
Reaction Efficiency=	10	%	
Mole Ratio=	2		
Mr (HF)=	20		
HF max=	21.2797619	mol/hr	
=	0.425595238	kg/hr	
=	7.093253968	g/min	
=	7.857142857	kg/tonAl	
HF predicted =	0.042559524	kg/hr	
=	0.785714286	kg/tonAl	

Figure A2.2 – The spreadsheet calculations for the model predicting cell technology I emissions.

A2.3 – Cell Technology II.

Constants *Cell Technology II*

Cell Data:

Current I =	265	kA	
V=	4.2	V	
Al Produced=	2000	kg/24hrs	
CE (%)=	94	%	
Bath Temp (T) =	962	oC	
=	1235.15	K	
Net Carbon=	0.41	kg/kgAl	
Superheat =	5.73	oC	
Na_3AlF_6=	80	wt%	
Excess AlF_3 =	12	wt%	
%CaF_2=	5	wt%	
% Al_2O_3=	3	wt%	
%LiF=	0	wt%	
%MgF_2=	0	wt%	
Primary LOI 300 =	0.98	%	
Primary LOI 1000 =	0.88	%	
p-alumina Na% =	0.42	%	
p-alumina F% =	0.4	%	
Secondary LOI 300=	2.31	%	
Secondary LOI 1000=	2.89	%	
S-alumina Na% =	0.61	%	
S-alumina F% =	2.09	%	
Average Overfeeding Rate =	3.31	kg/min	
Average Underfeeding Rate =	1.5925	kg/min	
Average Feeding Rate=	2.45	kg/min	
BR (WR)=	1.091		
CR=	2.182		

Mr	*wt%/Mr*	*mol%*
213	*0.3756*	*62.04*
87	*0.1379*	*22.78*
78	*0.0641*	*10.59*
108	*0.0278*	*4.59*
26	*0.0000*	*0.00*
62.3	*0.0000*	*0.00*

Mr	
Al	*26.982*
Na	*22.99*
F	*18.999*
HF	*20*
H_2O	*18*

Primary Generation Factors:

Open feeder holes	37.50	%	
Feeding Technology	3.00		1 Retrofit, 2 Middle, 3 Total Design
Overall Alumina Water R.E. =	34.9	%	~feeder hole states and technology
Dissolved Water Effect =	0.231	kg/h/wt%	Al_2O_3
%H in Anodes=	0.044	wt%	Experimental
Anode Reaction efficiency=	10	%	

Secondary Generation Factors:

Phumid=	2.5	kPa	Absolute Humidity
Pb =	101.3	kPa	Absolute Pressure

Particulates:

Crust Quality =	2.5	(1=poor, 2=good, 3=excellent)
Crust Integrity	59.17	% (~Crust Quality and Feeder holes)
HBA (Hydr by air)	37.42	% (vapour converted by thermal hydrolysis)

Volatilization of Bath. (from Haupin and Kvande (1993)).

Vapour Pressure of Molten Cryolite:

VP=	513.6937	Pa
VPb (Na_3AlF_6) =	0.0051	bar
A=	21898.22	
B=	23.97083	

Anode Gas Produced= 29.5711 kmol/tonAl

Partial Pressures:

PNaF=	2.94185E-05	bar
Kp=	0.1977	
PM ($NaAlF_4$)=	4.9820E-03	bar
PD ($Na_2Al_2Al_8$)=	1.2552E-04	bar

Volitilisation Fluoride Emission:

Fvp= 6.1296 kgF/tonAl

Hydrolysis of Pot Fume.

1/2NaAlF4(g) + 1/2H2O(g) = 1/6Al2O3(s)+1/6Na3AlF6(s) + HF(g)

PHF=	look into	
HBA (hyd by air)	1.1225	=hydrolysis %*3 (3 is lots, 1 is poor)

Hydrolysis Fluoride Emission:

FGP= 4.0722 kgF/tonAl

Results Summary:

	Type	kgF/tonAl	kgF/hr	%total	
	Vapourisation	6.130	0.511	20.60	Volatisation
	Entrained Bath	2.633	0.219	8.85	Entrained bath
	Hydrogen	0.716	0.060	2.41	Gaseous HF
	Dissolved Water	8.316	0.693	27.95	Gaseous HF
	Water	11.956	0.996	40.19	Gaseous HF
	Hydrolysis	4.072	0.339	13.69	Hydrolysis
With Hydrolysis:					
Total Particulate Fp=		4.691	0.391	15.77	
Total Gaseous fluoride =		25.060	2.088	84.23	
Total Fluoride Ft=		29.750	2.479	100.00	
HF Breakdown:	*Background =*	*13.104*	*1.092*		
	Alumina Water =	*11.956*	*0.996*		

Liquidus temperature calculation:

TL=	956.27	oC
Bath Temp=	962.00	oC
Superheat=	5.73	oC

Equation from Røstum (1990)

Entrained Bath.

Catch=	0.591666667	=Crust Integrity/100 - how good the cover is, 1 is good
SurfT=	125.3773	mN/m

Entrainment Fluoride Emission:

Fep= 2.6332 kgF/tonAl

Water Primary Generation.

1/3AlF3(in bath) +1/2H2O(g) = HF(g) + 1/6Al2O3(in bath)

Na% with bath materials=	0.19	%
s-alumina Alumina %=	99.30596281	%
Crystalline Water=	0.873892473	%
Other Water=	5.2	%
Reaction Efficiency=	34.9	%

Assuming only a percentage of the crystalline water reacts:

					kg/h	kg/tonAl
HF produced:	Overfeed=	0.022417	kg/min	=	1.344999	16.13999
	Underfeed=	0.010793	kg/min	=	0.647592	7.77110629
	Average=	0.016605	kg/min	=	0.996296	11.9555481

Dissolved Water

Emission Rate= 0.693 kg/h = 8.316 kg/tonneAl

Hydrogen Primary Generation

Na3AlF6(l)+3/2H2 = Al(l)+3HF(g)+3NaF(l) (1)
AlF3(l)+3/2H2=Al+3HF (2)

Aluminium Production=	2000	kg/day	
Carbon used=	820	kg/day	
Anode Hydrogen %=	0.044	%	
Hydrogen Produced=	0.3608	kg/day	
=	14.91402116	mol/hr	
Reaction Efficiency=	10	%	
Mole Ratio=	2		
Mr (HF)=	20		
HF max=	29.82804233	mol/hr	
=	0.596560847	kg/hr	
=	9.942680776	g/min	
=	7.158730159	kg/tonAl	
HF predicted =	0.059656085	kg/hr	
=	0.715873016	kg/tonAl	

Figure A2.3 – The spreadsheet calculations for the model predicting cell technology II emissions.